Studies on Space Structure, Quantum Thermodynamic Systems and Computation

PRITAM CHATTOPADHYAY

Supervisor: Goutam Paul

CRYPTOLOGY AND SECURITY RESEARCH UNIT

R.C. BOSE CENTRE FOR CRYPTOLOGY AND SECURITY

INDIAN STATISTICAL INSTITUTE

KOLKATA, WB-700108, INDIA

A dissertation submitted to Indian Statistical Institute, Kolkata
for the partial fulfilment of the requirements for the Degree of
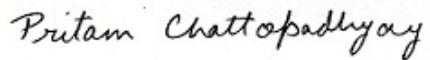*Doctor of Philosophy in Computer Science*

02nd August, 2021

I dedicate this thesis to

My Parents

DECLARATION OF AUTHORSHIP

I, **Pritam Chattopadhyay**, a student of Cryptology and Security Research Unit, R. C. Bose Centre for Cryptology and Security, of the Ph.D. program of Indian Statistical Institute Kolkata, hereby declare that the investigation presented in this thesis is based on my own work and, to the best of my knowledge, the materials contained in this thesis have not previously been published or written by any other person, nor it has been submitted as a whole or as a part for any degree/diploma or any other academic award anywhere before.

Pritam Chattopadhyay

Cryptology and Security Research Unit

R. C. Bose Centre for Cryptology and Security

Indian Statistical Institute Kolkata

Kolkata 700108, West Bengal, India

ACKNOWLEDGMENTS

ABSTRACT

Thermodynamics is one of the core disciplines of physics, and despite its long history it happens to be a very active area of research till date. With the advent of quantum information, we have perceived that it plays a crucial role to explain the various thermodynamic phenomenon. The paradox of Maxwell's demon was suitably explained with information theory. Even computation theory, whose primary motivation is to optimize the cost of computation has a direct connection with thermodynamics. The major component that a computer needs to run a process is energy, i.e., the thermodynamic cost. It got its foundation in the seminal work of Landauer, where it was commented that the computer spends $k_B T ln2$ amount of energy to erase a bit of information (here T is the temperature of the system and k_B represents the Boltzmann's constant). Thermal machines, which is one of the primary focus of thermodynamics are extensively explored for the last two centuries. It plays a major role in the development of the modern era that started with the invention of the steam engine. With the advancement in technology, we are now able to produce small devices in the nanoscale domain. We have to consider the quantum effect while analyzing the systems in this domain. So, with the advancement of technology, the researchers got interested to analyze thermal machines in the quantum domain, giving rise to the active research area of quantum thermodynamics. In this thesis, we explore the interconnection of quantum information and thermodynamics. Here we look at what kind of thermal devices can be constructed and how quantum behavior will affect them.

In this thesis, we develop the bounds on the uncertainty relation for two incompatible observables for a quantum system. Having this preliminary finding, we proceed to explore the Stirling engine with the information of the uncertainty relation of the quantum system that is considered as the working medium. We are able to provide a tighter lower bound as well as propose an upper bound on the efficiency of the engine with the help of uncertainty relation without performing any measurement. We have obtained the better bounds than the previous ones by optimizing the uncertainty relation over the complete set of bases. It is explored in the non-relativistic as well as in the relativistic regime. We wanted to explore an alternative approach to solve the problem as proposed: whether the change in the space structure can provide a boost to the efficiency and the coefficient of performance of thermal machines? For this purpose, we consider different quantum systems at a deformed space structure which is a generalization of the usual space structure. These quantum systems are considered as

the working medium for the analysis of thermal machines like the Stirling engine and Otto engine. The prime focus has been to explore whether the change in the space structure provides an advantage to the efficiency of the thermal machines over the usual space. We have done numerical analysis for deriving the solution of different equations in our work and have simulated the efficiency as well the coefficient of performance of the different thermodynamic cycles. Along with that, we have discussed a way to analyze thermodynamic cycles in a quantum computer. For the investigation of thermal machines, we need to simulate the fundamental thermodynamic process in a quantum computer. Finally, we have proposed a way to understand the black hole information paradox with the help of the pseudo density operator by simulating the system in the Rigetti quantum computer. Here in this work, we have also provided a Gedanken experiment for the exploration of gravitational waves.

List of Publications/Pre-print

1. **P. Chattopadhyay**, A. Mitra and G. Paul , "Probing Uncertainty Relations in Non-Commutative Space", *International Journal of Theoretical Physics* **58,** 2619–2631 (2019),

    DOI: https://doi.org/10.1007/s10773-019-04150-3,

    arXiv:1712.07748 [quant-ph].

2. **P. Chattopadhyay** and G. Paul, "Relativistic quantum heat engine from uncertainty relation standpoint ", *Scientific Reports* **9,** 16967 (2019),

    DOI: https://doi.org/10.1038/s41598-019-53331-x,

    arXiv:1908.06819 [quant-ph].

3. **P. Chattopadhyay**, "Non-Commutative space: boon or bane for quantum engines and refrigerators", *The European Physical Journal Plus* **135,** 302 (2020),

    DOI: https://doi.org/10.1140/epjp/s13360-020-00318-7,

    arXiv:1911.12766 [quant-ph]

4. A. Mitra, **Pritam Chattopadhyay**, G. Paul, V. Zarikas, "Binary Black Hole Information Loss Paradox & Future Prospects", *Entropy* **22(12)**, 1387 (2020),

    DOI: https://doi.org/10.3390/e22121387,

    arXiv:2004.04695 [gr-qc].

5. **P. Chattopadhyay**, A. Mitra, G. Paul and V Zarikas "Bound on efficiency of heat engine from uncertainty relation viewpoint", *Entropy* **23(4),** 439 (2021),

    DOI: https://doi.org/10.3390/e23040439,

    arXiv:1908.06804 [quant-ph].

6. T. Pandit, **P. Chattopadhyay** and G. Paul, "Non-commutative space engine: a boost to thermodynamic processes", *Modern Physics Letters A* **36(24),** 2150174 (2021),

    DOI: https://doi.org/10.1142/S0217732321501741,

    arXiv:1911.13105 [quant-ph].

7. **P. Chattopadhyay**, T. Pandit, A. Mitra and G. Paul, "Quantum Cycle in Relativistic Non-Commutative Space with Generalized Uncertainty Principle Correction", *Physica A: Statistical Mechanics and its Applications* **584,** 126365 (2021),

    DOI: https://doi.org/10.1016/j.physa.2021.126365,

    arXiv:2010.06672 [quant-ph].

8. **P. Chattopadhyay** and G. Paul, "Revisiting thermodynamics in computation and information theory",

   communicated to: *Reports on Progress in Physics*, submitted on 14 December, 2020, arXiv:2102.09981 [quant-ph].

...

...

CMB	Cosmic Microwave Background
FLRW	Friedmann–Lemaître–Robertson–Walker
PDO	Pseudo Density Operator
GHZ	Greenberger–Horne–Zeilinger
CKW	Coffman-Kundu-Wootters
BBO	β-Barium Borate
PDC	Parametric Down-Conversion
QWP	Quarter-Wave Plate
HWP	Half-Wave Plate
PBS	Polarizing Beam Splitter
MLE	Maximum Likelihood Estimation
LIGO	Laser Interferometer Gravitational-wave Observatory
LISA	Laser Interferometer Space Antenna

Contents

List of Figures

List of Tables

1 Introduction

There is a say that crisis and curiosity have been the foundation of the invention. Aeolipile [1], a device in Roman times was able to produce rotation from a jet of steam. This arose the curiosity and, it was a portent of the things to come. It was Carnot, in the 19th century, who desired to develop a steam engine that would help France to win the Napoleonic Wars that gave birth to thermodynamics [2]. This happens to be an era-defining invention that was adapted to provide power to machinery and has been a backbone for the industrial revolution which foster our modern way of life. Since the advent of the steam engine, there has been an endless quest to ameliorate the performance by using fewer resources. Thermodynamics, without any argument, is the backbone of modern physics which is set as a benchmark for novel physical theories. It not only delineates the functioning of engines, refrigerators, power plants but also has its impact on explaining the basic mechanism of climate change, chemical reactions. Even it is believed that thermodynamics can unravel the properties of black hole [3–5] and provide a physical description to unfold the mystery of our universe.

We encounter a paradigm shift in the 20th century from the macro world (classical) to the micro world (quantum) to unravel the aspects which were not explainable in the classical regime. The counterintuitive aspects in the quantum world are the concept of uncertainty relation, entanglement [6] and correlation [7]. Surprisingly, thermodynamics holds its success and universality even after the advent of quantum mechanics. The story behind the success is due to the fact that the concepts and the principle of thermodynamics were developed irrespective of any references to the microscopic mechanism. The framework is eventually based on general axioms [8–11]. These axioms are conveyed as the laws of thermodynamics. In this era of modern physics, it is an accepted fact that at the microscopic level the physical reality is described by quantum mechanics. So, one needs to accept the fact that the development of thermodynamics principles follows from quantum mechanics.

During the early stage of quantum mechanics, there was an idea of describing the quantum system from a thermodynamic viewpoint [12,13]. Later on, this opened the field of quan-

tum thermodynamics [14–18] which strives to understand how the quantum regime guided the way to develop the classical thermodynamic concepts.

The advent of quantum information and computation theory has shed light on the various aspects of quantum thermodynamics. Information theory, being in its incipient stage has made a decisive contribution to solving an age-old problem of thermodynamics, the extraction of work by Maxwell's demon [19, 20]. The demon is able to extract work from the system which is under study by having the knowledge of the microscopic details of the system, which apparently appears to violate the second law of thermodynamics. It was Leo Szilard who pointed the significance of information in thermodynamics while analyzing Maxwell's demon problem for a single atom engine [21]. In the later phase, Landauer coined the concept of "logical irreversibility" while examining the energy cost of erasing information [22], which conveys that "Information is physical" [23]. Along with that Bennett conveyed in this work [24], the amount of work that is required to erase the memory of the demon after the execution of the process is exactly equivalent to the amount of work gained by the demon. So it was Bennett and Landauer's concept which bridged a connection between thermodynamics and information theory. Even various aspects of statistical mechanics were explored from the information-theoretic viewpoint [25, 26]. Surprisingly information theory has played a crucial role in the formation of the framework of many important physical theories [27, 28] though once considered as an independent theory.

The theory of "Information is physical" conveys that every real-world computational process has some thermodynamic cost which means that, when we perform computation in the real world, some physical changes (entropy production or some heat generation) occur in the world which unfolds the physical consequences of computation processes. This bridges the interconnection between thermodynamics and computation theory. It is generally conveyed that every naturally occurring process like biological computers and even man-made computers has a thermodynamic cost. Translation of RNAs into amino acids is one such natural biological process where one encounters energy cost for the execution of the process. Work in this direction [29], has shown that the thermodynamics cost of this biological process is more efficient than the artificial process.

Out of all such artificial processes, one of the important ones is the existing digital computer system. It can be considered as an engine that dissipates energy for performing mathematical and logical tasks. According to the earlier scientists, they had a notion that there must be some fundamental thermodynamic limit to the efficiency of such engines irrespective of their hardware structure. According to Von-Neumann [30], a computer operated at a

temperature T must dissipate at least $k_B T \, ln(2)$ amount of heat. The thought experiment of Brillouin [31] boils down to the same conclusion as that of Von-Neumann with some error probability. But now, it is a well-known fact that today's computers can perform a large amount of reliable computation per $k_B T$ of energy dissipation. Though reliable computation can be executed per $k_B T$, but today's computer dissipates a vast quantity of energy compared to $k_B T$. Volatile memory devices (such as TTL flip-flops) are the reasons behind this huge waste. The volatile devices dissipate energy even when they are not being used. The macroscopic nature of the existing computers is one of the basic reasons for the inefficiency in the context of energy. Due to its macroscopic nature, the amount of energy required to trigger the system is quantitatively high, and this energy is dissipated instead of reusing it for the next pulse. It is similar to the case of applying brakes to stop a moving car than by saving its kinetic energy. One of the spectacular thermodynamically reversible computation models is the ballistic model, proposed by Fredkin and Toffoli [32]. Other models [33–35] were developed which were more physically realistic than that of Fredkin's version.

Now we provide a table 1.1 to get a clear picture of the contribution that we have made in the field of quantum thermal machines.

Table 1.1. Contribution to the domain of research

	Non-Commutative Space		**Commutative Space**	
Non-relativistic	Without Generalized Uncertainty relation (GUP) **Present work** [40, 41] Chapter 8, 9	With GUP (not yet explored)	Without Uncertainty Relation (UR) Other's work [37–39]	With UR **Present work** [36] Chapter 6
Relativistic	Without GUP (not yet explored)	With GUP **Present work** [42] Chapter 10	Without UR Other's work [44–46]	With UR **Present work** [43] Chapter 7

1.1   Outline of the thesis

The thesis is organized as follows:

- In chapter 2, we give a brief description of field of thermodynamics in the quantum regime. We first explore the developed classical thermodynamics and study quantum thermodynamics by one-to-one correspondence with the classical thermodynamics. The laws of thermodynamics in both the regime are discussed briefly. Along with that we have discussed about the various aspects of thermodynamics that are being explored in this domain. Followed by that we study the design of thermal machine in the nanoscale level with different quantum mechanical mediums. For the analysis we have considered Stirling cycle and Otto cycle with harmonic oscillator and potential well as the working substance. The basic intuition of uncertainty relation are described which are utilized for the analysis of thermal machines. In chapter 3, we have explored the basic aspects of commutation theory and then visualize the connection between thermodynamics and the commutation theory. This is explained through the thermodynamic interpretation of this computation models.

- In chapter 4, we give a brief introduction to the non-commutative space structure which is the deformed space of the usual space or in other words this is the generalized structure of the usual space. Along with that various quantum system (potential problems) are analyzed in this space structure which are used as the working medium for the analysis of thermal cycles. Along with that we have discussed briefly about the black hole information paradox in this chapter.

- In chapter 5, we have explored the uncertainty relation in the non-commutative space. Here we have proposed a upper and lower bound for the uncertainty relation and explored it with a quantum system in this space structure. With the help this intuition we are able to explore thermal machine from uncertainty viewpoint which is explored in chapter 6, and chapter 7. Here we have considered potential well as the quantum system for the working medium of the thermal machine. Stirling cycle with this quantum system is explore in non-relativistic as well as relativistic regime.

- A question whether the change in the space structure can provide any boost to the thermal machines has been explored in chapter 8 to chapter 10. Here, we have considered

thermal machines like Stirling and Otto cycles in the non-commutative space with different quantum systems (like harmonic oscillator, coupled harmonic oscillator, potential well) as the working medium. The concluding statement to this question for the considered thermal machine that are studied is that the change in the space structure provides a boost to the system.

- In the first phase of Chapter 11 we discuss the challenges to simulated a thermodynamic process in a quantum computer, then we go through the alternative ways to simulate some of the thermodynamics processes, which is the backbone for the analysis of thermal machines. We then covey that if we are able to propose how to simulate the thermodynamic process in quantum computers, then we can have an experimental analysis of thermal machines with the different working mediums in a quantum computer. In the second phase of the chapter, we describe the analysis of the black hole information paradox for the binary black hole system with a different formalism. Here, pseudo density operators are considered for the analysis of the process. The proposed method is simulated in a quantum computer to understand the information paradox. Along with that, we have proposed a table-top experiment for the analysis of the gravitational waves with the help of the quantum optical systems of the present technology.

- Finally, we conclude in chapter 12 with a brief description about the results in this thesis along with future directions which are interesting to explore.

The chapters 5, 6, 7, 8, 9, 10 and 11 are based on original and published work by us.

1.2   Computational Tools Used

We have used both classical as well as quantum computational tools for our analysis purpose.

Classical Computing Tool

We have done numerical analysis for deriving the solution of different equations in our work. We have used Mathematica and Python platform for the simulation purpose. Version 3.2 of Python in Jupyter environment and Mathematica 11.2 version were considered for simulating the results.

Quantum Computing Tool

We have used Rigetti quantum computer (https://www.rigetti.com/) for our computing purpose. We have used cloud based rigetti quantum computer.

2 Background on Thermodynamical Aspects of Quantum Systems

Contents

Thermodynamics is equivalent to deific if one considers physical theories to be folks. Thermodynamics got unfolded over three centuries ago. Even since that, it has witnessed many theories to rise and dwindle. And even surviving the revolution of physics like relativity and quantum mechanics. Einstein said that thermodynamics is "the only physical theory of universal content, which I am convinced, that within the framework of applicability of its basic concepts will never be overthrown." Every theory has to visit her for advice and abide by the concepts set by her. So no theories ever dare to contradict the concepts of thermodynamics. Even various aspects of modern physics like black hole entropy [47], gravity [48,49] comes to her for advice. The resilience power of thermodynamics is due to its simplicity. The concepts of thermodynamics happen to be the road map to exploit the said world like developing engines, hard drive formatting, and so on. It never endeavors to explain the mysteries of the universe, nor it peeps into the microscopic details of the prescribed system. It rather tries to perceive the operations which ease the cost of implementation.

Thermodynamics happens to be an operational theory. Such approaches are prominent in computer science, economics, mathematics, and even in quantum information theory. This is the reason why quantum information theory has brought so much in thermodynamics which leads to the foundation of quantum thermodynamics. In this chapter, we will first describe classical thermodynamics in brief and then its transitions to the quantum world.

2.1   Classical Thermodynamics

Classical thermodynamics laws are usually fabricated for the macro regime (i.e., large objects) where the system is at thermal equilibrium. The anecdote of the impact of thermodynamics commences with the innovation of the steam engine. So, the foundation of this theory was from experimental observation, and it leads to the formulation of the fundamental laws of thermodynamics. Out of all the existing physical laws, the thermodynamics laws have the most influence on our daily life. These thermodynamic laws create the framework where the thermodynamics processes are executed. The part of the universe where we will execute our studies is conveyed as the 'system'. While the remaining part of the universe

which lies outside the system is defined as the environment. Though the boundary between the system and the environment is well defined but in the case of a realistic scenario, the concept is not yet clear. The environment is generally conveyed as a reservoir with infinite heat capacity. Now we describe the thermodynamic laws [50–52] which provides the framework to describe the physical quantities of a system like temperature, energy, entropy, and so on. The thermodynamic laws are expressed as:

Zeroth law of thermodynamics:

Let us consider three systems A, B, and C. System A happens to be in thermal equilibrium with the system C, along with that if the system B is in thermal equilibrium with C, then the system A and B with also be in thermal equilibrium with each other. So this conveys the concept of temperature, i.e., the systems in thermal equilibrium will have the same temperature (T) (so it is an intensive variable). In other words, we can also convey that there is no exchange of heat when the systems are in equilibrium.

First law of thermodynamics:

The first law of thermodynamics conveys that the energy of a closed system is constant. The energy of the systems is of two types, one is heat which is uncontrollable and is wasted, whereas the other form is the work which is controllable and useful. Mathematically the change of the internal energy (U) of the system is depicted as:

$$dU = \bar{d}Q + \bar{d}W, \qquad (2.1.1)$$

where $\bar{d}Q$ and $\bar{d}W$ describes the changes in heat and work respectively and $\bar{d}$ is used to depict that it is a non-exact differential [53]. So, heat and work are not state functions. From this law, one can infer that although heat and work represent disparate physical quantities, it belongs to the same form of energy and they transfer to one another to conserve the energy of the system.

Second law of thermodynamics:

This law of thermodynamics is interpreted as one of the important and fundamental laws. It describes the irreversibility of the thermodynamics process. It conveys that in the universe the intensity of the disorder increases continuously, i.e., the system has a propensity to move towards a random state from the ordered one. The second law of thermodynamics conveys that heat will from the hot system to the cold one, not the other way round. The second law of thermodynamics is described in different ways. Carnot developed the condition of maximum extractable work from a heat engine when operated cyclically between two thermal reservoirs. Clausius provided a different formulation for the second law. It states that a spontaneous flow of heat is not possible from a cold to a hot system without any external work. Kelvin proposed his statement where he conveyed that it is physically not possible for any thermodynamic process to solely extract heat and convert it entirely into work from a reservoir.

It can also be described as a function of entropy. The concept of entropy was coined by Clausius, which measures the intensity of disorder that persists in the system. Mathematically it is described as:

$$dS = \frac{\bar{d}Q}{T}, \tag{2.1.2}$$

where dS is change in the entropy (d depicts the exact differential), $\bar{d}Q$ describes the amount of heat transfer in a reversible process. This statement of the second law conveys that the entropy of the system will either remain constant or increase with respect to time.

Third law of thermodynamics:

This thermodynamic law [54] provides the framework for the concept of absolute zero temperature. The system at this temperature will possess a minimum amount of energy, and so the available microstate at this point is only one. We know that the entropy of the system has a direct connection with the number of microstate for the system. Now for this system, the entropy $S \rightarrow 0$ as the system moves towards absolute zero temperature. Another form of this law which is popularly known as the Nernst theorem [55] conveys that it is physically impossible for a system to reach absolute zero temperature within a finite time.

2.2 Classical Thermal Machine

The laws of thermodynamics provide the required framework for the operation of thermal machines. A heat engine will transfer heat into work whereas, in the case of a refrigerator it will convert work into heat. Two thermal baths, a working medium, and a proper thermodynamic cycle are the basic ingredient to construct a heat engine. Out of which one of the thermal baths acts as a source (hot bath) of heat and the other bath is a sink (cold bath) of heat. Heat engines involve different cycles of operations. The working substance has a crucial role in the working process of a heat engine. The working medium helps in transfer of heat between the thermal baths during the operation of the thermodynamic cycle. One can define the efficiency of a heat engine as the ability engine to convert heat into work, mathematically we can define it as the ratio of "work-output" to "heat input". The pictorial representation of a heat engine and refrigerator is shown in Fig. 2.1. From Fig. 2.1, we can infer that the engine assimilates $Q_H > 0$ quantity of heat from the hot reservoir at T_H temperature to carry out a certain amount of work $W > 0$ and finally ejecting $Q_C < 0$ amount of heat to the sink reservoir (cold reservoir) at T_C temperature. The efficiency of the engine is mathematically expressed as:

$$\eta = \frac{W}{Q_H} = \frac{Q_H - |Q_C|}{Q_H}. \tag{2.2.1}$$

2.2.1 Classical Carnot Cycle

An ideal engine will convert heat into work with 100% efficiency. The pictorial representation of the Carnot cycle is shown in Fig. 2.2. It is a four-stroke engine. It was Carnot who showed that for all reversible thermodynamic cycles the maximum attainable efficiency by the engine is defined as:

$$\eta = 1 - \frac{T_C}{T_H}. \tag{2.2.2}$$

This form of efficiency is coined as Carnot efficiency, and it provides a bound on the efficiency of the engines. From Eq. (2.2.2), we can infer that the maximum efficiency is a function of the temperature, i.e., it has no dependency on the working substance as well as on the characteristics of the cycle.

(a)   (b)
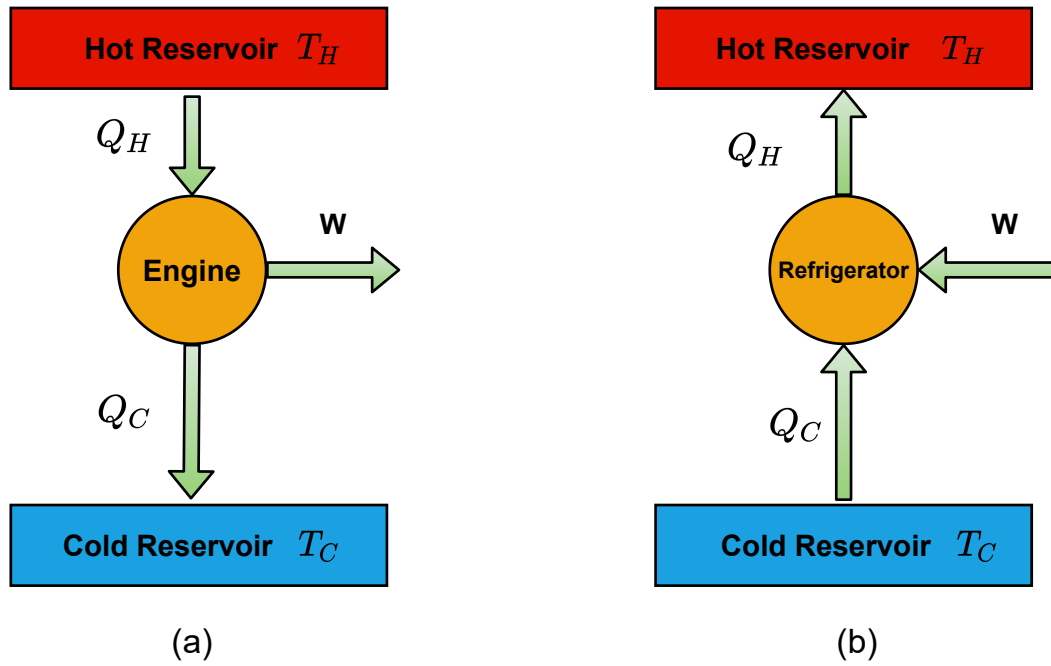
Figure 2.1. Schematic representation of a (a) heat engine and (b) refrigerator respectively.
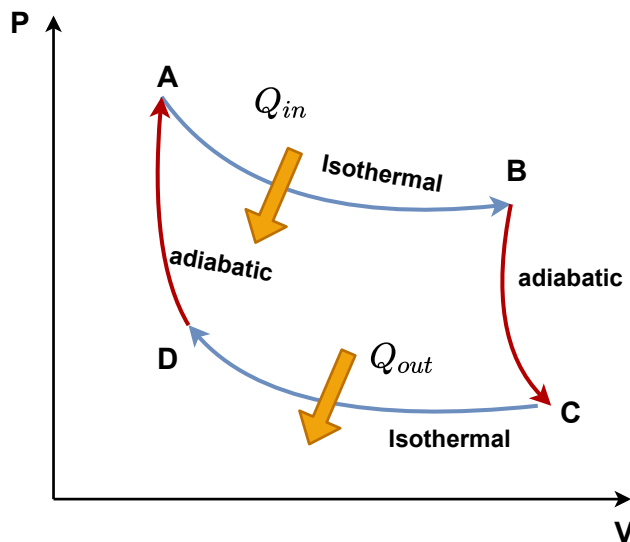
Figure 2.2. Schematic representation of the pressure vs. volume (P-V) diagram of a classical Carnot engine.

A refrigerator as depicted in Fig. 2.1 was a working principle that is just the reverse of a thermal engine. In this case, the working medium gallops heat from the cold reservoir at T_C temperature under the influence of a certain amount of external work W and ejects the energy to the hot reservoir at T_H temperature. The coefficient of performance (COP) of this model, that is coined as Carnot COP, sets an upper limit for the refrigerator as:

$$COP = \frac{T_C}{T_H - T_C}. \tag{2.2.3}$$

Now we will briefly discuss two of such engine models that have been analyzed in the quantum realm.

2.2.2 Classical Otto Cycle

In this modern era of technology, one of the most important engines is the Otto cycle. It was named after Nikolas A. Otto [56] who first proposed a successful four-stroke model of the internal combustion engine in 1876 with the guidance of the cycle that was proposed by Frenchman Alphonse Beau de Rochas in the year 1862. The Otto cycle is appropriate for the spark-ignition reciprocating engines where the piston-cylinder commences the combustion process of the fuel mixture. Otto engine is comprised of two isochoric and two adiabatic strokes, where stokes describe the movement of the piston. Otto engine has a wide range of applications in automobiles. The efficiency of this model of engine is bounded by the Carnot efficiency, and the engine efficiency is lower than that of the Carnot engine. The working substance for this engine model is the classical ideal gas, and the four strokes of the cycle are characterized by the volume (V) and the temperature (T) of the working substance. The classical Otto engine is pictorially represented by the P-V diagram in Fig. 2.3.

Now we will describe each stroke of the engine.

1st *Stroke* [Isochoric process (Hot), A (V_H, T_C') $\rightarrow$ B (V_H, T_H)] : This stroke is also popularly known as Ignition stroke. Here volume V_H and temperature T_C' describes the initial state A of the engine. In this phase of the cycle, the working system is attached with the hot reservoir at a constant volume having temperature T_H. The system remains in this phase until it attains equilibrium with the reservoir. So, during this stroke of the cycle, the working system will absorb heat from the hot bath which is depicted as Q_H in the Fiq.2.3,
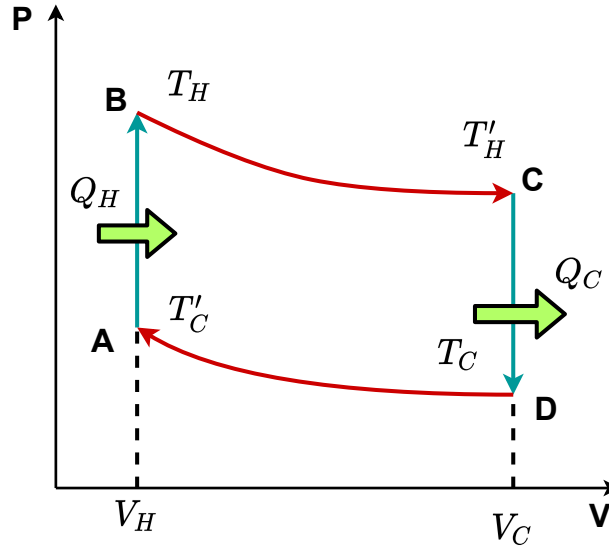
Figure 2.3. Schematic representation of the pressure vs. volume (P-V) diagram of a classical Otto engine.

and no work is executed in this process. The amount of heat absorbed can be expressed as $Q_H = mC_V(T_H - T'_C)$, where m and C_V represent the mass of the gas particles and the specific heat capacity for constant volume respectively. In the realistic scenario, we can compare this stage to the rapid combustion of the fuel mixture.

2nd *Stroke* [Isentropic process (expansion), $B\ (V_H, T_H) \rightarrow C\ (V_C, T'_H)$] : This stroke is popularly known as Expansion stroke. While this phase of the cycle is processed, the system will undergo an adiabatic expansion. The system encounters a volume change from V_H to V_C. There is no heat exchange with the reservoir, but we encounter that some of the work is done in this phase of the cycle due to which there is a drop in the temperature from T_H to T'_H. In the realistic scenario, we can compare this stage with the power stroke of the spark-ignition engine.

3rd *Stroke* [Isochoric process (Cold), $C\ (V_C, T'_H) \rightarrow D\ (V_C, T_C)$] : This stroke is popularly known as Exhaust stroke. While this phase of the cycle is processed, the system is connected to the cold reservoir at a constant volume having temperature T_C. The system is cooled in this process, and it ejects Q_C amount of heat to the cold reservoir. Similar to the 1st stroke, no work is performed in this phase of the cycle. The amount of heat rejected by the system can be expressed as $Q_H = mC_V(T_C - T'_H)$.

4th *Stroke* [Isentropic process (compression), $D\ (V_C, T_C) \rightarrow A\ (V_H, T'_C)$] : This stroke is popularly known as Compression stroke. While this phase of the cycle is processed, the system will undergo adiabatic compression. During this final phase of the cyclic process, the system encounters a volume change from V_C to its initial volume V_H. There is no heat

exchange with the reservoir, but we encounter that some of the work is done in this phase of the cycle due to which there is a rise in the temperature from T_C to T_C'. The system is reconnected to the hot reservoir to complete the cycle.

From the energy conservation law (the first of thermodynamic), the total work done by the system can be evaluated as:

$$W = Q_H + Q_C = mC_V \left(T_H + T_C - T_H' - T_C' \right). \tag{2.2.4}$$

So, the efficiency of the engine can be evaluated as:

$$\eta = \frac{W}{Q_H} = 1 - \left(\frac{V_H}{V_C} \right)^{\gamma - 1}, \tag{2.2.5}$$

where $\gamma = \frac{C_P}{C_V}$ is the specific heat ratio, and C_P is the specific heat capacity at constant pressure. From Eq. (2.2.5) we can infer that the Otto cycle efficiency has a dependence on the compression ratio of the engine and the specific heat ratio of the working substance.

2.2.3   Classical Stirling Cycle

The Stirling cycle proposed by Robert Stirling in 1816 is a relatively old power cycle. It was conceived as a replacement to the steam engines as the efficiency of the was high and along with that has the ability to use any heat source. Similar to the Otto cycle, the Stirling cycle is also a four-stroke thermal machine. Stirling engine is comprised of two isochoric and two isothermal strokes. Similar to the Otto engine, the Stirling cycle has a wide range of applications in automobile technology. The efficiency of the engine efficiency is equivalent to that of the Carnot engine. The working substance for this engine model is the classical ideal gas, and the four strokes of the cycle are characterized by the volume (V) and the temperature (T) of the working substance. The classical Stirling engine is pictorially represented by the P-V diagram in Fig. 2.4.

Now we will go through each stroke of the engine briefly.

1st *Stroke* [Isothermal process (expansion), $A \rightarrow B$] : This is the expansion stroke of the cycle. While this phase of the cycle is processed, we encounter heat addition to the system takes place externally. As the working substance gets heated, it expands simultaneously
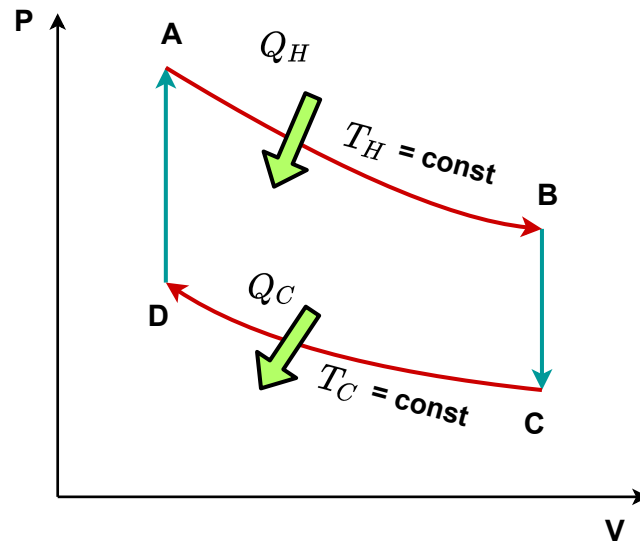
Figure 2.4. Schematic representation of the pressure vs. volume (P-V) diagram of a classical Stirling engine.

keeping the temperature of the process constant (T_H). The system encounters a volume change and a drop in pressure during this stroke of the cycle.

2nd *Stroke* [Isochoric process (Cold), $B \rightarrow C$] : This process is also known as heat removal process. While this phase of the cycle is processed, the system is connected to the cold reservoir at a constant volume having temperature T_C. So the system encounters a decrease in the temperature and pressure during this phase of the cycle.

3rd *Stroke* [Isothermal process (compression), $C \rightarrow D$] : This stroke is also known as compression stroke. In the third part of the cyclic process, heat is ejected by the system. As the system gets cooled down, it gets compressed. So we encounter a decrease in the volume and pressure at constant temperature T_C during the process.

4th *Stroke* [Isochoric process (hot), $D \rightarrow A$] : This is the last phase of the cycle. This process is also known as the heat addition process. In this final phase of the cyclic process, the system is reconnected to the hot reservoir at a constant volume. So the system encounters an increase in the temperature and pressure during this phase of the cycle. The system is reverted back to its initial state in this phase of the cycle.

The efficiency of the cycle is given by the Carnot efficiency.

2.3 Quantum Thermodynamics

In the 19th century, there was a quest for the development of more efficient steam engines. The framework of various practical applications was a remarkable contribution from the

phenomenological thermodynamic laws and various experimental concepts. In the latter half of the 19th century, atomic theory [57] took the ground and it was statistical mechanics who came to the rescue to explain the thermodynamic behavior of the macro world in terms of its constituent atoms [58, 59]. With the advancement of technology, the capability for the experimental analysis got enhanced, and it was possible to probe microscopic level systems that are predominantly controlled by quantum mechanics. So now, a considerable effort is dedicated to extending thermodynamics to the micro realm theoretically as well as with experimental concepts. Extending thermodynamics to the quantum realm, it was generally anticipated that new concepts will get surfaced. But one encountered a similarity of the quantum version with the classical one. The Carnot efficiency limit applies to the quantum realm [14, 60, 61] when the reservoirs are thermal. One also encountered the similarity in the fluctuation theorem [62–64] in both the regimes.

So the field quantum thermodynamics studies thermodynamic properties like temperature, heat, work in the micro realm which includes analysis on thermal machines in microscopic level [15, 65–74], thermalization [75–77], algorithmic cooling [78–82], single shot [83, 84] and so on. The deep connection between quantum information theory and thermodynamics is analyzed in the works [84, 85]. Along with that, the thermodynamic laws for the quantum realm gained importance. The details of these laws in the quantum world are thoroughly analyzed in the works [86–89]. One of the primary focuses of this domain is the analysis of the subtle relationship between the standard and the non-equilibrium thermodynamics. Now we will briefly discuss some of the major research domains of quantum thermodynamics. For the details regarding this domain, one can go through the review articles [27, 28].

Thermodynamic resource theory: Recently, the resource theoretic approach to quantum thermodynamics [90–92] has gained importance. The generic approach to deal with valuable resources like purity, entanglement is provided by resource theory. The primary focus of this theory is to find out the class of operations which can or cannot be executed on a quantum state. These constrained operations define a set of state which a given initial state can reach. In this framework, thermal operations are the set of allowed operations on the quantum system, which keep the total energy of the system constant as well as its thermal environment. The non-equilibrium states are the valuable resource states. The defined allowed operations should be consistent with the thermodynamic laws, and it is restricted that, one cannot extract work from a single thermal reservoir by applying these operations. This resource theoretic approach provides an innovative way, one can utilize to evaluate the amount of work that one

can extract from the quantum system having coherence or correlation, or the amount of work that is required to create quantum correlation or coherence. Resource theory of quantum thermodynamics has a profound effect on the analysis of the quantum thermal machine as well as on the efficiency of thermodynamic processes. Quantum information theory plays a crucial role (it is omnipresent) in the resource theory of quantum thermodynamics. Along with that, the resource theory of entanglement and coherence make a significant contribution in the framework of the resource theory of quantum thermodynamics due to its structural similarities.

Equilibration and thermalisation: It is an age-old matter where effort is given to the formulation of statistical mechanics from the evolution of an isolated quantum system. According to thermodynamics, the entropy of the system is ever-increasing, whereas from the concept of quantum mechanics we know that a system evolves unitarily, and so it preserves its purity. So, one might come to the conclusion that thermodynamic and quantum theory are incompatible. This apparent paradox can be bypassed by utilizing the concept of entanglement which was coined as "the spooky action at a distance" at the earlier stage. It was observed that when the system gets entangled with the rest of the universe, the entropy of the respective system increases. Through rigorous analysis, it has been conveyed that equilibration and thermalization are intrinsic to quantum mechanics [61]. Various works have shown that the cause of equal a prior probability is due to the consequence of Hilbert space. This domain is an active field of research.

Quantum fluctuation relations: The seminal works by Jarzynsi [93,94] and Crooks [95, 96] developed the relationship between the free energy and the work that is being executed or extracted during the transformation among the physical states. Now researchers are investigating the quantum version of Jarzynski and Crook relations. From the investigation, researchers were able to infer that these relations remain invariant under unitary quantum dynamics [97,98]. It also hold for open quantum dynamics [99,100]. In the seminal work [98], they conveyed that work is not an observable. So, it is a necessary task to develop the fluctuating quantum work as a two-point correlation function for closed dynamics to distinguish the jarzynski relation. So this conveys that we have to perform projective measurement both at the beginning as well as at the end of the process on an instantaneous eigenbasis of the evolving system. This provides the required information about the change in the energy that occurs during the evolution of the system, and so it provides the pathway for the develop-

ment of the work distribution function. Some experimental verification in this direction has also been analyzed, where a single trapped ion system is considered for the analysis of non-equilibrium work distribution [101] and for quantum Jarzynski equality [102, 103]. Along with all these approaches, a new measurement scheme is proposed based on the concept of an interferometric scheme of phase estimation for quantum systems [104]. In this work, they have shown that one can reconstruct the work distribution using this interferometric scheme [28] (by virtue of ancilla) rather than executing two projective measurements. In this scheme, the ancilla will interact with the system at the start and end of the process, so the state of the system obtains a phase from this interaction. This phase has a connection with the energy difference of the system, and one has to measure this ancilla to get the estimation of the energy difference of the system. This has been implemented experimentally in a nuclear magnetic resonance (NMR) [105]. Along with that positive operator valued measures (POVM) are also used for the study of quantum fluctuation relation and this has been analyzed experimentally using ultracold atoms [106].

Single shot thermodynamics: This is the domain of quantum thermodynamics which tries to find the application of statistical mechanics to the strongly correlated quantum systems which is plunged in the hot bath [83, 107, 108]. Equivalent to entanglement theory, the single-shot thermodynamics is also based on the concept of agents, i.e., a limited set of operations are allowed in this process. In other words, we can express this as the prohibition of multi-tasking, like extraction of work or handling the characteristics of coherence.

Quantum heat machines (QHMs) are another broad area of research in the field of quantum thermodynamics. The focus of this thesis is based on QHMs and will be described in detail.

2.3.1   Heat, Work and Entropy

Equipped with the knowledge of classical thermodynamics and its further development we are all set to analyze heat and work for the quantum systems. Following the analogy of the classical world, that all system is accompanied by energy which in the quantum regime is described by the Hamiltonian of the system. Now, when one wants to measure the internal energy of the system, it operates the observable to the state of the system which then collapses to one of the eigenstates. The corresponding eigenvalue for this eigenstate provides the output of the internal energy of the system [28]. In quantum mechanics, the measure-

ment has probabilistic nature. So the internal energy U can take values E_i with probability p_I where $i = 1, 2, \ldots, n$ denotes the dimension of the states space [61]. From now on, whenever we talk about the internal energy of the system we would simply mean the average internal energy of the system. The internal energy is mathematically described as:

$$U = \langle H \rangle = tr[\rho H] = \sum_i p_i E_i, \tag{2.3.1}$$

where H represents the Hamiltonian of the system, ρ is the state of the system. The energy changes in the system can be described in two forms:

- Heat (Q): Heat is described as the flow of energy among the system and the environment when the system is attached to the environment.

- Work (W): Work is described as the change in energy of the system caused due to external forces when acted on the system.

Now, the entropy of a system provides a measure of the uncertainty about the knowledge of a system. If we consider a pure singlet state, then we have all the information of this state. The entropy of such a state is zero. Now, if we consider a mixed state, then one cannot say with certainty which is the exact state of the system, but one can convey about the state with some probability. These states have some entropy. The lack of information in the quantum realm is measured using Von Neumann entropy:

$$S(\rho) = -tr[\rho \, ln\rho] = -\sum_i \lambda_i ln \lambda_i, \tag{2.3.2}$$

where λ_i is the eigenvalues of the state ρ. Now, from the 2nd law of thermodynamics, we know that for any heat flow there is an equivalent entropy flow in the system and is depicted as:

$$\Delta S = \sum_i \frac{\Delta Q_i}{T_i}. \tag{2.3.3}$$

From Eq. (2.3.2) and (2.3.3), we can analyze that the entropy of the system is a function of states, i.e., when the population of the system changes one will encounter a change in the entropy of the system, whereas no change is observed with the change of eigenvalues.

2.3.2   Thermodynamic laws in Quantum Regime

Here in this section, we are going to study the thermodynamic laws for quantum systems. One should be aware and keep in mind that the laws should approach their classical definitions within certain limits.

Zeroth law of thermodynamics:

As conveyed earlier in this chapter, the zeroth law of thermodynamics in the classical domain describes that thermal equilibrium is equivalent to an equality relationship between the states of the systems where the only parameter is the temperature which classifies the different equivalence classes. Whereas in the micro-world, the case is different due to the presence of quantum features. Quantum features like entanglement, quantum correlations dispense new insight to this regime which we have never encounter in the classical world. For any thermodynamic process, it is generally assumed that the system and the bath are uncorrelated, but there is a high probability that the system gets correlated during the process. If one considers the system to be correlated with the bath, then we will encounter the violation of zeroth law. So to encounter this problem, we have to reinterpret the concept of equilibrium. In the work [109], they have coined the general zeroth law of thermodynamics which conveys that we can infer mutual thermal equilibrium for a set of states only when no work is extractable from any combination of these states under the entropy-preserving operation. To satisfy this condition, each of the states should be a thermal state with the same temperature. For example, let us consider three systems where the states are defined as $\rho_C \otimes \rho_{AB}$, where these states are marginal thermal states. Now, if A happens to be in thermal equilibrium with B and B with C then all the systems have the same temperature. But if we consider that any two of the system are correlated say A and B, then this state are not in thermal equilibrium with each other.

First law of thermodynamics:

The model to analyze the internal energy of a system has been thoroughly explored in the work [110]. We will consider this model for the analysis of the first law of thermodynamics,

and a general system having a finite count of energy levels is considered as the working medium. So the Hamiltonian can be expressed as:

$$H = E_n|E_n\rangle\langle E_n|, \qquad (2.3.4)$$

where E_n is the eigen-energy and $|E_n\rangle$ describes the nth eigenstate. The internal energy of the system is defined as:

$$U = \sum_n P_n E_n, \qquad (2.3.5)$$

where P_n is the occupation probability of nth eigenstate. So the infinitesimal change in the internal energy fromEq. (2.3.4) can be expressed as:

$$dU = \sum_n (E_n dP_n + P_n dE_n). \qquad (2.3.6)$$

So comparing with the definition of first law (as described in classical regime), we can equate

$$\begin{aligned} dQ &= \sum_n E_n dP_n \\ dW &= \sum_n P_n dE_n, \end{aligned} \qquad (2.3.7)$$

in the quantum domain. Here dQ, dW describes the infinitesimal heat change and infinitesimal work done respectively. Interestingly, the definition of dQ (as defined in Eq. 2.3.7) is valid even if the working medium is not in thermal equilibrium, unlike the classical regime where $dQ = TdS$ (T, S defines the temperature and the entropy of the system) is applicable only when the system is in thermal equilibrium.

We can describe these quantities in another way. Let us consider a quantum state which is described by the density operator ρ, and the system Hamiltonian by H. The internal energy can be described as the expectation value of the Hamiltonian as:

$$U = \langle H \rangle = tr(\rho H). \qquad (2.3.8)$$

The rate of change of internal energy can be evaluated as:

$$\frac{dU}{dt} = tr(\dot{\rho}H) + tr(\rho\dot{H}). \qquad (2.3.9)$$

Now for a closed system evolution the dynamics is controlled by the Hamiltonian of the

system, so $tr(\dot{\rho}H) = 0$. So no entropy is generated in this process as the system is isolated and it follows the unitary evolution. So the remaining term in Eq. (2.3.9) describes the energy flow in the system.

Now, if we consider the system to be weakly interlinked with the bath and the Hamiltonian to be time-independent, then we can convey that the energy flow is due to the fact that there is a heat exchange between the system and the reservoir. As a consequence of this, the first term of Eq. (2.3.9) exists, and the second term equates to zero. The first term describes the heat current in the system. So this provides the alternative formalism to describe the first law of thermodynamics in the quantum domain.

Second law of thermodynamics:

The second law of thermodynamics plays a vital role in a wide scale of application. This law, when analyzed in the micro domain, produces fascinating outcomes. A different version of the second laws of thermodynamics are developed based on application and are discussed below.

Let us consider two density matrices ρ and σ which depicts two different states for a k-dimensional system. Let λ_j^{ρ} and λ_j^{σ} (where $j = 1, 2, \ldots, k$) is used to denote the eigenvalues of the states. We can convey that σ majorizes ρ [90, 111] if for all $m = 1, 2, \ldots, k$

$$\sum_{j=1}^{l} \lambda_j^{\downarrow\sigma} \geq \sum_{j=1}^{l} \lambda_j^{\downarrow\rho}, \quad \sum_{j=1}^{l} \lambda_j^{\sigma} = \sum_{j=1}^{l} \lambda_j^{\rho}, \tag{2.3.10}$$

where $\lambda_j^{\downarrow\sigma}$ and $\lambda_j^{\downarrow\rho}$ are developed by rearranging the eigenvalues in the decreasing order $\lambda_1^{\downarrow\sigma} \geq \lambda_2^{\downarrow\sigma} \geq \ldots \lambda_j^{\downarrow\sigma}$ and $\lambda_1^{\downarrow\rho} \geq \lambda_2^{\downarrow\rho} \geq \ldots \lambda_j^{\downarrow\rho}$. So we can infer from this $\sigma > \rho$. So the Shannon entropy of the density states should follow the relation $S(\rho) \geq S(\sigma)$. If the system additionally follows the condition as mentioned in Eq. (2.3.10) we can describe ρ as:

$$\rho = P_l U \sigma U^{\dagger} P_l, \tag{2.3.11}$$

where P_l described the projective operator for a certain eigenbasis and U is a unitary operator. From Eq. (2.3.11) we can infer that by operating a projective operation followed by the unitary evolution of the system, we can make a transition from a low entropic state to a higher one. So it confirms that there is no way to reach a lower entropic state by a unitary

process (like adiabatic process).

The second law, as conveyed earlier in this chapter (classical regime), states that the entropy of the closed system will either remain the same or increase with time. In the seminal work [112], they have shown if the system and the environment are not correlated, then the entropy change of the total system is always positive. Using this concept we can define the initial state (ρ_{total}^{in}) of the total system as a tensor product of the initial state of the system (ρ_{sys}^{in}) and that of the environment (ρ_{env}^{in}) as $\rho_{total}^{in} = \rho_{sys}^{in} \otimes \rho_{env}^{in}$. Now if we perform a global unitary operation to the total system, the unitary evolution of the total system can be expressed as $\rho_{total}^{fin} = U^{\dagger} \rho_{total}^{in} U$. So the change in the entropy can be expressed as:

$$
\begin{aligned}
\Delta S_{total} &= \Delta S_{sys} + \Delta S_{env} = \left(S(\rho_{sys}^{fin}) - S(\rho_{sys}^{in}) \right) + \left(S(\rho_{env}^{fin}) - S(\rho_{env}^{in}) \right) \\
&= \left(S(\rho_{sys}^{fin}) + S(\rho_{env}^{fin}) \right) - \left(S(\rho_{sys}^{in}) + S(\rho_{env}^{in}) \right),
\end{aligned} \tag{2.3.12}
$$

where ρ_{sys}^{fin} and ρ_{env}^{fin} describes the final state of the system and the environment respectively. The basic assumption that is considered in the analysis is that there is no correlation between the system and the environment. So we can express the second term of the Eq. (2.3.12) as $\left(S(\rho_{sys}^{in}) + S(\rho_{env}^{in}) \right) = S(\rho_{total}^{in})$. We know that Von-Neumann entropy is invariant under any unitary transformation so we can infer from this concept that $S(\rho_{total}^{in}) = S(\rho_{total}^{fin})$. So the total change in the entropy can be expressed as:

$$
\Delta S_{total} = \left(S(\rho_{sys}^{fin}) + S(\rho_{env}^{fin}) \right) - S\left(\rho_{total}^{fin} \right) = S\left(\rho_{total}^{fin} \| \rho_{sys}^{fin} \otimes \rho_{eve}^{fin} \right) \geq 0. \tag{2.3.13}
$$

We have also considered the fact that the relative entropy of the system is a non-negative quantity.

Third law of thermodynamics:

The third law of thermodynamics state that the entropy of the system is zero at absolute zero temperature provided that the system is having non-degenerate ground states at equilibrium [113]. The quantum version of this law [114] is an exciting area of research. This has gained importance in the context of thermodynamics [115–117] as cooling a system up to an absolute zero temperature has been executed [118], where one encounters that the quantum

fluctuation has a dominance over the thermal fluctuations.

2.4   Quantum Thermal Machine

The center stage of the field of thermodynamics was the development of thermal cycles. In a thermodynamic cycle, the system has to execute a series of strokes (stroke is a time span where one operation is executed like thermalization or extraction) which ultimately affects the internal energy of the system, and finally, the system returns to its original state, i.e., $\rho_{in} = \rho_f$ after the cycle is complete. Generally, there exist three types of engines with two thermal reservoirs. They are four-stroke, two-stroke, and continuous engines. There is various type of strokes a system can undergo [110]. Generally, two-stroke adjacent to each other does not commute, if such a relationship exists among them then they can be combined into a single stroke by just applying the operations simultaneously. Some of the notable strokes are:

- Isothermal process: During this process, there is an exchange of heat with the environment. The process is executed slowly enough so that the state of the system is a thermal state even after evolution. Work is done to change the energy levels so that thermalization is ensured.

- Adiabatic process: During this process, the system performs work by altering its Hamiltonian of the system. In this process, the system is detached from the environment. The process is executed slowly so that it can be adapted by the system, and the population of the system remains unchanged [119, 120].

- Isochoric process: During this process, the system interacts with the environment and exchanges heat without performing any work.

The thermodynamic cycle can be used repeatedly with a single system as the initial and the final state of the system happens to be the same. Two of the most common thermal machines are the thermal engine and the refrigerator. A thermal engine is a cyclic process that produces work when there is a heat flow from the hot reservoir to the cold one. The refrigerator is a cyclic process that is able to move work from a cold reservoir to the hot one. The measure of performance of a thermal engine is described by efficiency η. Efficiency is defined as the ratio of work produced by the system with the heat absorbed from the hot bath.

$$\eta = \frac{|W|}{Q_{input}} = \frac{Q_{out} + Q_{input}}{Q_{input}}. \tag{2.4.1}$$

The measure of performance for a refrigerator is described by the coefficient of performance. It is defined as the ratio of cooling with the work needed for that.

$$COP = \frac{Q}{|W|}. \tag{2.4.2}$$

Various thermodynamic cycles have been analyzed [110, 121–125]. Here, we are going to study about two such cycles, the Stirling cycle, and the Otto cycle.

2.4.1   Quantum Carnot Cycle

Carnot introduced the Carnot cycle which happens to be the efficient cycle and it gives an upper bound to the performance of the engines. It is a four-stroke engine. The strokes of the engine are described as follows:

- The first stroke of the engine is the isothermal process. During the execution of this phase of the cycle, the system is attached to the hot bath at T_h temperature.

- The second stroke of the engine is the adiabatic process. During the execution of this phase of the cycle, the system is disconnected from the hot bath, and the system Hamiltonian is changed ($H \rightarrow H_0$) during this phase of the cycle.

- The third stroke of the engine is the isothermal process. During this phase, the system is connected to the cold reservoir at T_c temperature.

- The fourth stroke of the engine is the adiabatic process. During the execution of the final phase of the cycle, the system is disconnected from the cold bath, and the Hamiltonian of the system is changed from H_0 to H.

The efficiency of the cycle is independent of the system parameters but depends only on the temperature of the reservoirs $\eta = 1 - \frac{T_c}{T_h}$. This is called the Carnot bound as it provides optimal efficiency. This is a reversible cycle, so there is no entropy production in this process. If one reverses the cyclic process, the working machines turn the thermal engine into a refrigerator. The measure of performance of the refrigerator, i.e., COP is solely function of temperature of the reservoirs, $COP = \frac{T_c}{T_h + T_c}$. Finite-time isothermal cycles has

been analyzed [126], and different working mediums for Carnot cycles are proposed and explored [66, 127–133]. With the utilization of non-equilibrium baths some engines are able to surpass the Carnot bound [134].

2.4.2   Quantum Otto Cycle

The Otto cycle is a combustion cycle. It is also a four-stroke cycle and the process is as follows:

- The first stage of the cycle is the adiabatic compression process. During the execution of this phase of the cycle, the change in the Hamiltonian ($H \rightarrow H_0$) of the system occurs.

- The second stage of the cycle is the isochoric heating stroke. During the execution of this phase of the cycle, the system is attached to the hot reservoir at T_h temperature.

- The third phase of the cycle is the adiabatic expansion process. During the execution of this phase of the cycle, the change in the Hamiltonian ($H_0 \rightarrow H$) of the system occurs.

- The fourth stage of the cycle is the isochoric cooling stroke. During this final part of the cyclic process, the system is attached to the cold bath at T_c temperature, where $T_c < T_h$.

Based on the order of the strokes one can develop an Otto engine or Otto refrigerator. The efficiency of the cycle is a function of the parameters that change during the adiabatic compression and the adiabatic expansion strokes. The ease to implement the isochoric process over the isothermal process has made the Otto cycle a popular one for analysis [135–145].

2.4.3   Quantum Stirling Cycle

Stirling cycle [146, 147] is also a four-stroke engine. Here we will analyze the four strokes of these cycles.

- The first stroke of the engine is the isothermal process. During this part of the cyclic process, the system is attached to the hot reservoir at T_h temperature. Change in the in Hamiltonian takes place in this phase.

- The second stroke of the engine is the isochoric process. During this part of the cyclic process, the system will execute an isochoric heat exchange. The system is attached to a reservoir with T_c temperature, so the heat gets released during this process.

- The third stroke of the engine is the isothermal process. During this phase, the system remains connected to the cold reservoir at T_c temperature.

- And in the final part of the cyclic process, the system is reverted back to the hot reservoir with T_h temperature.

The efficiency of this cycle is bounded by the Carnot efficiency. If one reverses the whole cyclic process, one can turn this thermal process into a refrigerator process. This cycle is also a reversible process.

2.5   Quantum Thermodynamic Processes

From classical thermodynamic, we are aware that there are four primary processes: isothermal process, adiabatic process, isobaric process, and isochoric process. Here, isothermal process describes the evolution of the system with constant temperature, whereas for the adiabatic process there is no heat exchange. Isobaric and isochoric process describes the evolution with constant pressure and volume respectively. With these four basic processes, one can develop various types of thermodynamic cycles like the Carnot cycle, the Otto cycle, the Stirling cycle, the Brayton cycle, and so on. One of the prime objectives in the analysis of quantum thermodynamics [17, 75, 148] is to extend the classical version in the quantum regime. In this section, we will describe the quantum analogy of these four fundamental processes in the thermodynamic process [121].

2.5.1   Quantum Isothermal process

In an isothermal process, the temperature of the system will remain the same. This process is executed by connecting the system with an external thermal bath which helps the system to maintain a constant temperature as that of the bath through heat exchange with the reservoir. Similarly, in the quantum regime [110], the working medium is kept in contact with the thermal bath at a constant temperature. The system can execute external work by absorbing heat from the reservoir if the occupation probability of the system and its energy gaps change simultaneously. This keeps the temperature of the system fixed at a particular temperature

alike the classical one. For example, a two-level system is considered for analysis. The state $|-\rangle$ and $|+\rangle$ describes the ground and the excited state respectively. The occupation probability and the eigenenergy for the ground state are P_- and E_- and that of the excited state is P_+ and E_+. To execute a quasistatic isothermal process the condition $(E_+(t) - E_-(t))$ needs to be satisfied, which conveys that the level spacing should change slowly with respect to the time t. So the ratio of occupation probabilities will follow the Boltzmann distribution.

$$\frac{P_+}{P_-} = e^{\frac{E_+(t) - E_-(t)}{k_B T}}, \tag{2.5.1}$$

where T describe the temperature of the reservoir.

2.5.2 Quantum Adiabatic process

In the classical regime of thermodynamics, the process where there is no heat exchange with the environment by the system is defined as an adiabatic process. The first law conveys that all the changes in the internal energy are due to the work done throughout the process. In the quantum regime, the process should be executed quasistatically so that it satisfies the generic adiabatic condition. So the evolution of the system parameter is quasistatic in nature.

We consider a system with eigenstate $|n(0)\rangle$ for the initial Hamiltonian at time $t = 0$. While we execute the process, the system will be in the n-th eigenstate $|n(t)\rangle$ for the instantaneous Hamiltonian of the system to satiate the quantum adiabatic theorem. So the occupation probability of the eigenstate $|n(t)\rangle$ is adiabatically invariant, i.e., work is done without any exchange of heat. This condition is totally a quantum phenomenon. This condition is not a mandatory condition in the classical regime. For example, if we execute the process fast then the quantum adiabatic process will not be satisfied due to the presence of the internal excitation in the system but without any heat exchange which is the required criteria to satisfy the classical adiabatic condition. So, one can infer that the classicala counterpart of the adiabatic process is more general than that of the quantum one.

In the analysis of quantum heat engines, the quantum adiabatic theorem is indispensable. Due to this fact, we will study this briefly. For detailed analysis, one can look into [149]. Let us consider a time-dependent Hamiltonian $(H(t))$. Hamiltonian for different time (t) will not commute, i.e., the eigenstate for the Hamiltonian for different time is not the same. So we can say that the eigenstate (ψ_n) and the eigenvalues (E_n) are time-dependent. So,

$$H(t)\psi_n(t) = E_n(t)\psi_n(t). \tag{2.5.2}$$

The Schrödinger equation for the state Ψ can be described as:

$$i\hbar\frac{\partial \Psi(t)}{\partial t} = H(t)\Psi(t). \tag{2.5.3}$$

The solution of Eq. (2.5.3) can be described as a linear combination of the eigenstates of the Hamiltonian at time t, as:

$$\Psi_n(t) = \sum_n C_n(t)\,\psi_n(t)\,e^{i\Theta_n(t)}, \tag{2.5.4}$$

where $\Theta_n(t) = -\frac{1}{\hbar}\int_0^t E_n(t')dt'$ is the phase factor. Now using Eq. (2.5.4) in Eq. (2.5.3) we get

$$i\hbar\left(C_n\dot{\psi}_n + \dot{C}_n\psi_n + iC_n\dot{\Theta}\right)e^{i\Theta_n} = \sum_n C_n H e^{i\Theta_n}. \tag{2.5.5}$$

Using Eq. (2.5.2), and executing some algebraic manipulation, we have

$$\sum_n \dot{C}_n\psi_n e^{i\Theta_n} = \sum_n C_n\psi_n e^{i\Theta_n}. \tag{2.5.6}$$

Now we consider the inner product with the state Ψ_m, and then applying the orthonormality condition, we get

$$\dot{C}_m(t) = -\sum_n C_n\langle\Psi_m|\Psi_n\rangle\,e^{i(\Theta_n-\Theta_m)}. \tag{2.5.7}$$

Now we will first execute the time derivative of Eq. (2.5.2), and then after that, we will take the inner product with Ψ_m and using the Hermiticity of the Hamiltonian in Eq 2.5.7 we have

$$\dot{C}_m(t) = -C_m\langle\Psi_m|\Psi_n\rangle - \sum_n C_n\frac{\langle\Psi_m|\dot{H}|\Psi_n\rangle}{E_n - E_m}\,e^{i(\Theta_n-\Theta_m)}. \tag{2.5.8}$$

Considering the adiabatic approximation, which conveys the fact that H is quite small so that we can equate the second term of the Eq. (2.5.8) to zero, so we have

$$\dot{C}_m(t) = -C_m\langle\Psi_m|\Psi_n\rangle. \tag{2.5.9}$$

Solving the equation we have

$$C_m(t) = C_m(0)\,e^{i\gamma_m(t)}, \tag{2.5.10}$$

where $\gamma_m(t) = i \int_0^t \langle \psi_m(t') | \dot{\psi}_m(t') \rangle \, dt'$. If $C_n(0) = 1$ and $C_m(0) = 0$ then we have

$$\Psi_n(t) = e^{i\Theta_n(t)} \, e^{i\gamma_n(t)} \, \psi_n(t). \tag{2.5.11}$$

From Eq. (2.5.11) one can infer that the system remains in its instantaneous eigenstate of the Hamiltonian with some global phase factor.

2.5.3 Quantum Isochoric process

In a classical isochoric process, the volume remains constant. As the volume is the same throughout the process, the system does not do any work. In this process, the system can exchange heat with the hot reservoir. The pressure and the temperature of the system changes during the evolution of the system in this process, and at the end of the process the system will attain thermal equilibrium with the hot reservoir. With the same analogy the quantum isochoric process, the system is kept in touch with the hot reservoir. During this process, the system exchanges some amount of heat with the reservoir without performing any work. The occupation probability P_n changes, although the energy spacing E_n will remain the same:

$$dW = \sum_n P_n dE_n = 0. \tag{2.5.12}$$

The entropy of the system S will change until the system equilibrates with the hot reservoir at the end of the process, and the occupation probabilities in each eigenstate will satisfy Boltzmann distribution. For example, if one considers a spin system as a working medium, the analogy of the concept of volume can be described with the energy spacing of the system. The spacing will remain constant throughout the process.

2.5.4 Quantum Isobaric process

In the classical regime, the isobaric process states that the pressure will remain constant throughout the process. This is executed by controlling the volume (V) expansion or contraction so that it is able to neutralize the pressure changes that will occur due to the heat exchange by the system with the reservoir. During this process, another parameter, i.e., the temperature of the reservoir needs to be controlled. The system thus follows the condition $T \propto V$ and the generalized force Y_N is defined as $Y_N = -\frac{dW}{dy_N}$, where y_N is the generalized coordinate. The first law for this process takes the form

$$dU = dQ + dW = T\,dS + Y_N dy_N, \qquad (2.5.13)$$

where S is the entropy of the system. Using this analogy, in the quantum regime, the force for a one-dimensional quantum system is defined from the quantum first law of thermodynamics.

$$F = -\frac{dW}{dL} = -\sum_n P_N \frac{dE_N}{dL}, \qquad (2.5.14)$$

where L describes the generalized coordinate system corresponding to the force F. This is equivalent to the pressure in the quantum regime. To execute an isobaric process for the one-dimensional quantum system the temperature of the system should be proportional to the width of the potential, i.e., $T \propto L$. This is equivalent to the condition $T \propto V$ in the classical regime.

The comparative study of the classical and the quantum thermodynamic processes is described in the table 2.1.

2.6 Uncertainty relation and connection to information theory

Heisenberg, in his seminal work [150], analyzed a hypothetical observation of an electron with photons and came out with a proposal that the product of the measurement error will be governed by a relation:

$$\Delta a \Delta b \geq \frac{\hbar}{2}, \qquad (2.6.1)$$

where a and b are two canonical observables. In quantum theory, two observables are called canonical if they satisfy the commutation relation $[a,b] = \hbar/i$ (in this case it is x and p). Kennard [151] and Weyl [152] inspired by this idea derived it mathematically and conveyed that it is a constraint on the measurement outcome for an ensemble with identical systems. Schrödinger [153] generalized Eq. (2.6.1) with a correlation term and Robertson [154, 155] derived the relation for two non-commutative Hermitian operators. It is similar to the relation proposed by Schrödinger. This relation is also known as the canonical uncertainty relation. Now it is considered that it provides a fundamental limit on the properties of the quantum systems. Eq. (2.6.1) is the bound which conveys that one cannot simultaneously attribute

Table 2.1. Thermodynamic processes in macro and micro regime

	Classical domain		Quantum domain	
	Variant	**Invariant**	**Variant**	**Invariant**
Isothermal Process Heat absorbed or released Work done	Pressure, Volume	Internal energy, Temperature	Internal energy, Eigenenergy, Occupation distribution probability	Temperature
	Variant	**Invariant**	**Variant**	**Invariant**
Adiabatic Process No heat exchange Work done	Pressure, Temperature, Volume	Entropy	Eigenenergy, Effective Temperature	Occupation distribution probability
	Variant	**Invariant**	**Variant**	**Invariant**
Isochoric Process Heat absorbed or released No work done	Pressure, Temperature	Volume	Effective Temperature, Occupation distribution probability	Eigenenergy
	Variant	**Invariant**	**Variant**	**Invariant**
Isobaric Process Heat absorbed or released Work done	Volume, Temperature	Pressure	Effective Temperature, Eigenenergy, Occupation distribution probability	—

definite values to the canonical observables.

According to Bohr [156], temperature and energy are complementary to each other as that of position and momentum. It says that a definite temperature can only be attributed to a system when submerged in a heat bath where we can neglect the energy fluctuations. Similarly, we can assign definite energy to the system when it is thermally isolated which simultaneously excludes the determination of temperature. Rosenfeld [157] extended this

with quantum mechanics and obtained an uncertainty relation which is of the form:

$$\Delta U \Delta(1/T) \geq k_B. \tag{2.6.2}$$

This is called the thermodynamic uncertainty relation. Different forms of the thermodynamic uncertainty relation are present in the literature which are developed for various aspects. Here, in this thesis, we have transferred the better bounds that have been proposed for canonical uncertainty relation to thermodynamic uncertainty relation, which will guide us to propose a bound in the efficiency of the thermal machine.

In recent years quantum information theory has encountered rapid progress. It was inspired by the seminal work of Einstein, Podolsky, and Rosen (EPR) paradox [158]. Schrödinger coined the term 'entanglement' [159] to explain the paradoxical feature that was proposed by EPR. The position-momentum uncertainty relation was the first testable formalism for the explanation of the EPR paradox. Quantum steering [160], which is the modern formalism of EPR concept, is based on the violation of the steering inequality which gained its form with the help of uncertainty relation of entropic form. This is similar to that of the Bell-type inequality [161, 162].

With the advent of quantum information theory, the researchers were able to uncover several other applications of uncertainty relations in this domain. It has been used as a tool for the discrimination between separable and entangled states [163, 164]. Whereas, the Robertson version of the uncertainty relation is used in the discrete variable domain to discriminate between the pure and the mixed states of the bipartite and qutrit systems [165–169]. One can utilize the uncertainty relation to explore the non-locality of the physical systems [170]. It has been explored for bipartite [170] and tripartite [171] systems as well as for biased non-local games [172]. In quantum cryptography, the uncertainty relation is the backbone for security purposes. For example, the security of the quantum key distribution protocols is based on quantum uncertainty relation [173]. One can visualize that the amount of key that is extractable from each state has a direct link with the lower limit of the entropy uncertainty relation [174,175]. So we can visualize the importance of the uncertainty relation in quantum information processing and quantum computation.

2.6.1   Uncertainty relation for a particle in a potential well

Here we are going to study the potential well problem in the relativistic as well as non-relativistic regime and then analyze the uncertainty relation for the system in their respective regimes. The UP (popularly known as Heisenberg's uncertainty principle [176]) states that no two canonically conjugate variables can be determined simultaneously with an accuracy greater than the fundamental constant named as plack constant $\hbar$. Mathematically, it can be defined in terms of the standard deviations of the pair of variables [177]. For two of such variables x and p which describes the position and momentum of a system, it is defined as

$$\Delta x \Delta p \geq \frac{\hbar}{2}, \tag{2.6.3}$$

There is a subtle difference in two closely associated terms, namely: UP and the UR. The UP as stated in [154, 178–180], describes the inevitability of joint measurement for any two canonical pair of variables. Whereas UR doesn't convey the measurement-induced disturbances, rather, it refers to the state-induced spread in the measurement outcome.

One can find various forms of UR, which are developed over the years starting from Heisenberg's UR [176]. The most common form of the UR was given by Robertson [154] as:

$$\Delta A \Delta B \geq \left| \frac{1}{2} \langle [A, B] \rangle \right|, \tag{2.6.4}$$

where A and B are two incompatible observables. One can reproduce Eq. (2.6.3) from the Robertson relation by substituting the corresponding commutation relation for $[x, p]$. Schrödinger is his UR form addaed an extra anti-commutator term [178, 179], which further strengthened the bound

$$\Delta A^2 \Delta B^2 \geq \left| \frac{1}{2} \langle [A, B] \rangle \right|^2 + \left| \frac{1}{2} \langle \{A, B\} \rangle - \langle A \rangle \langle B \rangle \right|^2 . \tag{2.6.5}$$

With the evolution of quantum information, the essence and importance of uncertainty relation in technology got enriched. It has various applications in quantum technology like quantum cryptography [181–183], entanglement detection [184–187], even in quantum metrology [188] and quantum speed limit [189–192]. In recent times, the work [193–195]

have authenticated the uncertainty relation experimentally.

let us first revisit the one-dimensional potential well for the non-relativistic scenario. It is an age-old textbook problem. The one-dimensional potential well is a well-known problem in quantum mechanics [196, 197]. Here, we consider a particle of mass m inside a one-dimensional potential box of length $2L$. The wave-function of this system for the n-th level is $|\psi_n\rangle = \sqrt{\frac{1}{L}} sin(\frac{n\pi x}{2L})$. So, when the wavefunction of the model under study is known, we can calculate the eigenvalue of the system. Eigenvalues of 1-D potential well is $E_n = \frac{n^2\pi^2\hbar^2}{2m(2L)^2}$, where $\hbar$ is Planck's constant.

With the wavefunction of the model in our hand, we are all set to derive the uncertainty relation of the position and the momentum for this system. The uncertainty relation for our model is described as [196, 197]

$$\Delta x \Delta p \quad = \quad \frac{\hbar}{2}\sqrt{\left(\frac{(n\pi)^2}{3} - 2\right)} \quad \geq \frac{\hbar}{2}, \tag{2.6.6}$$

where $\Delta x^2 = \langle x^2 \rangle - \langle x \rangle^2$ and $\Delta p^2 = \langle p^2 \rangle - \langle p \rangle^2$ and we have $\langle p \rangle = 0$ for all eigenstate. The expectation values of $\langle x \rangle$, $\langle x^2 \rangle$ and $\langle p^2 \rangle$, can be easily evaluated by considering the defined wavefunction of the considered system.

Unlike the potential well problem in non-relativistic quantum mechanics, the potential well problem with a relativistic particle confined in it is not a textbook material traditionally. Here, we will now revisit the analysis of uncertainty relation for a relativistic particle in a potential well. For our convenience, we have used '≡' for defining a new symbol or quantity.

Here, for the analysis, we have considered the relativistic potential well model as our working substance. The solution of the free Klein-Gordon (KG) equation [198] using Feshbach-Villars formalism [199] is

$$\psi_{\vec{p}}^{\pm}(\vec{x}, t) \quad \equiv \quad A_{\pm}\begin{pmatrix} \phi^{\pm}(\vec{p}) \\ \eta^{\pm}(\vec{p}) \end{pmatrix} e^{(\mp E_p t - \vec{p}\,\vec{x})/\hbar}$$

$$= \quad A_{\pm}\phi^{\pm}(\vec{p})e^{(\mp E_p t - \vec{p}\,\vec{x})/\hbar}, \tag{2.6.7}$$

where $\pm$ represents the positive and negative energy solution respectively and $E_p = \sqrt{p^2 c^2 + m^2 c^4}$, $A_{\pm}$ is the normalization constant and m, p, c is the mass, momentum and the velocity (of the order of speed of light) of the particle respectively.

The mathematical forms for $\phi^{\pm}(\vec{p})$ and $\eta^{\pm}(\vec{p})$ of Eq. (2.6.7) are given by

$$\phi^{\pm}(\vec{p}) \equiv \frac{\pm E_p + mc^2}{2\sqrt{mc^2 E_p}},$$

$$\eta^{\pm}(\vec{p}) \equiv \frac{\mp E_p + mc^2}{2\sqrt{mc^2 E_p}}.$$

The procedure we generally take to solve for a particle in a box in the relativistic case leads to the 'Klein paradox'. Klein paradox tells that the flux of the reflected plane wave in the walls of the potential well is larger than that of the incident waves. The reason behind this is the wavefunction which starts to pick up components from the negative energy states. The way to solve this paradox is to presume the mass of the system as a function of x. So it is defined as:

$$m(x) \equiv \begin{cases} m, & x \in L, \\ M \to \infty, & x \notin L, \end{cases}$$

where L is the length of the potential box. So, the wave function inside the box results in

$$\Psi(x) \equiv \sqrt{\frac{2}{L}}\phi^{+}(p)\sin(p\,x/\hbar). \tag{2.6.8}$$

Here $pL = n\pi\hbar$ and $n = 1, 2, \cdots, \infty$. The quantized energy of the system takes the form

$$\begin{aligned} E_n &\equiv \sqrt{\frac{n^2\pi^2\hbar^2 c^2}{L^2} + m^2 c^4} \\ &\approx mc^2 + \frac{n^2\pi^2\hbar^2}{2mL^2} + \cdots, \end{aligned} \tag{2.6.9}$$

where in the last line a small $p/(mc) = n\pi\hbar/(Lmc)$ expansion is made. The second term arises by solving the Schrödinger equation. The mc^2 term represents the rest energy, and the dots represent second and higher-order terms of L which are being neglected for our analysis.

Now, for our purpose, we consider a relativistic particle of mass m inside a one-dimensional potential box of length $2L$ with a bath at temperature T. We have considered the potential box of length $2L$ for calculation convenience when we insert a partition in the middle of the potential box. So, the wavefunction of the system for the n-th level, similar to the Eq. (2.6.8) which takes the form

$$\psi(x) = \sqrt{\frac{1}{L}}\phi^+(p)\sin(px/\hbar), \quad where \quad p(2L) = n\pi\hbar. \tag{2.6.10}$$

So, the quantized energy of the considered system takes the form similar to Eq. (2.6.9) as:

$$
\begin{aligned}
E_n &= \sqrt{\frac{n^2\pi^2\hbar^2 c^2}{(2L)^2} + m^2 c^4} \\
&\approx mc^2 + \frac{n^2\pi^2\hbar^2}{2m(2L)^2} + \cdots .
\end{aligned} \tag{2.6.11}
$$

Having the information about the wavefunction and the eigenvalues, we are all set to analyze the uncertainty relation of the position and the momentum operator of the system. The mathematical form of the uncertainty relation for the position and the momentum operator of the system is

$$
\begin{aligned}
\Delta x \Delta p &\equiv \sigma_x \sigma_p \\
&= \frac{\hbar L}{2}\phi^+(p)\Big[\Big(\frac{1}{3} - \frac{2}{(n\pi)^2} - \phi^{+2}(p)\Big) \times \Big(\frac{\pi^2 n^2}{L^2} + \frac{8m^2 c^2}{\hbar^2}\Big)\Big]^{\frac{1}{2}} \\
&\geq \frac{\hbar}{2},
\end{aligned} \tag{2.6.12}
$$

where $\Delta x^2 = \langle x^2 \rangle - \langle x \rangle^2$ and in the case of momentum, Δp^2 can be defined similarly. The mathematical form of the expectation values of $\langle x \rangle$, $\langle p \rangle$, $\langle x^2 \rangle$ and $\langle p^2 \rangle$ for the relativistic particle confined in the potential well are

$$
\begin{aligned}
\langle \psi_n | p | \psi_n \rangle &= 0 \\
\langle \psi_n | x | \psi_n \rangle &= L\phi^{+2}(p) \quad n = 1,2,\cdots \\
\langle \psi_n | x^2 | \psi_n \rangle &= 4L^2 \phi^{+2}(p)\Big[\frac{1}{3} - \frac{1}{2(n\pi)^2}\Big] \; n = 1,2,\cdots \\
\langle \psi_n | p^2 | \psi_n \rangle &= \Big(\frac{\pi\hbar n}{2L}\Big)^2 + 2m^2 c^2, \quad n = 1,2,\cdots
\end{aligned} \tag{2.6.13}
$$

where we have considered the wavefunction ψ_n as shown is Eq. (2.6.10).

2.7 Thermal engine with different working medium

In this section, we are going to analyze different thermal engines like quantum Stirling engine and quantum Otto engine with potential well and harmonic oscillator (HO) as the working medium. Here we will provide the general idea of the engines with the working substance,

the details based on the respective working medium will be analyzed later.

2.8   Stirling cycle with potential well

Here we are going to analyze the Stirling cycle with potential well as the working medium in a generic way. A Stirling cycle [123, 146, 147, 200] is composed of four stages, two isothermal processes, and two isochoric processes. During the first stage, we insert a barrier isothermally in the middle of the well. While this quasi-static insertion process is being done, the working medium stays at an equilibrium condition with a hot bath at a temperature T_1. During the second stage, we perceive an isochoric heat extraction of the working medium by connecting it with a bath at a lower temperature of T_2. In the next stage of the cycle, there is an isothermal removal of the barrier where we retain the engine in equilibrium at temperature T_2. Now in the final stage, we bridge the engine to the hot bath at the temperature T_1 and this gives rise to isochoric heat absorption. It is represented pictorially in Fig. 2.5.
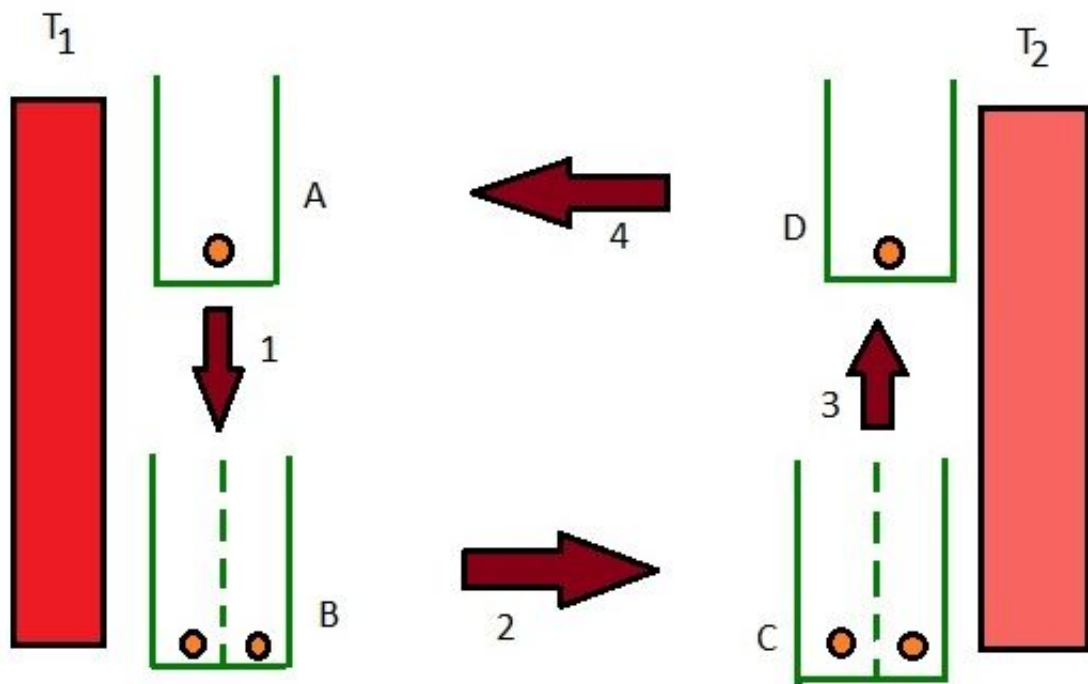
Figure 2.5. The figure shows the four stages(two isothermal and two isochoric process) of the Stirling cycle modeled using potential well.

A detailed description of the phases of the cycle is described below:

(i) First stage of the Stirling cycle is the *isothermal (A→B)* process. In this phase, we insert a barrier isothermally in the 1-D well, which divides the well into two equal halves.

The positioning of the partition (i.e. barrier) in the middle of the infinite 1-D well converts it to an infinite 1-D double potential well. In our analysis, we have taken into account that the delta potential grows in strength from zero to that height, which would be enough to prevent the tunneling process through the barrier. This provides us the assurance that the probability tends to zero for the tunneling process considering that the time required for the execution of the tunneling process is more than the time required for any thermodynamic processes to complete. During this phase of the cycle, the working medium is attached to a hot bath with a temperature T_1. Throughout this process, the system remains at its equilibrium condition when the quasi-static insertion of the barrier is being done.

(ii) The second phase: *isochoric (B→C) process*. In this stage of the cycle the working medium experiences an isochoric heat extraction. The system is connected to the cold bath at temperature T_2 where $T_1 > T_2$.

(iii) The third phase: *isothermal (C→D) process*. In this stage of the cycle, we remove the barrier from the 1-D well isothermally. The execution of this stage is carried out keeping in mind that the tunneling probability tends to zero, and it remains in equilibrium at temperature T_2.

(iv) The fourth stage: *isochoric (D→A) process*. During this last phase of the cycle, isochoric heat absorption is observed when the working medium is connected back to the bath at a temperature T_1. The schematic representation of the cycle is shown in Fig. (2.5).

2.8.1   Otto cycle with harmonic oscillator

We will briefly describe the quantum Otto engine proposed by Kieu [201]. It is also explored with different mediums [61, 144]. For our analysis, we have adopted a quantum system, namely, harmonic oscillator as the working substance for the engine cycle. The adiabatic increase and decrease in the quantum realm are controlled by the change in the energy levels which occurs due to the change in the frequency of the oscillator. The isochoric process in the quantum version is represented by the thermalization processes, during which it exchanges heat with the bath. Work is done during the adiabatic process of the cycle. The change in the mean energies guides us to calculate the work and heat for the cycle, where mean energy for the system is represented by the state ρ and the Hamiltonian H. It is defined as $Tr[\rho H]$. his is the general representation of the Otto cycle with harmonic oscillator [202] as the working medium. The pictorial representation of the whole process is described in Fig. 2.6.
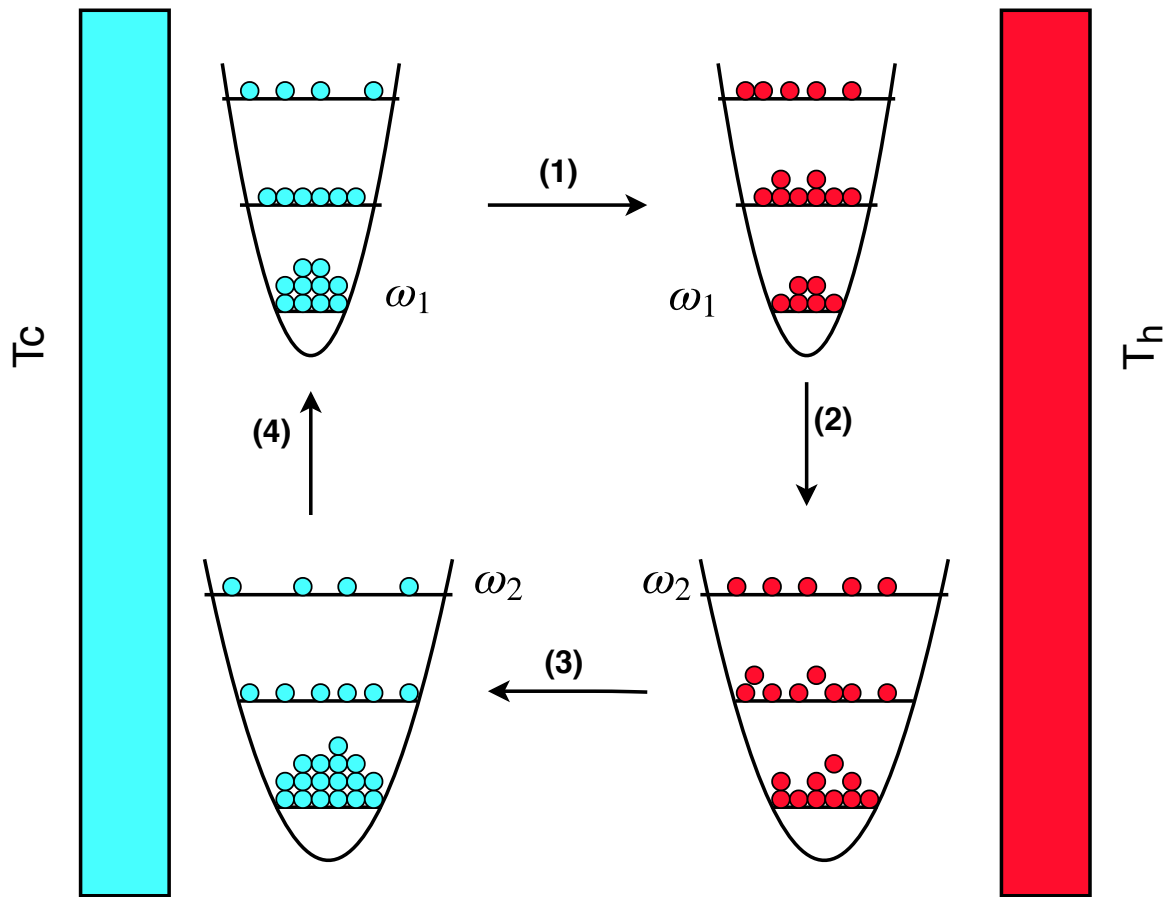
Figure 2.6. (Color online) The schematic representation of a quantum Otto cycle is shown. The working substance of the cycle is a coupled harmonic oscillator. The first stage and the third stage of the cycle are the thermalization processes, and the second phase and the fourth phase corresponds to the adiabatic processes.

2.8.2   Stirling cycle with harmonic oscillator

We will analyze the Stirling cycle with coupled HO as the working substance. The isochoric process in the quantum version is represented by the thermalization processes during which it exchanges heat with the bath. The isothermal expansion and compression in the quantum realm are controlled by the change in the energy levels due to the variation in the frequency of the oscillators. The Stirling cycle is a quantum regime with coupled HO as the working substance is depicted in Fig. (2.7). The four stages of the quantum Stirling cycle are

This is the generic representation of the Stirling engine with a harmonic oscillator as the working medium. The detailed analysis of the engine with the different Hamiltonian structures of our work is described later.

ω_1, T_h Isothermal ω_2, T_h

$$A \longrightarrow B$$

Isochoric $\uparrow$ $\downarrow$ Isochoric

$$D \longleftarrow C$$

ω_1, T_c Isothermal ω_2, T_c

$$\omega_1 > \omega_2, \quad T_h > T_c$$
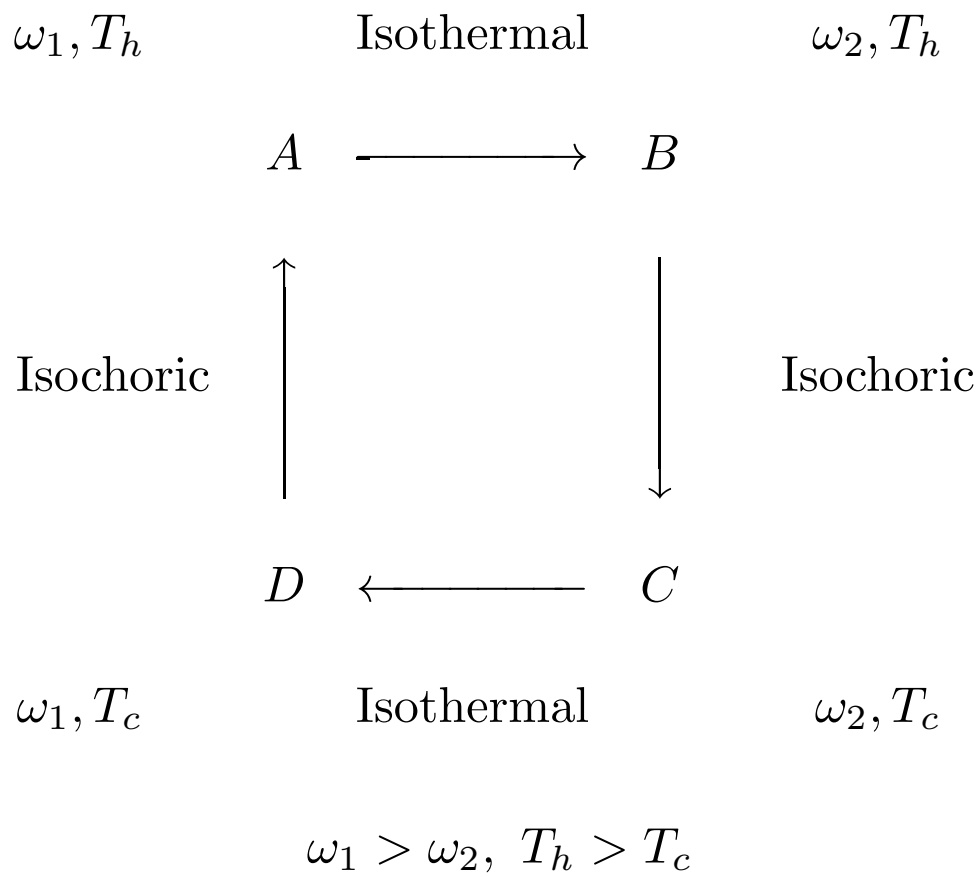
Figure 2.7. Schematic representation of the Stirling cycle in quantum realm with harmonic oscillator as the working substance. ζ represents the coupling strength of the coupled harmonic oscillator.

3   Background on Thermodynamics of Computation and Information Theory

Contents

The contents in this chapter are based on the review article in Ref. [203].

From Landauer's principle, we know that when a bit of information is written on a memory device the entropy of the system decreases by $k_B T \, ln(2)$, so at least the same amount of work has to be done. In the works [24, 204], they have stated that we can have systems that are able to compute with no lower bound with respect to the thermodynamic cost. With the theoretical advancement of stochastic thermodynamics [205] and information thermodynamics [206], a better understanding of the physical foundation of the information processing is possible. Though these frameworks are concentrated on proto-computation [207–210], few attempts are taken to apply information thermodynamics to computer science. However, the works [211, 212], suggest that one can consider the fundamental limit to the thermodynamics cost of computation while analyzing the system in the quasi-static limit. One can also describe the thermodynamic cost for a computation process as a sum of the energy that is required to provide an extra bit in the due course of the computation process, plus the energy required to destroy [24] the generated garbage bits. This part of the computation is non-reversible, and so according to Landauer's principle, this part of the computation process dissipates heat. The "Fundamental Theorem" [213] provides the upper and the lower bounds over the thermodynamic cost of the computation process. It is also stated that a slow computational process releases less amount of energy [24]. In the article [214], they have provided proof of the existence of this statement mathematically, that with the increase of the time of computation, there exists a time-energy trade-of hierarchy for diminishing the energy cost of the process. From real-life examples, we know that garbage needs to be compressed and this needs time. Along with the increase of interest to investigate the connection of thermodynamics with computation, connection with information-theoretic notions can gain importance. Now, information theory is treated as a physical science, and the bridge between information theory and thermodynamics provides a trade route between them. The investigation to connect thermodynamics with information theory is highly pursued.

We are going to first revisit the basics of computation and information theory in this chapter. Then we will study some alternative models of computation that are thermodynamic cost-friendly. Along with that, we will visualize the effect of thermodynamics in various computation models, information theory, and its contribution to the algorithmic study.

Now let us first define some mathematical variables that we will be considered throughout this chapter. For any defined set $\mathbb{S}$, the collections of the set of all finite strings of the elements from $\mathbb{S}$ is denoted by $\mathbb{S}^\star$. In computer, we use $\mathbb{S} = \{0, 1\}$. Here $\mathbb{S}^\star$ denotes the set of all binary strings.

For the analysis, we are going to consider the output 1 as Boolean 'TRUE' and consider the 0 output as 'FALSE'. For any Boolean function $g(a)$ the indicator function is expressed as:

$$\mathbb{I}(g) = \begin{cases} 1, & g(a) = 1, \\ 0, & \textit{otherwise}. \end{cases} \tag{3.0.1}$$

We will denote the length of a finite string $\mathbb{M}$ as $l(\mathbb{M})$. The concatenation of two strings $\mathbb{M}$ and $\mathbb{M}'$ is defined as $\mathbb{M}\mathbb{M}'$. For ceiling operators, we will use $\lceil \bullet \rceil$, and for flooring operators $\lfloor \bullet \rfloor$ wherever required.

In probability theory, the random variables are described by upper case letters, and the instances of these random variables are expressed by the lower case letters. Given a set A, the distribution over this set can be expressed as $p(a)$. Now, there exists any $A' \subseteq A$ for which we can write $p(A') = \sum_{a \in A'} p(a)$. For a distribution p over a set A the conditional distribution $\pi(y|a)$ is defined as:

$$(\pi p)\, y := \sum_{a \in A} \pi(y|a)\, p(a), \tag{3.0.2}$$

where πp is the distribution over Y.

3.1   Basic Aspects of Computation Theory

Theoretical computer science covers different areas starting from the algorithm, data structure, computation to computational number theory. In this section, we are going to study about two of the basic computation aspects of computer science. In the further section, we will see the impact of thermodynamics on these aspects. From a computational perspective, the system is defined in this form to describe that it is one of the members of the Chomsky hierarchy [215].

3.1.1   Finite Automata

The formal definition of the finite automaton is as follows

Definition 1. A finite automaton is a 5-tuple $M = (Q, \Sigma, \delta, q, F)$, where,

- Q represents a finite set of states.

- Σ also represents a finite set of symbols called the alphabet.

- $\delta : Q \times \Sigma \rightarrow Q$ represents the transition function where $\delta(q,a) = q'$. Here q' describes the next state.

- $q \in Q$. It represents the start state.

- $F \subseteq Q$ describes the set of final accepting states.

One can infer from the definition that, the transition function denoted by δ represents the program of the finite automaton $M = (Q, \Sigma, \delta, q, F)$. The input words accepted by the automaton specifies a language that is described as a regular language, i.e., any finite language (words of finite length) can be called a regular language. So, we can conclude that a finite automaton has the power to compute input words of arbitrary length.
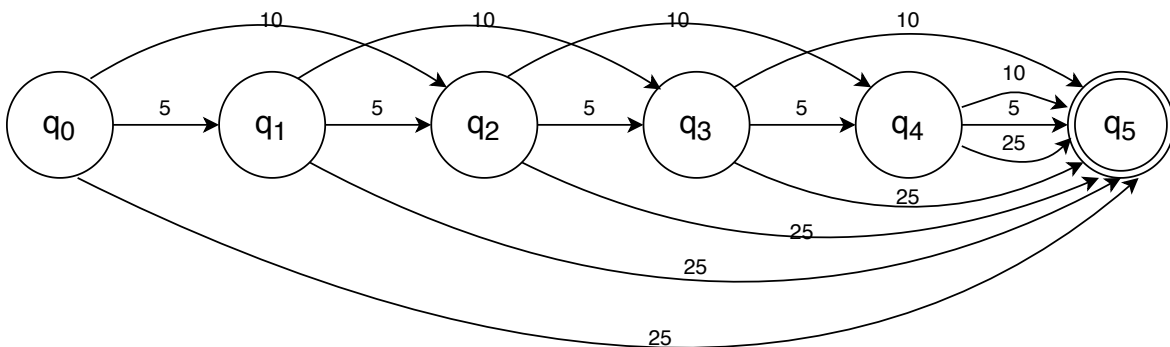
Figure 3.1. Transition diagram of the system.

We will first consider an example of an automaton that appears naturally. Let us consider a *toll gate*. Now, we will design a computer that will control this *toll gate*. The gate from the toll pass remains closed until the vehicle pays the required amount. For example, we consider that when the driver pays 25 bucks the toll gate opens, and the driver is allowed to go. We assume that there exist only three sets of coins: 5, 10, and 25 bucks. Whenever a driver appears at the toll gate, he will insert coins into the machine. So, the machine decides whether it will open the gate or not, in other words, whether the driver has fulfilled the payment of the required amount (i.e., 25 bucks or more). The machine can be in any of the six states based on which it will decide whether it will open the gate or not. The six states of the machine during the execution of the process are:

- If the machine does not collect any money, the machine state is described by q_0.

- When the machine receives 5 bucks, the machine moves to the state q_1.

- Now, when it gets 10 bucks, the state of the machine is q_2.

- When it has 15 bucks, the state is q_3.

- When it has 20 bucks, the state is q_4.

- When it has 25 bucks, the state is q_5.

Now, let us consider a situation where a vehicle comes to the toll gate, then the machine will be at its initial state. Now the driver inserts 25 bucks in the sequence (5, 5, 10, 5). The state of the machines evolves through the process as follows:

- After the driver inserts 5 bucks to the machine, the machine evolves from the state q_0 to q_1.

- Similarly, the driver inserts the next 5 bucks to the machine, the machine now moves from the state q_1 to the state q_2.

- After that the driver inserts 10 bucks, the machine jumps by two steps and moves to the state q_4 from state q_2.

- Finally, the driver inserts its last 5 bucks, the machine moves to its final state q_5. The toll gate opens up. We assume that the driver provides that exact amount else the machine responds abort and restart the process.

The state diagram with all the combinations is shown in Fig. 3.1. Here, the state q_5 is depicted by two circles. The two circle state represents the final state of the system (or the halt state). Now, if the machine reaches this state, the gate will open otherwise the gate remains closed. In this case, one can observe that the machine only has to remember the state where it belongs at any instant of time.

Finite automata have a great impact in different fields of studies which include computer science, biology, mathematics, logic, linguistics, engineering, and even in philosophy. Finite automaton has a wide scale of applications in computer science like designing hardware, designing compilers, network protocols, and in computation.

Finite automata have different forms like deterministic and stochastic (alternatively called "probabilistic automaton") finite automaton. In the stochastic automaton, the single-valued transition function δ will be replaced by a conditional distribution. One can observe multiple

accepted states which are described in the literature as 'terminal states' for the system. Even one can encounter multiple start states in the process.

3.1.2   Turing Machine

Alan Turing in his seminal work [216], first coined the term Turing Machine (TM). He conveyed that it is an abstract computation device, which will help to investigate the extent and as well the limitation of what we can compute. It was devised mainly for the computation of real numbers. So, the renowned form of the computational machine studied in computer science is Turing machines [215, 217]. It is generally conveyed in the literature that one can model every computational machine using a universal Turing machine [218]. Church-Turing thesis [219] conveys the statement a bit formally, it states that "A function on the natural numbers is computable by a human being following an algorithm, ignoring resource limitations, if and only if it is computable by a Turing machine." It was further modified in the ' Physical Church-Turing thesis', where it has been conveyed that the set of functions which one can compute by utilizing the mechanical algorithmic method, which abides by the laws of physics [220–224], are also computable with the help of Turing machine.

Various forms of definitions of the Turing machine exist in the literature which is computationally equivalent to each other. As the various definition are equivalent to each other, computation done in one type of Turing machine can be executed equivalently in other forms of the Turing machine. The formal definition of the Turing machine is

Definition 2. A Turing machine is defined by 7-tuple $(Q, \Lambda, \Gamma, \delta, q_0, q_a, q_r)$, where

- Q is a finite set which describes the set of states.

- Λ is also a finite set that depicts the input alphabets.

- $\Gamma \supset \Lambda$ represents a finite set of tape alphabet.

- $\delta : Q \times \Gamma \to Q \times \Gamma \times \{L, R, S\}$ is called the transition function.

- q_0 represents the start state of the Turing machine.

- q_a is called the accepted state or in other words, halting state.

- q_r is called the rejected state.

Here, $\{L, R, S\}$ describes the direction of the movement of the head of the tape. Based on the command, the head moves left, right, or stays in that same position of the tape. In other

equivalent computational definitions of the Turing machine, one can encounter multiple sets of accepting states, in other words, halting states.
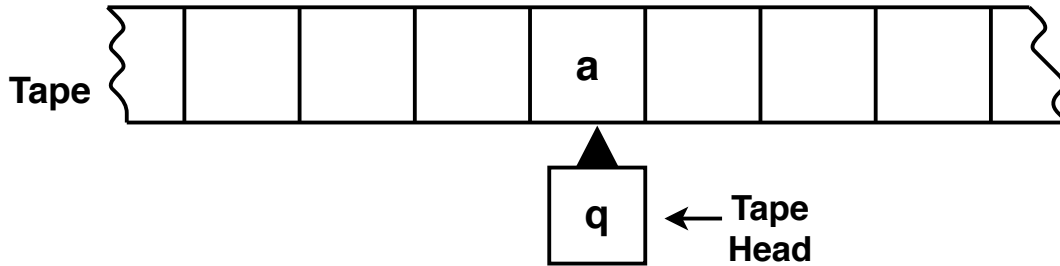
Figure 3.2. A schematic of TM. The tape of a TM is an infinite tape whose state is specified by q. The infinite tape is divided into equidistance square boxes filled with tape alphabets. The TM will scan the tape with its tape head. The tape head has access to move to the left or right of the tape.

At each step of the computation, the state of the TM reads the alphabet in the square where the tape head is placed, and subsequently move on to a new state q'. It writes a new alphabet (a') on the tape, and then it moves its tape head either to the left or to the right. This process is repeated until the system attains the accepted state. Mathematically this map can be expressed as $\delta(q,a) = (q',a',d)$, where d denotes the right or left movement of the tape head. For a given TM, the arguments of the transition states are called "instantaneous description" (IDs) of the TM. One can also sometimes encounter TM's with no halts.

A function f is called recursive, if there exist a TM with input alphabets x where $x \in \Gamma^{\star}$, for which the TM computes $f(x)$. Similarly, the function f is a partial recursive function, if we are able to compute $f(x)$ using a TM, where x is input alphabets of the TM. Turing has conveyed in his work that all functions are not recursive, which remains a fundamental limitation.

Turing machine has a great impact on the analysis of computational complexity [215, 225]. One of the profound open problems in mathematics that remains a concern for the exploration of the Turing machine is whether $P = NP$ [226]. The limitations of mathematics, like Gödel's incompleteness theorem [227], have a deep intimacy with the computational device theory of the Turing machine, and even in some parts of philosophy as well [228]. As all devices are physical, it has been argued in some works [229, 230] that one might bring some restriction to the foundation of physics by utilizing some properties of Turing machines.

It is a well-known fact that there exist many variants of TM like multitape, both way tape etc. Here, we have described the formal definition for a single tape. One of the popular variants of TM is the multiple tapes, where one of these tapes contains the input of the computational model, and one of them contains the output of the TM when it reaches its halting state. Other intermediate tapes in the multiple tape TM are called the 'work tapes' that are used as scratch pads. It is a complicated variant than that of the single tape. It is used in the literature as it is easy to prove theorems than single tape TMs. The computational power for all of these variants is equivalent. The interesting fact about these two variants is that one can convert a multiple tape TM into a single tape TM and similarly a single tape TM into a multiple one [218, 231, 232]. One of the variants of TM is the universal TM, which has the computational power to compute any other TM. In general, it is considered that TM is a formal structure of algorithm whereas a universal Turing machine (UTM) (which takes other TM's as input) is a formal structure of a computer.

3.2 Basics Aspects of Information Theory

In this section, we will discuss some basics concepts of information theory that are required for our analysis, and then we move on to discuss the error correction theory for the classical system as well as the quantum system. Thermodynamics has an impact on various aspects of quantum information theory. Here we are concerned about the error correction as it has a great impact on computational as well as communication aspects.

3.2.1 Notion on Information Theory

Here, we will guide ourselves through some of the basic aspects of information theory. The Shannon entropy over a set T is defined as:

$$S(T) = -\sum_{t \in T} p(t) \, log_b \, p(t),$$

where, for the cases when $b = e$ (nats) it will be generally conveyed as ln throughout the article. Here, $p(t)$ is the probability of the event t. For other conditions like $b = 2$ (bits) and so on it will specifically be mentioned in the analysis.

Using the above definition, we can describe the conditional entropy of a random variable X_r, which is conditioned on another random variable Z_r. The mathematical representation of

conditional entropy is

$$
\begin{aligned}
S(X_r|Z_r) &= \sum_{z \in Z_r} p(z)\, S(X_r|z) \\
&= \sum_{z \in Z_r,\, x \in X} p(z)\, p(x|z)\, ln\, p(x|z).
\end{aligned}
$$

Similarly, one can define the mutual information for two random variables X_r and Z_r as:

$$
\begin{aligned}
I_p(X_r; Z_r) &= S(X_r) + S(Z_r) - S(X_r, Z_r) \\
&= S(X_r) - S(X_r|Z_r).
\end{aligned}
$$

We have described some of the basics definitions of information theory. Readers who are interested to have a deep understanding of information theory (both in classical and quantum systems) can go through the referred books [233–237].

3.2.2 Classical Error Correction

In a communication process, the data is transmitted from the sender to the receiver end through a channel that is prone to noise, i.e., it is transmitted through a noisy channel. The data string is a sequence of 0's and 1's. The string to be communicated is encoded with an additional number of bits (redundant bits). On the receiver's end, the receivers reconstruct the actual message by decoding and examining the corrupted message. This reconstruction process is conveyed as decoding.

In the late '40s of the 20th century, the seminal work of Shannon [238] leads to the foundation of this field and extended by Hamming in his work [239]. Since then, this field has gained importance for developing better communication. The extent to which error correction of the missing bits is possible depends on the design of the error-correcting code. Generally, there exists two types of error-correcting codes, they are **block code** and **convolutional code**. We will be mainly focusing on the linear code of the block code. There are other models of error correction codes that are not covered here, interested readers can go through [240, 241] for further information.

The formal definition of the error correcting code is defined as:

Definition 3. The error correcting code can be defined as an injecting map form n symbols (messages bits) to m symbols:

$$
Enc : \Lambda_n \to \Lambda_m,
$$

where Λ represents the set of symbols.

- We define a variable a which describes the cardinality of our alphabet set ($a = |\Lambda|$). For binary code system $a = 2$.

- The domain of the set, i.e., Λ_n represents the message space, and Λ_m represents the message that will be transmitted from the channel. Here n denotes the message length.

- Block length: Block length is denoted by m, it describes the message which is mapped to m-bit strings.

- Code: The message to be transmitted will be encoded with a codeword. This codeword is called the code. In general , $m \geq n$.

- Rate: It is defined as the ratio of n over m. it describes the efficiency of the protocol.

Now we move on to analyze the linear code protocol. A linear code is a type of error correction code, where the linear combination of codewords also represents a codeword. The channel through which we will communicate is a binary channel, generally known as a binary symmetric channel. In this type of noisy channel, the bit gets affected independently. The symmetric nature of the channels conveys that the channels cause error $0 \rightarrow 1$ and $1 \rightarrow 0$ with equal probability. Let us consider a message of n symbols as $u = u_1 u_2 \ldots u_n$ which are encoded into a codeword $x = x_1 x_2 \ldots x_m$. Here, the first part of the codeword is the original message (i.e. $x_{1 \rightarrow m} = u_1 u_2 \ldots u_n$) to be transmitted and the remaining are the check symbols (i.e. $x_{n+1} \ldots x_m$) which satisfies the condition:

$$H_p x = 0,$$

where the matrix H_p $((m-n) \times m)$ is called the parity check matrix for the code [242].

This codeword is now transmitted through the noisy channel. The receiver at the receiver's end, receives a different message say $y = y_1 y_2 \ldots y_m$ which is quite different from x. Let us denote the error in the message as $e = y - x = e_1 e_2 \ldots e_m$. Here, $e_j = 0$ with probability $1 - p$, will depict that the j symbols in the message is correct whereas, $e_j = 1$ with probability p conveys that the j symbol is incorrect. So in the decoding process, the receiver has to identify the message u from the received message y, which actually boils down to identify the error vector e. The decoder will try to choose the most likely error vector so that it can reduce the probability of making a mistake in decoding the correct message. This is gener-

ally defined as maximum likelihood decoding. The whole communication process is shown in Fig 3.3.
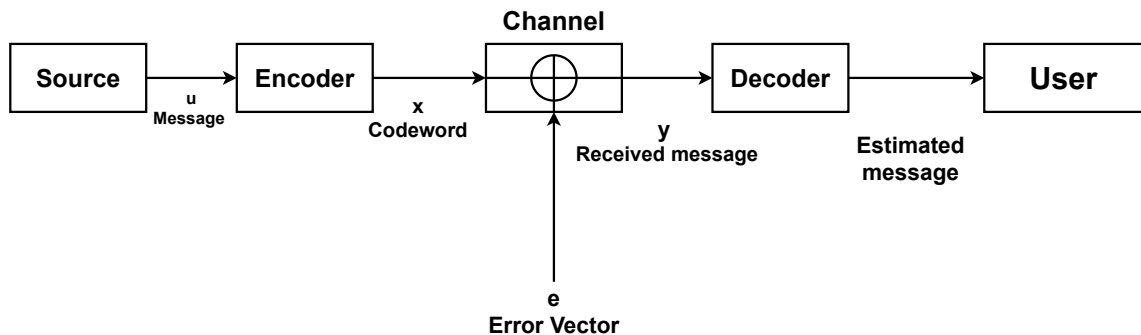
Figure 3.3. A schematic representation of the whole process in a communication system is depicted here. The channel is the communication medium through which the message is transmitted from the source to the receiver end.

So let us analyze how the decoder chooses the most likely error vector when it receives the message. Before we proceed, we will discuss two important definitions.

Definition 4. *Hamming distance*: The hamming distance between two given vectors $x = x_1 x_2 \ldots x_m$ and $y = y_1 y_2 \ldots y_m$ is described by number of positions the corresponding vectors differs. It is mathematically denoted by:

$$Dis(x, y) = |k : y_k \neq x_k|.$$

Definition 5. *Hamming weight*: The hamming weight is defined as the number of non-zero x_j in a vector x. It is denoted by $wt(x)$.

From the above two definitions, we can infer that $Dis(x, y) = wt(y - x)$. Based on the above-given definitions, we will formalize a parameter. The parameter is called the minimum hamming distance of a code, which is defined as $Dis_{min} = min\{Dis(x, y)\} = min\{wt(x - y)\}$, where x and y vary across all codewords. So the strategy of the decoder is to take that error e, which will have the least weight. This process is called nearest neighbor decoding. The decoder will compare the message y with all the possible combinations of the codewords, and then select the closest one. This brute force process is fine for small n. If n is very large this process becomes tedious, and coding theory aims to develop new schemes to decode these messages faster.

A linear code is generally called a $[m, n, d]$ code, where m describes the length of the codeword, n denotes the length of the message string, and d describes the minimum hamming distance.

3.2.3   Quantum Error Correction

Here in this section, we will discuss error correction in the quantum regime. Classical error correction is a well-developed theory based on the demand for better communication systems. One-to-one mapping from classical to quantum error correction is not possible as the quantum world has some constraints of its own. Qubit (quantum bits) are bounded by the no-cloning principle, which states that in quantum information theory one cannot copy a state which is possible in the case of classical information theory. Another aspect that we encounter in the quantum regime is that the wavefunction collapses when a measurement is performed over the state. These constraints were the reasons which make the quantum world unique over the classical, and these pose a challenge to the feasibility of quantum computing. It was the seminal work of Peter Shor [243], where they proposed the first quantum error correction protocol. Shor in his work has demonstrated that quantum information can be encoded by exploiting the idea of entanglement of qubits. Works in this direction [244–247], have demonstrated that one can suppress the error rate in the quantum regime provided the qubits met some physical conditions. Interested readers can go through the reviews [248–251] in this direction which covers quantum error correction and its subfields. In this article, we will describe the basic intuition of quantum error correction that we will explore in the latter half from a thermodynamics point of view.

Quantum errors in digitalize form

In the classical world, the units of information are bits, which belong to set $\mathbb{S}$ whereas, in the case of quantum the units of information are the qubits. The general definition of a qubit state is

$$|\psi\rangle = \alpha|0\rangle + \beta|1\rangle, \tag{3.2.1}$$

where α and β represents complex number satisfying the condition $|\alpha|^2 + |\beta|^2 = 1$. So, a qubit has the power to encode in the superposition of the computational basis states which are denoted by $|0\rangle$ and $|1\rangle$. The only error that is possible in the classical regime is the bit flip, i.e., $0 \to 1$ or viz versa. In the quantum realm, the qubit state is continuous in nature. So, this property of the qubits is the main challenge in developing the error correction code in the quantum world. The qubits are subjected to an infinite number of errors.

To get a clear idea about the errors let us describe the qubit state defined in Eq. (3.2.1)

as:

$$|\psi\rangle = \cos\frac{\theta}{2}|0\rangle + e^{i\phi}\sin\frac{\theta}{2}|1\rangle. \tag{3.2.2}$$

This is the geometric representation of the qubits. The condition of the probability amplitude is maintained as defined. The qubit state in Eq. (3.2.2) is described by a point in the Bloch sphere.

There can be errors due to a variety of physical processes. The rotation of the qubit from one point to another in a Bloch sphere will cause an error. Mathematically one can denote this type of error by a unitary operator $U(\Delta\theta, \Delta\phi)$ which will evolve the qubit state expressed in Eq. (3.2.2) to

$$U(\Delta\theta, \Delta\phi)|\psi\rangle = \cos\frac{\theta + \Delta\theta}{2}|0\rangle + e^{i(\phi + \Delta\phi)}\sin\frac{\theta + \Delta\theta}{2}|1\rangle. \tag{3.2.3}$$

The error that is caused by the rotation of the qubits shows that it is continuous in its nature. But we are quite lucky that we can digitalize this error with the help of the Pauli operators (i.e. Pauli matrices). The rotation process described in Eq. (3.2.3) can be described in terms of the Pauli matrices as:

$$U(\Delta\theta, \Delta\phi)|\psi\rangle = a_0\sigma_0|\psi\rangle + a_1\sigma_1|\psi\rangle + a_2\sigma_2|\psi\rangle + a_3\sigma_3|\psi\rangle, \tag{3.2.4}$$

where a_i ($i = 0, 1, 2, 3$) represents the coefficients, and σ_i ($i = 0, 1, 2, 3$) the respective Pauli operators. So, any error due to this rotation of the qubit can be described by the Pauli operators $[\mathbb{I}, \sigma_x, \sigma_y(\sigma_x\sigma_z), \sigma_z]$. The error correction code, which will have the computational power to correct the error caused by the Pauli matrices will make the message flawless. This procedure causes the digitalization of the error, which will have a great impact on the quantum error correction code.

Types of Quantum error

The error counts in the quantum realm boil down to two fundamental errors due to the digitization of the errors. The quantum code has to encounter these two types of errors. One is the X-type error (X describes the Pauli matrix σ_x), and the other is the Z_{pau}-type error (Z_{pau} describes the Pauli matrix σ_z). The X-type error is a bit flip error, which is similar to the classical errors where the state $|0\rangle \rightarrow |1\rangle$ when operated by the Pauli X operator and viz versa.

The other error, i.e., Z_{pau}-type error, causes a phase flip of the qubits. There is no classical counterpart of this type of error. Phase flip of the qubit state is described as $Z_{pau}|0\rangle = |0\rangle$ and $Z_{pau}|1\rangle = -|1\rangle$.

Though the digitalization of the errors has reduced the error counts, but we still have some challenges in the quantum world which are unique and have no classical analog. One of this challenge is that we cannot clone (xerox) a quantum state, i.e., we cannot construct a universal unitary operator (universal xerox machine) U_c, which can xerox or copy a state as:

$$U_c|\psi\rangle|0\rangle = |\psi\rangle|\psi\rangle.$$

Whereas, in the classical realm one has the power to copy a state as required.

The second challenge is that the message to be transmitted from quantum channels is exposed to both bit-flip and phase-flip error simultaneously. So the quantum error correction code should be able to detect both these errors simultaneously. Along with these challenges, one has to keep in mind that in the quantum world measurement of a state causes wavefunction collapse, which we have no counterpart in classical theory. In classical systems, one has access to measure arbitrary properties without compromising information loss.

Stabilizer Code

In this section, we will study how to create a $[[m,n,d]]$ stabilizer code. Here m represents the total count of qubits, the count of the logical qubits is given by n, and d describes the code distance. The stabilizer represents an abelian subgroup of the m-fold Pauli group and it encodes n logical qubits into m physical qubits. We have represented the notation of the quantum codes in double brackets to differentiate it from the classical code, which is shown by a single bracket.

The structure of an $[[m,n,d]]$ stabilizer code is depicted in Fig. 3.4. From the Fig. 3.4, we can infer that n qubits $|\psi\rangle_M$ are entangled with $m-n$ qubits $|0\rangle_{m-n}$ by an encoding operation. The output state after this process is $|\psi\rangle_{Out}$. So the data that was confined in $|\psi\rangle_M$ is now distributed in the expanded Hilbert space. To detect the error that occurs during the communication, $(m-n)$ stabilizer measurements are performed. For every stabilizer P_j shown in Fig. 3.4, the syndrome extraction process is described as:

$$|\Psi\rangle|0\rangle_{m-n} \xrightarrow{\text{syndrome extraction}} \frac{1}{2}(\mathbb{1}^{\otimes n} + P_j)|\Psi\rangle|0\rangle_{A_j}$$
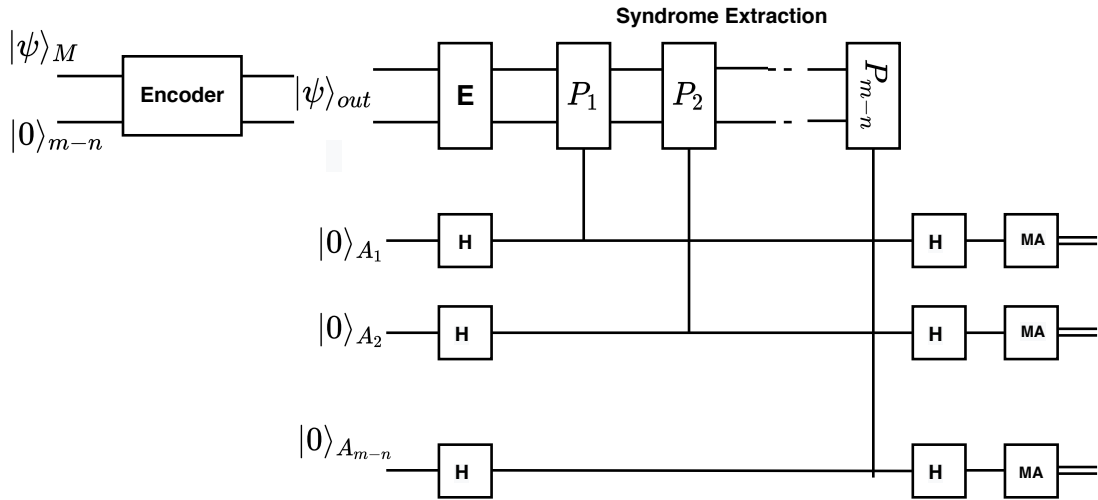
Figure 3.4. A schematic representation of the circuital analysis of $[[m,n,d]]$ stabilizer code is depicted here. $|\psi\rangle_M$ represents the message, and $|0\rangle_{m-n}$ represents the ancilla qubits. H is the Hadamard operator, and MA denotes the measurement.

$$+ \qquad \frac{1}{2}(\mathbb{1}^{\otimes n} - P_j)|\Psi\rangle|1\rangle_{A_j},$$

where $|\Psi\rangle = E|\psi\rangle_M$. The commutation relation of the stabilizer P_j with the error E provides the measurement outcomes. If P_j commutes with E the ancilla returns "0", whereas when it anti-commutes, we get "1" as the measurement outcome. The fabrication of a good code boils down to the fact that we have to find stabilizers that anti-commutes with the errors.

<div align="center">

Error correction with Stabilizer code

</div>

So we are left with the process of decoding the message. The process is to find the best fitted unitary operation $\mathbb{K}$, which would return the state to the codespace. The process of decoding the message will be successful if the action of the error E, and $\mathbb{K}$ on the codes state return the exact state, i.e., $\mathbb{K}E|\psi\rangle_{out} = (+1)|\psi\rangle_{out}$, and fails if it returns $\mathbb{K}E|\psi\rangle_{out} = S_a|\psi\rangle_{out}$, where S_a represents a logical operator.

3.3 Alternative Computation Model

The computational models that are being explored in section 3.1 are not thermodynamically efficient ones. In this section, we are going to analyze some alternative computational systems which are thermodynamically more efficient, i.e., the thermodynamic cost for the

computation is quite less due to its reversible nature. We will first discuss about the Ballistic computer, which was proposed by Fredkin and Toffoli [32], and then describe its limitation. Followed by that, we will analyze the Brownian computer which utilizes the thermal fluctuation to perform a computational process.

For the analysis of the ballistic and Brownian computer, the programming style requires a change in its form to irreversible operation from reversible one. The erasure principle of overwriting of data by other data cannot be addressed for these models. Ballistic computer fails totally to operate with irreversible operations but the Brownian computers have the power to tolerate a small amount of irreversibility in the logical operation. But it fails miserably for a large number of irreversible operations.

3.3.1   Ballistic Computer

The simple basic idea, that an idealized machine has the power to compute without dissipating any amount of kinetic energy forms the principle of the "ballistic" computation model [32]. This model consists of a hard-sphere that collides between themselves and with a fixed reflective barrier. In the input side of this computer model, we have a "starting line" from which a huge number of hard spheres are fired with equal velocity. We will be considering a ball in the starting line if we encounter a '1' in the input, and in the cases where we will get '0', there will be no ball in the starting line. The computer has some mirrors inside it with which it collides. Due to this collision process, the ball changes its direction and collides with the other balls. All the collision processes are considered to be elastic in nature, and between the collisions, the ball moves in a straight-line path with a constant velocity. The balls after a finite number of collisions reach to its finishing point. This signifies the output of the computer. The presence of a ball in the output line is considered as 1 in the output, and the absence of it as 0. The mirror of this computer is equivalent to the logic gates of our digital computers, and the balls are equivalent to the signals. The pictorial representation of this computer is shown in Fig. 3.5.

We can infer that this computer is unable to compute non-conservative Boolean functions. It has the power to implement functions whose output has an equal number of ones as in input, and it can implement bijective functions. But Toffoli has shown that one can transform any Boolean function into a conservative, bijective function. So, this model has the power to compute all functions. Though it conveys to decrease the amount of cost in energy, we encounter some drawbacks of this setup. Two main drawbacks of this system are
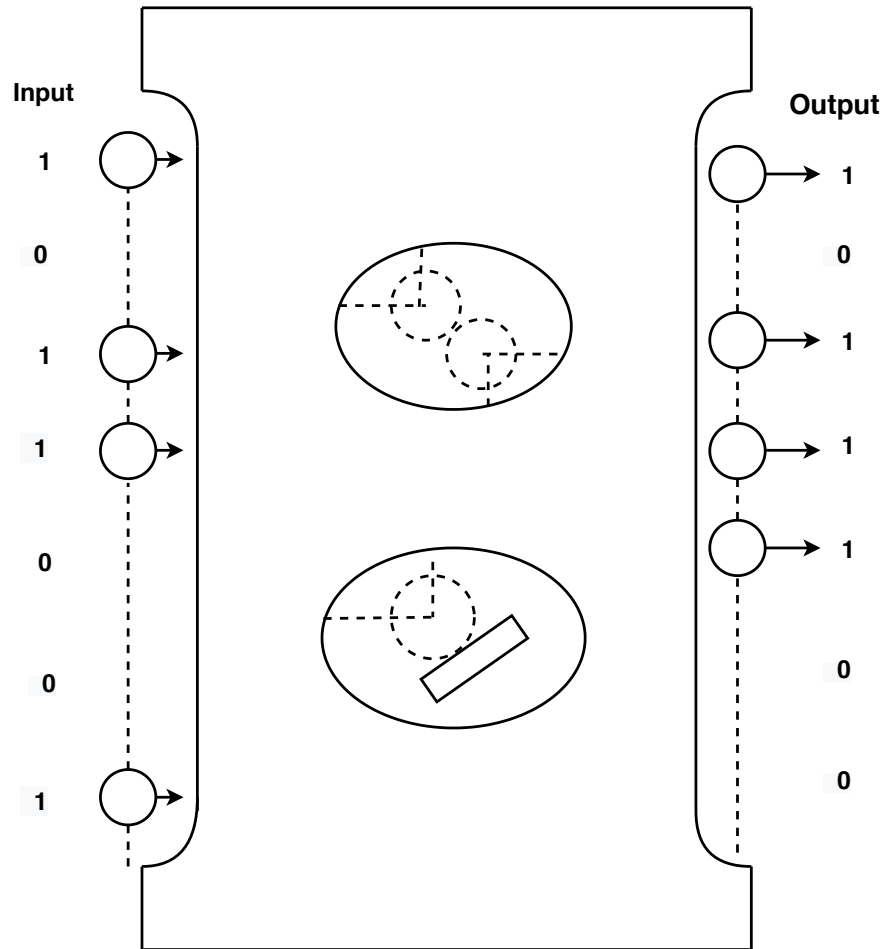
Figure 3.5. A schematic representation of a Ballistic computer proposed by Toffoli is depicted. The condition of having the same number of 1's in the input and the output should be satisfied, i.e., the boolean function should be conservative and reversible in nature.

its sensitivity to small perturbative change, and the second one is related to the collision of the balls. It is quite difficult to make each collision elastic. A small error in the positions and velocities gets amplified after each collision by a factor of 2, so the trajectory of the balls becomes unpredictable after a few numbers of collisions. The stronger the noise source the sooner the trajectory is spoiled. To get better performance we have to eliminate these noises.

One of the ways to overcome this collision problem is to correct the instability in the velocity and position of the ball after the execution of each collision process. Though this provides a solution but it makes the system thermodynamically irreversible one, but due to its low energy cost it has some practical importance. To culminate the effect of noise one can think of considering square balls instead of using spherical. It culminates the exponential growth of the errors as the balls are always parallel to the wall and to each other. Although it seems possible but it is quite unnatural as there is no proof of the existence of square atoms

in nature. Quantum effects can stabilize the system from noise, but they will bring some new instability. The wave-packet spreading causes instability in the system in the quantum realm. Benioff [252] in his work has discussed about a quantum version of the ballistic computer, where he has proposed a way to culminate the effect of the noise due to the wave packet spreading by utilizing time-independent Hamiltonian.

3.3.2   Brownian computer

We can infer from the previous section that thermal randomization is inevitable, so it is unavoidable and one can exploit this. Brownian computers [24] are such a model that exploits these properties for computation. In this model, the trajectory of the dynamical part of the system is influenced by thermal randomization in such a way that it attains Maxwell velocity. The trajectory becomes equivalent to a random walk. Despite of the chaotic nature, the Brownian computer is able to execute useful computations. The high potential barriers prevent the trajectory to escape from the system. So, within these confined walls created by the potential barriers, the system performs a random walk in the forward direction of the computation.

The state transition for the Brownian computer happens due to the random thermal movement of the part which carries the information with it. Due to its random nature, the transition can backtrace (move backward) in the computational process, undoing the transition executed recently. In the macro regime, the execution of computation using a Brownian computer seems counter-intuitive, but this is an obvious situation in the micro regime. In the case of chemical reactions, we encounter such things where the Brownian motion of the particle of the reactants orients the reactants as required for the execution of the reaction. This is equivalent to the transition state for the computational process.

Bennett has shown that one can execute a Turing machine using this thermal randomness. It is made up of clockwork which is frictionless, and rigid in form. The parts of the clockwork Turing machine should be interlocked so that they have the freedom to jiggle around locally, but restricted from moving an appreciable amount for the execution of a logical transition. In computational complexity, Reif [253] considered a similar model to analyze **P = PSPACE**.

In Fig. 3.6, the framework of the Brownian Turing machine has been depicted. The head of the Turing machine is scanning the square b of the tape. In this configuration, each tape is interlocked with some E-shaped bit storage device denoted by (e) in the figure. If it is placed up, then it represents 1, if down then 0. The device which is shown in the figure as
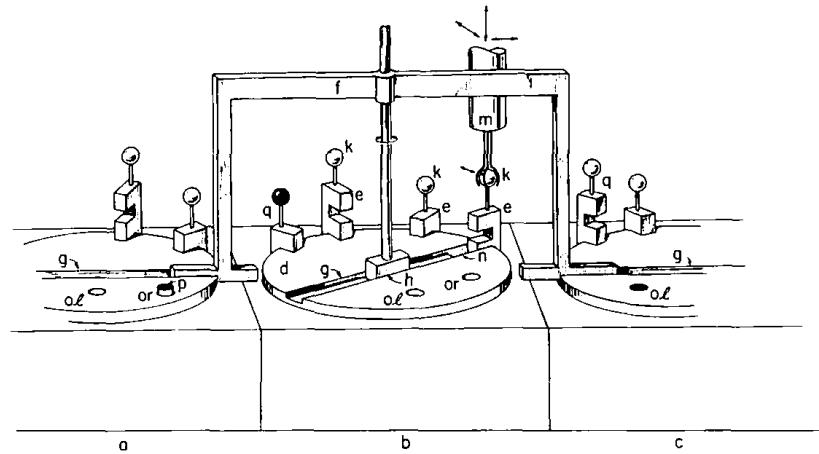
Figure 3.6. Pictorial reprentation of Brownian Turing machine. The symbols (a, b, c) depicts the Turing machine tape and the read, write and shift equipments is shown in the figure. [Adapted from Ref. [24]. Copyright 1982, Springer Nature]

(f) restricts the movement of the two adjacent squares of the tape. To change the bits of the system the knob (k) guides the way to slide the bit storage device (e) up or down with the help of the manipulator (m). To constrain the disks on the square blocks of the tape that are not scanned, a special knob (q) is attached to each square of the tape. To execute the shifting operation in this model the screwdriver of the system allows the knob (g) to get aligned with the framework (f). Now the manipulator of the framework grasps a knob and moves it to the right or left of the scanned tape. In this whole set up no springs are allowed so as to prevent friction in the system. Friction is not allowed in the system as it leads to thermodynamic dissipation.

In Bennett's model of Brownian computation, it is considered that each of the computational states will possess a unique antecedent state. A unique antecedent state is only possible when the computer executes reversible operations like the **NOT** gate. So, the antecedent state of the present state with memory 0 is 1, and vice versa. For a computer that executed irreversible operations, the antecedent state can be 0 or 1 when the memory cells have 0 value.

To acquire a unique antecedent state for each state of the system, the interlocking of the device should be executed in such a way that the device has one degree of freedom, i.e., the computational process of this device meander within this single degree of freedom. This model has limitations like it requires a configuration space with a huge accessible portion.

Bennett, in his work, has presumed that the driving force to execute the computation requires some energy gradient but, in the work [254], they have shown that one can sufficiently drive the computation process with the entropic force.

3.4   Finite state machine: Thermodynamic Interpretation

We are going to explore finite state machine (FSM) from a thermodynamics point of view [255] in this section. For the analysis, we will consider two processes, which will be the fundamental blocks that will guide us to build physical models of FSM. These models help us to describe FSM from a thermodynamic viewpoint. We will describe these two processes as $N-it$ setter and $N-it$ flips. These two processes are the generalization of bit-set and bit-flip operation. Here, we will consider three energy level systems with multiple numbers of states. The schematic representation of these two processes is shown in Fig. 3.7.
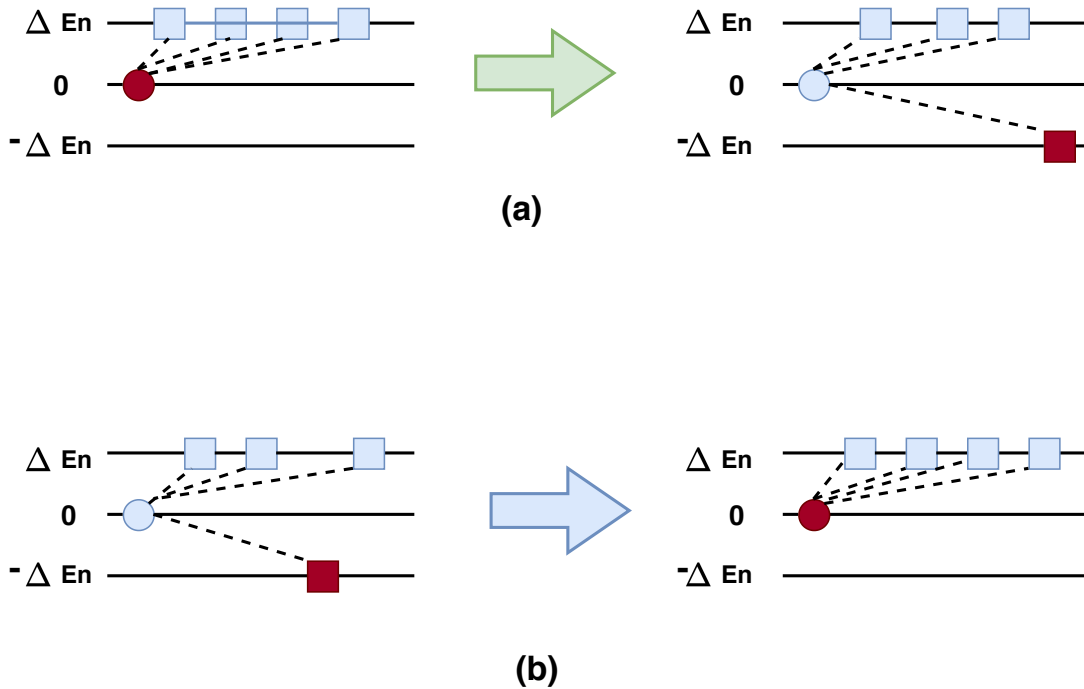
Figure 3.7. Schematic diagram of the $N-it$ setter and $N-it$ flip is shown in (a) and (b) respectively for $N=4$. The label states are depicted by circles, and the dynamic states are described by squares. The favorable state is shown in brown color. For $N-it$, setter the final target state is transferred from high energy level to the lower one whereas, in the case of $N-it$ flip, the reverse procedure is followed.

We will consider a two level system $\{c_1, c_2\}$ to conceive the idea of bit-flip and bit-set. Let us first explore about the bit-flip process. For this process, we consider the state of the process is correlated with energy level $\{-\Delta En, 0\}$. The system for this model will be kept in contact with an heat bath at some constant temperature T. The probability that the system in the state c_1 after a long time is $p(C_1) = e^{\Delta En/kT}/(1+e^{\Delta En/kT})$. For the allowed transitions between the states of the system, the energy levels are depicted as $r_{c_1 \to c_2}$ and $r_{c_2 \to c_1}$ where

$r_{c_1 \to c_2} = r^-$ and $r_{c_2 \to c_1} = r^+$ initially. According to the proposed postulates in [256], we know that the system should be balance, i.e., $r^+/r^- = e^{\Delta En/kT}$. To execute the bit-flip operation the energy level is raised to $En_1 = \Delta En$. So the transition states in this condition is $r_{c_1 \to c_2} = r^+$ and $r_{c_2 \to c_1} = r^-$. The work done to execute this whole process is:

$$\langle W_a \rangle = \frac{2r^+}{r^+ + r^-} \, ln\Big(\frac{r^+}{r^-}\Big), \tag{3.4.1}$$

and the entropy of the system is

$$S_{total} = \frac{r^+ - r^-}{r^+ + r^-} \, ln\Big(\frac{r^+}{r^-}\Big). \tag{3.4.2}$$

Similarly, one can get the Gibbs free energy for the system from the entropy. Whereas, for the bit-set operation the work done for the execution of the process can be described as

$$\langle W_a \rangle = -\frac{1}{2} \, ln\Big(\frac{r^+}{r^-}\Big), \tag{3.4.3}$$

and the entropy of the system is

$$S_{total} = ln\Big(\frac{r^+ + r^-}{2\sqrt{r^+ r^-}}\Big). \tag{3.4.4}$$

Now we will explore the process described as $N - it$ setter and $N - it$ flips from this simple model analysis. First we will explore $N - it$ setter, then we will move on to explore $N - it$ flips. Similar to the bit-flip and bit-set operation, here also we will alter the energy levels of the systems. For this multiple level systems with $N + 1$ states, the operation is complicated than that of the bit-flip operations. The multi-level states are denoted as $\{V_0, V_1, V_2, \ldots, V_N\}$ with energy levels $\{0, \Delta En, \Delta En, \ldots, \Delta En\}$ at the initial stage. After the execution of the process the energy level at the final stage is described as $\{0, \Delta En, \Delta En, \ldots, -\Delta En, \ldots, \Delta En\}$ for the states $\{V_0, V_1, V_2, \ldots, V_i, \ldots, V_N\}$. One can compute the probability of the state V_i for the initial stage analogous to the bit-flip method as $p(V_i) = \frac{e^{-\Delta En}}{1 + Ne^{-\Delta En}}$, and the probability of the state V_i for the final stage is $p(V_i) = \frac{(r^+)^2}{(r^+)^2 + r^+ r^- + (N-1)(r^-)^2}$. So the work done for the execution of the process is $W_a = \frac{2r^-}{r^+ + Nr^-} \, ln\Big(\frac{r^+}{r^-}\Big)$. Now one can compute the entropy of the system as $S_{total} = \frac{2r^-}{r^+ + Nr^-} \, ln\Big(\frac{r^+}{r^-}\Big) + log\Big(1\frac{r^+}{r^-} + \frac{r^-(N-1)}{r^+}\Big) - log\Big(1 + \frac{Nr^-}{r^+}\Big)$.

We will now explore the second operation, i.e., $N - it$ flip. Similar to the bit-flip and bit-set operation, here also we will alter the energy levels of the systems. Similarly to the $N - it$ setter the states are described by $\{V_0, V_1, V_2, \ldots, V_N\}$. One can compute the probability

of the state V_i for the initial stage analogous to the $N - it$ setter as $p(V_i) = \frac{e^{\Delta En}}{e^{\Delta En}+1+Ne^{-\Delta En}}$, and the probability of the state V_i for the final stage is $p(V_i) = \frac{r^+}{r^++Nr^-}$. So the work done for the execution of the process is $W_a = \frac{(r^+)^2}{(r^+)^2+r^+r^-+(N-1)(r^-)^2} ln\left(\frac{r^+}{r^-}\right)$. So, one can compute the entropy of the system as $S_{total} = \frac{(r^+)^2}{(r^+)^2+r^+r^-+(N-1)(r^-)^2} ln\left(\frac{r^+}{r^-}\right) + log\left(1 + \frac{Nr^-}{r^+}\right) - log\left(1\frac{r^+}{r^-} + \frac{r^-(N-1)}{r^+}\right)$.

Physical model for FSM

To analyze the thermodynamics of FSM, we have to construct a model for FSM which is thermodynamically consistent. FSM is equivalent to an inhomogeneous Markov chain, where the transitions depend on the tape symbol. To design a model for the physical implementation of FSM, one has to keep in mind about the transition based on the tape symbol. First, we will consider a Markov chain model M_c, which is nothing but a naive translation of FSM. But, the naive translation of FSM will not provide a sufficient mechanism to implement the physical system. The naive transformation is done as follows:

1. The states of M_c are described as ϑ_i. These are equivalent to the states defined for FSM.

2. The transition $tran_{ij}$ from a state to another state, i.e, from ϑ_i to some ϑ_j conditioned that it is associated with an input symbol a.

3. When an internal transition takes place, the external tape executes a movement in the forward direction, and then it takes the machine to the next tape element which has the symbol a. During this transition, the transition rate $r_{ij} = 1$ if and only if the machine is in the tape with some input symbol.

Now, if we try to implement this model, we encounter some difficulties, and we will need some helper states which are described as dynamic states [257]. The difficulties come from the transition process. To see this, let us consider a transition from ϑ_i to ϑ_j, where it is assumed that this transition occurs with a low transition rate r^- with an input symbol a. So, the different transition form ϑ_i to ϑ_m is associated with the symbol a. For the execution of this transition, the state ϑ_j should be at a high energy level. Now, it might be possible that there exists some transition from $\vartheta_k \neq \vartheta_i$ to ϑ_j with a transition rate r^+, which demands ϑ_j to be at a lower energy level. Just by adjusting the energy levels, we are not able to tackle this situation. To overcome this, helper states are required which is described as the 'dynamic state'.

For each logical state we will consider n number (n is the number of symbols) of dynamic states which will keep a track of all transition even the self-transition. The dynamic states

of the system for a input symbol a is defined as $Ds_a = \{Ds_a^{1\to 1a}, \dots, Ds_a^{M\to Ma}\}$, where M denotes the number of internal states. Similarly, the dynamic states for the system correlated with the label states ϑ_i is $Ds^i = \{Ds_a^{1\to 1(a)}, Ds_b^{1\to 1(b)}, \dots\}$. The changes in the modified form of the Markov model from the pre-defined form is

1. Now for every label state, we have n number of dynamic states with tape symbols.

2. All the forms of transition are taken into account by these dynamic sets of states.

The schematic of an FSM model using the Markov model is shown in Fig. 3.8.
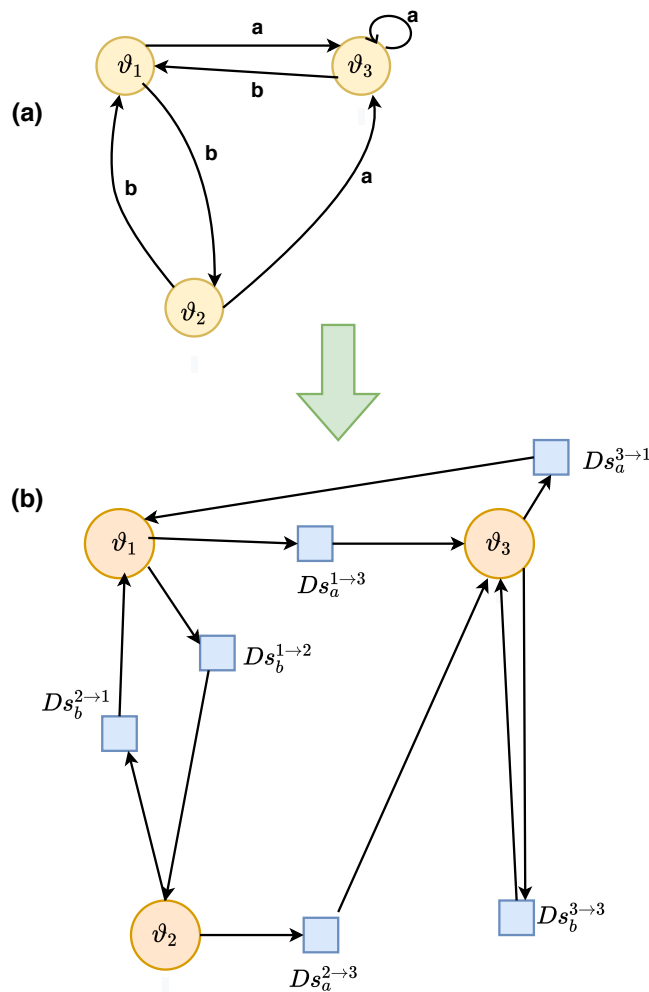
Figure 3.8. A state diagram of an FSM with three states where the accepting state is represented by ϑ_3 is shown in (a). The details to develop a state diagram for a computational process have been described in detail with an example while we were exploring finite automata in the section 3.1. The transition diagram of the Markov model designed for the same FSM is shown in (b). The dynamic states are described by the square blocks and the label state by the circles. The direction of the computation is shown by the arrows.

Now we will use this proposed Markov model to simulate any FSM. To do that one has to consider three energy levels $\{0, \pm\Delta En\}$, where the label states are at 0 energy level and the dynamic states at $\pm\Delta En$. The schematic representation of the cycle to execute an FSM is

shown in Fig. 3.9. This protocol will be analyzed for an FSM. The protocol is independent of the prior knowledge of the states. We will now describe the protocol step by step.
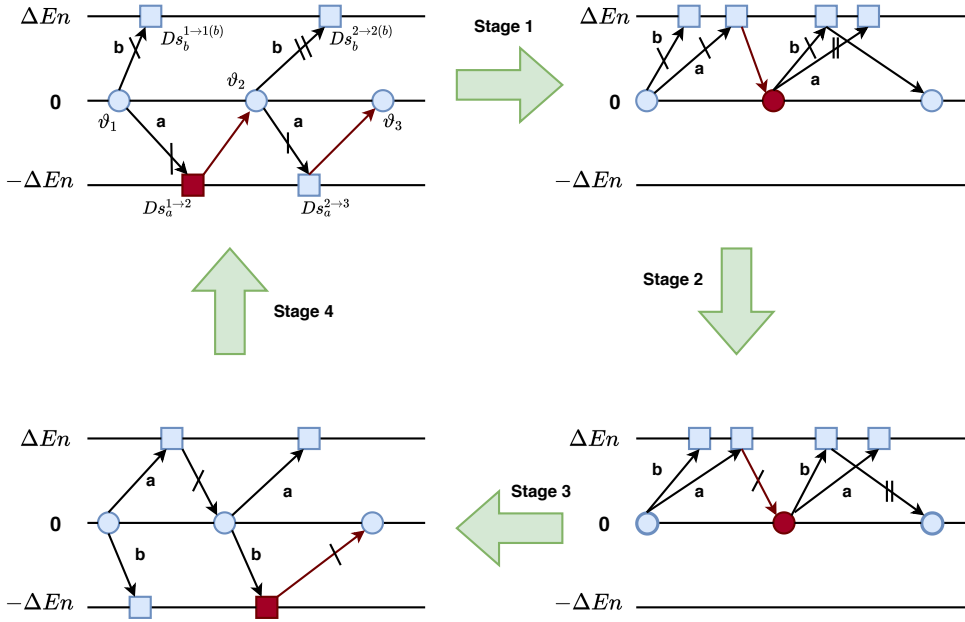
Figure 3.9. A schematic representation of the cyclic process for the computation is shown. The bluish circle and the squares describe the label states and dynamic states. The input tape is marked with brown color having the current symbol and also the current state is highlighted by brown color.

We consider an arbitrary stage for the beginning stage of the cycle of operation, where the label states ϑ_i have energy 0. The corresponding dynamic state $Ds_a^{i \to i(a)}$ of the system for the specific label state ϑ_i have energy $Enr = -\Delta En$, and the other dynamic state for symbol other than a have energy $Enr = \Delta En$. We may visualize errors in the computation as one will find the machine in different initial states. Now we will describe the four stages of the cycle.

Stage 1: In this stage of the cycle, the dynamic states are transmitted to the energy level ΔEn. In this stage of the cycle, the bit flip operation is performed. The system in this stage of the cycle gets relaxed at the label state ϑ_j after a certain period of time. Before the transition of the cycle from stage 1 to stage 2, the system should be provided with some relaxation time.

Stage 2: In this phase of the cycle, the energy barriers are removed. For the new configurations, new energy barriers are created. Such type of energy barriers helps us to reduce the energetic cost for the system and produce results with less error probability. This also helps in coarse-graining label states, which are required for the execution of the processes.

Stage 3: In this phase of the cycle, the energy levels of the dynamic states are set based on the tape symbol of the system. Before the transition of the system to the next phase of

the cycle, the system is provided some time for relaxation. In this stage of the cycle, we implement the $N - it$ setter. So the system enters the dynamic state $Ds_a^{i \to i(a)}$ for the label state ϑ_i with tape symbol a. Here the dynamic states Ds_a are transmitted from the higher energy to the lower energy, whereas the other dynamical states remain at the high energy level.

Stage 4: In this last phase of the cycle, the energy barrier is again removed and new are created for the outgoing configuration. So this stage brings back the system to its initial stage for the further execution of the process.

In this whole computational process, work is done only in two stages of the cycle, stage 1 and stage 3. In stage 1, work is done for raising the energy levels, and in stage 3, work is extracted for lowering the dynamic state for the execution. So the work done in stage 1 can be expressed as:

$$W_1 = \frac{2(r^+)^2}{(r^+)^2 + r^+ r^- + (N-1)(r^-)^2} \, ln\left(\frac{r^+}{r^-}\right).$$

And the work done in stage 3 can be expressed as

$$W_3 = -\frac{2r^-}{r^+ + nr^-} \, ln\left(\frac{r^+}{r^-}\right).$$

So the total work done for the execution of the process is:

$$\begin{aligned}
W_{total} &= \left(\frac{2(r^+)^2}{(r^+)^2 + r^+ r^- + (N-1)(r^-)^2} - \frac{2r^-}{r^+ + nr^-}\right) \\
&\quad \times \ ln\left(\frac{r^+}{r^-}\right), \\
&= 2ln\left(\frac{r^+}{r^-}\right) + \mathcal{O}\left(\frac{r^-}{r^+} ln\left(\frac{r^+}{r^-}\right)\right).
\end{aligned}$$

For $r^+ >> r^-$ the results show no dependence on the symbol count and also on the size of the machine. Along with energy cost for the execution of the cyclic process for the computation, there is also some additional energy cost. Some amount of energy is required to reset the machine to its initial state. So one can infer the thermodynamic cost is directly proportional to the number of states of an FSM but has no dependence on the number of computational steps that are executed in the process.

3.5   Turing Machine: Thermodynamic Interpretation

In this section, we are going to analyze the thermodynamic cost for the different physical models that are considered for Turing machines. First, we will discuss about the entropic one-way-ness which confirms the existence of one-way computation. Secondly, we will analyze the reversible Turing machine using different physical models and evaluate its thermodynamic costs. Stochastic thermodynamic is considered for the analysis of the dynamics of this model of TM. From the analysis, we will be able to infer that the thermodynamic complexity is bounded, whereas the Kolmogorov complexity happens to be unbounded.

3.5.1   One-way-ness

For the analysis of one-way-ness in the input machine (Turing machine), we will consider Bennett's Turing machine model [204, 258]. A one-way function is easy to compute on the set of input but it is hard to invert it being provided with the image of the random inputs. Binary memory and the measuring system are the logical structure of this model, and the logical states are controlled by the controlled-NOT gate (C-NOT gate).

In Bennett's algorithm, two non-commutative stages are utilized for the restoration and measure of the states of the memory. To execute the process, a partition is inserted in the adiabatic box that divides it into two equal half. It is assumed that no thermodynamic work is done during this insertion. Due to this insertion, the memory split up into two states. Before the execution of this process, the memory state is stored in the target bit by applying the C-NOT gate. Due to the insertion of the partition the logical state of the measuring and the measured system gets correlated. The pictorial representation of the process is shown in Fig. 3.10. The operation executed in this process randomizes the memory state.
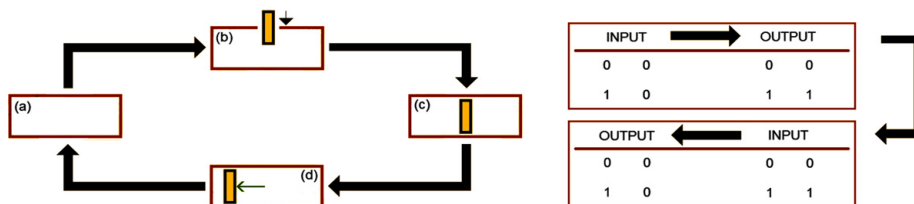
Figure 3.10. A pictorial representation of Bennett's algorithm for the Szilard one-molecule engine is shown. There exists a one to one correspondence between the initial and the final state for these reversible Turing machines. The thermodynamic analysis for this model comprises of the transition that takes place in this cycle where non-random data is changed to the random and vis versa in the cycle. [Adapted from Ref. [259]. Copyright 2014 Elsevier]

Now we are left with the merging of the two states of the system. Due to the merging of the memory state, we are going to observe certain changes in some of the macroscopic variables. Thermodynamically this operation is represented by the isothermal expansion of the system, i.e., the adiabatic box. This is equivalent to the process of compressing the piston in a Szilard engine model [21]. To execute the merging of the states, the partition is moved toward the left side of the chamber. Due to this operation, the measured and the measuring system gets detached from each other. This is represented by the fourth stage of the cycle shown in Fig. 3.10. The system is reverted back to the initial stage, and the memory is restored to its initial state. This process is equivalent to the information erasure process. Due to this erasure, we can infer from Landauer's principle, that heat will be generated in the adiabatic chamber. This will cause an increase in the entropy by an amount of $\varDelta S \geq k_B \, ln\,(2)$. The thermodynamic reversibility is maintained by the equivalent amount of decrease in the entropy of the random data.

Due to the thermodynamic reversibility of the process, one can reverse and rebuild the memory. Thermodynamically this operation can be described by the isothermal compression of the measured state as shown in Fig. 3.11. The process is executed by moving the partition wall from the left side of the chamber with volume ($\mathscr{V}$), to the center of the chamber ($\frac{\mathscr{V}}{2}$) to distribute it into two equal half. During the execution of the process, heat is extracted, and it gets converted to thermodynamic work. So in the whole process where erasure and its reversal process take place, we observe no net entropy change, as shown in Eq. (3.5.1).

$$\int_{\mathscr{V} \to \frac{\mathscr{V}}{2}} k_B \frac{d\mathscr{V}}{\mathscr{V}} + \int_{\mathscr{V} \leftarrow \frac{\mathscr{V}}{2}} k_B \frac{d\mathscr{V}}{\mathscr{V}} = 0. \tag{3.5.1}$$

where $\leftarrow$ indicates the change volume of the chamber from V to $\frac{V}{2}$, whereas the $\rightarrow$ describe the change of the volume $\frac{V}{2}$ to V.

The problem that one encounters is the closing of the cycle. An approach to solve this problem has been proposed in [259]. The approach one can think of is by moving the partition wall to the extreme right of the chamber as shown in Fig. 3.11(d′′′). The measured and the measuring system gets detached when the partition is moved to the extreme left of the chamber. Now we will discuss the method to execute this process.

The change that occurs in the memory state $\mathscr{M}_{\mathscr{D}}$ can be expressed as:

$$\frac{d}{dt}\mathscr{M}_{\mathscr{D}} = {}_{\mathscr{A}}\langle \varsigma, \mathscr{M}_{\mathscr{D}} \rangle,$$
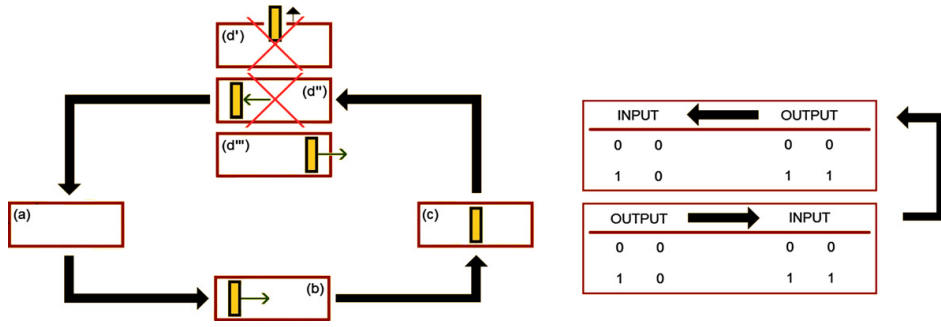
Figure 3.11. The reverse cycle for the two non-commutative stages is shown. Three approaches for the completion of the reverse cycle are considered, out of which one satisfies all the conditions. The other two processes are discarded as shown by the crossover on the box. The other two approaches were removing the partition wall without dissipation, and the other approach was to move the wall towards the extreme left of the chamber. In the adopted approach, the wall is moved towards the right of the chamber. [Adapted from Ref. [259]. Copyright 2014 Elsevier]

where ς describes the outcome of the measurement, and $\mathscr{A}$ represents the matching metric that describes the correlation between the measuring and the measured system. If $\mathscr{A} = 1$, then there exists a perfect correlation of the feedback control for Bennett's Turing machine. Whether one runs the forward cycle or the reverse cycle the dynamics can be expressed in terms of the correlation as:

$$\frac{d}{dt}\mathscr{M}_{\mathscr{D}} = \begin{cases} \varsigma\mathscr{M}_{\mathscr{D}}, & -ve\,feedback, \\ -\varsigma\mathscr{M}_{\mathscr{D}}, & +ve\,feedback. \end{cases} \tag{3.5.2}$$

So, one can define the erasure in the reverse process from Eq. (3.5.2) as

$$-\varsigma\Delta t\Big|_{+ve\,feedback} = \int_{\mathscr{M}_{\mathscr{D}a}}^{\mathscr{M}_{\mathscr{D}b}} \frac{d\mathscr{M}_{\mathscr{D}}}{\mathscr{M}_{\mathscr{D}}} = ln\left(1 + \frac{\Delta\mathscr{M}_{\mathscr{D}}}{\mathscr{M}_{\mathscr{D}a}}\right),$$

where $\mathscr{M}_{\mathscr{D}a}$, $\mathscr{M}_{\mathscr{D}b}$ describes the initial and the final state. When $\frac{\Delta\mathscr{M}_{\mathscr{D}}}{\mathscr{M}_{\mathscr{D}a}} = -\frac{1}{2}$, the information that is discarded in the process is $\varsigma = ln(2)$. This occurs when the two logical states get merged, and prevents the loss of randomness. For the forward direction, the amount is $\varsigma = -ln(2)$. As the system is immersed in an isothermal heat reservoir, the erasure of information will have a thermal effect by a factor $k_B T$. So for the reverse cycle, the system prevents the entropy increase by an amount of $\Delta S \leq k_B ln(2)$, where the equality holds for the perfect correlation. For the forward cycle, we encounter the reverse process where the system prevents the decrease in the entropy of the system by an amount $\Delta S \geq k_B ln(2)$, where the equality holds for the perfect correlation. So one can infer that the entropic one-way-ness guarantees the existence of one-way permutation.

3.5.2   Thermodynamics of reversible TM

Thermodynamically, one can consider a machine to be coupled with a heat reservoir at temperature T and a work reservoir. The primary motivation of the work reservoir is to thrive the computational process in a definite direction. The Turing machine defined in section 3.1 is irreversible in its form. If in computation, we overwrite the input tape with the output one, then the computation will be an irreversible one. So to have a reversible TM, it demands two tape one for the input and the other for the output. In a reversible TM, we will be able to retrace the computational path and trace it back to the initial state of the TM.

A logically reversible TM for the computational process was proposed by Bennett. In his work, he have shown that a irreversible TM needs four times less number of steps for the execution of a computation, than that of the logically reversible TM. Now in a recent work [212], they have modified the Bennett's treatment. Bennett in his work considered a single computation, whereas in this model they develop a TM which has the power to process a continuous stream of input string like $(\ldots, a, \mathscr{S}'_{inp}, a, \ldots, a, \mathscr{S}_{inp}, a, \ldots)$. The input tape is an infinite tape with input string described by $\mathscr{S}'_{inp}, \mathscr{S}_{inp}$. They will be separated from each other by blank symbols. The blank symbols will denote the beginning and the end of the input string. Following this, the output string can be described as $(\ldots, a, \mathscr{S}'_{out} = \mathbb{U}(\mathscr{S}'_{out}), a, \ldots, a, \mathscr{S}_{out} = \mathbb{U}(\mathscr{S}_{out}), a, \ldots)$, where $\mathbb{U} : \mathscr{S}_{inp} \to \mathscr{S}_{out}$. This model is equivalent to the model studied in other works [85, 260–264], where one manipulates the external tape to extract work.

The new TM model consists of four tapes, out of which two are the input and the output tape, and the other two are working tape and history tape. The machine comprises the working and the history tape, and the other two tapes are provided externally. This model also consists of a computation cycle. It is a five-stage cycle. The stages of this cycle are described as follows:

Stage 1: In the first stage of the cycle, the system receives an input. This input is copied from the input tape to the working tape.

Stage 2: In the second stage of the cycle, the system performs the computation process. So after the execution of the computation, the working tape has the output data. During the process, the history tape keeps the track of each step of the computational process to satisfy the reversibility of the model.

Stage 3: In this phase of the cycle, the output data in the working tape is copied to the output tape, and the working tape is reset to zero.

Stage 4: This stage of the cycle is just the reverse of the *Stage 2*. The reverse computation is done in this stage of the cycle using the data of the history tape, and then the history tape is reset.

Stage 5: In the last stage of the cycle, the working tape having the input data is copied to the input tape, and the working tape is reset to zero. This process completes the computational cycle.

This TM can be model by a continuous Markov process. The markovian master equation for this Markov process for the system $\mathscr{Y}$ with states $\mathbb{Y}$ is:

$$\frac{d}{dt}p_y(t) = \sum_{y'} \mathscr{W}_{y,y'} p_{y'}(t),$$

where $\mathscr{W}_{yy'}$ represents the rate matrix, and $p_y(t)$ is the probability to find the system in the state $y \in \mathbb{Y}$. Now for the thermodynamic interpretation of this TM, we will consider that each state of the system will be associated with an energy E_y. Due to this, an additional property is attached with the rate matrix, which is defined as $ln[\mathscr{W}_{y,y'}|\mathscr{W}_{y',y}] = -\beta(E_y - Ey')$ where $\beta = \frac{1}{k_BT}$. So, the markovian master equation [265] gets associated with the reversible TM by allowing the transition in the computation process for both the forward as well as the backward direction. In this model, it has been taken care that each state has at most two adjacent states the predecessor and the successor state. If there exist more branches then the system will have multiple predecessors and successors, which will cause the computational process to lose its reversibility. So the final form of the markovian master equation is:

$$\begin{aligned} \frac{d}{dt}p_\eta(t) &= -\left(\mathscr{W}_{\eta+1,\eta} - c_{\eta-1,\eta}\right)p_\eta(t) \\ &+ \mathscr{W}_{\eta,\eta+1}p_{\eta+1}(t) + \mathscr{W}_{\eta,\eta-1}p_{\eta-1}(t), \end{aligned} \qquad (3.5.3)$$

where $\eta \in \mathbb{Z}$, and $\mathscr{W}_{\eta,\eta+1}$, $\mathscr{W}_{\eta,\eta-1}$ describes the forward and the reverse rate respectively. The rate matrix $\mathscr{W}$ will be decomposed into blocks for each input during the computation process in stage 2 and stage 4. The transition between the different blocks of the rate matrix is prohibited during the computation process.

For the thermodynamic analysis of this model, we will couple the system with an energy landscape, which happens to be linear in its form for the computational path, i.e., the logical and the successor state are separated from each other by a constant amount ϵ_c. Due to this addition of energy, the forward and the backward transition rate should obey the local detail

balance. This in turn fixes the temperature for the environment. Now we will move on to the thermodynamic interpretation of the computation process using this TM model.

We will analyze the thermodynamics of this model at a coarse-grained level, subject to the condition that the system (computer) was active for quite some time, so that the variance $(\langle \eta^2 \rangle - \langle \eta \rangle^2)$ is large than unity. The linearity of the energy is necessary as we are interested in the steady-state regime for the analysis. So the rate of transition for this model can be described as:

$$\mathcal{W}_{\eta,\eta+1} = \Gamma_a e^{-\beta \epsilon_c/2}, \quad \mathcal{W}_{\eta+1,\eta} = \Gamma_a e^{\beta \epsilon_c/2},$$

where Γ_a represents the overall time-scale. The Fokker-Planck equation (FPE) using Eq. (3.5.3) for this model can be expressed as:

$$\frac{1}{\Gamma_c} \frac{\partial}{\partial t} p_\eta(t) = \frac{\partial}{\partial \eta} \left(-2 sinh(\frac{\beta \epsilon_c}{2}) + cosh(\frac{\beta \epsilon_c}{2}) \frac{\partial}{\partial \eta} \right) p_\eta(t).$$

The expectation value of the parameter η, which describes the count of the computational steps, and the speed of the computational process is described as:

$$\langle \eta \rangle(t) = 2\Gamma_c t \, sinh\left(\frac{\beta \epsilon_c}{2}\right),$$
$$vel \equiv \frac{d}{dt} \langle \eta \rangle(t) = 2\Gamma_c \, sinh\left(\frac{\beta \epsilon_c}{2}\right), \tag{3.5.4}$$

where vel depicts the speed of the computational process. So the variance over the parameter which counts the number of computational steps can be expressed as:

$$\langle \eta^2 \rangle(t) - \langle \eta \rangle^2(t) = 2\Gamma_c t \, cosh\left(\frac{\beta \epsilon_c}{2}\right).$$

The entropy cost for the execution of the process for this model which one can describe by the Shannon entropy is evaluated as:

$$S(t) = -\int d\eta \, p_\eta(t) \, ln p_\eta(t) = \frac{1}{2} ln\left(4\pi \Gamma_c t \, cosh\left(\frac{\beta \epsilon_c}{2}\right) \right).$$

Using Eq. (3.5.4), we can transform the Shannon entropy in term of the parameter η as:

$$S(t) = ln\left(2\pi \Gamma_c t \, cosh\left(\frac{\beta \epsilon_c}{2}\right) \langle \eta \rangle(t) \right).$$

So the entropy production rate, which in other terms is described as the rate of change of

the Shannon entropy for the computational process can be expressed as:

$$
\begin{aligned}
\dot{S}(t) &= \frac{d}{dt}S(t) + \beta \epsilon_c \, vel, \\
&= \frac{1}{2t} + 2\Gamma_c \beta \epsilon_c \, sinh\left(\frac{\beta \epsilon_c}{2}\right) \geq 0.
\end{aligned}
\tag{3.5.5}
$$

Therefore the defined model works in a thermodynamically reversible manner without any dissipation. The rate of entropy production becomes small for the condition where $\eta \to 0$ doesn't imply, and the overall production rate of the entropy throughout the process will be zero. This model also satisfies Norton's notion regarding this matter [254, 266].

We will now explore a very recent work [267] in this direction. They have considered that their physical system is associated with heat reservoirs, and its dynamics are influenced by the driving schemes [206, 268, 269]. They have considered stochastic thermodynamics for the analysis of the dynamics of these physical processes. Interested readers can go through the review article [222] which provides a detailed analysis of the stochastic thermodynamics in different aspects of computation. The state of this physical system can be equated to some logical state of a Turing machine. In this work, the authors have considered two physical processes for TM, and have analyzed three thermodynamic quantities for each physical process. The three quantities that are analyzed are as follows:

(1) The heat generated during the execution of the realization of TM will be processed for each input z. It is denoted as $Q(z)$.

(2) The heat generation for the entire computation that mapping the input z to the output y.

(3) The average heat generation $\langle Q \rangle$ minimizes the entropy production in the physical process while evaluating the input.

The physical process that is considered for analysis is the 'coin-flipping' process for the UTM. This physical model is a thermodynamically reversible model, where the input is samples of the 'coin-flipping' distribution $p(z) \propto 2^{l(z)}$, where $l(z)$ depicts the string length. The heat generation for this process of UTM is described as:

$$
Q_{cofp}(z) = l(z) + K(UTM(z)) + \mathcal{O}(1),
\tag{3.5.6}
$$

where $UTM(z)$ describes the output of UTM for the given input z, and $K(UTM(z))$ describes the *Kolmogorov complexity* for the given input string z. For a given universal Turing machine,

one can define the Kolmogorov complexity for a given bit string $z \in \mathbb{S}^{\star}$ as:

$$K_{UTM}(z) = \min_{UTM(z)=y} l(z).$$

The defined Kolmogorov complexity is an unbounded function. From the definition given in Eq. (3.5.6), one can infer that the thermodynamic complexity is a bounded function.

Being motivated by the *physical Church-Turing thesis* [270], the alternative physical process that the authors have considered in their work is a semi-computable process coined as *domination realization*. Similarly to the first physical process, the heat generation or rather heat function of the process is described as:

$$Q_{dore}(z) = K(z|TM(z)) + \mathcal{O}(1), \tag{3.5.7}$$

where $K(z|TM(z))$ represents the condition Kolmogorov complexity for the TM. This heating effect holds for this process even if TM is not even a UTM. For a semicomputation process we have $Q_{dore}(z) \leq Q(z) + \mathcal{O}(1)$. This conveys the fact that the heat generation in this process is less than the heat generation for any other semicomputable process of TM.

Now we will analyze the 'coin-flipping' process in detail. The coin-flipping distribution is expressed as:

$$CP(z) = 2^{-l(z)} \delta(f(z), y) \quad z \in dom\ UTM. \tag{3.5.8}$$

where it is conveyed that the UTM will not halt, if the input $z \notin dom\ UTM$. $CP(z)$ describes the probability of successive feeding of the bits in the UTM, where this UTM halts after receiving z number of bits. We will now calculate the thermodynamic cost of this physical process. To do this, we first normalize the distribution shown in Eq. (3.5.8) as:

$$p_z^{cofp} = \frac{CP(z)}{\sum_{z \in dom\ UTM} CP(z)}.$$

Similar to this we can define the universal distribution $CP(y) = \sum_{UTM(z)=y} 2^{-l(z)}$ and its normalized distribution is $p(UTM(z)) = \frac{CP(UTM(z))}{\sum_{z \in dom\ UTM} CP(UTM(z))}$. The heat function for this coin flipping distribution is expressed as:

$$
\begin{aligned}
Q_{cofp}(z) &= l(z) + lnCP(UTM(z)), \\
&= l(z) - K(UTM(z)) + \mathcal{O}(1). \tag{3.5.9}
\end{aligned}
$$

The minimum amount of heat required for the generation of the output for this physical process can be described as:

$$\min_{UTM(z)=y} Q_{cofp}(z) = K(y) + lnCP(UTM(z)).$$ (3.5.10)

Using Eq. (3.5.9) in Eq. (3.5.10) we have

$$\min_{UTM(z)=y} Q_{cofp}(z) = \mathscr{O}(1).$$

The average heat that is generate for a set of input strings generated from the distribution of p_z^{cofp} is:

$$\langle Q \rangle_{p_z^{cofp}} = \left[S(p_z^{cofp}) - S(p(UTM(z))) \right] + \Upsilon(p_z^{cofp}),$$

where $\Upsilon(p_z^{cofp})$ describes the entropy production in a thermodynamic process.

Now, we will analyze the second physical process coined as *dominating realization*. The heat function for this process has two properties, one is that it is semi computable, and the second is that it is optimal for the physical process. The associate function for a given TM, which is not universal is defined as:

$$\mathscr{G}_b(z) = K(z|TM(z)).$$

For a defined TM the heat function Q_{dorl} happens to be an upper semicomputable function. To compute the heat function for this process, let us consider a TM that reads some long and incompressible data of m_v bits for some input program ip. The heat function for this process can be evaluated as:

$$Q_{dorl}(ip) = K(ip|TM(ip)) \approx m_v.$$

Now when we consider the TM to be a universal TM, it guarantees us that there exists some desired output for a well-defined program. This provides us the required element of information for the analysis of the thermodynamic complexity for this physical process. So we can now compute the minimum amount of heat that is required for the computational process to execute its operation to give a desired output y. The amount is bounded by a constant and is expressed as:

$$\min_{UTM(z)=y} Q_{dorl}(z) = \mathscr{O}(1).$$

Through thorough analysis, it has been conveyed that this bound holds even if the TM is not a universal TM.

Finally, we can analyze the expected heat that is being generated while this physical process executes some computation. For the analysis, we will consider the input to be a random sample from the input distribution. For the comparison between the two processes, we will consider that the input distribution will result in minimum entropy production. The analysis shows that the expectation of heat that is being generated by this physical process during the execution of computation for a given input distribution is infinite.

To get a clear view of the two physical processes we will give a short comparison between the physical processes.

(1) For both the physical process, the minimum amount of heat that is required for the computation to generate output y is bounded by a constant. The constant defined for these two processes has no relation among them, but the thermodynamic cost for the dominating physical process is larger in principle than that of the coin-flipping.

(2) For the coin flipping process, one has to know the shortest route for the output y to get the bounded form of the heat production, whereas, in the case of dominating process the condition is quite simple and advantageous. The condition says that we can get the bounded form if the computation is fed by input which demands the print of the output y.

(3) The heat function happens to be an upper semicomputable function for the dominating physical process, whereas it is a lower semicomputable function for the coin-flipping process. So $Q_{dorl}(z) - Q_{cofp}(z) > c_\gamma$ where c_γ is a real number. The excess amount of heat that is generated in the dominating physical process is bounded. It is expressed as $Q_{dorl}(z) - Q_{cofp}(z) \leq lnK(UTM(z))$.

The above methods have provided an insight into the physical realization of the TM from a thermodynamic viewpoint. Turing machine happens to be the center of attraction to both physics and computer science. So the physical realization of TM with a more feasible and realistic model needs further investigation.

3.6   Error Correction: Thermodynamic Interpretation

After the advent of quantum error correction theory [243, 271, 272], it has experienced a rapid development. Some of the quantum codes were just mapped from the classical error correction codes mainly the classical error correction codes (CSS codes) [272]. It was then further generalized to the stabilizer codes [273–276]. Firstly, we will discuss an unsophisti-

cated model for the analysis of error correction as described in the work [277]. Here in this work, the authors have considered a reversible cycle to explain the error correction process. This cycle is a modified version of Bennett's 'Maxwell's demon'. We will explain the classical codes from a thermodynamics point of view, then we will explore the quantum error correction theory using this reversible cycle. From a thermodynamics viewpoint, quantum error correction is equivalent to a refrigerator process. In this process, one tries to sustain a steady entropy for the system even when it is subjected to environmental noises. Due to the decrease in entropy, one might intuitively think that the protocol defined for the quantum error correction violates the second law of thermodynamics. A careful analysis of the process will show that it does not violate the second law.

The author in their work [277] has considered a singlet atom confined in a box to link the information with thermodynamics. The classical information can be modeled using this system, where the atom when happens to be on the 'left-hand side' (LHS) is described as 0, and when on the 'right-hand side' it will be described as 1. Now we allow the system to expand isothermally considering that the atom exists on one of the sides. Due to this expansion, one encounters an increase in the entropy by an amount of $\Delta S = k_B \ln 2$. The atom has an equally likely probability to jump on either side of the box from its initial state. This comprises the error that can occur in the system. The protocol of the error correction is described below:

(1) We will consider that the atoms are in the LHS and RHS of the respective boxes.

(2) Let us consider that some error occurs to the particle in the box $\mathscr{A}_\alpha$. The error is defined as the probability of the atom in the box $\mathscr{A}_\alpha$ to be in the LHS or RHS of the box.

(3) Another system $\mathscr{B}_\alpha$ is kept to keep track of the system $\mathscr{A}_\alpha$. The system $\mathscr{B}_\alpha$ correlates itself with the system $\mathscr{A}_\alpha$.

(4) Based on the state of the system $\mathscr{B}_\alpha$ one will move the system $\mathscr{A}_\alpha$ to its respective side. This leaves the system $\mathscr{B}_\alpha$ in a randomized state. The execution of this process needs no work.

(5) This is the last step of the protocol where the system $\mathscr{B}_\alpha$ is brought back to its initial state by isothermal compression.

The pictorial representation of the protocol is described in Fig. 3.12. The energy of the atom in the system $\mathscr{A}_\alpha$ is $k_B T \ln 2$. Due to the error, the system undergoes a decrease in the energy by an amount $\Delta F = -k_B T \ln 2$, and the entropy of the system increase by an amount $S = k_B \ln 2$. In the third stage of the cycle, the system $\mathscr{B}_\alpha$ has the information of the $\mathscr{A}_\alpha$ as they happen to be correlated. And in the final stage of the cycle, the $k_B T \ln 2$ amount of work

is done in the system $\mathcal{B}_\alpha$ to reset the system. The amount of entropy change during this stage of the process is $S = -k_B ln2$. So the error that has been described in this model is nothing but the inability to do work. So to make the system free of this inability the system is correlated to another system. This makes the second system possess the same inability. In the reset, step entropy is wasted so the system regains its initial state. Now we will analyze the error correction in the quantum realm using this protocol.
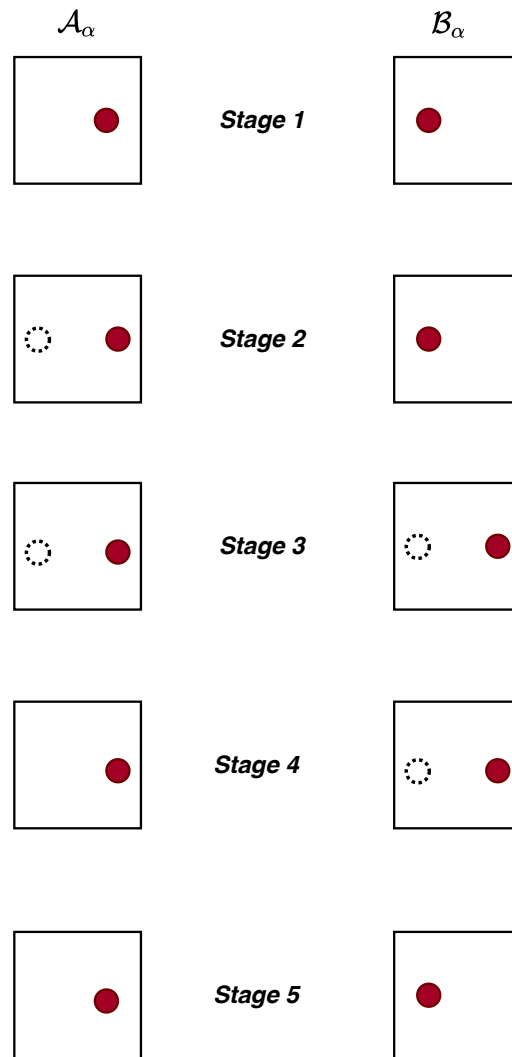
Figure 3.12. A pictorial representation of the reversible cycle which implement the classical error correction protocol is depicted. The detail description of each stage of the cycle are given in the text.

The main motivation of the quantum error correction theory is to preserve the quantum state. The protocol is described below for the pure states. One can similarly describe the protocol for the mixed states. The protocol is as follows:

(1) The state of the system after the introduction of the error is described as $\sum_j Err_j|\psi_{cs}\rangle|m\rangle|env_j\rangle$, where $|\psi_{co}\rangle$ describes the encoded state, $|m\rangle$ represents the state of the measurement device,

and the environmental state is described $|env\rangle_j$. The environmental states are orthogonal in nature. Here, it has been assumed that $\langle env_j|env_k\rangle = \delta(j,k)$.

(2) Now in the next phase of the protocol, the environmental effect is traced out. The state of the system after tracing out is $\sum_j Err_j|\psi_{co}\rangle\langle\psi_{co}|Err_j^\dagger \otimes |m\rangle\langle m|$.

(3) In this phase of the protocol, one observes the system, due to which correlation is generated between the measurement apparatus and the system. The state of the system is described as $\sum_j Err_j|\psi_{co}\rangle\langle\psi_{co}|Err_j^\dagger \otimes |m_j\rangle\langle m_j|$, where $\langle m_j|m_k\rangle = \delta(j,k)$. We have to keep in mind that if the observation is not perfect, then the protocol will not work properly, as we will not be able to get the orthogonal states of the system.

(4) During this phase of the cycle, the system gets uncorrelated. In this phase, the correction of the error is done. The state of the system after the execution of this step is $|\psi_{co}\rangle\langle\psi_{co}| \otimes \sum_j |m_j\rangle\langle m_j|$. This is not the exact state that we have started with. We have to reset the measurement state to its initial state.

(5) This is the last stage of the protocol, where we reset the measurement system to its initial state. To do this, we include a garbage system to the system. Now, the state of the system is $|\psi_{co}\rangle\langle\psi_{co}| \otimes \sum_j |m_j\rangle\langle m_j| \otimes |m\rangle\langle m|$. The state of the system by swapping the garbage system and the measurement system can be expressed as $|\psi_{co}\rangle\langle\psi_{co}| \otimes |m\rangle\langle m| \otimes \sum_j |m_j\rangle\langle m_j|$. Now the system is reset for another cycle of quantum error correction.

Similar to the analysis done for the classical code, we will analyze the entropy change that takes place throughout the protocol. The entropy of the system after the first stage of the cycle is $\Delta S = S(\rho_{ab})$, where $\rho_{ab} = \sum_j Err_j|\psi_{co}\rangle\langle\psi_{co}|Err_j^\dagger$ is the density matrix. We don't encounter a change in the entropy for the other steps except for the reset step. The entropy of the system during this reset step is $\Delta S = -S(\rho_{ab})$. The garbage system encounters a gain in the entropy of the system. The information gain by the system during the correlation step is $S(\rho_{ab})$. So from the observation, we can infer that the gain in the entropy by the garbage system is more than the information gain. This confirms that the error correction protocol is successful from a thermodynamic viewpoint.

In the work [278], the author has further extended the model described in the work [277] to include the non-maximally mixed states for the analysis of quantum error correction. In their work, they have conveyed that their system exhibits a constant entropy even when subjected to the impact of environmental noises. In their model, they have introduced some ancilla qubits which keeps a track of the error. In the refrigeration process, this is equivalent to the transfer of information of the error from the data qubit to the ancillary qubit. This causes an entropy change and cools downs the data qubits. They have also explored the

changes that occur in the quantum error correction cycle when the measurement system is not perfect, and also the information gain is not optimal. Another important aspect, i.e., how the non-orthogonal states will have an impact on the thermodynamic analysis of the error cycle is also addressed in this work.

Now we will explore a modern formalism to describe quantum error-correcting condition from a thermodynamic viewpoint as studied in the work [279]. Different interaction in a system has been modeled through various Hamiltonian, like spin chain model. One have encounter applicability of spin model in quantum information theory like in space free from decoherence [280], entanglement [281], gates [282], and even in topological quantum computing [283, 284]. Here in this work, the authors have used spin chain formalism to develop the condition of the quantum codes.

In the seminal works [244, 247, 285, 286], they have proposed the necessary and the sufficient condition for the quantum codes to correct the errors. The condition to correct the errors *err* that appears during transmission, or during storage in quantum devices can be defined as $\langle\psi|Err_a^\dagger Err_b|\psi\rangle$, where ψ is a vector $\in \mathbb{C}$, and Err_a, $Err_b \in err$. The errors are defined as a set of linear operators $err = \{Err_a : \mathbb{B} \to \mathbb{B}\}$, where $\mathbb{B}$ represents the encoding space. This encoding space has a set of orthonormal basics defined as $\{|\psi_i\rangle\}$. So, one can alternatively define the condition for quantum error correction as $\langle\psi_j|Err_a^\dagger Err_b|\psi_i\rangle = \varpi_{ab}\delta(i,j)$, where ϖ_{ab} is a constant.

For the analysis, the authors have first considered the XXO model. The Hilbert space for this model is $\mathbb{B} \simeq (\mathbb{C}^2)^{\otimes n_c}$, where n_c represents the size of the model or one can convey it as the length of the lattice. The Hamiltonian of the system is described as:

$$\mathcal{H} = -\sum_{i=1}^{n_c}\left(\sigma_j^x\sigma_{j+1}^x + \sigma_j^y\sigma_{j+1}^y + \iota\,\sigma_j^z\right), \tag{3.6.1}$$

where σ^a for $a = x, y, z$ describes the Pauli matrices and ι describes the magnetic field, and it is real in its form. This spin chain model is also called as "isotropic XY model", and was proposed in the seminal work [287]. For any thermodynamical analysis, we need the partition function Z of the system, then we can extract the information of other thermodynamic variables. The partition function for this system for $T > 0$ can be evaluated as:

$$Z = tr(2^{-\mathcal{H}/T}) = \sum_{En} 2^{n_c S}\,2^{-En/T}, \tag{3.6.2}$$

where 2^{nS} describes the degeneracy that exists within the energy levels, and S depicts the

entropy of the system. For this system, we observe that the energy and the entropy are directly proportional to n_c.

Now for this model, the partition function of the system can be evaluated as:

$$
\begin{aligned}
Z &= tr_{\mathscr{C}1}(2^{-\mathscr{H}/\mathscr{T}}) \\
&\sim \frac{n}{\pi} \int_{-\pi}^{\pi} ln(1 + 2^{-e(p)/T}) dp,
\end{aligned}
$$

where $e(p) = -4\cos p + 2\iota$. Here, the trace is taken over the subspace $\mathscr{C}1$. So, the free energy for the system can be described as $F_{en} = \frac{1}{2\pi} \int_{-\pi}^{\pi} ln(1 + 2^{-e(p)/T})$. So the entropy of the system can be described as:

$$
\begin{aligned}
S = \int_{-\pi}^{\pi} &\Big(\frac{1}{2\pi} ln\Big(\frac{1}{2\pi}\Big) - \mathscr{J}(p) ln[\mathscr{J}(p)] \\
&- \{\Big(\frac{1}{2\pi}\Big) - \mathscr{J}(p)\} ln\Big[\Big(\frac{1}{2\pi}\Big) - \mathscr{J}(p)\Big]\Big),
\end{aligned} \tag{3.6.3}
$$

where $\mathscr{J}(p_i) = \frac{1}{n_c(p_{i+1}-p_i)}$. Here $[p]$ denotes the collection of the momentum of the particles. Now we define a correlation function $\langle \mathbb{O} \rangle_T$, where $\mathbb{O}$ represents the product of Pauli operators in linear combination. The mathematical definition of this function is defined as:

$$
\langle \mathbb{O} \rangle_T = tr \frac{2^{-\mathscr{H}/T}\mathbb{O}}{Z}.
$$

This is also called as the thermodynamic correlation function. For this model, the correlation is evaluated as:

$$
\langle \mathbb{O} \rangle_T = \lim_{n_c \to \infty} \frac{\langle [p]|\mathbb{O}|[p] \rangle}{\langle [p]|[p] \rangle}.
$$

The eigenvector for this system happens to be in thermo-equilibrium space with the same $\mathscr{J}$. The thermodynamic correlation function is independent of the wave vectors $|\psi\rangle$.

In the field of statistical mechanics the probability that the system collapses in an eigenstate $|\phi_b\rangle \in \mathbb{B}$ with eigenvalue $E(|\phi_b\rangle \in \mathbb{B})$ is $\frac{2^{-\mathscr{H}/T}}{Z}$. So the subspace of this system is at the thermo-equilibrium state and one can compare this with Schumacher's subspace. This subspace asymptotically converges to the quantum error correction criteria for all types of errors. One can equivalently define the quantum codes to be an approximation of the 'thermo-equilibrium space'. To get a clear idea about this spin chain model in quantum error correction, practical implementation of this process using gates and measurement tools is required.

3.7 Some Deeper Aspects of Thermodynamic Computation

3.7.1 Engine as computer

In a simple sense, one can convey that the Carnot heat engine extracts an amount of heat Q_{hot} from the hot reservoir at temperature T_{hot} and transfers an amount of heat Q_{cold} to the sink at temperature T_{cold}. The work done to execute this process is $W_{hot \to cold} = Q_{hot} - Q_{cold}$. One will observe optimal efficiency if

$$\mathscr{L}_{hot} - \mathscr{L}_{cold} = 0,$$

where $\mathscr{L}_{hot} = -Q_{hot}/T_{hot}$ is the negentropy that is imprinted in the engine. So the loss that occurs in the process is just throwing away the negentropy of amount Q_{cold}/T_{cold}. Now we move on to analyze the computer equivalently as a Carnot cycle as shown in the work [288]. We know from the work [31, 289], that one encounters zero work balance for an ideal computer and the amount of information that is delivered during a process is $ln2\,dl = \mathscr{L}_{hot} - \mathscr{L}_{cold}$ where l denotes the amount of information.

So in the case of an ideal computer, we also encounter a loss by throwing out an equivalent amount of negentropy as in the case of the Carnot cycle.

3.7.2 Nonergodic systems and its thermodynamics

A memory device can be designed using a multistable system applied to the condition that, the transition between the states is not allowed. Alternatively, we can say that information can be stored only in a nonergodic system where the 'time average' of the system differs from the 'phase space average' of the system. In the work [290], the authors have analyzed the thermodynamics of computation with the notion that information is recorded in a multistable system. These multistable states are considered as a nonergodic states.

We will interpret the memory register in terms of thermodynamics. According to the Landauer principle, the system will confront a decrease in entropy due to restore to one (RTO) operation. Whereas in the work [290], the authors have proved that there is no change in the thermodynamic entropy even after the RTO operation. The Clausius definition of

thermodynamic entropy for a system in two states ST_a and ST_b is expressed as:

$$\Delta S = \int_{ST_a}^{ST_b} dQ/T,$$

where dQ represents the heat change in the system and T the temperature of the system. So to prove the statement proposed in the work [290] the author considered a thought experiment. The thought experiment is that we will consider a system where the particle is in a bistable-monostable potential well. This system will interact with a heat reservoir. Goto and his co-workers in their work [291, 292] coined this model as "quantum flux parametron". For the analysis, the state of the system will be described as one when the particle is found on the right side of the potential well and zero when one finds the particle to be on the left-hand side of the well. The thought experiment is as follows:

- The system is considered to be initiated in state zero. This will be the initial state of the system. The entropy of the system is S_{zero}.

- The left well of the system is lowered by applying a bias potential.

- Now the 'double-well potential' is converted to a single well. This is executed by removing the partition between this well.

- In the next stage of the process, we will remove the bias potential that was applied to the left well of the system. The system is now in a neutral state and we denote it as ST_{ne}. The state of the system of being in one or zero is denoted by ST_m.

- The bias potential is again applied, but now on the right side of the single potential well. This lowers the right side of the well.

- In the next stage of the protocol, we then revert back the single potential well into the double potential well just by recreating the partition between the left and right side of the well.

- In the final stage of the process, we remove the bias potential. The system is now in state one, and the entropy of the system is S_{one}.

The schematic representation of the thought experiment is shown in Fig. 3.13.

The first four steps of the thought experiment are called the erasing process, and the final three steps represent the writing process. If we apply RTO to the system, and the system is in the state zero, we will observe the same configuration even after the RTO operation
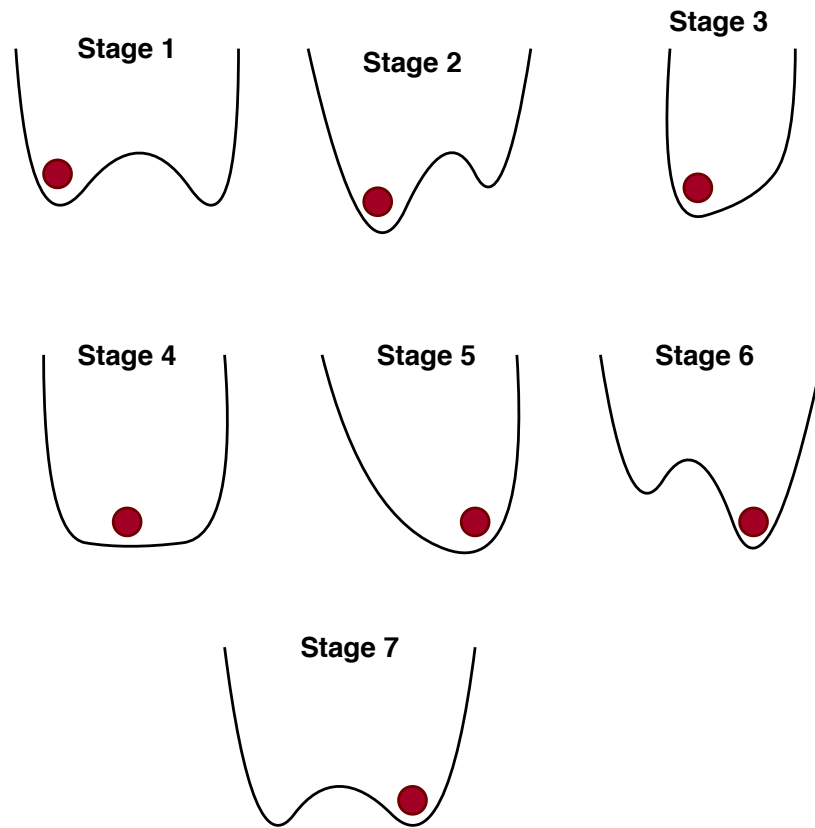
Figure 3.13. A schematic representation of the thought experiment step by step is depicted. The red solid sphere is the single atom of the system

($S_{zero} = S_{one}$), subjected to a condition that the state is known before the execution of this experiment.

From an information point of view, entropy is defined as a measure of lack of information, i.e., the lesser the information we gather about the system the higher is the entropy of the system. So, the entropy of the unknown state ST_{ukn} should have large entropy than that of the known state. Based on this notion, Landauer argued that the system will observe a decrease in entropy after RTO operation.

It is a well-known fact that when a computer runs repeated recordings and erasure occurs in a memory device. The physical equivalence of this process can be thought of as a sequence of evolution of the system from an ergodic state to a nonergodic state, and vice versa. Now we will analyze the thermodynamics of this evolution using two different models. The first model that we are going to analyze is the Szilard engine model, and the second one is the bistable-monostable potential well.

Szilard engine with one atom is the widely studied model for a memory device. This model helps us to understand the physics behind the computation. The Szilard engine model

is associated with a heat reservoir at temperature T. When the system has the partition wall the state of the system is in nonergodic state ST_{nerg} and it will be in the ergodic state ST_{erg} when one removes the partition. Now we will describe the writing process for this model. The initial state of the system is considered as ST_{erg}. Now the partition is inserted in the middle of the chamber, so work is done on the atom in the system. The work done can be expressed as $\langle W_{writing} \rangle = k_B T \, ln2$ and the heat that is generated to execute the process of writing is

$$\langle Q_{writing} \rangle = T(S_{ST_{erg}} - S_{ST_{nerg}}) = k_B T \, ln2. \tag{3.7.1}$$

The process is executed a large number of times to evaluate the expectation of the work done and the heat generation during the execution of the process.

Along with the writing process, the system goes through the erasure process. For the writing process, we have two types of erasure process. One is reversible in nature and the other is irreversible in its form. For the reversible process the work done and the creation of heat in the surrounding can be expressed as $\langle W_{erasure} \rangle = -\langle W_{writing} \rangle$ and $\langle Q_{erasure} \rangle = -\langle Q_{writing} \rangle$. So for the process, where one executes the writing process as well as the erasure process using the reversible form, one can infer that the total work is done and the heat generation is zero. One will be able to execute the reversible erasure process if the state of the system is known before the process is executed.

The second model of the erasure process is the irreversible process. The initial state of the system is now not known to us. To execute this process one removes the partition from the chamber without any prior information about the state of the memory. The removal of the partition evolves the state of the system from the nonergodic state to the ergodic state. The work done and the heat generation for this erasure process is zero but we encounter an increase in the entropy of the system. The increase of this entropy can be evaluated as $S_{erg} = k_B ln2$. So for the total process of writing and as well as the erasure process, the total work done and the heat production can be expressed as:

$$\langle W_{tirr} \rangle = \langle Q_{tirr} \rangle = k_B \, ln2, \tag{3.7.2}$$

where $\langle W_{tirr} \rangle$ and $\langle Q_{tirr} \rangle$ represents the work and heat for the total process.

Now we will explore the second model, i.e., the bistable-monostable potential well model.

In this process, the partition of the Szilard engine gets replaced by a potential wall. The writing process and the erasure process for this model are described in the thought experiment. For the writing process, the amount of work done and the heat production can be evaluated as:

$$
\begin{aligned}
\langle W_{writing} \rangle &= k_B T \ln\left(\frac{Z_{ST_{ne}}}{Z_{ST_m}}\right), \\
\langle Q_{writing} \rangle &= E_{ST_{ne}} - E_{ST_m} + k_B T \ln\left(\frac{Z_{ST_{ne}}}{Z_{ST_m}}\right),
\end{aligned}
$$

$$(3.7.3)$$

where E and Z represents the energy and partition function of the system. The partition function for the system can be evaluated as:

$$
\begin{aligned}
Z_{ST_{ne}} &= \int_{-\infty}^{\infty} e^{-V_{ne}/kT} dx, \\
Z_{ST_m} &= \int_{0}^{\infty} e^{-V_m/kT} dx,
\end{aligned}
$$

where V_{ne}, V_m describes the potential energy of the double and the single potential well. The partition function of the system is defined based on the assumption that we have considered the nonergodicity of the system. The potential wall should be chosen in such a way that it is greater than $k_B T$. The potential wall is chosen in this manner to reduce the error during the operation.

The erasure process considered for this model is the irreversible one. The irreversible erasure process is executed by diminishing the potential wall height (i.e. reducing the height of the hill), and along with that, we will not use the bias potential in this process. Due to this lowering of the height of the wall, we encounter entropy production S_{ern} in the system by an amount of $k_B ln2$. The work done and the heat production for the execution of the erasure process can be expressed as:

$$
\begin{aligned}
\langle W_{erasure} \rangle &= -\langle W_{writing} \rangle + T S_{ern}, \\
\langle Q_{erasure} \rangle &= -\langle Q_{writing} \rangle + T S_{ern}.
\end{aligned}
$$

So for the total process of writing and as well as the erasure process, the total work done and the heat production is equivalent to the results (Eq. (3.7.2)) obtained in the irreversible process of the Szilard model.

3.7.3   Thermodynamics of algorithm

It is generally believed that the advent of quantum computers will help to solve some age-old problems in number theory, physical as well as combinatorial search faster than the existing classical computers. To get a better understanding of quantum speedups, one has to consider a realistic model of computation. The realistic model should consider the time-complexity and time-space tradeoffs during analysis. Some works [293–296] have analyzed these type of models. A recent work [297] in this direction has analyzed the quantum speedups from a thermodynamic viewpoint. To analyze the cost of the algorithm (in classical and quantum regimes) from the thermodynamic perspective Brownian model of computation is considered.

For the thermodynamic interpretation of algorithms, the authors in their work [297] have considered collision finding algorithm and preimage search for their analysis. Before we move on to the thermodynamic analysis of the algorithm, we would describe the algorithms briefly. First, we will learn about the collision finding algorithm and then about the preimage search algorithm.

The parallel collision search algorithm proposed by Van Oorshot and Wiener [298] happens to be the best classical collision finding algorithm. This algorithm can detect a collision in an expected serial depth of $\mathscr{O}(\sqrt{G}/G_\alpha)$, where G denotes the range of the function and G_α depicts the parallel processes with memory $\mathscr{O}(1)$. It is assumed that the communication cost among the thread is negligible than the overall computation costs. Brassard, Hoyer and Tapp (BHT) algorithm extended this algorithm in the quantum realm in their work [299]. The operations for this algorithm is $\mathscr{O}(G^{\frac{1}{3}})$ with memory size $G^{\frac{1}{3}}$. One can further generalize this algorithm to a parallel algorithm with n_β parallel processors having memory size G_β. This generalized algorithm satisfies this condition $n_\beta < G_\beta < \mathscr{O}\big((Gn_\beta)^{\frac{1}{3}}\big)$ with a serial complexity $\mathscr{O}\big(\sqrt{\frac{G}{G_\beta n_\beta}}\big)$.

Bernstein has shown in their work [295] that the BHT algorithm, when measured in terms of memory and serial depth does not encounter any improvement over the classical algorithm, but one encounters an improvement in terms of query complexity. Giovanetti in their work [300], counters the memory cost by proposing a quantum RAM model, where they convey that memory access operation can be executed at logarithmic energy cost despite large gate complexity. So the question remains whether one can propose a realistic model where one encounters improvement of the complexity of the quantum algorithm over the classical one. Now we will see whether the Brownian model of computation provides a

solution to this proposed problem. To do so, we will first analyze the quantum version of the algorithm. For a given time t and memory size G_β, we are going to calculate the total energy that is required for the collision search. We will consider that in the BHT algorithm the energy complexity is subjugated by oracle queries over the memory access. So the energy for per operation is $\mathscr{O}\left(\frac{\left(\sqrt{\frac{G}{G_\beta n_\beta}}\right)}{t}\right)$. So the total energy for the process can be expressed as:

$$E_{quantum} = \mathscr{O}\left(n_\beta \times \sqrt{\frac{G}{G_\beta n_\beta}} \times \frac{\left(\sqrt{\frac{G}{G_\beta n_\beta}}\right)}{t}\right) = \mathscr{O}\left(\frac{GG_\beta}{t}\right).$$

Now if we consider the classical case the energy for per operation is $\mathscr{O}(\frac{\sqrt{G}}{G_\beta t})$, and the total energy for the process is:

$$E_{classical} = \mathscr{O}\left(G_\beta \times \frac{\sqrt{G}}{G_\beta t} \times \frac{\sqrt{G}}{G_\beta}\right) = \mathscr{O}\left(\frac{G}{G_\beta t}\right).$$

So we can infer from the results that this realistic model does not provide any advantage of the quantum algorithm over the classical one. So, it requires further investigation to verify whether any realistic model will provide an advantage of the quantum algorithm over the classical algorithm. One can think of applying a similar analysis for the Claw Finding problem. Its objective is to find the collision between two functions with different domain sizes, e.g., Do_1 and Do_2. The quantum version of this algorithm was explored in the work [301]. The energy cost for finding the collision in quantum regime is $\mathscr{O}\left(max\left(\frac{Do_1 Do_2}{G_b etat}, \frac{Do_1}{t}, \frac{Do_2}{t}\right)\right)$, wherein the case of classical it is $\mathscr{O}\left(\frac{(Do_1 + Do_2)^3}{G_\beta^2 t}\right)$.

Now we will analyze the second algorithm, i.e., the pre-image algorithm. One can find preimages of a function having a domain size N_γ using Grover's algorithm. The serial complexity for this algorithm is $\mathscr{O}(N_\gamma)$. An optimal serial complexity can be obtained if one considers M_γ parallel processes with memory $\mathscr{O}(1)$. The serial complexity of this optimal model is $\mathscr{O}\left(\sqrt{\frac{N_\gamma}{M_\gamma}}\right)$. This was verified in the work [302]. If one implement Grover's algorithm with Brownian computation model the energy for per operation is $\mathscr{O}\left(\frac{\sqrt{\frac{N_\gamma}{M_\gamma}}}{t}\right)$, and the total energy of the process for this quantum version is:

$$E_{quantum} = \mathscr{O}\left(\frac{\sqrt{\frac{N_\gamma}{M_\gamma}}}{t} \times M_\gamma \times \sqrt{\frac{N_\gamma}{M_\gamma}}\right) = \mathscr{O}\left(\frac{N_\gamma}{t}\right).$$

If we naively apply the Brownian computation for the classical search the total energy

for the process boils down to $E_{classical} = \mathcal{O}\left(\frac{N_\gamma^2}{M_\gamma t}\right)$. To improve the complexity of the process, one allows the Brownian motion to steer the system on a random work. If one implements the computation with M_γ parallel processes, then the complexity of the algorithm becomes equivalent to that of the quantum version. So we encounter the same asymptotic performance for the algorithm in the classical and quantum regimes.

If one compares Grover's algorithm with the classical search algorithms instead of quantum versus classical collision search, then one will encounter that Grover's algorithm is more efficient than the classical version (where powered and unpowered Brownian computation model is considered for the analysis). If the assumption of scale invariance for memory size and the energy consumption is removed for unpowered primage search, then one encounters that the preimage algorithm is memory intensive. If one considers oracle queries then also the unpowered preimage algorithm happens to be less significant than Grover's algorithm.

The results that have been discussed so far suggest that the cost of hardware happens to the prime factor that determines the advantage of the algorithms. If the cost of the hardware can be reduced, then one can even use the classical search algorithms over Grover's algorithm. One can even encounter that unpowered classical preimage search surpasses Grover's algorithm provided that the memory costs are very close to the fundamental thermodynamic limit. These results also guide us in the field of post-quantum cryptography, especially in choosing the key size of the block ciphers. It can be inferred from this analysis that doubling the key size is unnecessary. Instead of that one can make a small increase from 128 to 192 bits for better protection.

4 Background on Non-commutative Space and Quantum Information Paradox

Contents

4.1 Introduction

The formulation of quantum mechanics is greater than a century old. The starting point of its development came from the interpretation of the phenomena of black body radiation in 1900. Einstein in 1905, used the intuition of quantum-based hypothesis to analyze the photoelectric effect. Quantum theory got its new dimension when it got reframed around 1925 with the guidance of fundamental Heisenberg commutation relation and the associated uncertainty relation which conveys that no two canonical observable will commute with each other. This is called non-commutative which is the central mathematical concept expressing the uncertainty in quantum mechanics.

Quantum field theory being surfaced during the 1930s, one of the problems was to find a solution to the infinities that appeared in the theory. One of the ideas that came to the mind of the researchers was to extend the non-commutativity to the coordinates which will be to remove the infinite quantities that are appearing in this domain. This was suggested by Werner Heisenberg. This intuitive idea of Heisenberg gave birth to the concept of quantum space-time which is the generalized form of the usual space-time. In this new space-time, some of the variables which are commutative in nature in the usual space-time are assumed to be noncommuting. This gives rise to a different Lie algebra.

Peierls, who was the doctoral student of Heisenberg, used this idea in the late 1930s [303] in their work to understand the Landau problem. They also explored during their studies that in quantum space the electrons surrounded in a magnetic field can be considered as moving. This idea was carried forward to Pauli and Oppenheimer [304]. Snyder, who was the doctoral student of Oppenheimer, proposed the first concrete example in the year 1947 [305].

With the advent of renormalization theory and it's success snitched the concept of non-commutative coordinates. Later while during 1980s Connes developed noncommutative geometry [306, 307]. Connes theory was very successful and it was compelling the attention of particle physicists and string theorists [308–317].

So, the first question that pops up in one's mind is how to define a "non-commutative space-time". So, non-commutative space-time represents the deformation of the usual space-time in which the space-time coordinates x_i, which is expressible by Hermitian operators $\hat{x}_i$, will not commute with each other. Mathematically it is depicted as:

$$[x_i, x_j] = i\theta_{ij}. \tag{4.1.1}$$

Here θ_{ij} depicts the deformation parameter. It will boil down to ordinary space-time when $\theta_{ij} \to 0$. Conventionally it is considered as a real tensor [318] and antisymmetric in nature under $i \leftrightarrow j$. The dimension of this parameter is length-squared. Now, what is the physical implication of this parameter? θ_{ij} can be considered as a small patch of the area in the ij- plane which can be deemed as "observable". This is analogues to the role that is being played by $\hbar$ in $[x_i, p_j] = i\hbar\delta_{ij}$. So we can say that non-commutative space-time is a parametrization of the space time with a limit which probes in the space-time when the system approaches more towards the miniature scale. This form of space-time is sometimes called "fuzzy", as one is not to provide a explicit meaning to a "point".

The consequences of the non-commutativity of space-time are:

- One can transit from the usual quantum field theory to the action of field theory in the non-commutative space-time by substituting the field product by Moyal star-product [319].

- The uncertainty relation for the respective position operator will lead to nonlocal theory.

- The parameter θ_{ij} violates the Lorentz invariance principle then the dimension of the space-time is considered greater than two.

- The ultraviolet divergence is still persistent in this non-commutative quantum field theory.

- The non-commutativity of the space and time lead to the violation of causality [320].

Though there are some flawless features that persist in this model but still there has been a strong motivation for the exploration of non-commutative space-time. There was a strong belief that in quantum theories which also include gravity the change in space-time is natural at distance comparable to the Planck scale. The non-commutative theories are also explored as to its analogs theory to the Yang-Mills theory. One has encountered that Eq. (4.1.1) describes the low-energy limit of string theory where θ_{ij} is equivalent to the antisymmetric background field B_{ij} in the existence of D-brane. One can also encounter the essence of non-commutative field theory in condensed matter theory. Analysis of electrons placed in a magnetic field that is extrapolated to the lower Landau level is popularly depicted as the Quantum Hall problem. And it is contemplated as non-commutative Chern-Simons theory [321].

An example of the presence of non-commutative coordinates can be encountered in the analysis of non-relativistic charged particles in a strong magnetic field. Let us consider the motion of the particle to be in the X, Y plane under the influence of a magnetic field that is applied in the Z direction. The Lagrangian for the considered system is expressed as:

$$L = \frac{1}{2}mv^2 + \frac{e}{c}v.A - V(X,Y),\tag{4.1.2}$$

where m and e are the mass and charge of the particle respectively, $A_i = \{0,0,0,B_X\}$ and $V(X,Y)$ is some conserved potential. If we consider the field to be strong enough i.e., $B \to \infty$ then the Lagrangian of the system converge to

$$L = \frac{eB}{c}X\dot{Y} - V(X,Y).\tag{4.1.3}$$

Eq. (4.1.3) is equivalent to the form of $p\dot{q} - h(p,q)$ if $(\frac{eBx}{c}, Y)$ is considered as the canonical coordinates i.e., $\{X,Y\} = \frac{c}{eB}$ [322–324]. This has a close correspondence with the origin of non-commutative in string theory.

In this we will study quantum mechanics on non-commutative space rather focusing on quantum field theory. For the introduction of non-commutative space it is well suited that we consider the non-commutative quantum mechanics with commutative time evolution for our analysis rather than non-commutative quantum field theory. Non-commutative quantum mechanics is explored and analyzed in various works [325–358]. Here we will study the formulation and interpretation of quantum mechanics. Then we will see the affect of this space structure to quantum thermodynamics.

4.2 Different formalism of non-commutative quantum mechanics

In this section, we will explore some of the various formalisms of non-commutative quantum mechanics. There are various formalism to explore quantum mechanics in the commutative space. Now we will explore the various formalism that exist for the analysis of non-commutative quantum mechanics. We would explore whether they are equivalent or give some different insight into each formalism.

4.2.1   Canonical Formalism

In this formalism, we will study three different approaches to describe this formalism.

4.2.1.1   New Coordinates System

The noncommutative space can be realized with the coordinate operators satisfying Eq. (4.1.1). The phase space can be considered as:

$$[x_i, x_j] = i\theta_{ij}, \quad [x_i, p_j] = i\hbar\delta_{ij}, \quad [p_i, p_j] = 0. \tag{4.2.1}$$

We can generalize this by considering the non-commutativity of the momentum operator. This is represented as:

$$[x_i, x_j] = i\theta_{ij}, \quad [x_i, p_j] = i\hbar\delta_{ij}, \quad [p_i, p_j] = i\eta_{ij}. \tag{4.2.2}$$

where η_{ij} describes the non-commutative properties of the momentum operator in the non-commutative space.

In this form of formalism, the approach is to describe the set of non-commutative coordinates as a linear combination of the canonical variables. For this approach which is mostly used for analysis, the Hilbert space of the non-commutative space can be considered the same as that of the Hilbert space considered for the commutative space systems. The dynamics of the state can be described with the help of the usual Schrödinger equation $H|\psi_v\rangle = i\hbar\frac{\partial}{\partial t}|\psi_v\rangle$, where H is the Hamiltonian of the system in the non-commutative space.

The coordinate of the system can be expressed as:

$$\hat{x}_i = x_i + \frac{1}{2\hbar}\theta_{ij}\hat{p}_j, \quad \hat{p}_i = p_i. \tag{4.2.3}$$

This new variable satisfies the usual commutation relation and can be described as:

$$[\hat{x}, \hat{x}_j] = 0, \quad [\hat{x}, \hat{p}_j] = i\hbar\delta_{ij}, \quad [\hat{p}, \hat{p}_j] = 0. \tag{4.2.4}$$

The non-commutative parameter θ as described in Eq. (4.2.3) is very small. So one can consider the non-commutative effect as some perturbation to the commutative system by the θ parameter to its first order. Due to this reason, one can use the wavefunction and probabilities that are usually used for the analysis of the system in the commutative space.

So, the dissimilarity between the commutative and the non-commutative quantum mechanics can be described by the choice of polarization.

The non-commutative observables which for our case is the position and momentum can be described from Eq. (4.2.3) as:

$$x_i = \kappa \hat{x}_i - \frac{1}{2\hbar\kappa}\theta_{ij}\hat{p}_j, \quad p_i = \kappa\hat{p}_i + \frac{1}{2\hbar\kappa}\eta_{ij}\hat{x}_j. \qquad (4.2.5)$$

where κ is the scaling constant which is related to the non-commutativity of phase space [359, 360].

4.2.1.2   Bopp's Shift and Star Products

Fritz Bopp in this seminal paper [361] discussed the statistical implication of quantization. He also described the pseudo-differential operators which are obtained from symbol using the quantization rule

$$x \to x + \frac{1}{2}i\hbar\delta_p \quad p \to p - \frac{1}{2}i\hbar\delta_x. \qquad (4.2.6)$$

He used this transformation [361] instead of using the usual one $x \to x$ and $p \to -\frac{1}{2}i\hbar\delta_x$. In the literature, the operators that are defined in Eq. (4.2.6) are called the Bopp shift. The quantization described by Bopp in his seminal work is called Bopp quantization. The star product ($\star$-product) has a connection with Bopp's shift which is described by the associative deformation of the ordinary products on the phase space. Groenewold in his seminal paper [362] defined the $\star$-product as:

$$\star \equiv e^{\frac{i\hbar}{2}(\overleftarrow{\delta_x}\overrightarrow{\delta_p} - \overleftarrow{\delta_p}\overrightarrow{\delta_x})}. \qquad (4.2.7)$$

Bopp's shift is induced by the $\star$-product [363] in the sense that it has been evaluated through the translation of functions argument as:

$$f(x,p) \star g(x,p) = f\left(x + \frac{i\hbar}{2}\overrightarrow{\delta_p}, p - \frac{i\hbar}{2}\overrightarrow{\delta_x}\right)g(x,p). \qquad (4.2.8)$$

So one can say the non-commutative quantum mechanics that is described in this approach can be defined on a manifold where it is considered that the product of the functions will be the Moyal one [364]. The Moyal product for two given functions $f(x)$ and $g(x)$ is described as:

$$(f \star g)(x) = e^{i\theta_{ij}\delta_i^{[1]}\delta_j^{[2]}} f(x_1)g(x_2) |_{x_1 = x_2 = x}. \qquad (4.2.9)$$

So, the time-dependent Schrödinger equation for this non-commutative space approach is the same as that of the usual one and can be expressed as:

$$i\frac{\partial \psi(x,t)}{\partial t} = \left(\frac{p^2}{2m} + V(x)\right)\psi(x,t),$$ (4.2.10)

where the potential of the system is shifted as $V(x - \frac{p}{2})$ where $V(x) \star \psi(x,t) \to V(x - \frac{p}{2})\psi(x,t)$. This shows that the study of quantum mechanics in the non-commutative plane is nontrivial. This is due to the fact that the in principle the shifted potential has the arbitrary power of the momenta. So due to this reason, we will only encounter a large number of derivatives in the Schrödinger equation.

One can reduce the non-commutative approach to a variant of Bopp calculus. The variant of Bopp's shift is depicted in the map

$$x_i = \hat{x}_i - \frac{1}{2\hbar}\theta_{ij}\hat{p}_j, \quad p_i = \hat{p}_i.$$ (4.2.11)

This is equivalent to the Eq. (4.2.1).

4.2.1.3 Seiberg–Witten Map

Seiberg and Witten, in their seminal paper, which was based in the context of string theory and non-commutative geometry gave birth to the Seiberg–Witten (SW) map [312]. It was argued in the paper that, the usual gauge theory will be a gauge that is similar to the non-commutative Yang-Mills field theory. This gave rise to the bridge between the non-commutative gauge theory and the usually used i.e., the conventional gauge theory. Let us now understand what it means by the SW map. For analysis, let's consider a Minkowski space. In this space structure, the coordinates x_i are considered to self-adjoint in the considered Hilbert space which satisfies:

$$[x_i, x_j] = i\theta_{ij}.$$ (4.2.12)

where θ_{ij} is real and antisymmetric in nature. So the field theory considered happen to be equivalent to the flat manifold where the usual product is substituted by the non-local $\star$-product as:

$$(f \star g)(x) = \int \frac{d^4k}{(2\pi)^4} \int \frac{d^4p}{(2\pi)^4} e^{-i(k_i+p_i)x_i} e^{\frac{1}{2}\theta^{ij}k_ip_j} \bar{f}(k)\bar{g}(p).$$ (4.2.13)

Here f and g are the function of the manifold. The action of the non-commutative Yang-Mills theory is defined as:

$$\hat{\Omega} = -\frac{1}{4}\int d^4x \hat{F}_{ij} \star \hat{F}^{ij} = -\frac{1}{4}\int d^4x \hat{F}_{ij}\hat{F}^{ij}, \tag{4.2.14}$$

where

$$\hat{F}_{ij} = \partial_i\hat{A}_j - \partial_j\hat{A}_i - i\hat{A}_i \star \hat{A}_j + i\hat{A}_j \star \hat{A}_i. \tag{4.2.15}$$

Here $\hat{A}_i$ is the U(1) gauge field. The variable $\hat{A}_i$ is Hermitian in nature. So, the non-commutative gauge transformation is expressed as:

$$\hat{\partial}_{\hat{\lambda}}\hat{A}_i = \partial_i\hat{\lambda} - i\hat{A}_i \star \hat{\lambda} + i\hat{\lambda} \star \hat{A}_i \equiv \hat{D}_i\hat{\lambda}. \tag{4.2.16}$$

Here $\hat{\lambda}$ is the known as the gauge parameter and $\hat{\lambda} = \hat{\lambda}^\star$. Seiberg and his colleague in their paper have shown that when one expands θ, it leads to a map that connects the non-commutative gauge field $\hat{A}_i$ with the usual commutative gauge field A_i. The relation persists for the gauge parameters also. This is known as the SW map which is depicted as:

$$\begin{aligned}\hat{A}_i(A) &= A_i - \frac{1}{2}\theta^{kl}A_k(\partial_l A_i + F_{ki}) + \mathcal{O}(\theta^2) \\ \hat{\lambda}(\lambda, A) &= \lambda - \frac{1}{2}\theta^{kl}A_k\partial_l\lambda + \mathcal{O}(\theta^2).\end{aligned} \tag{4.2.17}$$

Here F_{Ki} is the Abelian field strength which is evaluated as:

$$F_{ki} = \partial_k A_i - \partial_i A_k. \tag{4.2.18}$$

It is a general notion that non-commutative quantum mechanics are generally referred to as the SW map linear transformation which relates the extended Heisenberg algebra [365] with that of the standard form of the Heisenberg algebra. The definition of an SW map is not unique [366]. With the help of one of the transformations, i.e., using a particular SW map, one can develop a representation for the non-commutative observables which are the operators acting on the Hilbert space of the usual quantum mechanics. So, the state of the system can be represented by the usual wave functions that are being used in the ordinary Hilbert space. This SW map is often considered as a alteration of the Bopp's shift [331, 367–369].

4.2.2 Path Integral formalism

Let us considered a deformed Heisenberg algebra as:

$$[\hat{x}_1, \hat{x}_2] = i\theta, \quad [\hat{x}_1, \hat{p}_1] = i\hbar, \quad [\hat{x}_2, \hat{p}_2] = i\hbar,$$

$$[\hat{p}_1, \hat{p}_2] = i\eta, \quad [\hat{x}_2, \hat{p}_1] = 0, \quad [\hat{x}_1, \hat{p}_2] = 0. \tag{4.2.19}$$

We will now study the path-integral formulation of quantum mechanics [370] which will be consistent with the Eq. (4.2.19). For the analysis, one formulates the phase space path-integral, and with the help of this, the commutation relation in Eq. (4.2.19) and the equation of motion is derived. This will be formulated in this section. The classical action in the (2+1) dimension space-time is described as:

$$S = \int_0^T dt \left(\frac{1}{2} \omega_{ij} x_i \dot{x}_j - H(x) \right), \tag{4.2.20}$$

where H is the Hamiltonian of the system and $\omega_{ij} = (\Theta^{-1})_{ij}$. Here ω_{ij} and Θ_{ij} is depicted as:

$$\omega_{ij} = \frac{1}{1 - \theta\eta} \begin{pmatrix} 0 & \eta & -1 & 0 \\ -\eta & 0 & 0 & -1 \\ 1 & 0 & 0 & \theta \\ 0 & 1 & -\theta & 0 \end{pmatrix} \qquad \Theta_{ij} = \begin{pmatrix} 0 & \theta & 1 & 0 \\ -\theta & 0 & 0 & 1 \\ -1 & 0 & 0 & \eta \\ 0 & -1 & -\eta & 0 \end{pmatrix}.$$

Here $\hbar = 1$ and the matrix Θ_{ij} is non-singular in its nature. So, $\theta\eta \neq 1$. The equation of motion and the Poisson bracket for this formalism are respectively represented as:

$$\dot{x}_i = \{x_i, H\} = \Theta_{ij} \frac{\partial H}{\partial x_j} \quad and \quad \{x_i, x_j\} = \Theta_{ij}. \tag{4.2.21}$$

The path-integral formulation for the quantum mechanics for the given action in Eq. (4.2.20) is given by

$$Z_\alpha = \int \prod_{k=1}^4 Dx_k e^{iS} = \int \prod_{k=1}^4 Dx_k e^{i \int dt \left(\frac{1}{2} \omega_{ij} x_i \dot{x}_j - H(x) \right)}. \tag{4.2.22}$$

The variable Z_α describes the transition amplitude between two states. The time ordering of the operators given by the path-integral is:

$$\int Dx O_1 O_2 e^{iS} = \langle T\{\hat{O}_1 \hat{O}_2\} \rangle. \tag{4.2.23}$$

With the discretization of the path integral as shown in the Eq. (4.2.22) and with the help of the time ordering of operators, the commutation relation can be expressed as:

$$[\hat{x}_i, \hat{x}_j] = i\Theta_{ij} = i(\omega^{-1})_{ij}. \tag{4.2.24}$$

and the extended equations of motion is described as:

$$\frac{d}{dt}\hat{x}_i = \Theta_{ij}\frac{\partial \hat{H}}{\partial \hat{x}_j} = -[\hat{x}_i, \hat{H}]. \tag{4.2.25}$$

With the commutation relation in hand as defined in Eq. (4.2.19) we derive the path-integral as shown in Eq. (4.2.22). It shows that there exists an equivalence between the path-integral and operator formalism.

Let us now highlight some of the points of the path-integral formalism:

- For the formulation of the path-integral formalism, the dimension of the space-time is considered to be (2+1). It can be extended to a higher dimension for the analysis.

- If we are able to control the commutative case then no such complication will arise for the evaluation of the non-commutative partition function due to the presence of the additional quadratic coupling between the phase space variables.

- If the matrix Θ_{ij} is singular in its form, then the two-dimensional problem get boil down to the one-dimensional problem.

For the detail understanding of the path-integral formalism for the non-commutative quantum mechanics one can take look on the referred articles [370–375].

4.2.3   Weyl Wigner Formalism

Let us consider a n-dimensional space. The extended Heisenberg algebra for this space with non-commuting position and momentum observable can be expressed as:

$$[\hat{q}_\mu, \hat{q}_\nu] = i\theta_{\mu\nu}, \quad [\hat{q}_\mu, \hat{p}_\nu] = i\hbar\delta_{\mu\nu}, \quad [\hat{p}_\mu, \hat{p}_\nu] = i\eta_{\mu\nu}, \tag{4.2.26}$$

where $\eta_{\mu\nu}$ and $\theta_{\mu\nu}$ are antisymmetric and real $(n \times n)$ matrices and $\delta_{\mu\nu}$ is the Kronecher delta function. We assume that

$$\zeta_{\mu\nu} = \delta_{\mu\nu} + \frac{1}{\hbar^2}\theta_{\mu k}\eta_{k\nu}. \tag{4.2.27}$$

is an invertible matrix. What it conveys is that for the matrix elements η and θ, the product among these two elements is smaller than $\hbar^2$, i.e., $\eta\theta \ll \hbar^2$. The algebra in Eq. (4.2.26) is related to the Heisenberg algebra via the SW map. this is depicted as:

$$\hat{q}_\mu = A_{\mu\nu}q_\nu + B_{\mu\nu}p_\nu \quad \hat{p}_\mu = C_{\mu\nu}q_\nu + D_{\mu\nu}p_\nu. \tag{4.2.28}$$

Here A, B, C, D are real matrices. This transformation is irreversible. For the formulation of the Weyl-Wigner formalism for the non-commutative quantum mechanics, let re recapitulate some concepts briefly. When we consider the usual quantum world, we can consider the map (i.e. the Weyl-wigner map) to be isomorpic in nature based on Heisenberg algebra in the usual space. This provides us the simplest approach of all for deriving the mathematical structure of the traditional phase space of the quantum mechanics [362, 376, 377]. This map which is covariant in its form has been analyzed in the seminal work [378].

The generalization of the covariant form of the Weyl-Wigner transformation and that of the SW map is the backbone for the formulation of the Weyl-Wigner formalism of the non-commutative quantum mechanics. For the exploration of non-commutativity, an extended Weyl-Wigner map is constructed, which is isomorphic in its form between the operator space and the phase representation of the extended algebra. It has been shown by the researchers, that the non-commutative Weyl-Wigner transforms, and thus the entire formulation will not have any dependency on the choice of the SW map.

Some salient features of this approach are as follows:

- We can obtain the non-commutative Wigner function by using the extended Weyl–Wigner transformation over the density matrix.

- Derivation of the extended $\star$-product and the extended Moyal bracket are executed.

- The dynamical of the system and the eigenvalue equations for non-commutative quantum mechanics are equivalent to the usual ones.

For further details of this approach, one can go to the ref. [379, 380].

4.2.4 Systematic Formalism

Here in this section, we will first introduce the non-commutating analog of the field derivatives. In the non-commutative approach, let us consider a Hermitian operator e.g., position

in our case $\hat{x}_i$ with satisfies the following commutation relation

$$[\hat{x}_i, \hat{x}_j] = i\lambda^2 \epsilon_{ij}, \qquad (4.2.29)$$

where λ is a positive constant with a dimension of length. The field derivatives for the non-commutative systems are defined as:

$$\partial_i \hat{\psi} = \epsilon_{ij} \frac{i}{\lambda^2} [\hat{x}_j, \hat{\psi}]. \qquad (4.2.30)$$

Eq. (4.2.30) satisfies the Leibniz rule, and thus it will reduce to the usual one in the commutative limit. From the definition given in Eq.. (4.2.30) the momentum operator can be defined as:

$$\hat{p}_i = i\hbar\lambda^{-2} \epsilon_{ij} ad_{x_j}, \qquad (4.2.31)$$

where $ad_{x_j}\hat{B} = [\hat{x}_i, \hat{B}]$ for an operator B.

Here we are going to present a formalism that will be completely analogous to conventional quantum mechanics. Here we consider a system that is in Hilbert space where Hilbert-Schmidt operators will be operated on the non-commutative space. The creation and the annihilation operator of the system for two-dimension which satisfies the Fock algebra [381] can be expressed as:

$$a = \frac{1}{\sqrt{2\theta}}(\hat{x}_i + i\hat{x}_2), \quad a^\dagger = \frac{1}{\sqrt{2\theta}}(\hat{x}_i - i\hat{x}_2). \qquad (4.2.32)$$

The operators satisfies the condition $[a, a^\dagger] = 1$. The non-commutative configuration space, which is isomorphic to the boson Fock space, can be expressed as:

$$\mathscr{H}_c = span\left\{|n\rangle \equiv \frac{1}{\sqrt{n}}(a^\dagger)^n|0\rangle\right\}_{n=0}^{\infty}, \qquad (4.2.33)$$

where it is considered that the span over the field of complex numbers. Let us now consider the operation of Hilbert–Schmidt operators on the non-commutative configuration space which is depicted as:

$$\mathscr{H} = \left\{\psi(\hat{x}_1, \hat{x}_2) : \psi(\hat{x}_1, \hat{x}_2) \in \mathscr{B}(\mathscr{H}_c), tr_c(\psi(\hat{x}_1, \hat{x}_2)^\dagger \psi(\hat{x}_1, \hat{x}_2)) < \infty\right\}, \qquad (4.2.34)$$

where tr_c represents the trace which is taken over the non-commutative configuration space, $\mathscr{B}(\mathscr{H}_c)$ describes the set of bounded operators on $\mathscr{H}_c$. On the other way round, we can say that the Hilbert space depicts the trace class, which envelops the Fock configuration

space algebra. As these operators happen to be bounded, so this is again a Hilbert space. To distinguish the classical configuration space from the quantum version, we will use *cl* and *qu* as a subscript. This notation is also used to distinguish operators in the classical or quantum Hilbert space.

The Heisenberg algebra, for our system, is substituted by the non-commutative Heisenberg algebra [382]. For the two dimensional systems, it is depicted as:

$$[x_i, p_j] = i\hbar\delta_{ij}, \quad [x_i, x_j] = i\theta_{ij}, \quad [p_i, p_j] = 0. \tag{4.2.35}$$

We consider operators $\hat{X}_i$ and $\hat{P}_i$ which is the unitary representation of the algebra which acts on the Hilbert space H_q. This is an analogous representation of the Schrödinger form of the Heisenberg algebra and is depicted as:

$$
\begin{aligned}
\hat{X}_i\psi(\hat{x}_1, \hat{x}_2) &= \hat{x}_i\psi(\hat{x}_1, \hat{x}_2) \\
\hat{P}_i\psi(\hat{x}_1, \hat{x}_2) &= \frac{\hbar}{\theta}\epsilon_{ij}[\hat{x}_j, \psi(\hat{x}_1, \hat{x}_2)].
\end{aligned} \tag{4.2.36}
$$

The coordinates are only considered as non-commutative in Eq. (4.2.35). This is considered so that we can define the expression Eq. (4.2.36) which requires the commutating momentum to be consistent. Now we will consider systems where the momentum component is also non-commutative in nature. So the commutation relation for the modified form is expressed as:

$$[x_i, p_j] = i\hbar\delta_{ij}, \quad [x_i, x_j] = i\theta_{ij}, \quad [p_i, p_j] = i\Gamma_{ij}. \tag{4.2.37}$$

To apply the defined formalism, we have to boil down the commutation relation in Eq. (4.2.37) to the commutation relation described in Eq. (4.2.35) by applying a linear transformation over the momentum and the coordinates. The newly transformed coordinates y_i and momentum π_i is expressed as:

$$
\begin{aligned}
y_i &= x_i \\
\pi_i &= \alpha p_i + \beta\epsilon_{ij}x_j.
\end{aligned} \tag{4.2.38}
$$

where $\alpha = \frac{\pm\hbar}{\sqrt{\hbar^2 - \Gamma\theta}}$ and $\beta = \frac{\hbar}{\theta}(1 - \alpha)$. For this values of α and β the new coordinate and the momentum will satisfy the commutation relation given in Eq. (4.2.35). We have a critical value for the parameter Γ which is described as $\Gamma = \frac{\hbar^2}{\theta}$. If $\Gamma < \frac{\hbar^2}{\theta}$ then the system is unitary in its nature and if $\Gamma > \frac{\hbar^2}{\theta}$ then the system lose its unitary.

In non-commutative quantum mechanics, the Gazeau–Klauder coherent states are studied using this formalism. This approach is used to describe the non-commutative quantum mechanics in terms of the extended objects. For details, one can look into the ref. [383, 384].

We will be considering canonical formalism for our analysis. We will develop a better bound on the extended uncertainty relation and analyze the impact of the non-commutative parameter on the thermodynamic cycles.

4.3   Non-commutative harmonic oscillator (NHO)

Now we will explore different potential problems like a harmonic oscillator, coupled harmonic oscillators, and infinite potential well problems for the different non-commutative space structures. We will be considering these systems as the working medium for the analysis of the thermodynamics process. So, we are going to explore the working principle of these working mediums in the chapter. We initiate our discussion with the basic notion of squeezed state. We can obtain the squeezed states by applying the Glauber's unitary displacement operator $D(\alpha)$ on the squeezed vacuum state [385]. The mathematical form is $|\alpha, \xi\rangle = D(\alpha)A(\xi)|0\rangle$, where $D(\alpha) = e^{(\alpha a^\dagger - \alpha^* \alpha)}$ and $A(\xi) = e^{(\xi a^\dagger a^\dagger - \xi^* aa)}$. Here α, ξ are the displacement and squeezing parameters, respectively, and $A(\xi)$ is the unitary squeezing operator. The ordering of the displacement and the squeezing operator are equivalent and it amounts to a change of parameter [385]. We can also construct the squeezed state $|\alpha, \xi\rangle$ using the ladder operator. It is obtained by performing the Holstein-Primakoff/Bogoliubov transformation on the squeezing operator [385]. It is defined as $(a + \xi a^\dagger)|\alpha, \xi\rangle = \alpha|\alpha, \xi\rangle$ where $a, \xi \in \mathbb{C}$. The operators $a, a^\dagger$ are the bosonic annihilation and creation operators, i.e., $a^\dagger|n\rangle = \sqrt{k(n+1)}|n+1\rangle$ and $a|n\rangle = \sqrt{k(n)}|n-1\rangle$, where $k(n)$ is a general function which leads to different generalized models.

The one-dimensional harmonic oscillator in the non-commutative space is defined as [386–388]:

$$H = \frac{P^2}{2m} + \frac{1}{2}m\omega^2 X^2 - \hbar\omega\left(\frac{1}{2} + \frac{\gamma}{4}\right), \tag{4.3.1}$$

satisfying the relations:

$$[X, P] = i\hbar(1 + \tilde{\gamma}P^2), \quad X = (1 + \tilde{\gamma}p^2)x, \quad P = p. \tag{4.3.2}$$

Here γ is a dimensionless constant and $\tilde{\gamma} = \gamma/(m\omega\hbar)$ has the dimension of inverse squared momentum. The observables X, P representing the non-commutative space shown in (4.3.2)

are expressed in terms of the standard canonical variables x, p satisfying $[x, p] = i\hbar$. The Hamiltonian defined in (4.3.1) is non-hermitian with respect to the inner product. The non-commutative Hamiltonian of the one-dimensional harmonic oscillator is derived from the standard one-dimensional harmonic oscillator which satisfies the condition $[X_i, P_j] = i\hbar(1 + \tilde{\gamma}P^2)$. The last term on the right-hand side appears during this transformation. The right side of the equation has a parameter γ, which represents the non-commutative parameter. We can tune the energy spectrum of the system by varying the non-commutative parameter.

We can construct the Hermitian counterpart of the defined non-Hermitian Hamiltonian shown in (4.3.1), if we assume the Hamiltonian H to be a pseudo-Hermitian, i.e., the non-Hermitian Hamiltonian H and the Hermitian Hamiltonian h are interlinked by a similarity transformation $h = \mu H \mu^{-1}$. Here $\mu\mu^{\dagger}$ is the positive definite operator, and it plays the role of the metric. Now, we can represent the eigenstates of the Hamiltonians H and h as $|\phi\rangle$ and $|\varphi\rangle$, respectively. They are related as $|\phi\rangle = \mu^{-1}|\varphi\rangle$. The Dyson map μ takes the form $\mu = (1 + \tilde{\gamma}p^2)^{-1/2}$. The Dyson map μ is defined by the same set of operators as that of the Hamiltonian. The Dyson map can be expressed in the general form as shown in previous works [389, 390] with some assumption. Following the same methodology, the relation between the Dyson map μ and the Hamiltonian parameters can be developed, which in turn satisfies the commutation relations $[x_i, x_j] = i\theta_{ij}$, where θ_{ij} is considered as a constant antisymmetric tensor. Considering this metric, we can compute the Hamiltonian h as:

$$
\begin{aligned}
h &= \mu H \mu^{-1} \\
&= \frac{p^2}{2m} + \frac{1}{2}\omega^2 x^2 + \frac{\omega\mu}{4\hbar}\left(p^2 x^2 + x^2 p^2 + 2xp^2 x\right) \\
&\quad - \hbar\omega\left(\frac{1}{2} + \frac{\mu}{4}\right) + \mathscr{O}(\mu^2).
\end{aligned}
\tag{4.3.3}
$$

Now we will use the perturbation treatment to decompose the Hamiltonian (4.3.3) into $h = h_0 + h_1$, where h_0 is taken to be the standard harmonic oscillator and h_1 as the perturbation part. Using the perturbation theory, the energy eigenvalues of H and h evolves to:

$$
E_n = \hbar\omega(An + Bn^2) + \mathscr{O}(\mu^2),
\tag{4.3.4}
$$

where $A = (1 + \mu/2)$ and $B = \mu/2$. The corresponding eigenstates of the system are

$$
\begin{aligned}
|\psi_n\rangle &= |n\rangle - \frac{\gamma}{16}\sqrt{(n-3)^{(4)}}|n-4\rangle \\
&+ \frac{\gamma}{16}\sqrt{(n+1)^{(4)}}|n+4\rangle + \mathcal{O}(\mu^2),
\end{aligned}
\tag{4.3.5}
$$

where $P = \Pi_{k=0}^{n-1}(P+k)$ represents the Pochhammer symbol with the raising factorial. Now we have all the prerequisites for the analysis of the thermodynamic cycles in these space structures.

4.4 Coupled Harmonic Oscillator

We will examine a coupled harmonic oscillator (HO) [391, 392] system specified by the coordinates x_1, x_2 and masses m_1, m_2. One can describe this using the Hamiltonian as the sum of free and interacting parts

$$
H_\alpha = \frac{p_1^2}{2m_1} + \frac{p_2^2}{2m_2} + \frac{1}{2}\left(C_1 x_1^2 + C_2 x_2^2 + C_3 x_1 x_2\right),
\tag{4.4.1}
$$

where C_1, C_2, C_3 are constant parameters and p_1, p_2 are the momentum of the two oscillators. Re-scaling the position variables of the oscillators we have:

$$
x_\alpha = \left(\frac{m_1}{m_2}\right)^{\frac{1}{4}} x_1, \quad x_\varpi = \left(\frac{m_2}{m_1}\right)^{\frac{1}{4}} x_2,
\tag{4.4.2}
$$

and similarly for the momentum we have:

$$
p_\alpha = \left(\frac{m_2}{m_1}\right)^{\frac{1}{4}} P_1, \quad p_\varpi = \left(\frac{m_1}{m_2}\right)^{\frac{1}{4}} P_2.
\tag{4.4.3}
$$

So, the Hamiltonian H_α in Eq. (4.4.1) using Eq. (4.4.2), (4.4.3) takes the form:

$$
H_{\alpha_1} = \frac{1}{2m}(p_\alpha^2 + p_\varpi^2) + \frac{1}{2}(c_1 x_\alpha^2 + c_2 x_\varpi^2 + c_3 x_\alpha x_\varpi),
\tag{4.4.4}
$$

where the parameters take the form:

$$
m = (m_1 m_2)^{1/2}, \quad c_3 = C_3, \quad c_1 = C_1\sqrt{\frac{m_2}{m_1}}, \quad c_2 = C_2\sqrt{\frac{m_1}{m_2}}.
$$

The Hamiltonian (4.4.4) represents the interaction between the two oscillators. The analysis of the system for this Hamiltonian is not so straightforward. To streamline the situation

we transform to new phase variables

$$y_i = M_{ij}x_j, \qquad q_i = M_{ij}p_j, \tag{4.4.5}$$

where M_{ij} takes the form $M_{ij} = \begin{pmatrix} cos\frac{\theta}{2} & -\sin\frac{\theta}{2} \\ \sin\frac{\theta}{2} & \cos\frac{\theta}{2} \end{pmatrix}$. Here, M_{ij} is a unitary rotation operator with the angle θ. Using this transformation (4.4.5) the Hamiltonian (4.4.4) takes the form

$$H_{final} = \frac{1}{2m}(q_\alpha^2 + q_\varpi^2) + \frac{K}{2}(e^{2\zeta}y_\alpha^2 + e^{-2\zeta}y_\varpi^2), \tag{4.4.6}$$

where $K = \sqrt{c_1c_2 - c_3^2/4}$, $e^\zeta = \frac{c_1+c_2+\sqrt{(c_1-c_2)^2+c_3^2}}{2K}$. Here e^ζ describes the coupling between the two coupled oscillators. The Hamiltonian has to satisfy the conditions $4c_1c_2 > c_3^2$ and $\alpha = \frac{c_3}{c_2-c_1}$. Solving the Hamiltonian (4.4.6) for the eigenvalues we get

$$E_{n_1,n_2} = \hbar\omega_\vartheta \left(e^\zeta \left(n_1 + \frac{1}{2} \right) + e^{-\zeta} \left(n_2 + \frac{1}{2} \right) \right). \tag{4.4.7}$$

Eq. (4.4.7) represents the energy spectrum of the two coupled harmonic oscillators in commutative space and ω_ϑ represents the frequency of the oscillator.

4.4.1 Coupled HO for non-commutative space

Now, we will analyze two coupled HO in NC spacetime. Based on the Heisenberg-Weyl algebra [393] the NC space structure abides the commutation relation

$$[x_i, x_j] = i\theta_{ij}, \ [x_i, p_j] = i\hbar\delta_{ij}, \ [p_i, p_j] = 0,$$

where $\theta_{ij} = \epsilon_{ij}\theta$ is the non-commutative parameter and δ_{ij} is the Kronecker delta which results in one when $i = j$ and zero otherwise. Here ϵ_{ij} is an antisymmetric matrix and so the non-commutative parameter θ_{ij} is a real and anti-symmetric matrix. The non-commutative parameter in the space-space like the case, i.e., when the space coordinate and the time commutes with each other, the dimension of θ_{ij} is $(length)^2$ and in the case of space-time, the dimension of this parameter is $length.time$. In our space structure models, the non-commutative parameters and their associated fundamental lengths are of the order of the Planck length. In this work, we have studied the models and their effects on thermodynamic cycles in natural units where $\hbar = 1$ and $c = 1$. One can derive this relation by using the star

product definition

$$f(x) \star h(x) = \exp\left\{\frac{i}{2}\theta_{ij}\partial_{x^i}\partial_{y^j}\right\}f(x)h(y)\Big|_{x=y}, \tag{4.4.8}$$

where f and h are two arbitrary functions of two variables x and y. This defines the general-ized quantum mechanics which boils down to the standard one when $\theta = 0$. We can develop the Hamiltonian for this space structure by using the definition (4.4.8) in Eq. (4.4.4), for NC space structure. The Hamiltonian takes the form

$$
\begin{aligned}
H^{NC}_{\alpha_1} &= \frac{1}{2m}\left(p_1^2 + p_2^2\right) + \frac{c_1}{2}\left(x_1 - \frac{\theta}{2\hbar}p_2\right)^2 + \frac{c_2}{2}\left(x_2 + \frac{\theta}{2\hbar}p_1\right)^2 \\
&\quad + \frac{c_3}{2}\left(x_1 - \frac{\theta}{2\hbar}p_2\right)\left(x_2 + \frac{\theta}{2\hbar}p_1\right).
\end{aligned} \tag{4.4.9}
$$

By transforming the Hamiltonian (4.4.9), we can develop a compact form for the Hamil-tonian. It takes the form

$$H^{NC}_1 = \frac{1}{2M}\left(\Xi_1^2 + \Xi_2^2\right) + \frac{K}{2}\left(\Theta_1^2 + \Theta_2^2\right) + \frac{K\theta}{2\hbar}\left(\Theta_2\Xi_1 - \Theta_1\Xi_2\right), \tag{4.4.10}$$

where M depicts the effective mass of the system. It is described as $M = \frac{m}{1+\left(\frac{m\omega_\vartheta\theta}{2\hbar}\right)^2}$. The effective mass, M, boils down to the defined mass m when $\theta = 0$. To establish the compact form of the Hamiltonian, we have rescaled the variables to new coordinates Ξ_i and Θ_i. If we compare Eq. (4.4.10) with Eq. (4.4.6), we will encounter an extra term in the Hamiltonian of NC space which is a function of θ. The new co-ordinates defined in Eq. (4.4.10) (Θ, Ξ) which represents the position and the momentum variables respectively are expressed in terms of creation and annihilation operators as:

$$\Theta_i = \sqrt{\frac{\hbar\Omega}{2K}}\left(b_i + b_i^\dagger\right), \quad \Xi_i = i\sqrt{\frac{M\hbar\Omega}{2}}\left(b_i^\dagger - b_i\right), \tag{4.4.11}$$

which satisfy the relation

$$[b_i, b_j^\dagger] = \delta_{ij},$$

where $b_i, b_j^\dagger$ are the annihilation and creation operator respectively. The effective frequency Ω is a function of θ and is described as $\Omega = \sqrt{\frac{K}{M}}$. We can re-define the Hamiltonian in Eq. (4.4.10) by transforming it with another set of operators. The new Hamiltonian takes the form

$$H^{NC}_{final} = \hbar\Omega_1 B_1^\dagger B_1 + \hbar\Omega_2 B_2^\dagger B_2 + \hbar\Omega, \tag{4.4.12}$$

where $\Omega_1 = \Omega + \frac{K\theta}{2\hbar}, \Omega_2 = \Omega - \frac{K\theta}{2\hbar}$. The new operators are expressed as

$$B_1 = \frac{1}{\sqrt{2}}(b_1 + ib_2), \quad B_2 = \frac{1}{\sqrt{2}}(-b_1 + ib_2), \quad B_1 = \frac{1}{\sqrt{2}}(b_1^\dagger - ib_2^\dagger), \quad B_2 = \frac{1}{\sqrt{2}}(-b_1^\dagger - ib_2^\dagger),$$

where b_1, b_2 are the annihilation operator and $b_1^\dagger, b_2^\dagger$ are the creation operator. The most compact form of the Hamiltonian for the considered NC space structure is defined in Eq. (4.4.12). Solving this Hamiltonian the energy eigenvalues results as

$$E^{NC}_{n_1,n_2} = \hbar\Omega_1 n_1 + \hbar\Omega_2 n_2 + \hbar\Omega. \qquad (4.4.13)$$

The energy spectrum for the coupled HO for the considered NC space structure is depicted in the Eq. (4.4.13).

4.4.2 Coupled HO for generalized NC space

We will consider a generalized NC space for our analysis. We call this generalized NC space because the deformation is considered for both the co-ordinate ad momentum space, i.e., the commutation relation for both these space structures results in non-zero. The position and the momentum of this space structure satisfies the following commutation relation

$$[\hat{x}_i, \hat{x}_j] = i\gamma_{ij}, \quad [\hat{p}_i, \hat{p}_j] = i\xi_{ij}, \quad [\hat{x}_i, \hat{p}_j] = i\hbar\delta_{ij},$$

where $\gamma_{ij} = \epsilon_{ij}\gamma, \xi_{ij} = \epsilon_{ij}\xi$ is the non-commutative parameter and δ_{ij} represents the Kronecker delta. Here ϵ_{ij} represents an antisymmetric matrix. We can define the Hamiltonian for this space structure (as in [392]) by separating out the Hamiltonian (4.4.6) into two parts which are described as:

$$\mathcal{H}_1^{GNC} = \left(\frac{e^\zeta \sqrt{K} \sin a}{\sqrt{2}} y_\alpha + \frac{\cos a}{\sqrt{2m}} q_\varpi\right)^2 + \left(\frac{e^{-\zeta} \sqrt{K} \sin b}{\sqrt{2}} y_\varpi + \frac{\cos b}{\sqrt{2m}} q_\alpha\right)^2,$$

$$\mathcal{H}_2^{GNC} = \left(\frac{e^\zeta \sqrt{K} \cos a}{\sqrt{2}} y_\alpha - \frac{\sin a}{\sqrt{2m}} q_\varpi\right)^2 + \left(\frac{e^{-\zeta} \sqrt{K} \cos b}{\sqrt{2}} y_\varpi - \frac{\sin b}{\sqrt{2m}} q_\alpha\right)^2. \quad (4.4.14)$$

Here a and b take values such that:

$$\sin(a-b) = \frac{\hbar\sqrt{Km}(e^\zeta + e^{-\zeta})}{\lambda_1}, \cos(a-b) = \frac{Km\gamma - \xi}{\lambda_1},$$

$$\sin(a+b) = \frac{\hbar\sqrt{Km}(e^\zeta - e^{-\zeta})}{\lambda_2}, \cos(a+b) = -\frac{Km\gamma + \xi}{\lambda_2},$$

where $\lambda_1 = (e^\zeta + e^{-\zeta})\hbar \sqrt{Km} \sqrt{1 + \Delta_1}$, and $\lambda_2 = (e^\zeta - e^{-\zeta})\hbar \sqrt{Km} \sqrt{1 + \Delta_2}$. Here Δ_1 and Δ_2 denote the non-commutative effect of the phase space. When $\gamma = \xi = 0$, we have $\Delta_1 = \Delta_2 = 0$, and it returns to the ordinary commutative phase space. Δ_1, Δ_2 is evaluated as $\Delta_1 = \frac{(Km\gamma - \xi)^2}{(e^\zeta + e^{-\zeta})^2 \hbar^2 Km}$, and $\Delta_2 = \frac{(Km\gamma + \xi)^2}{(e^\zeta - e^{-\zeta})^2 \hbar^2 Km}$.

By further simplification the compact form for a and b is evaluated as

$$a = \frac{1}{2}\Big(\arctan\Lambda + \arctan\varkappa\Big),$$

$$b = \frac{1}{2}\Big(\arctan\Lambda - \arctan\varkappa\Big),$$

where $\Lambda = \frac{\hbar \sqrt{Km}(e^\zeta - e^{-\zeta})}{-(Km\gamma + \xi)}$, and $\varkappa = \frac{\hbar \sqrt{Km}(e^\zeta + e^{-\zeta})}{Km\gamma - \xi}$. To obtain the eigenvalues we have to solve the Hamiltonian (4.4.14). So, the energy eigenvalues of the Hamiltonian for the considered NC space results to

$$\begin{aligned} E_{n_1,n_2} &= E_{n_1}^{(1)} + E_{n_2}^{(2)} \\ &= \frac{1}{2m}\Big((n_1 + n_2 + 1)\lambda_1 + (n_1 - n_2)\lambda_2\Big) \\ &= \frac{\hbar\omega_\vartheta}{2}\Big((n_1 + n_2 + 1)(e^\zeta + e^{-\zeta})\sqrt{1 + \Delta_1} + (n_1 - n_2)(e^\zeta - e^{-\zeta})\sqrt{1 + \Delta_2}\Big) \\ &= \hbar\Big(n_1\omega_a + n_2\omega_b + \frac{\omega}{2}(e^\zeta + e^{-\zeta})\sqrt{1 + \Delta_1}\Big), \end{aligned} \qquad (4.4.15)$$

where the frequencies are defined as:

$$\begin{aligned} \omega_a &= \frac{\omega_\vartheta}{2}\Big\{(e^\zeta + e^{-\zeta})\sqrt{1 + \Delta_1} + (e^\zeta - e^{-\zeta})\sqrt{1 + \Delta_1}\Big\} \\ \omega_b &= \frac{\omega_\vartheta}{2}\Big\{(e^\zeta + e^{-\zeta})\sqrt{1 + \Delta_1} - (e^\zeta - e^{-\zeta})\sqrt{1 + \Delta_1}\Big\}. \end{aligned} \qquad (4.4.16)$$

So, the energy spectrum of coupled harmonic oscillator for the generalized NC space is depicted in Eq. (4.4.15).

4.5   Generalized Uncertainty Principle in relativistic regime

Here, we explore the analysis of generalized uncertainty principle [394] in the relativistic regime. The well known quadratic GUP was first proposed in the work [395], which takes the form as:

$$[x^i, p^j] = i\hbar\delta^{ij}(1 + g(p^2)), \qquad (4.5.1)$$

where $i, j \in \{1, 2, 3\}$, with δ^{ij} being the Kronecker delta function which results to 1 when $i = j$ and zero otherwise. Here, x and p represent the position and momentum of a particle respectively. This form of the space structure was proposed for the non-relativistic regime. The position operators for this model obeys the commutation relation

$$[x^i, x^j] = -i\hbar g(p^2)(x^i p^j - x^j p^i). \tag{4.5.2}$$

For our analysis we consider a non-commutative space [394] which obeys the following commutation relation

$$[x^i, p^j] = i\hbar \left(\left[1 + (\epsilon - \alpha)\zeta^2 p^\delta p_\delta \right] \eta^{ij} + (\beta + 2\gamma)\zeta^2 p^i p^j \right), \tag{4.5.3}$$

where $i, j \in \{0, 1, 2, 3\}$ and α, ϵ, β, γ are dimensionless parameters. The parameter ζ takes the form $\zeta = \frac{1}{cM_{pl}}$ and has the dimension of inverse momentum and η^{ij} takes the signatures $\{-, +, +, +\}$ of the Minkowski spacetime. Here, M_{pl} is the Planck mass. Eq. (4.5.3) reduces to non-relativistic limit (Eq. (4.5.1)) when $c \to \infty$, and when $\zeta \to 0$ the system boils down to the non-GUP limit where the standard Heisenberg algebra works.

If we take a clear note, we can visualize that the physical observables (the position and the momentum) of the system are not canonically conjugate. By introducing the variables x_0^i and p_0^i (where $p_0^i = -i\hbar \frac{\partial}{\partial x_{0i}}$) which are canonically conjugate in nature the position and the momentum can be expressed up to the second-order of ζ as[1]

$$
\begin{aligned}
x^i &= x_0^i - \alpha\zeta^2 p_0^\delta p_{0\delta} x_0^i + \beta\zeta^2 p_0^i p_0^\delta x_{0\delta} + \gamma\zeta^2 p_0^i, \\
p^i &= p_0^i (1 + \epsilon\zeta^2 p_0^\delta p_{0\delta}).
\end{aligned}
\tag{4.5.4}
$$

Using Eq. (4.5.4) the commutation relation for the position operators becomes

$$[x^i, x^j] = i\hbar\zeta^2 \frac{2\alpha + \beta}{1 + (\epsilon - \alpha)\zeta^2 p^\delta p_\delta}(x^i p^j - x^j p^i). \tag{4.5.5}$$

The last two terms in the expression of x^i of Eq. (4.4.4) break the isotropy of the space-time and violates the relativity principles while introducing the preferred direction of p_0^i. So, from now onward we will consider $\beta = \gamma = 0$ for further analysis.

---

[1]Einstein's summation convention is followed throughout this work.

4.6   One-dimensional potential problems in NC space with relativistic and GUP correction

In this section, we are going to revisit the analysis of some of the one-dimensional (1-D) potential systems for this non-commutative space structure. For the analysis, we substitute $\epsilon = \alpha$ in Eq. (4.5.4) (we use this condition to keep the Poincare algebra undeformed) and neglecting the last two terms of x^i we have:

$$
\begin{aligned}
x^i &= x_0^i - \alpha\zeta^2 p_0^\delta p_{0\delta} x_0^i, \\
p^i &= p_0^i (1 + \alpha\zeta^2 p_0^\delta p_{0\delta}).
\end{aligned}
\tag{4.6.1}
$$

The Klein-Gordon (KG) equation in terms of the variables p_0^i is

$$
p_0^\delta p_{0\delta}(1 + 2\alpha\zeta^2 p_0^\rho p_{0\rho}) = -m^2 c^2,
\tag{4.6.2}
$$

where m is the mass of the relativistic particle. Solving Eq. (4.6.2) in terms of $p_0^\delta p_{0\delta}$ we get:

$$
\begin{aligned}
p_0^\delta p_{0\delta} &= -\frac{1}{4\alpha\zeta^2} + \left(\frac{1}{(4\alpha\zeta^2)^2} - \frac{m^2 c^2}{2\alpha\zeta^2}\right)^{\frac{1}{2}}, \\
&\simeq -m^2 c^2 - 2\alpha\zeta^2 m^4 c^4 - \mathcal{O}(\zeta^4).
\end{aligned}
\tag{4.6.3}
$$

The higher-order terms are discarded, and along with that, the other solution of the KG equation is not taken into account as it does not reduce to $m^2 c^2$ when $\zeta \to 0$.

One can rewrite Eq. (4.6.3) as:

$$
-E^2 + c^2 p_0^2 + m^2 c^4 + 2\alpha\zeta^2 m^4 c^6 = 0.
\tag{4.6.4}
$$

Now solving the Eq. (4.6.4), we can evaluate the expression of the energy for the system. It takes the form

$$
E = mc^2(1 + \alpha\zeta^2 m^2 c^2) + \frac{p_0^2}{2m}\left(1 - \frac{1}{2}\alpha\zeta^2 m^2 c^2\right) - \frac{p_0^4}{8m^3 c^2}\left(1 - 3\alpha\zeta^2 m^2 c^2\right).
\tag{4.6.5}
$$

The energy expression consists of the rest mass term, the non-relativistic kinetic energy term, along with that it possesses relativistic and GUP corrections. Now, the Schrödinger equation with relativistic and the GUP corrections, is defined as:

$$
\begin{aligned}
i\hbar\frac{\partial}{\partial t_0}\psi(t_0,x_0) &= \Big[mc^2(1+\alpha\zeta^2 m^2 c^2)+\frac{\hbar^2}{2m}(1-\frac{1}{2}\alpha\zeta^2 m^2 c^2)\nabla_0^2 \\
&+ \frac{\hbar^4}{8m^3 c^2}(1-3\alpha\zeta^2 m^2 c^2)\nabla_0^4 + V(x)\Big]\psi(t_0,x_0).
\end{aligned}
\tag{4.6.6}
$$

One can solve Eq. (4.6.6) for a different potential problem with relativistic and GUP correction, to develop the wavefunction and the physical energy of the considered problem. We will consider two such potential problems for our analysis. One of which is the one-dimensional infinite potential well, and the other is the harmonic oscillator.

4.6.1 One Dimensional Potential Well

The 1-D potential well for 1+1 dimensional case is defined as:

$$
V(x) = \begin{cases} V_0, & for\ \ 0 < x < L, \\ \infty, & for\ \ x \le 0 \ \cup \ x \ge L. \end{cases}
\tag{4.6.7}
$$

The physical dimensions of the 1-D box for the system under consideration can be evaluated from Eq. (4.6.1). It s expressed as:

$$
L = L_0[1 + \alpha\zeta^2 m^2 c^2 + \mathcal{O}(\zeta^4)].
\tag{4.6.8}
$$

Solving the Schrödinger equation (Eq. (4.6.6)) for this potential problem, the energy of the system results to

$$
E_n = -\frac{n^2\hbar^2\pi^2}{2mL^2}\Big[1+\frac{3}{2}\alpha\zeta^2 m^2 c^2\Big] - \frac{\hbar^4}{8m^2 c^2}\Big[\frac{n\pi}{L}\Big]^4.
\tag{4.6.9}
$$

Here, the first term in the Eq. (4.6.9) corresponds to the non-relativistic energy of the system with GUP-corrections, whereas, the last term of the expression depicts the relativistic corrections.

4.6.2 Harmonic Oscillator

Harmonic oscillator is a well-defined potential problem. Here we are going to analyze the harmonic oscillator for the system under consideration in a 1+1 dimensional case. The

harmonic oscillator potential is

$$V(x) = \frac{1}{2}m\omega^2 x^2.$$

Using this potential in the Schrödinger equation (Eq. (4.6.6)) and solving it, we can evaluate the expression of the energy for this non-commutative spacetime model. The expression of the energy is

$$E_n \;=\; \hbar\omega\left(n+\frac{1}{2}\right)\left[1-\frac{1}{2}\alpha\zeta^2 m^2 c^2\right] - \frac{\hbar^2\omega^2}{32mc^2}\left[1-4\alpha\zeta^2 m^2 c^2\right]\left(5n(n+1)+3\right).$$

(4.6.10)

If one calculates the landau levels similar to the previously defined work [396], one will come up with a bound on α. The bound is

$$\alpha \leq 10^{41}.$$

Hereafter, for our analysis, we will consider $\alpha \sim 10^{41}$.

The primary motivation for the exploration of the deformed space structure for the analysis of thermal systems was triggered by the question of whether the change in the space structure can enhance the performance of the thermal machines. For that, we have considered different deformed space structures with different working models for the analysis of thermal engines. This is an open area for exploration.

4.7 Quantum Information Loss Paradox

At the turn of the twentieth century, Einstein formulated the general theory of relativity [397]. With its development, our basic understanding of the fabric of the Universe (space-time and its geometry) became mathematically more clear. With time, one of the strongest predictions of the general theory of relativity (GR) became the existence of black holes. The theory of GR is fundamentally based on the Einstein equations. It's a set of ten coupled nonlinear partial differential equation (PDE) with four independent parameters [398, 399].

$$G_{ab} = R_{ab} - \tfrac{1}{2}Rg_{ab} = \frac{8\pi G T_{ab}}{c^4} + \Lambda g_{ab},$$

(4.7.1)

where R_{ab} is the Ricci curvature tensor, R is the Ricci scalar, g_{ab} is the metric tensor, G is Newton's gravitational constant, T_{ab} is the stress-energy tensor, c the usual speed of light, and Λ the cosmological constant. [2] Exact solutions to this set of PDEs can describe black holes (among other things) with different physical properties (static : Schwarzchild solution [400], rotating : Kerr- (Newman) solution [401], static with electric charge : Reissner-Nordström solution ([398, 399, 402–405]) etc. However, Stephen Hawking showed [5] that any given black hole following the principles of quantum field theory, naturally emits thermal radiations inversely proportional to its mass (M), with a given temperature (T_H) of

$$k_b T_H = \frac{\hbar}{2\pi \lambda_k},\tag{4.7.2}$$

where $\lambda_k = 2r_s/c$ is the characteristic time (in case of rotating black holes, there is an additional dependence on the angular momentum), $r_s (= \frac{2GM}{c^2})$ is the Schwarzchild radius, while k_b and $\hbar$ are the usual Boltzmann constant and the reduced Planck constant.[3]

This is the Hawking radiation. It arises from the pair production of particles from quantum fluctuations from the horizon of the black hole. One of these particles (one with positive energy and outside the event horizon) leaves as radiation from the black hole to infinity and the other stays trapped within the black hole. As a result of the radiation, it is suggested that the black hole in the process loses mass (and hence the surface area) through the outgoing particles and hence evaporates with time. This is called the evaporation of a black hole. Observationally, it is very difficult to detect Hawking radiation as its temperature is many orders less in comparison to the cosmic microwave background (CMB) temperature $T \sim 3K$, which overwhelms it (it is the reason why in last five decades of dedicated study we have not been able to still detect any such signatures of black holes). This process, however, has some deeper consequences. For one it violates the classical Hawking area theorem [406] (black hole evaporation is a quantum effect) and other, an evaporating black hole, with losing mass, means that the black hole's lifetime is limited and beyond that period it potentially loses all the information that was inside it. This creates a direct violation of the quantum information conservation[4]. Quantum information which is quantified via the von-Neumann

---

[2]Inclusion of Λ in the Einstein equation takes into consideration of the background cosmology for a Friedmann–Lemaître–Robertson–Walker (FLRW) model. Although we don't need this term for our analysis here, but from the point of view of gravitational wave propagation, the evolution of background cosmology is governed by an FLRW universe, and hence for completeness, we presented the Einstein equation with the cosmological constant term.

[3]Hawking temperature of the black hole can be approximated from the values of the constant as $T_H \simeq 10^{-7} K$.

[4]Both in classical and quantum domain information conservation is fundamental, in classical physics this is governed by the Liouville's theorem of the conservation of the phase space volume [407], in the quantum

entropy [111], similar to classical physics maintains the conservation principle, that the information in a closed isolated system will be conserved [408–412]. It is intuitive to show that Hawking radiation generating from an initial pure state black hole, with the evolution of time, would end up with mixed states as remnants, thus violating the unitary evolution principle of the quantum mechanics and hence information lost during the process [413]. If the Hawking radiation were somehow able to carry an imprint of the quantum information [414] from within the horizon in its flight away from the black hole to infinity, it would still give rise to new incongruency by violating the no-cloning theorem [413, 415].

In black hole theory, it was evident that energy can flow into the system, but it become apparent from further research works [416, 417] that it can also flow out of the system. So, it can act as an intermediary in the energy exchange process. The efficiency of energy extraction from the system is maximum only when the horizon area remains unchanged [4, 418, 419]. The analogy of the process with that of the thermodynamic behavior was a striking feature where the horizon area plays the role of entropy. Since the advent of this analogy in the 1970s, it is vigorously being pursued to get a deep understanding of black hole theory. We can infer that there must be a relation between dM (the change of mass of the black hole) and dA (the change in horizon area). In Penrose process [399, 420] one can find that when $dA = 0$, one has $dM = \Omega_\alpha dJ + \Phi_\alpha dQ$, where Q and J are the charge of the black hole and the angular momentum respectively, whereas Ω_α and Φ_α are the angular velocity and the electric potential of the horizon respectively. This describes the change in the energy of the black hole during the reversible process alike to the process of work done in a thermodynamic system. It is equivalent to the First law of thermodynamics with the heat term missing. This missing term is provided by $\kappa dA/8\pi G$ where κ depicts the surface gravity of the horizon. One can define the surface gravity of the stationary black hole by assuming the event horizon as a Killing horizon.

The analogy between the thermodynamic variable (i.e., temperature for this case) and the surface gravity helps temperature to enter the first law of black hole theory which provides the equivalence with the thermodynamic law [421–423]. Now, the fact that the temperature will remain constant over the horizon provides the equivalence with the Zeroth law of thermodynamics, and the fact that it is near impossible to reduce it to zero provides the equivalence with the third law [424]. Now according to the seminal work [425], a black hole with thermodynamic temperature can be defined in terms of the efficiency of the heat engine. This is proportional to the surface gravity of the black hole. We know that the temperature

---

domain, this is preserved via the unitarity of the S-matrix.

can be expressed by virtue of the second law of thermodynamics which states that in a cycle we cannot pump heat from a colder body to a hotter body with no other changes. The ratio of the thermodynamic temperature for two equilibrium states is defined as $T_{in}/T_{out} = Q_{in}/Q_{out}$, where the ratio Q_{in}/Q_{out} describes the heat in to that of the heat out during a reversible heat cycle operated between two heat reservoirs. The most efficient engine is the one that has the power to dump its heat into the cold bath. If we apply this definition to the black hole theory, we encounter that the temperature of the black hole must be zero since with perfect efficiency one has the empower to extract the entire rest mass of a particle as work. This is executed by dumping the heat into the black hole by lowering it to the horizon. To do so, we have to consider the condition of lowering the heat all the way to the horizon. This indicates the analogy between the thermodynamic cycle with that of the black hole. So, we can infer that the black hole itself is a thermodynamic object.

We can imbibe the concept of information paradox by means of a thought experiment. Let us consider a pure state comprised of n EPR pairs, and the black hole happens to be in a pure state initially. As the state of the system is pure in its form, the Von Neumann entropy of the system, which quantifies the information vanishes. Now we throw one of the qubits of each pair of the system into the black hole. Due to this incidence, the new entanglement entropy, i.e., Von Neumann entropy of the states that remain outside of the black hole (obtained by performing the trace out an operation on the interior of black hole qubits) is $n\,ln2$, where $ln2$ is for each pair. The entropy measure for the black hole is also the same. After a certain period of time, the black hole gets evaporated, but the entropy of the external states remains unchanged. It is obvious that the qubits that have fallen into this black hole, i.e., the horizon of the black hole cannot have an influence over the matter that is outside the black hole. If this happens, then it will violate the causality principle. So, we can infer that in the thought experiment we started from zero initial entanglement entropy and at the end, we have $S = 2\,ln2$. On another way round, we can say that we started with a pure state and ended up with a mixed state. This thought experiment thus outlines the paradox.

While analyzing the black hole information paradox, one must be careful that the results of unitarity should only be applied to closed systems which ensures that the information is conserved. From field theory, we know that a particle and an antiparticle are formed in the vacuum, which is known as vacuum fluctuations. From the uncertainty principle ($\Delta E \Delta t \sim \hbar/2$), we know that these particles, which are also known as 'virtual particles', annihilate with each other. Hawking has conveyed that vacuum fluctuations occur near the event horizon of the black hole. He also showed that there is a high probability that one of the particles might

escape the black hole horizon after its creation, and it depends on the temperature of the black hole. The Hawking emission of using this vacuum fluctuation can be expressed as:

$$\alpha(T)|1\rangle_A|1\rangle_B + \beta(T)|0\rangle_A|0\rangle_B, \tag{4.7.3}$$

where $|1\rangle$ describes the presence of virtual particle and $|0\rangle$ describes the presence of the particle. $\alpha(T)$ and $\beta(T)$ denote that the emission process is thermal in nature. In this situation, the particle A is outside the horizon, and the particle B is inside the horizon. So, the Hawking radiation can be expressed as:

$$|\psi_{Hawking}\rangle = \frac{|1\rangle|1\rangle + |0\rangle|0\rangle}{\sqrt{2}}. \tag{4.7.4}$$

From Eq. (4.7.4), we can infer that the black hole can be explored through information theory. Here, in our case, we will study the information paradox using a quantum computer. We consider a quantum computational tool for the exploration of the black hole information paradox.

Many theories have surfaced to address the black hole information paradox. One of them is the black hole complementarity principle [426], which tries to fix this problem by suggesting that the occurrence of in-falling events are temporally relative based on the observer frame, hence non-simultaneous and so unverifiable. Other theories include the holographic principle [427], which states that the maximum number of states (degrees of freedom) in a confined volume is proportional to its surface area. Recently, in their work [428], they have proposed a new approach to tackle this problem while not disturbing the existing framework of the black hole information paradox, of the violation of the monogamy principle and the black hole evaporation process occurring simultaneously. Instead, they applied a pseudo-density operator to account for temporal and spatial entanglement between maximally entangled particles inside and outside of the black hole event horizon. With the use of the state tomography process, they simulated the scenario and successfully produced the pseudo-random operators for the model, and gave measurements that were in excellent agreement with the theoretical state's value.

5 Bound on Uncertainty Relation in Non-commutative Spacetime

The contents in this chapter are based on the article in Ref. [429].

The importance of UR is undeniable in almost all branches of physics and the recent works [210, 430–438] convey it's importance, especially those involving experiments in quantum domain. Recently, various experimental tests have been performed to verify the UR's [193–195]. They are the main tool necessary for formulating quantum mechanics [193, 439, 440] and even quantum gravity [441]. Technologically, in present time, it is even more important, as it has applications in quantum cryptography [181–183], and also in quantum entanglement detection [184–187]. It is also used in quantum metrology [188] and quantum speed limit research [189, 189–192, 442]. Likewise it is also used in space-time [443] and gravity analysis [444]. It has important relevance in string theory [445] as well.

Further recently, Pati and Maccone [180] were able to develop a stronger UR, called Pati-Maccone UR (PMUR), with a tighter lower bound. Using the algebraic square of sums $((a \pm b)^2 = a^2 + b^2 \pm 2ab)$, they turned the product form of the uncertainty relation into an

additive form:

$$\Delta A^2 + \Delta B^2 \geq max(\mathscr{L}_1, \mathscr{L}_2), \qquad\qquad (5.0.1)$$

where $\mathscr{L}_1$ and $\mathscr{L}_2$ are defined as $\pm i \langle [A, B] \rangle + \left| \langle \psi | A \pm iB | \psi^\perp \rangle \right|^2$ and $\frac{1}{2} |\langle \psi_{A+B}^\perp | A + B | \psi \rangle|^2$ respectively. Here $|\psi_{A+B}^\perp\rangle$ is the state, orthogonal to the state of the system $|\psi_{A+B}\rangle$. The sign is chosen in such a way that $\pm i \langle [A, B] \rangle$ yields a positive number.

Unlike the previously developed UR's, the PMUR is able to provide a non-trivial solution to the lower bound. For example, in the case of the relation (2.6.5), if one considers A and B as incompatible for the states of the system $|\psi\rangle$, then the whole relation reduces to a trivial case. However, for the case of PMUR, the lower bound happens to be almost always non-trivial (i.e., non-zero) for the cases where $|\psi\rangle$ is a common eigenstate of A and B, and when it is not. In the work [446], they have made a thorough derivation of PMUR relations, while in the work [447], they have provided an experimental validation for the PMUR relation. It is easy to see that the previous UR's can be shown as special cases of the PMUR relation.

Here in this chapter, we will present our development on deriving the UR's from Schrödinger's expression Eq. (2.6.5) and also the PMUR, both in product and as well as the sum of variance forms in non-commutative space. The complete analysis is done following the methodology of [448] but in non-commutative space, being motivated by the fact that the UR's scenario in NC space was strongly fueled by its mathematical background. Existing frameworks of modern classical geometry are outlined by Riemann's hypotheses of geometry [449], defined by two important concepts of the manifold and line elements [450, 451]. The validity of the infinitely small line element is connected to the basis of the respective metric of the space [449]. However, in quantum mechanics, the domain of the space being operated on fails to be a manifold. Along with that, we are also going to present the analysis using reverse UR, which is formulated in the work [448]. This is also useful in capturing the essence of the quantum uncertainties [452–456]. During the analysis an interesting result comes out for the non-linear model in NC space. It yields two different expressions for Schrödinger and Heisenberg UR. The identification for these two relations does not arise in commutative space, and even in the linear model of NC space.

5.1 Tighter Uncertainty relation in Non-Commutative Spacetime for Linear Harmonic Oscillator (LHO)

Till date, various NC space models have been proposed and analyzed. The proposed linear models can be generalized as:

$$X_i = A_{i,j}x_j, \tag{5.1.1}$$

where $X_i = [X_1, X_2, \ldots, X_{2n}]^T$, $x_i = [x_1, x_2, \ldots, x_{2n}]^T$, and

$$A_{i,j} = \begin{bmatrix} a_{1,1} & a_{1,2} & a_{1,3} & \ldots\ldots a_{1,2n} \\ a_{2,1} & a_{2,2} & a_{2,3} & \ldots\ldots a_{2,2n} \\ a_{3,1} & a_{3,2} & a_{3,3} & \ldots\ldots a_{3,2n} \\ \vdots & \vdots & \vdots & \vdots \\ a_{2n,1} & a_{2n,2} & a_{2n,3} & \ldots\ldots a_{2n,2n}. \end{bmatrix}$$

Here X_j are the coordinates of the non-commutative phase space, and x_j are the known commutative space coordinates. The variables a_{ij} can take any constant values. Any linear model can be easily procured from the generalized form given in Eq. (5.1.1) by replacing the values of the components of A_{ij}. In this chapter, we will present two NC models, (one linear and the other, non-linear). The models are presented below.

5.1.1 Model 1: Linear model

We take

$$\hat{X}_1 = \hat{x}_1 - \frac{\lambda}{2}\hat{p}_2, \qquad\qquad \hat{X}_2 = \hat{x}_2 + \frac{\lambda}{2}\hat{p}_1, \tag{5.1.2}$$
$$\hat{P}_1 = \hat{p}_1 + \frac{\gamma}{2}\hat{x}_2, \qquad\qquad \hat{P}_2 = \hat{p}_2 - \frac{\gamma}{2}\hat{x}_1,$$

where λ and γ are constants (extracted from the matrix A_{ij} for the current model, where $n = 2$.) This model is being used for the analysis of quantum gravity. The commutation relation for these observables can be written as:

$$[\hat{X}_1, \hat{X}_2] = i\lambda\hbar, \qquad [\hat{P}_1, \hat{P}_2] = i\gamma\hbar, \tag{5.1.3}$$
$$[\hat{X}_1, \hat{P}_1] = [\hat{X}_2, \hat{P}_2] = i\hbar\left(1 + \frac{\lambda\gamma}{4}\right).$$

The Robertson-Schrödinger uncertainty relation (RS) for position (X) and momentum

(P) operators are represented as:

$$\Delta\hat{X}^2\Delta\hat{P}^2 \geq \left|\frac{1}{2}\langle[\hat{X},\hat{P}]\rangle\right|^2 + \left|\frac{1}{2}\langle\{\hat{X},\hat{P}\}\rangle - \langle\hat{X}\rangle\langle\hat{P}\rangle\right|^2. \tag{5.1.4}$$

The expectation values, commutation and anti-commutation relations for the position X_1 and the momentum P_1 operators for LHO with respect to our known canonical variables are:

$$[\hat{X}_1,\hat{P}_1] = i\hbar\left(1 + \frac{\lambda\gamma}{4}\right), \tag{5.1.5}$$

$$\langle\hat{X}_1\rangle\langle\hat{P}_1\rangle = \langle\hat{x}_1\rangle\langle\hat{p}_1\rangle + \frac{\gamma}{2}\langle\hat{x}_1\rangle\langle\hat{x}_2\rangle - \frac{\lambda}{2}\langle\hat{p}_2\rangle\langle\hat{p}_1\rangle - \frac{\lambda\gamma}{4}\langle\hat{p}_2\rangle\langle\hat{x}_2\rangle, \tag{5.1.6}$$

and

$$\{\hat{X}_1,\hat{P}_1\} = \{\hat{x}_1,\hat{p}_1\} - \frac{\lambda}{2}\{\hat{p}_2,\hat{p}_1\} + \frac{\gamma}{2}\{\hat{x}_1,\hat{x}_2\} - \frac{\gamma\lambda}{4}\{\hat{p}_2,\hat{x}_2\}, \tag{5.1.7}$$

respectively. Plugging in Eq. (5.1.5), (5.1.6), (5.1.7) in Eq. (5.1.4) we get:

$$\Delta\hat{X}_1^{\,2}\Delta\hat{P}_1^{\,2} \geq \frac{\hbar^2}{4}\left(1 + \frac{\lambda\gamma}{4}\right)^2. \tag{5.1.8}$$

So we can see that the RS inequality yields the same results as we can develop from the Heisenberg UR relation (2.6.3). For the commutative space, there is no uncertainty in the position or momentum operator. But in NC space, the uncertainties in the position and momentum operators appear naturally.

The uncertainty of the position operator can be generated from Eq. (2.6.5) just by replacing it with X_1 and X_2. Plugging in the commutation, anti-commutation and the expectation relation in Eq. (2.6.5) for its corresponding X_1 and X_2 form, we get:

$$\Delta\hat{X}_1^{\,2}\Delta\hat{X}_2^{\,2} \geq \frac{\hbar^2\lambda^2}{4}. \tag{5.1.9}$$

Similarly, for the momentum operator, we can develop the uncertainty relation for the NC space by replacing the variables A and B by P_1 and P_2 in Eq. (2.6.5). Using the same formalism as above, we get:

$$\Delta\hat{P}_1^{\,2}\Delta\hat{P}_2^{\,2} \geq \frac{\hbar^2\gamma^2}{4}. \tag{5.1.10}$$

So we can conclude that the RS relation is equivalent in nature to the well known Heisenberg relation for LHO.

Figure 5.1. Shown above are the lower (Eq. (5.1.12)) and the upper bound (Eq. (5.2.3)) for the product of uncertainty of X and P of ***Model 1***, for $|\psi\rangle = cos\theta|\psi_0\rangle - sin\theta|\psi_1\rangle$. Here ψ_0 is the ground state and ψ_1 is the first excited state of LHO. The green shaded region describes the right side of the SR relation Eq.(2.6.5). The doted line is the plot of SR relation. Here it is shown that the lower bound of (Eq. (5.1.12)) is better than Eq.(2.6.5).

Now we proceed to compute the **tighter UR** relation. The expression is given as:

$$\Delta A^2 \Delta B^2 \geq \max_{\{|\psi_n\rangle\}} \frac{1}{4}\Big(\sum_n \big| \langle [\bar{A}, \bar{B}_n^\psi] \rangle_\psi + \langle \{\bar{A}, \bar{B}_n^\psi\} \rangle_\psi \big|^2 \Big). \tag{5.1.11}$$

Eq. (5.1.11) is tighter from Eq. (2.6.5) in the sense that it is achieved by optimizing the UR over the complete orthonormal bases. We want to optimize our UR in NC space using Eq. (5.1.11).

For the (X_1, P_1) pair, it reduces to

$$\Delta X_1^2 \Delta P_1^2 \geq \max_{\{|\psi_n\rangle\}} \frac{1}{4}\Big(\sum_n \big| \langle [\bar{X}_1, \bar{P}_{1n}^\psi] \rangle_\psi + \langle \{\bar{X}_1, \bar{P}_{1n}^\psi\} \rangle_\psi \big|^2 \Big), \tag{5.1.12}$$

where

$$\langle [\bar{X}_1, \bar{P}_{1n}^\psi] \rangle_\psi = \langle \psi | \bar{X}_1 | \psi_n \rangle \langle \psi_n | \bar{P}_1 | \psi \rangle - \langle \psi | \psi_n \rangle \langle \psi_n | \bar{P}_1 \bar{X}_1 | \psi \rangle. \tag{5.1.13}$$

Similarly, the anti-commutation relation follows.

Here, we have considered $|\psi\rangle$ as the state of the system and $\{|\psi_n\rangle\}$ as the basis states of the LHO. We have considered the states of LHO in NC space equivalent to the states of our known commutative space, as the models are developed by coupling the canonical variables of commutating space.
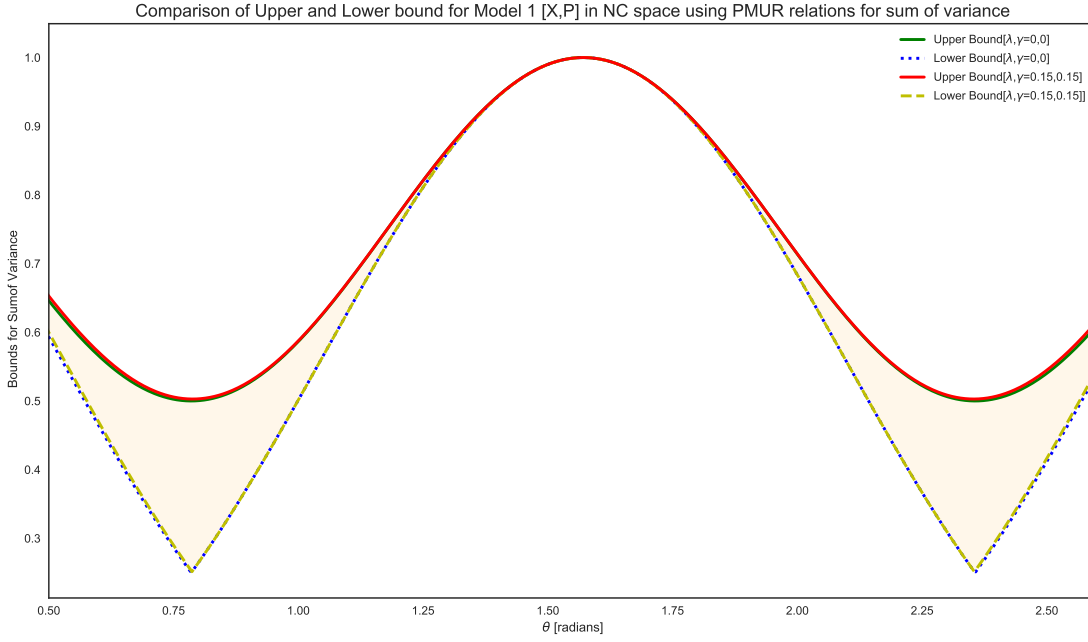
Figure 5.2. Similar to Fig. 5.1 we plot for $\lambda = \gamma = 0$ and $\lambda = \gamma = 0.15$. This plot shows that it is difficult to detect the NC space from the commutating space as the difference is too small.

The better lower and upper bound of the system for our first model, as shown in Fig. 5.1, are obtained by optimizing the UR over the compete set of bases of the considered system. Again, we have simulated Eq. (5.1.12) and Eq. (5.2.3) using Python with linear complexity.

Sum of UR in NC space is an interesting mathematical object for study. The product of variance can be trivial even for two incompatible observable. This is where the sum of uncertainty comes into play, where it captures the uncertainty in the observables even when it is non-trivial. Stronger UR has been put forward before in the work of [180]. Here we are using the definition proposed by Mondal *et al.* that yields better bounds than the previous ones, without requiring any further optimization.

The Sum of UR for two incompatible observable is:

$$\Delta A^2 + \Delta B^2 \geq \frac{1}{2} \sum_n \left(\left| \langle \psi_n | \bar{A} | \psi \rangle \right| + \left| \langle \psi_n | \bar{B} | \psi \rangle \right| \right)^2. \tag{5.1.14}$$

For the current model, we replace $A = X_1$ and $B = P_1$, giving

$$\Delta X_1^2 + \Delta P_1^2 \geq \frac{1}{2} \sum_n \left(\left| \langle \psi_n | \bar{X}_1 | \psi \rangle \right| + \left| \langle \psi_n | \bar{P}_1 | \psi \rangle \right| \right)^2. \tag{5.1.15}$$

Similar to Eq. (5.1.15), we can develop the sum of uncertainty for the position and momentum operators of the NC space equivalently.

The better lower and upper bound of the system for our first model, as shown in Fig. 5.2,

are obtained by optimizing the UR over the compete set of bases of the considered system. To do so, we have simulated Eq. (5.1.15) and Eq. (5.2.6) in Python with a complexity that is linear in the number of bases.

5.1.2   Model 2: Non-linear model

In this section, we will present the analysis of a second model, non-linear in nature. One of its applications is in string theory [457]. The representation of position and momentum operator for this non-linear model are:

$$\hat{X}_1 = \hat{x}_1, \qquad \hat{X}_2 = \hat{x}_2, \tag{5.1.16}$$

$$\hat{P}_1 = \hat{p}_1(1 - \alpha\hat{p}_1 + 2\alpha^2\hat{p}_1{}^2), \qquad \hat{P}_2 = \hat{p}_2(1 - \alpha\hat{p}_2 + 2\alpha^2\hat{p}_2{}^2),$$

where $\alpha = \frac{\alpha_0 l_{pl}}{\hbar}$ and α_0 is of order of 1 and $l_{pl} = 10^{-35}m$ (Planck length).

The commutation relation of this non-linear model includes the linear and the quadratic term in p, in the Planck regime [457].

$$[\hat{X}_j, \hat{P}_j] = i\hbar[1 - \alpha\hat{p}_j + 4\alpha^2\hat{p}_j{}^2], \qquad j = 1, 2. \tag{5.1.17}$$

We are going to develop Eq. (5.1.4) for this current model in a similar fashion. Evaluating the expectation of the position and the momentum operator, we get:

$$
\begin{aligned}
\langle\hat{X}_1\rangle\langle\hat{P}_1\rangle &= \langle\hat{x}_1\rangle\langle\hat{p}_1 - \alpha\hat{p}_1{}^2 + 2\alpha^2\hat{p}_1{}^3\rangle \\
&= \langle\hat{x}_1\rangle\langle\hat{p}_1\rangle - \alpha\langle\hat{x}_1\rangle\langle\hat{p}_1{}^2\rangle + 2\alpha^2\langle\hat{x}_1\rangle\langle\hat{p}_1{}^3\rangle.
\end{aligned}
\tag{5.1.18}
$$

The anti commutation relation for this model is given as:

$$
\begin{aligned}
\{\hat{X}_1, \hat{P}_1\} &= \{\hat{x}_1, (\hat{p}_1 - \alpha\hat{p}_1{}^2 + 2\alpha^2\hat{p}_1{}^3)\} \\
&= \{\hat{x}_1, \hat{p}_1\} - \alpha\{\hat{x}_1, \hat{p}_1{}^2\} + 2\alpha^2\{\hat{x}_1, \hat{p}_1{}^3\}.
\end{aligned}
\tag{5.1.19}
$$

Plugging in the above relations in Eq. (5.1.4), we get:

$$\Delta X_1^2 \Delta P_1^2 \geq \frac{1}{4}\hbar^2[1 - \alpha p + 4\alpha^2 p^2]^2 + \frac{1}{4}C^2 n[(n-1)^{\frac{1}{2}} + (n+1)^{\frac{1}{2}}]^2, \tag{5.1.20}$$

where $C = 6\alpha^2\hbar(\frac{\hbar}{2})^{\frac{3}{2}}(m_a\omega)^{\frac{1}{2}}$, m_a is the mass of the particle and ω is the angular frequency. For Eq. (5.1.20), n takes integer values from $[1, \infty]$. The state of the system is having n states,
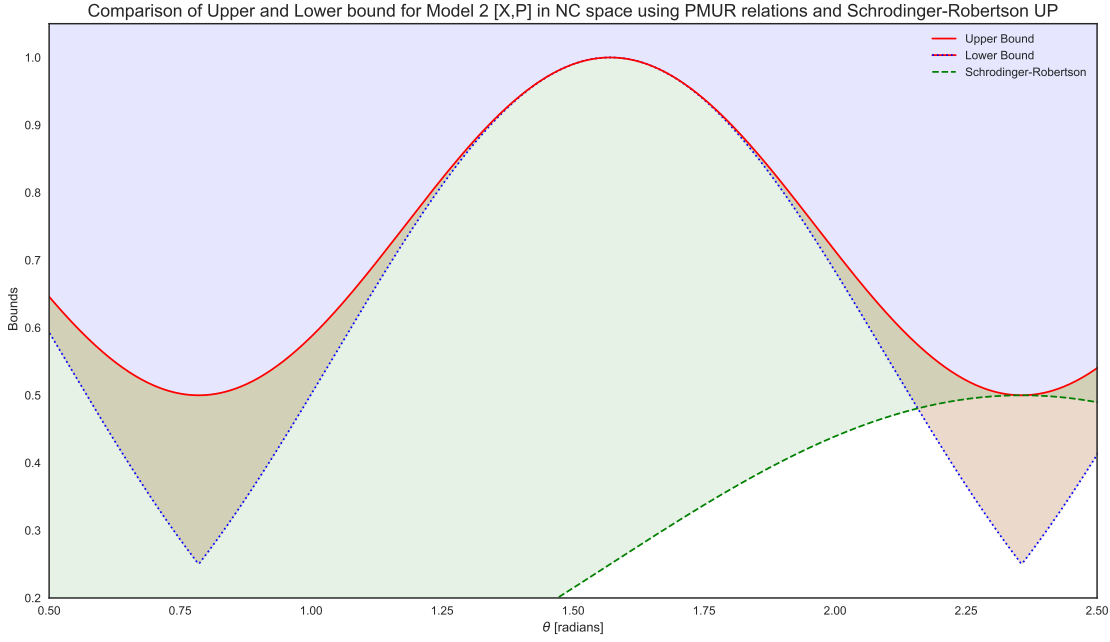
Figure 5.3. Shown above are the lower (Eq. (5.1.12)) and the upper bound (Eq. (5.2.3)) for the product of uncertainty of X and P of **Model 2**, for $|\psi\rangle = cos\theta|\psi_0\rangle - sin\theta|\psi_1\rangle$. Similar to the linear model the lower bound of (Eq. (5.1.12)) is better than the Eq.(2.6.5) for non-linear model.

where $n = 0$ corresponds to the ground state and $n = 1$ correspond to the first excited state and so on.

We will optimize the UR from the well-known form as in Eq.(5.1.12), where one can describe the different components using Eq. (5.1.13).

We have encountered an interesting difference while dealing with this linear and non-linear model. For the linear model of NC space and even in the case of commutative space there was no scope of differentiating the Heisenberg and SR relation. But in the case of the non-linear model, we encountered an extra scaling factor for SR relation in Eq. (5.1.20) along with the form that we get while deriving the Heisenberg relation.

The better lower and upper bounds of the system for our second model, as shown in Fig. 5.3, are obtained by optimizing the UR over the compete set of bases of the considered system. We have simulated Eq. (5.1.12) and Eq. (5.2.3) in Python with linear complexity.

5.2   Reverse uncertainty relations for NC spacetime

The computation of the reverse UR for NC space models is presented in this section. It allows putting a constraint on the upper limit of the uncertainty bound. First, we are going to develop the upper bound in uncertainty for the linear model followed by the non -linear model. For this, we are going to use reverse Cauchy-Schwarz inequality [458–461]. It is

defined as:

$$\sum_{i,j} c_i^2 d_j^2 \le \frac{CD+cd}{4CDcd}\left(\sum_{i,j} c_i d_j\right)^2,$$ (5.2.1)

where $0 < c \le c_i \le C < \infty$, $0 < d \le d_i \le D < \infty$ for some constants c, d, C and D for all $i = 1,...n$.

One can obtain the product of variance of two observables using the above inequality as:

$$\Delta A^2 \Delta B^2 \le \frac{\Lambda_{\alpha\beta}^{\psi}}{4}\left(\sum_n \left|\langle[\,\overline{A},\overline{B}_n^{\psi}]\rangle + \langle\{\overline{A},\overline{B}_n^{\psi}\}\rangle\right|\right)^2,$$ (5.2.2)

where $\Lambda_{\alpha\beta}^{\psi\Psi} = \frac{\left(M_{\psi\Psi}^{\alpha}M_{\psi\Psi}^{\beta}+m_{\psi\Psi}^{\alpha}m_{\psi\Psi}^{\beta}\right)^2}{4M_{\psi\Psi}^{\alpha}M_{\psi\Psi}^{\beta}m_{\psi\Psi}^{\alpha}m_{\psi\Psi}^{\beta}}$ with $M_{\psi\Psi}^{\alpha} = \max\{|\alpha_n|\}$, $m_{\psi\Psi}^{\alpha} = \min\{|\alpha_n|\}$, $M_{\psi\Psi}^{\beta} = \max\{|\beta_n|\}$ and $m_{\psi\Psi}^{\beta} = \min\{|\beta_n|\}$. Here α_n, β_n are the real constants, whose square form represents the probability of finding the particle in that state. For **Model 1**, we have to replace $A = X_1$ and $B = P_1$ in Eq. (5.2.2), giving

$$\Delta X_1^2 \Delta P_1^2 \le \frac{\Lambda_{\alpha\beta}^{\psi}}{4}\left(\sum_n \left|\langle[\,\overline{X_1},\overline{P_1}_n^{\psi}]\rangle + \langle\{\overline{X_1},\overline{P_1}_n^{\psi}\}\rangle\right|\right)^2.$$ (5.2.3)

Unlike the conventional commutative space, one has to develop Eq. (5.2.3) separately for both the position and the momentum operators. This can be generated by substitution of the variables in Eq. (5.2.2) by the position and the momentum operators.

The reverse uncertainty relation for the sum of variance can be developed using the Dunkl-Williams inequality [461]. Using this inequality, we get:

$$\Delta A + \Delta B \le \frac{\sqrt{2}\Delta(A-B)}{\sqrt{1 - \frac{Cov(A,B)}{\Delta A.\Delta B}}}.$$ (5.2.4)

Squaring both sides of the Eq. (5.2.4) we get the upper bound of the sum of variance for two variables as:

$$\Delta A^2 + \Delta B^2 \le \frac{2\Delta(A-B)^2}{1 - \frac{Cov(A,B)}{\Delta A \Delta B}} - 2\Delta A \Delta B.$$ (5.2.5)

For our linear model we replace $A = X_1$ and $B = P_1$ of the corresponding Model 1 in Eq. (5.2.5) to get

$$\Delta X_1^2 + \Delta P_1^2 \le \frac{2\Delta(X_1-P_1)^2}{1 - \frac{Cov(X_1,P_1)}{\Delta X_1 \Delta P_1}} - 2\Delta X_1 \Delta P_1,$$ (5.2.6)

where

$$Cov(X_1,P_1) = \frac{1}{2}\langle\psi_n|\{X_1,P_1\}|\psi\rangle - \langle\psi_n|X_1|\psi\rangle\langle\psi_n|P_1|\psi\rangle$$ (5.2.7)
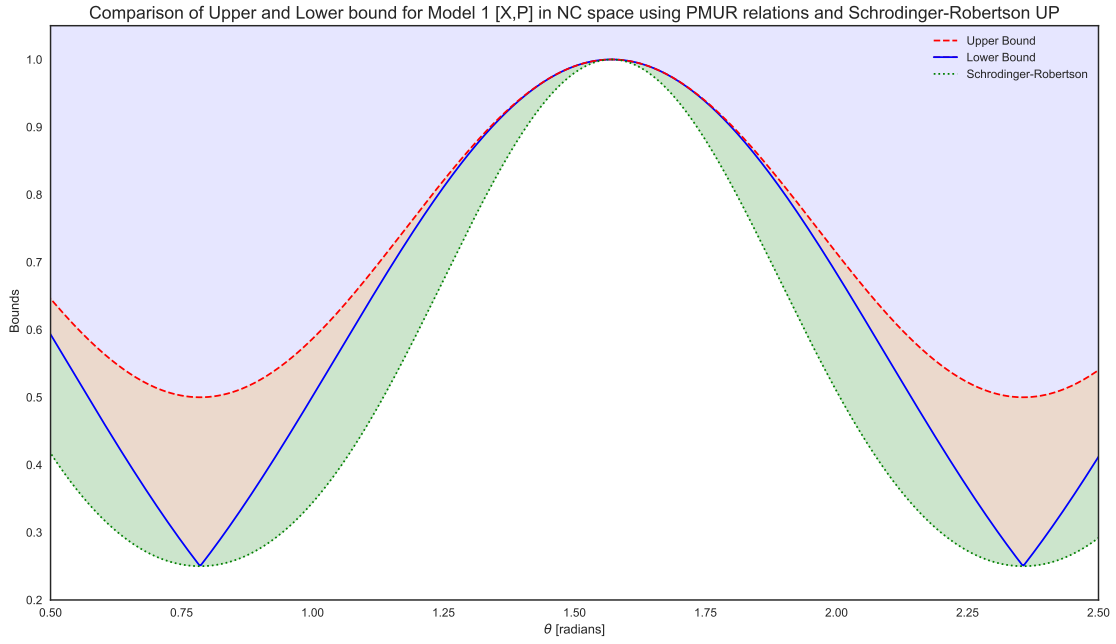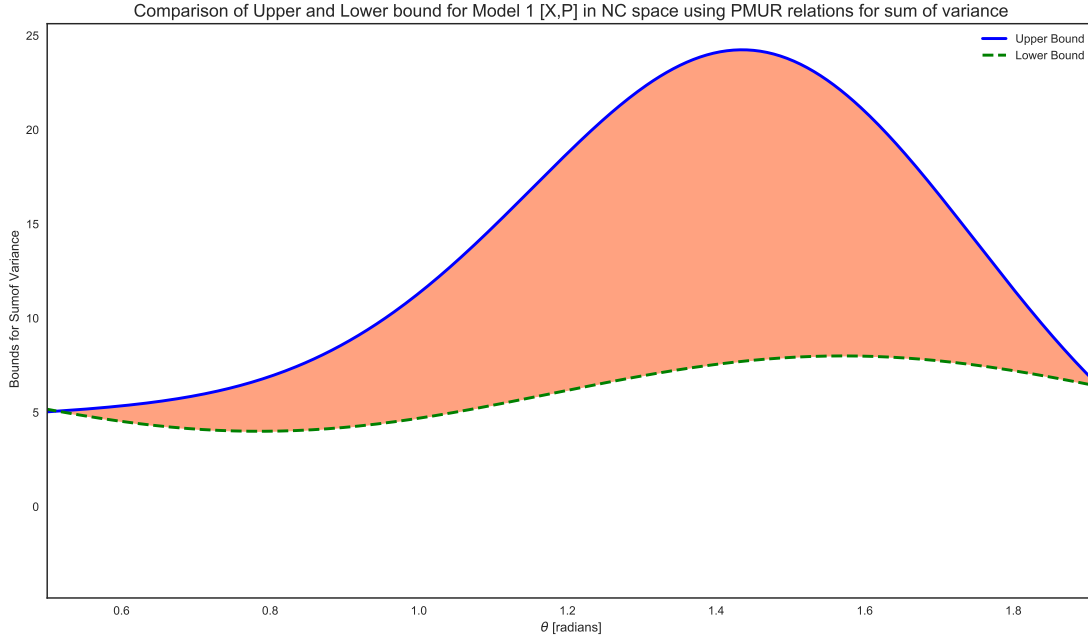
Figure 5.4. Shown above are the lower (Eq. (5.1.15)) and the upper bound (Eq. (5.2.6)) for the sum of uncertainty of X and P of ***Model 1***, for $|\psi\rangle = cos\theta|\psi_0\rangle - sin\theta|\psi_1\rangle$. This is a general plot with arbitrary (theoretical) values of γ, λ.

and

$$\Delta(X_1 - P_1)^2 = \langle\psi_n|(X_1 - P_1)^2|\psi\rangle - \langle\psi_n|(X_1 - P_1)|\psi\rangle^2. \qquad (5.2.8)$$

Unlike the commutative space, to develop the sum of variance for the position operator for our model, we have to consider $A = X_1$ and $B = X_2$ respectively. Similarly, to generate the sum of variance for the momentum operators, we have to substitute $A = P_1$ and $B = P_2$ in Eq. (5.2.5). The covariance can be calculated in the same fashion as shown in Eq. (5.2.7).

The treatment for the upper bound for the sum of variances of **Model 2** is exactly similar to that of the Model 1. Replacing $A = X_1$ and $B = P_1$ in Eq. (5.2.5) of Model 2, we obtain the expression of this model in the form, of Eq. (5.2.6).

The tighter bound of the uncertainty relation conveys that for a fixed amount of spread in the measurement outcome of one of the observables the amount of spread for the other observable is bounded from both sides. The experimental realization to probe deformations of the canonical commutator [462] and non-commutative theories [463] using quantum optics have been explored. So, the bound in the uncertainty measure in non-commutative space can be experimentally verified by extending the approach followed in the work [193].

The better lower and upper bounds for the sum uncertainty relation of the system for both the model, as shown in Fig. 5.4, and Fig. 5.5 are obtained by optimizing the UR over the compete set of bases of the considered system. To do so, we have simulated Eq. (5.1.15) and Eq. (5.2.6) in Python with a complexity linear with the number of bases.
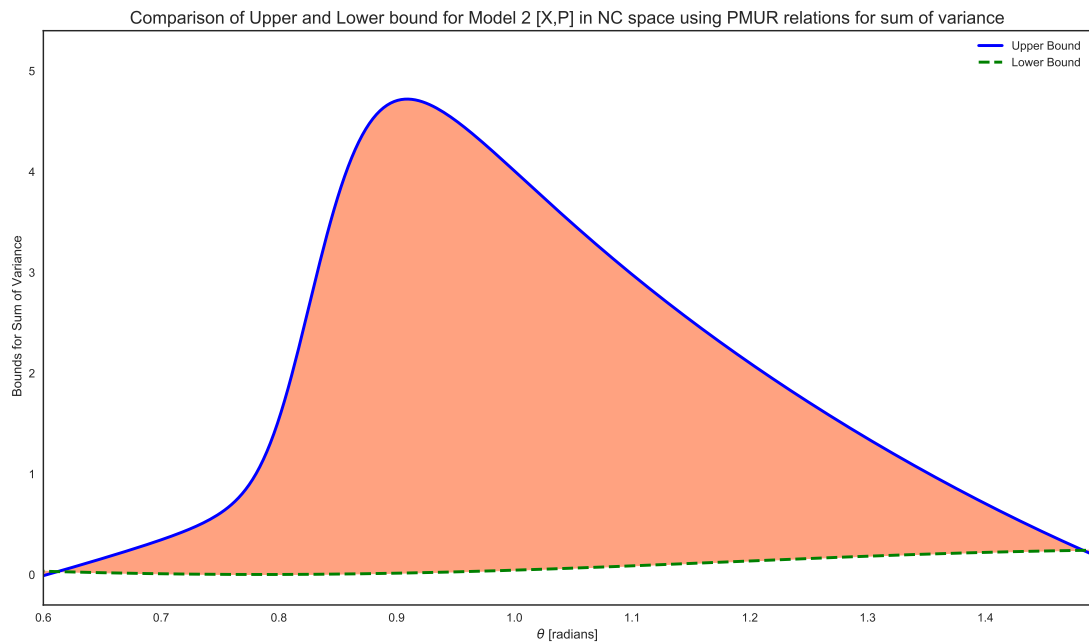
Figure 5.5. Similar to Fig. 5.4, but computed with the **Model 2**.

The bound in the uncertainty will be an important factor in the quantum metrology in non-commutative space structure. It will pose an upper bound in the error of the measurement and quantum evolution.

5.3   Chapter Summary

We see from the plots, that our computation of the LHO using NC models is consistent yet not similar to the results obtained from the traditional commutative space models. From Fig. 5.1, we can infer that the lower bound (blue curve) is better than the SR relation (green dotted curve). In Fig. 5.2, we have re-plotted Fig. 5.1 (excluding the SR relation), but for two different set of parameter values (γ, λ, $[0, 0.15]$). Where, the first case $\gamma, \lambda = 0$, is a special case where the model reduces to the standard commutative space case. Here we can see that the difference between the bounds of the commutative space($\gamma, \lambda = 0$) and the non-commutative space ($\gamma, \lambda = 0.15$) is very small. We speculate that this is why differentiating between the commutative and NC space is practically challenging. Fig. 5.3 is generated with the non-linear model. This plot further verifies the consistency of the PMUR relations in the NC space. However, owing to the non-linear nature of this model, the curve from the SR relation appears to have a deviation from nature exhibited in Fig. 5.1 and 5.2. We can also see that, in a small part the SR relation exceeds the lower bound provided by the PMUR in this model (shaded drab region), thus making it open for speculation on the tightness of

the bound over the SR lower bound in such non-linear NC models. In Fig. 5.4 and 5.5 we have presented the upper and the lower bound from the sum of variances using the PMUR relations. The plot gives us an allowed region for the range of uncertainty (for PMUR using the sum of variances only) to be valid. One can see that the linear model (Fig. 5.4) gives a less strict/more wider allowed range(shaded orange region) for the PMUR relation in comparison to Model 2, which is non-linear. The reason for such difference between the models is open for further speculations. Future experimental verifications of these results could help the community better with the understanding of the nature of working of these two models. In addition from Eq. (5.1.20), we have shown to the best of our knowledge for the first time that there is a difference in-bounds between the SR relation and the Heisenberg relation for a non-linear model operating in NC space. The URs have been the cornerstone of quantum theory. Even after nine decades of evolution of the URs, it is still open for further analysis and speculations.

Here, we have established the tighter URs for a linear and a non-linear model for two incompatible variables in NC space. We have also established the upper bound of the UR for the sum and product of our models. Together these URs and the bounds can play an important role in quantum cryptography and quantum metrology. For example, depending on the error margin of the underlying space, one can select an error-correcting code to design an error-free algorithm and protocols in that space. This can potentially lead to optimization of error analysis in the quantum domain.

This work has lead to the foundation and motivation for analyzing thermodynamic variables and systems from the eye of uncertainty relation where we have developed a bridge between the uncertainty relation of the working medium with the thermodynamic variables. The detail analysis and foundation are described in the next two chapters regarding this. Another aspect that evolved was that whether the change of the space structure can provide that much non-equilibrium effect to the system such that it boost's the efficiency of the thermal machines.

6

Quantum Thermal Engine's Efficiency Bound from Uncertainty Relation in Non-relativistic Regime

Contents

The contents in this chapter are based on the article in Ref. [36].

Out of the various aspects of quantum thermodynamics, one of them comprises of the analysis of heat engines and refrigerators in microscopic regime [15, 68, 69, 74, 110, 116, 134, 464, 465], and also in thermalization mechanism [76]. Various working models for heat-engine in the quantum regime have been realized and studied. Along with that its experimental setup has also been proposed in some works [466–470]. Heat engines are generally discrete or continuous in their nature. Two-stroke and four-stroke engines fall into the discrete group whereas a turbine belongs to the continuous engine.

Numerous quantum systems are considered for analysis of the quantum thermodynamics cycle, such as particles in a potential well [37, 471], harmonic oscillator [38], and spin 1/2 particles system [39]. For example, the quantum Szilard engine has been modeled using potential well. One-dimensional infinite potential well [196, 197] is the simplest problem in

non-relativistic quantum mechanics. This exemplifies how the wave nature of the particle quantizes the energy. When we place a barrier inside the middle of the well, the single potential well gets converted to a two-chambered potential well i.e., a double potential well. The thorough analysis of this model has been shown in the work [472]. Now modeling relativistic heat engines using potential well is not so straightforward. As in relativistic quantum mechanics, the study of the one-dimensional potential well is not so straightforward. New features appear in the energy spectra due to spin and energy-momentum relation. The solution for the relativistic model of the potential well is shown while keeping in mind that 'Klein's paradox' is taken care of [473]. Other problems that we face while we deal with the relativistic problem are the boundary conditions, which are not the same as in the case of non-relativistic problems. This is well discussed in [474, 475].

This chapter is dedicated to the exploration of thermal machines from a more fundamental concept of quantum mechanics. We will develop a bridge that connects the efficiency of the thermal engine with the fundamental uncertainty relation of two canonically conjugate operators. For the analysis one-dimensional potential well is considered as the working substance for the quantum thermal engines, which will work in the quantum regime for the non-relativistic scenario. In the next phase of our work, we establish a bridge between the uncertainty relation of position and momentum observable of the proposed model with our well-known thermodynamic variables. So, the proposed model depicts an effective method for the analysis of the useful work without executing any measurement, but by using two reservoirs of different temperatures. The analysis of the work done by the engine has been explored from the uncertainty relation viewpoint.

6.1   Thermal uncertainty relation

In the first phase of our analysis, we will evaluate the thermal uncertainty relation (which is one of the special cases of the general uncertainty relation) for a particle in one dimensional potential well.

Now, we formulate the uncertainty relation of the system at a certain temperature T from thermodynamics viewpoint. The formulation of the thermal uncertainty relation is performed by the analysis of the partition function of the system. The partition function [476], Z, for 1-D potential well is expressed as $Z = \sum_{n=1}^{\infty} e^{-\beta E_n} \approx \frac{1}{2} \sqrt{\frac{\pi}{\beta \alpha}}$, where $\beta = \frac{1}{k_B T}$, k_B is Boltzmann's constant and $\alpha = \frac{\pi^2 \hbar^2}{2m(2L)^2}$. The expression of Z converges to the form mentioned, as the product of β and α is a small quantity. We are using the Gaussian integral as the approximation

considering the error in the integration is negligible as the product of β and α is a small quantity. The mean energy for this system evolves to $\langle E \rangle = -\partial lnZ/\partial \beta = \frac{1}{2\beta}$. The average of the quantum number for the system under study can be conveyed as $\bar{n} = \frac{\sum_n ne^{-\beta E_n}}{\sum_n e^{-\beta E_n}} \approx \frac{1}{\sqrt{\pi \alpha \beta}}$.

Having the mathematical form of the partition function in our hand, we have all the resources to develop the thermal uncertainty relation. Now, we focus on the development of the dispersion relation of the position and the momentum operator at a certain temperature. The dispersion in position can be expressed as:

$$
\begin{aligned}
(\Delta X)_T^2 &= \langle (\Delta X)^2 \rangle_T = \langle X^2 \rangle_T - \langle X \rangle_T^2 \\
&= \frac{L^2}{3} - \frac{2L^2}{\pi^2} \times \frac{e^{-\alpha \beta} - \sqrt{\pi \alpha \beta} \times erfc(\sqrt{\alpha \beta})}{\frac{1}{2} \sqrt{\frac{\pi}{\alpha \beta}}} \\
&= \frac{L^2}{3} - \frac{4L^2 \sqrt{\alpha \beta}}{\pi^{5/2}} \times (e^{-\alpha \beta} - \sqrt{\pi \alpha \beta}).
\end{aligned} \tag{6.1.1}
$$

Erfc is the complementary error function, which appears while solving $\langle x^2 \rangle$. The dispersion relation of the momentum operator can be analyzed similarly. It is expressed as:

$$
\begin{aligned}
(\Delta P)_T^2 &= \langle (\Delta P)^2 \rangle_T = \langle P^2 \rangle_T - \langle P \rangle_T^2 \\
&= \frac{\pi^3 \hbar^2 \bar{n}^2}{8L^2}.
\end{aligned} \tag{6.1.2}
$$

So, the thermal uncertainty relation for the system at temperature T can be evaluated from Eq. (6.1.1), and Eq. (6.1.2) as:

$$
\begin{aligned}
(\Delta X)_T (\Delta P)_T &= \frac{\hbar \bar{n} \pi^{3/2}}{2\sqrt{2}} \left[\frac{1}{3} - \frac{4\sqrt{\alpha \beta}}{\pi^{5/2}} (e^{-\alpha \beta} - \sqrt{\pi \alpha \beta}) \right]^{\frac{1}{2}} \\
&\geq \frac{\hbar}{2}.
\end{aligned} \tag{6.1.3}
$$

The product uncertainty relation loses its importance when the system under consideration is an eigenstate of the observable under study. The sum of uncertainty [180] was introduced to capture the uncertainty in the observables when the system happens to be an eigenstate of the observables. The sum of uncertainty for this system at a particular temperature T is expressed as:

$$
(\Delta X)_T + (\Delta P)_T = L \left[\frac{1}{3} - \frac{4\sqrt{\alpha \beta}}{\pi^{5/2}} (e^{-\alpha \beta} - \sqrt{\pi \alpha \beta}) \right]^{\frac{1}{2}} + \frac{\hbar \bar{n} \pi^{3/2}}{2\sqrt{2}L}. \tag{6.1.4}
$$

The parameter that are considered for the analysis are shown in the table 6.1.

Table 6.1. Values of the parameters

Parameter	Values
$\bar{n}$	1, 2
Length (L)	0-5 nm
Hot bath (T_1)	320K
Cold bath (T_2)	80K
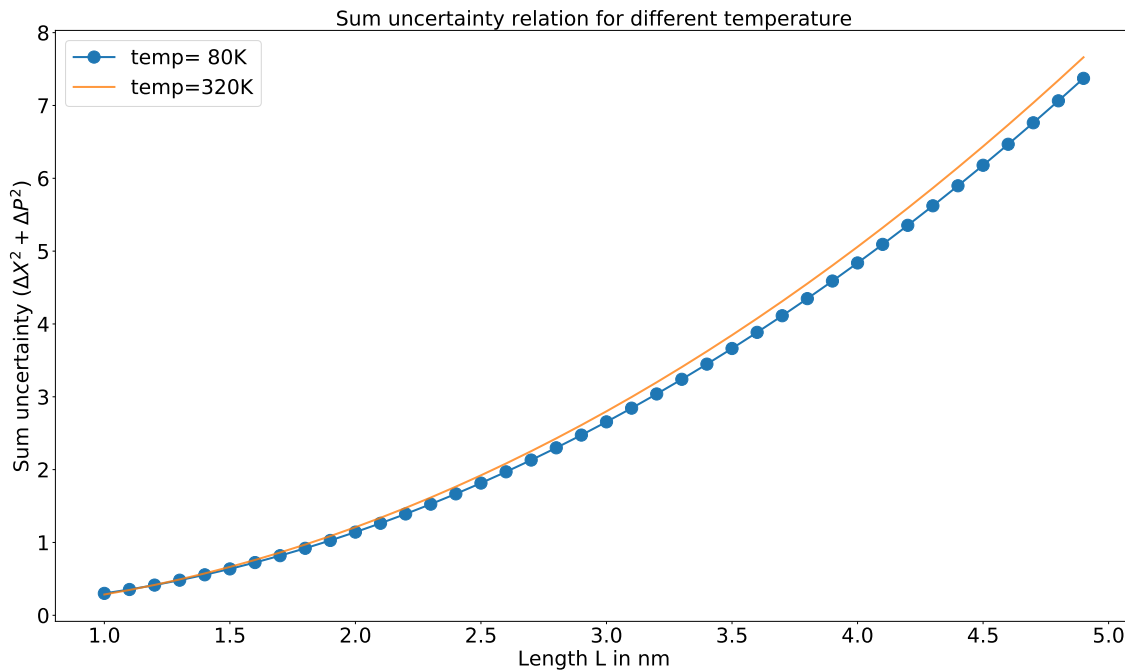
Figure 6.1. The variation of sum uncertainty relation (Eq. (6.1.4)) for different temperature. The dotted line is for lower and the solid line is for higher temperature

In Fig. 6.1, the variation of sum uncertainty relation (Eq. (6.1.4)) with respect to different temperature is shown. The thermal uncertainty relation that we have developed (Eq. (6.1.4)) for the considered system encounters a negligible amount of variation when the length of the potential well is small, whereas the difference is large for higher values of L (the order of the length is considered in nanometer).

The variation of uncertainty relation for different levels is shown in Fig. 6.2. Similar to the case of temperature analysis the variation is negligible for lower values of L and is large for higher values.
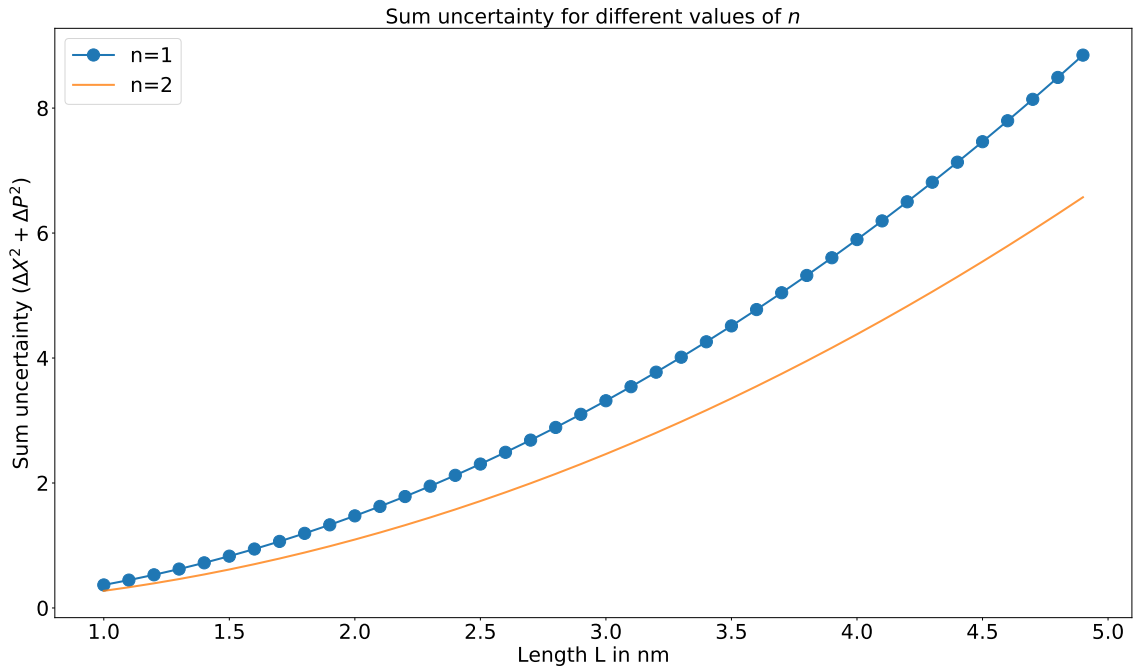
Figure 6.2. Similarly, this shows variation for different values of *n*.

6.2 Bound on sum uncertainty for one dimension potential well

In this section, we will first develop the bound on the uncertainty for the non-relativistic scenario. No better lower bound was known to us until it was explored in the work [448]. They have not only given a better lower bound than the previously known PMUR but also developed an upper bound for the uncertainty relation. It is popularly known as the reverse uncertainty relation.

The product of variances is sometimes unable to capture the uncertainty for two incompatible observables. If the state of the system is an eigenstate of one of the observables, then the product of the uncertainties vanishes [429, 448]. To overcome this, the sum of variances is introduced to capture the uncertainty of two incompatible observables. For any quantum model, the sum of variance of two incompatible observable which results in the lower bound is defined as:

$$\Delta A^2 + \Delta B^2 \geq \frac{1}{2} \sum_n \left(\left| \langle \psi_n | \bar{A} | \psi \rangle \right| + \left| \langle \psi_n | \bar{B} | \psi \rangle \right| \right)^2. \tag{6.2.1}$$

For our system, we calculate the lower bound of sum uncertainty for position and momentum

operator. So, we replace $A = X$ and $B = P$, which yields to:

$$\Delta X^2 + \Delta P^2 \geq \frac{1}{2} \sum_n \left(\left| \langle \psi_n | \bar{X} | \psi \rangle \right| + \left| \langle \psi_n | \bar{P} | \psi \rangle \right| \right)^2. \tag{6.2.2}$$

The computation of the reverse uncertainty relation of two observables results in the upper bound of uncertainty relation. To develop the upper bound, we have to utilize the definition of the Dunkl-Williams inequality [461]. The mathematical form of this inequality is:

$$\Delta A + \Delta B \leq \frac{\sqrt{2}\Delta(A-B)}{\sqrt{1 - \frac{Cov(A,B)}{\Delta A.\Delta B}}}. \tag{6.2.3}$$

Squaring both sides of the Eq. (6.2.3) we get the upper bound of the sum of variance for two variables as:

$$\Delta A^2 + \Delta B^2 \leq \frac{2\Delta(A-B)^2}{1 - \frac{Cov(A,B)}{\Delta A \Delta B}} - 2\Delta A \Delta B, \tag{6.2.4}$$

where $Cov(A, B)$ is defined as $Cov(A, B) = \frac{1}{2}\langle\{A, B\}\rangle - \langle A \rangle \langle B \rangle$, and $\Delta(A - B)^2 = \langle (A - B)^2 \rangle - \langle (A - B) \rangle^2$. $\Delta(A - B)^2$ is the variance of the difference of the two incompatible observable.

Now, for our one-dimensional potential well system which we have considered as a working substance, we calculate the upper bound of the sum of variance for the position and the momentum operator. So, we have to replace $A = X$ and $B = P$ in Eq. (6.2.4) and it results to:

$$\begin{aligned} \Delta X^2 + \Delta P^2 &\leq \frac{2\Delta(X-P)^2}{1 - \frac{Cov(X,P)}{\Delta X \Delta P}} - 2\Delta X \Delta P \\ &\leq \frac{L^2}{3} - \frac{2L^2}{(n\pi)^2} + \frac{\pi^2 \hbar^2 n^2}{4L^2}. \end{aligned} \tag{6.2.5}$$

In the above equation, i.e, Eq. (6.2.5) the upper bound of the system from the standard method is developed using the definition described in Eq. (6.2.4). Now, we develop the sum of variance of the same incompatible observables from the thermodynamic standpoint. The expression for the sum of variance of the system at a particular temperature evolves as:

$$\Delta X^2 + \Delta P^2 \leq \frac{4L^2}{3} - \frac{8L^2 \sqrt{\alpha\beta}}{\pi^{5/2}} \times (e^{-\alpha\beta} - \sqrt{\pi\alpha\beta}) + \frac{\hbar^2 \bar{n}^2 \pi^3}{4L^2}. \tag{6.2.6}$$

The bound of sum uncertainty relation (from thermodynamic perspective developed using Eq. (6.2.2) for lower bound and the Eq. (6.2.6) describes the upper bound for the considered system) with a particular temperature for different levels is shown in Fig. 6.3. The upper part of the plot is for $n = 1$, and the lower one is for $n = 2$. From Fig. 6.3, we can infer that
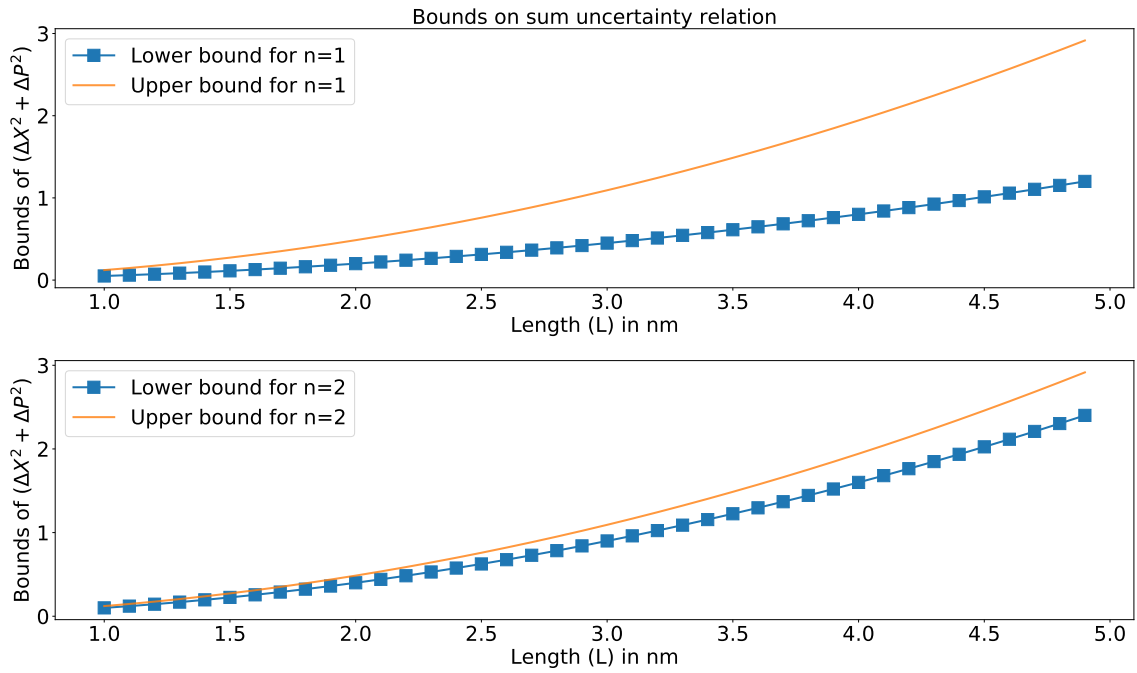
Figure 6.3. The bound of uncertainty relation (Eq. (6.2.2) and (6.2.6)) for a particular temperature for different values of *n* from thermodynamic standpoint.

the effect of the bounds of uncertainty relation is prominent for higher values of the length of the potential well. The bound is less prominent for lower values of *L*. The lower and upper bounds of the system are obtained by optimizing the UR over the compete set of bases of the considered system. To do so, we have simulated Eq. (6.2.6) and Eq. (6.2.2) in Python with a complexity in linear number of bases.

6.3   Correlation of thermodynamic quantities with uncertainty

In the next phase of our analysis, we want to establish a bridge between the thermodynamic quantities with the uncertainty relation.

We consider the sum of variance to overcome the flaw that will appear if we consider the product form of uncertainty if the system is an eigenstate of the observables. We will first demonstrate a connection of partition function with our uncertainty relation. The mathematical form of this is given by:

$$Z \;=\; \frac{\pi\bar{n}}{2} = \frac{L\sqrt{2}}{\hbar\sqrt{\pi}}\big(\varDelta X_T + \varDelta P_T + C_T\big), \tag{6.3.1}$$

where $C_T = -\frac{L}{3} + \frac{2L}{\pi^{5/2} \sqrt{\alpha\beta_T}}[\alpha\beta_T - \sqrt{\pi}(\alpha\beta_T)^{3/2} - 1]$ is a constant for a specific temperature, which is derived by expanding the Eq. (6.1.4) and neglecting the higher order terms as α and β are small.

Since we are able to bridge a relationship between the uncertainty relation and the partition function, we are all set to explain all the thermodynamic variables in terms of uncertainty relations. We develop the Helmholtz free energy [476], F, from an uncertainty viewpoint which takes the form as:

$$
\begin{aligned}
F &= \frac{-1}{\beta} lnZ \\
&= \frac{-1}{\beta} ln\Big[\frac{L\sqrt{2}}{\hbar\sqrt{\pi}}\big(\Delta X_T + \Delta P_T + C_T\big)\Big].
\end{aligned}
\tag{6.3.2}
$$

Entropy is expressed in terms of Helmholtz free energy. So, we uncover the relationship between the variance of position and momentum with entropy. The mathematical form for the entropy from uncertainty viewpoint is:

$$
\begin{aligned}
S &= -\frac{\partial F}{\partial T} \\
&= k_B \, ln\Big[\frac{L\sqrt{2}}{\hbar\sqrt{\pi}}\big(\Delta X_T + \Delta P_T + C_T\big)\Big] + \frac{\hbar\sqrt{\pi}k_B(\nu+\gamma)}{\sqrt{2}L\beta(\Delta X_T + \Delta P_T + C_T)},
\end{aligned}
\tag{6.3.3}
$$

where $\nu = \frac{\frac{L^2\sqrt{\alpha}}{\sqrt{\beta}\pi^{5/2}}\left(e^{-\alpha\beta} - \sqrt{\pi\alpha\beta}\right) - \frac{2L^2\sqrt{\alpha\beta}}{\pi^{5/2}}\left(\alpha e^{-\alpha\beta} - 1/2\sqrt{\frac{\pi\alpha}{\beta}}\right)}{\left[\frac{L^2}{3} - \frac{4L^2\sqrt{\alpha\beta}}{\pi^{5/2}}\left(e^{-\alpha\beta} - \sqrt{\pi\alpha\beta}\right)\right]^{\frac{1}{2}}}$ and γ is expressed as $\gamma = -\frac{L}{\pi^{5/2}\sqrt{\alpha}\beta^{3/2}}(\alpha\beta - \sqrt{\pi}(\alpha\beta)^{3/2} - 1) + \frac{2L}{\pi^{5/2}\sqrt{\alpha\beta}}(\alpha - \sqrt{\pi}\beta\alpha^{3/2})$

In Fig. 6.4, the variation of entropy in terms of uncertainty relation is shown. We can observe an increase in the entropy with an increase in the uncertainty for different temperatures. With an increase in uncertainty, the disorder in the system increases, causing an increase in entropy. The entropy of the system are obtained by optimizing the UR over the compete set of bases of the considered system in Python with linear complexity.

6.4 Stirling cycle and bound on efficiency

Here we are going to analyze the Stirling cycle in the non-relativistic regime. The generic description of the process is discussed in section 2.8. We are going to evaluate the work and efficiency of the engine for both scenarios.
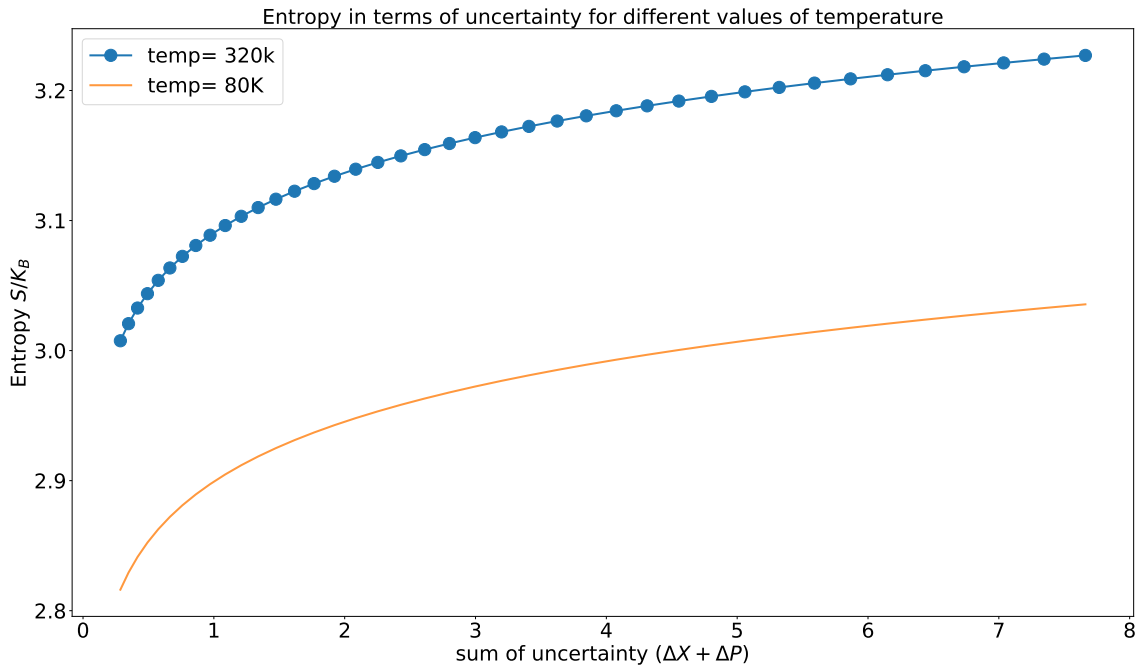
Figure 6.4. The variation of entropy (Eq. (6.3.3)) for different values of temperature. The scattered plot is higher and solid line is for lower temperature.

Similarly to [472], we calculate the work done and the efficiency but in terms of uncertainty relation. To develop the work done of the engine, a one-dimensional well of length $2L$ is considered with a particle of mass m at a temperature of T_1. The energy of this system is $E_n = \frac{n^2 \pi^2 \hbar^2}{2m(2L)^2}$. The partition function Z_A for the system is $Z \approx \frac{1}{2}\sqrt{\frac{\pi}{\beta \alpha}}$. Now, a wall is being inserted isothermally, which converts the potential well into an infinite double-well potential. Due to this insertion of the wall, the energy level for even values of n remain unchanged, but the odd ones shift and overlap with their nearest neighboring energy level. So the energy of the newly formed partitioned one-dimensional potential box is:

$$E_{2n} = \frac{(2n)^2 \pi^2 \hbar^2}{2m(2a)^2}. \tag{6.4.1}$$

So, the new partition function stands as:

$$Z_B = \sum_n 2e^{-\beta_1 E_{2n}}. \tag{6.4.2}$$

The internal energies for the system is calculated from the partition function. The internal energy U_A and U_B is defined as $U_i = -\partial ln Z_i / \partial \beta_1$ where $i = A, B$ and $\beta_1 = \frac{1}{k_B T_1}$. This results to:

$$U_A = U_B = \frac{1}{2\beta_1}. \tag{6.4.3}$$

The heat exchanged in this isothermal process can be expressed as:

$$Q_{AB} = U_B - U_A + k_B T_1 ln Z_B - k_B T_1 ln Z_A. \qquad (6.4.4)$$

Now the system is connected to a heat bath at a lower temperature T_2. The partition function for this lower temperature where the energy remains the same is defined as:

$$Z_C = \sum_n 2 e^{-\beta_2 E_{2n}}. \qquad (6.4.5)$$

The heat exchanged for this stage of the cycle is the difference of the average energies of the initial and the final states i.e.,

$$Q_{CB} = U_C - U_B. \qquad (6.4.6)$$

Where $U_C = -\partial ln Z_C / \partial \beta_2$ and $\beta_2 = \frac{1}{k_B T_2}$. The system being connected to the heat bath at temperature T_2 we remove the wall isothermally which we call as stage 3. The energy is now of the form $E_n = \frac{n^2 \pi^2 \hbar^2}{2m(2L)^2}$. The corresponding partition function is given by:

$$Z_D = \sum_n e^{-\beta E_n}. \qquad (6.4.7)$$

We can calculate the internal energy U_D similarly as U_C. The heat exchanged during this process is given by:

$$Q_{CD} = U_D - U_C + k_B T_2 ln Z_D - k_B T_2 ln Z_C. \qquad (6.4.8)$$

In the fourth stage of the cycle, the system is connected back to the heat bath at temperature T_1. The corresponding energy exchange for this stage can be expressed as:

$$Q_{DA} = U_A - U_D. \qquad (6.4.9)$$

So the total work done for the process in terms of variance of the position and the momentum operator evolves to:

$$
\begin{aligned}
W &= Q_{AB} + Q_{BC} + Q_{CD} + Q_{DA} \\
&= \frac{8L^2 \alpha}{\hbar^2 \pi^2} \Big[D ln\Big(\frac{Z_B}{Z_A}\Big) + E ln\Big(\frac{Z_D}{Z_C}\Big) \Big].
\end{aligned} \qquad (6.4.10)
$$

The efficiency of Stirling cycle engine stand as:

$$
\begin{aligned}
\eta &= 1 + \frac{Q_{BC} + Q_{CD}}{Q_{DA} + Q_{AB}} \\[2mm]
&= \frac{\left(\bar{n}_{T_2}^2 \, ln\!\left(\frac{Z_D}{Z_C}\right) + \bar{n}_{T_1}^2 \, ln\!\left(\frac{Z_B}{Z_A}\right) \right)}{\left(-\bar{n}_{T_2}^2/2 + \bar{n}_{T_1}^2 \left(ln\!\left(\frac{Z_B}{Z_A}\right) + 1/2 \right) \right)} \\[2mm]
&= \frac{\left[D \, ln\!\left(\frac{Z_B}{Z_A}\right) + E \, ln\!\left(\frac{Z_D}{Z_C}\right) \right]}{\left[-E/2 + D\left(ln\!\left(\frac{Z_B}{Z_A}\right) + 1/2 \right) \right]} \, . \quad (6.4.11)
\end{aligned}
$$

Where $D = \frac{8L^2}{\pi^3 \hbar^2}(\Delta X_{T_1} + \Delta P_{T_1} + C_{T_1})^2$ and $E = \frac{8L^2}{\pi^3 \hbar^2}(\Delta X_{T_2} + \Delta P_{T_2} + C_{T_2})^2$.
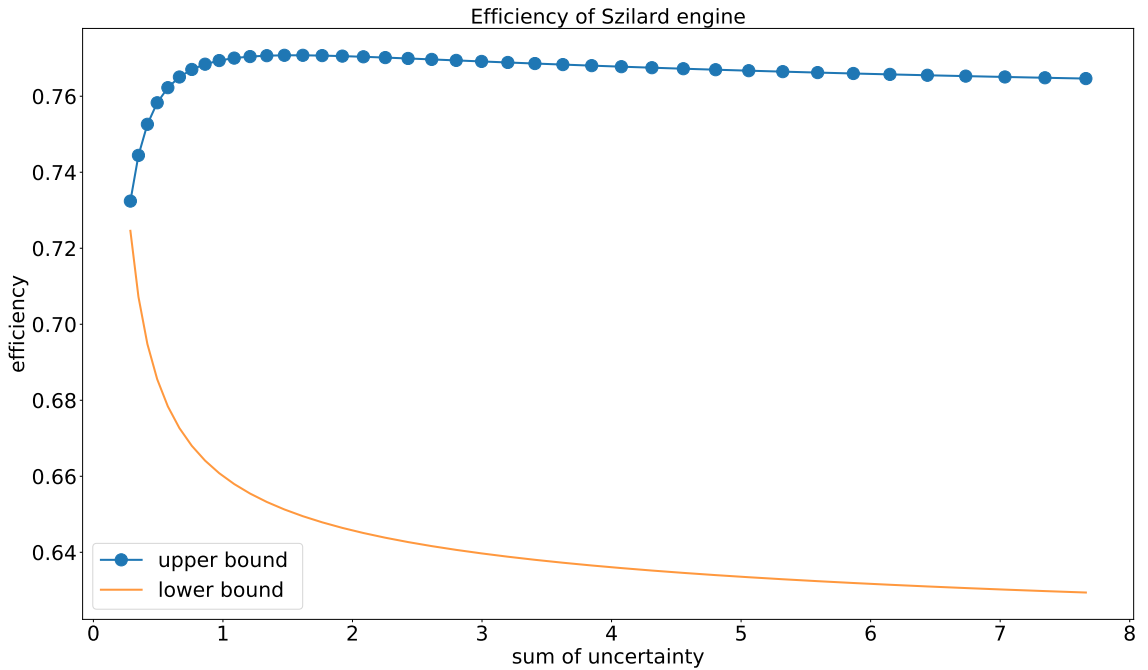
Figure 6.5. The bounds on the efficiency by heat engine in term of uncertainty relation. The scattered plot represents the upper bound and the solid line the lower bound of the efficiency.

In Eq. (6.4.11), the upper and the lower bound of the efficiency is evaluated in terms of the bound that is being analyzed for the thermal uncertainty relation of the position and the momentum operator. Here, the expression of D and E (for the working model considered for the analysis of the heat engine) gives the required uncertainty relation for the illustration of the bound of the efficiency.

In this work, we are able to bridge a connection between the efficiency of the heat engine with the variance of the position and the momentum operator. The upper bound of the efficiency for the heat engine is near about constant when the uncertainty is high, whereas it dips a little when uncertainty is less. As shown in Fig. 6.5, the lower bound of the efficiency is high when the uncertainty in measurement is less and dips gradually with the increase in

uncertainty. Thus, with an increase in uncertainty, we can visualize that the lower bound of the efficiency decreases. From Fig. 6.5, one can infer that the lower and the upper bound of the efficiency is near about the same when the uncertainty in the position and the momentum operator is quite small. The lower and upper bounds of the efficiency as described in Fig. 6.5 are obtained by optimizing the UR over the compete set of bases of the considered system in Python with linear complexity.

The Carnot efficiency for low temperature limit is expressed as $\left(1 - \frac{T_2}{T_1}\right)$ where T_2 and T_1 are the temperature of the cold and hot bath respectively. The upper bound of the efficiency from an uncertainty viewpoint is consistent with the bound given by the Carnot cycle. So, we can infer that the position and the momentum of the particle have a direct linkage with the thermodynamic variables. The work [477] suggests that the efficiency of engines that are powered by non-thermal baths can be higher than the usual convention. This can be testified from an uncertainty viewpoint.

In the quantum regime, after measurement, the system collapses to one of its eigenstates. So, to describe and analyze the efficiency of the engine for different conditions we must have a multi-copy of the system. Whereas, if we know the uncertainty relation of the model considered for analysis, we can describe and analyze different conditions without any measurement being done on the system. So, multiple copies of the system are not required for our analysis. This also reduces the measurement cost for the analysis of the system.

6.5 Chapter summary

The quantum heat engine has a predominant role in better understanding of the quantum engines, information, and quantum thermodynamics. This work develops a relationship between the thermodynamic variables with the position and momentum of the particle in the system. We give the analytic formulation of the work and efficiency of the engine in terms of the thermal uncertainty relation. Though we have considered a specific model for our analysis, this analysis has a global effect, i.e, it can be used to explain the efficiency of the various engines with different quantum models as the working substance. Based on these formulations, the physical properties of the heat engine and the thermodynamic variables that we have encountered are as follows.

(a) The total work and the efficiency depending on the position and momentum of the particle. The change in the uncertainty of the position and the momentum has a direct impact on the efficiency rate and the work of the engine.

(b) Every quantum thermodynamic variable has a direct connection with the uncertainty relation. Helmholtz's free energy shows the dependence of the internal energy of the thermodynamic system with the uncertainty relation of the incompatible observables. The detailed analysis of entropy with the uncertainty relation shows that entropy increases when the uncertainty of any one of the observables increases for a definite temperature. The rate of increase is different for different temperatures.

(c) The uncertainty relation which is the fundamental principle of quantum mechanics, is able to predict the efficiency and the total work of the engine without performing any measurement. So the measurement cost for the system gets reduced if we are able to model the system under study with a quantum model for which we can develop the uncertainty relation.

The bridge of the uncertainty related to the thermodynamic variable raises the question of whether we can analyze the phase transition (Landau theory) from an uncertainty perspective.

Most of the known methods for the measurement of entanglement converge to the analysis of entropy [478]. Now, if we can model the system that is being analyzed with a quantum model, we can construct the entanglement from the uncertainty relation for the system. This would be a standard method to measure the entanglement property of the system which might be a solution to the open problem of entanglement measure.

7 Quantum Thermal Engine's Efficiency Bound from Uncertainty Relation in Relativistic Regime

Contents

The contents in this chapter are based on the article in Ref. [43].

In this chapter, we have first proposed a model which will exclusively work in the quantum regime for the relativistic scenario. So, for the analysis of the relativistic version of heat engine, we have considered one-dimensional potential well as the working substance. In the next phase of our work, we establish a bridge between the uncertainty relation of position and momentum observable of the proposed model with our well-known thermodynamic variables. So, the proposed model depicts an effective method for the analysis of the useful work without executing any measurement, but by using two reservoirs of different temperatures. The analysis of the work done by the engine has been explored from the uncertainty relation viewpoint where the incompatible observables are the position and the momentum operators

of the relativistic particle in a potential well.

7.1   Thermal uncertainty relation for relativistic particle

In the first phase of our analysis, we will evaluate the thermal uncertainty relation (which is one of the special cases of the general uncertainty relation) for a particle in one dimensional potential well.

Now, we will formulate the uncertainty relation of this system from the thermodynamic standpoint. To evaluate the thermal uncertainty relation we have to analyze the partition function of the system. The partition function [476], Z, for 1-D potential well where a relativistic particle is confined in it is expressed as

$$Z \equiv \sum_{n=1}^{\infty} e^{-\beta E_n} \approx \frac{1}{2} \sqrt{\frac{\pi}{\beta \alpha}} \, e^{-\beta mc^2}, \tag{7.1.1}$$

where $\beta = \frac{1}{k_B T}$, k_B being Boltzmann's constant and $\alpha = \frac{\pi^2 \hbar^2}{2m(2L)^2}$. The expression of Z takes this form as the product of β and α is a small quantity. The expectation of the n-th state of the system is

$$\bar{n} \equiv \frac{\sum_n n e^{-\beta E_n}}{\sum_n e^{-\beta E_n}} \approx \frac{1}{\sqrt{\pi \alpha \beta}}. \tag{7.1.2}$$

After the evaluation of the partition function of the system, we now have all the available resources to develop the thermal uncertainty relation for the relativistic particle in a 1-D potential well. So, to evaluate the uncertainty relation for the position and the momentum operator we have to calculate the variance of the position and the momentum operator for this system. For the evaluation of the expectation of the position operator we consider the n-th state of the system and using Eq. (2.6.13) we get

$$
\begin{aligned}
(\varDelta X)_T^2 &\equiv \langle (\varDelta X)^2 \rangle_T = \langle X^2 \rangle_T - \langle X \rangle_T^2 \\
&\equiv \frac{1}{Z} \Big(\sum_{n=1}^{\infty} \langle \psi_n | X^2 | \psi_n \rangle e^{-\beta E_n} - \sum_{n=1}^{\infty} \langle \psi_n | X | \psi_n \rangle e^{-\beta E_n} \Big) \\
&= -\frac{2L^2}{\pi^2} \phi^{+2}(p) \frac{e^{-\alpha\beta} - \sqrt{\pi\alpha\beta} \times erfc(\sqrt{\alpha\beta})}{\frac{1}{2} \sqrt{\frac{\pi}{\alpha\beta}}} + \frac{4L^2}{3} \phi^{+2}(p) - L^2 \phi^{+4}(p) \\
&= -\phi^{+2}(p) \frac{4L^2 \sqrt{\alpha\beta}}{\pi^{5/2}} \times (e^{-\alpha\beta} - \sqrt{\pi\alpha\beta}) + L^2 \phi^{+2}(p) \Big(\frac{4}{3} - \phi^{+2}(p)\Big).
\end{aligned}
\tag{7.1.3}
$$

Here, $erfc$ is the complementary error function [479], which emerges while evaluating the

expression $\langle X^2 \rangle$.

Similar to the expression of the dispersion relation of the position operator, the variance of the momentum operator is

$$
\begin{aligned}
(\Delta P)_T^2 &\equiv \langle (\Delta P)^2 \rangle_T = \langle P^2 \rangle_T - \langle P \rangle_T^2 \\
&\equiv \frac{1}{Z} \sum_{n=1}^{\infty} \langle \psi_n | P^2 | \psi_n \rangle e^{-\beta E_n} \\
&= \frac{\pi^3 \hbar^2 \bar{n}^2}{8L^2} + 2mc^2.
\end{aligned} \tag{7.1.4}
$$

So the uncertainty relation from Eq. (7.1.3) and Eq. (7.1.4), at a thermal condition for the potential well model is expressed as

$$
\begin{aligned}
\Delta X_T \, \Delta P_T &= \frac{\hbar}{2} \left[-\phi^{+2}(p) \frac{4L^2 \sqrt{\alpha\beta}}{\pi^{5/2}} \times (e^{-\alpha\beta} - \sqrt{\pi\alpha\beta}) + L^2 \phi^{+2}(p) \left(\frac{4}{3} - \phi^{+2}(p) \right) \right]^{1/2} \\
&\quad \times \left(\frac{8mc^2}{\hbar^2} + \frac{\pi^3 \bar{n}^2}{2L^2} \right)^{\frac{1}{2}} \\
&\geq \frac{\hbar}{2}.
\end{aligned} \tag{7.1.5}
$$

Along with the product uncertainty relation, we also evaluate the thermal sum uncertainty relation of the position and the momentum operator for the potential well problem. Here, we have calculated the sum uncertainty as we are concerned about the fact that the product uncertainty relation is unable to capture the uncertainty of the incompatible observables when the wavefunction is an eigenfunction of one of the observables. The sum of uncertainty for these observables is

$$
\begin{aligned}
\Delta X_T + \Delta P_T &= \left[-\phi^{+2}(p) \frac{4L^2 \sqrt{\alpha\beta}}{\pi^{5/2}} \times (e^{-\alpha\beta} - \sqrt{\pi\alpha\beta}) + L^2 \phi^{+2}(p) \left(\frac{4}{3} - \phi^{+2}(p) \right) \right]^{1/2} \\
&\quad + \frac{\hbar}{2} \left(\frac{8mc^2}{\hbar^2} + \frac{\pi^3 \bar{n}^2}{2L^2} \right)^{1/2} \\
&\geq \frac{\hbar}{2}.
\end{aligned} \tag{7.1.6}
$$

Fig. 7.1 describes the variation of uncertainty with respect to different temperatures. The value of the uncertainty relation is almost constant for lower values of the length of the well. There is a sudden drop in the measure of uncertainty of the observables as the length of the well exceeds from 0.3 Å. The dip is more for higher values of L.

In Fig. 7.2, we can see that there is almost a gradual fall in the measure of uncertainty for $\bar{n} = 1$. Whereas, for $\bar{n} = 2$, we can visualize a small change for higher values of L.
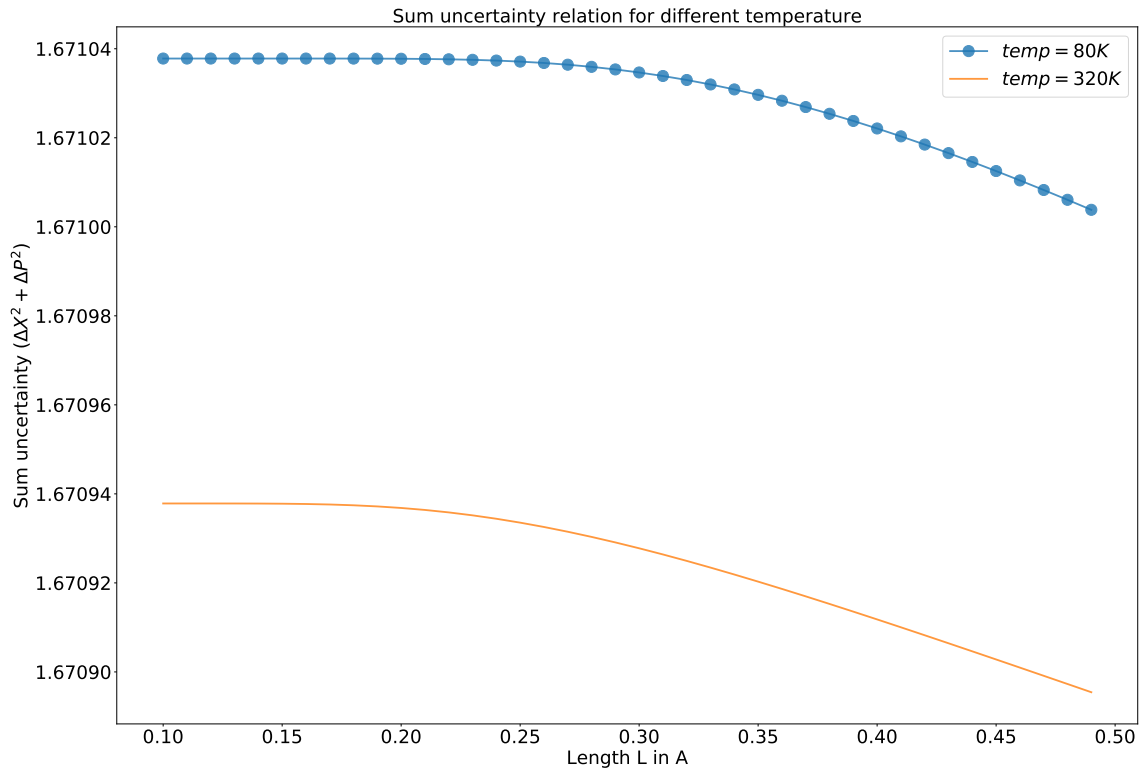
Figure 7.1. The variation of sum uncertainty relation for different temperature. The dotted line is for lower and the solid line is for higher temperature.

Table 7.1. Values of the parameters

Parameter	Values
$\bar{n}$	1, 2
Length (L)	0.1-0.5 Å
Hot bath (T_1)	320K
Cold bath (T_2)	80K

For the analysis of Fig. 7.1, we have replaced $\bar{n}$ from Eq. (7.1.2) in the expression of Eq. (7.1.6). Whereas, for the analysis of Fig. 7.2, we have replaced the required term of Eq. (7.1.6) as a function of $\bar{n}$ using Eq. (7.1.2) (for a fixed temperature '$T = 100K$'), to have a clear understanding of the dependency of the uncertainty relation with temperature and the average 'n'.

The parameters that are considered for the analysis are shown in the table 7.1.

In our model, the particle is confined to a box of length '$2L$'. The uncertainty in the position is a function of 'L', i.e., the particle has to be somewhere in the box. So, with the increase in length, there is an increase in the "uncertainty of position", i.e., ΔX increases with increase in length. From the definition of Heisenberg uncertainty, the uncertainty of
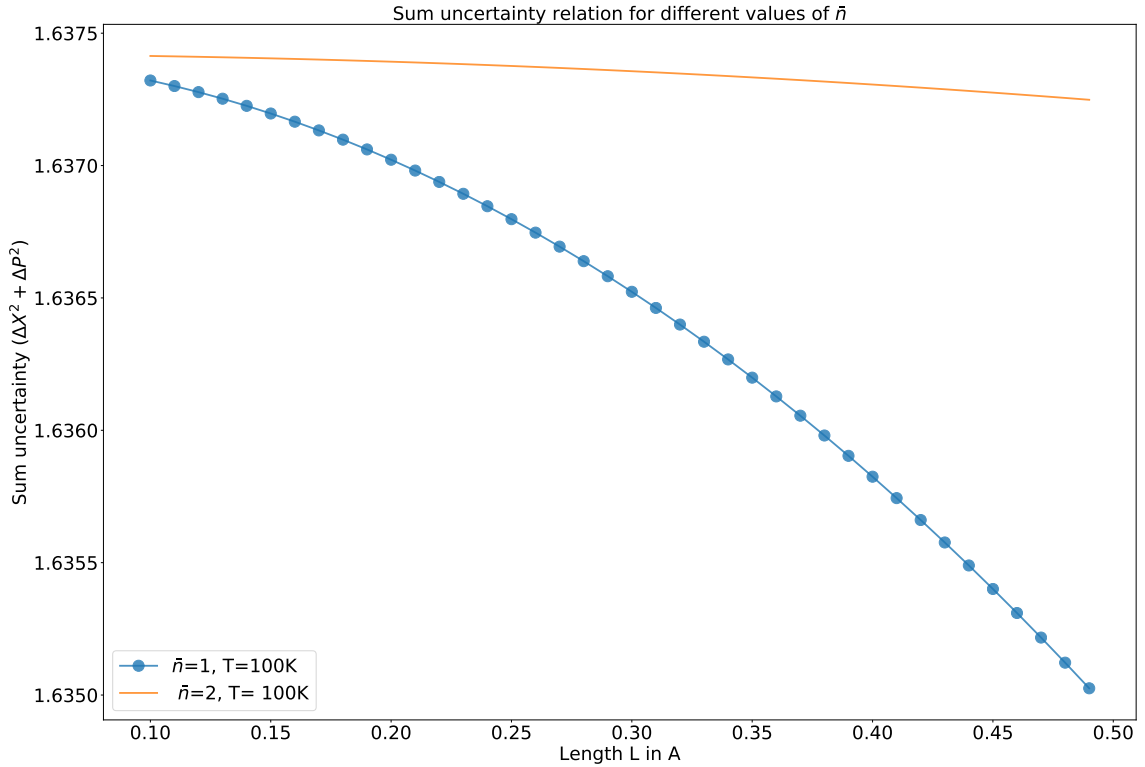
Figure 7.2. This shows the variation of sum uncertainty relation for different values of *n*.

momentum decreases with length, as it is inversely proportional to the length. So, according
to Heisenberg's definition, the overall uncertainty remains a constant (i.e $\hbar/2$). Following
the same ideology in case of our analysis, the "uncertainty of position" (ΔX of Eq. (7.1.3))
should show more dominance over the contribution of ΔP for an increase in the length of the
potential well in Eq. (7.1.6). We encounter a decrease in the "total uncertainty" for higher
values of *L* which is depicted in Fig. 7.1. The reason behind this is the dominance of the
first term of the expression of ΔX over the second term in Eq. (7.1.3) due to its exponential
nature, which causes an overall decrease in the "total uncertainty". We encounter the same
nature in Fig. 7.2. The reason for this nature is obviously similar to the analysis made for
Fig. 7.1.

7.2   Correlation of the thermodynamic quantities with uncertainty relation of relativistic particle

As far as our knowledge, the expression of the thermodynamic quantities from uncertainty
relation for a relativistic particle has not yet been provided. We have developed the relation-
ship between the basic thermodynamic quantities with the variance of the position and the

momentum operator.

The partition function [476] of the system, Z, in terms of the variance by using Eq. (7.1.6) for replacing $\bar{n}$ in Eq. (7.1.1) is expressed as

$$Z = \frac{\pi}{2} e^{-\beta mc^2} \left[\frac{16c\sqrt{2mc}}{\pi^3 \hbar^2} (\Delta X_T + \Delta P_T + C_T) \right]^{\frac{1}{2}}, \tag{7.2.1}$$

where $C_T = L\phi \sqrt{(\frac{4}{3} - \phi^2)} \left[\frac{2(\alpha\beta - \sqrt{\pi}(\alpha\beta)^{3/2} - 1)}{\pi^{5/2} \sqrt{\alpha\beta}(\frac{4}{3} - \phi^2)} - 1 \right] - \sqrt{2mc}$. Similarly, the internal energy of the canonical system can be evaluated using the variance of two incompatible operators. For our analysis these two incompatible operators are the position and the momentum operator. The internal energy of the system from Eq. (7.2.1) evolves to

$$\begin{aligned} \langle E \rangle &\equiv -\partial lnZ/\partial\beta \\ &= mc^2 + \frac{\zeta + \eta}{\pi[\frac{16c\sqrt{2mc}}{\pi^3 \hbar^2}(\Delta X_T + \Delta P_T + C_T)]}, \end{aligned}$$

where ζ is expressed as $\zeta = \frac{16c\sqrt{2mc}}{\pi^3 \hbar^2} \left[\frac{2L\phi}{\pi^{5/2}\sqrt{\alpha\beta(\frac{4}{3} - \phi^2)}}(\alpha - \alpha^{3/2}\sqrt{\pi\beta}) - \frac{L\phi}{\pi^{5/2}\beta^{3/2}\sqrt{\alpha(\frac{4}{3} - \phi^2)}}(\alpha\beta - \sqrt{\pi}(\alpha\beta)^{3/2} - 1) \right]$ and after calculation η is conveyed as $\eta = \frac{\frac{4L^2\phi^2}{\pi^{5/2}}\left[\sqrt{\frac{\alpha}{4\beta}}(e^{-\alpha\beta} - \sqrt{\pi\alpha\beta}) + \sqrt{\alpha\beta}(-\alpha e^{-\alpha\beta} - \sqrt{\frac{\pi\alpha}{4\beta}}) \right]}{2\left[L^2\phi^2(\frac{4}{3} - \phi^2) - \frac{4L^2\phi^2\sqrt{\alpha\beta}}{\pi^{5/2}}(e^{-\alpha\beta} - \sqrt{\pi\alpha\beta}) \right]^{\frac{1}{2}}}$.

Having the information of the link between the uncertainty relation and the partition function of the system we are set to describe all the thermodynamic variables in terms of the uncertainty relation of the position and the momentum operator of the considered system. One of the basic thermodynamic quantity is Helmholtz free energy [476] 'F'. The Helmholtz free energy for the relativistic particle in terms of the uncertainty relation is

$$\begin{aligned} F &\equiv \frac{-1}{\beta} lnZ \\ &= mc^2 - \frac{1}{\beta} ln\left[\frac{4c\sqrt{2mc}}{\pi\hbar^2}(\Delta X_T + \Delta P_T + C_T) \right]^{\frac{1}{2}}. \end{aligned}$$

We know that we can define entropy from Helmholtz free energy. So, we are now able to express entropy in terms of uncertainty relation which is expressed as

$$\begin{aligned} S &\equiv -\frac{\partial F}{\partial T} \\ &= k_B ln\left[\frac{4c\sqrt{2mc}}{\pi\hbar^2}(\Delta X_T + \Delta P_T + C_T) \right]^{\frac{1}{2}} + \frac{\tau + \chi}{\pi\beta[\frac{16c\sqrt{2mc}}{\pi^3 \hbar^2}(\Delta X_T + \Delta P_T + C_T)]}, \tag{7.2.2} \end{aligned}$$

where τ is expressed as $\tau = \frac{16c\sqrt{2mc}}{\pi^3\hbar^2}\Big[\frac{2Lk_B\phi}{\pi^{5/2}\sqrt{\alpha\beta(\frac{4}{3}-\phi^2)}}(\alpha-\alpha^{3/2}\sqrt{\pi\beta})-$

$\frac{Lk_B\phi}{\pi^{5/2}\beta^{3/2}\sqrt{\alpha(\frac{4}{3}-\phi^2)}}(\alpha\beta-\sqrt{\pi}(\alpha\beta)^{3/2}-1)\Big]$ and the form of χ after evaluation (using Eq. (7.1.6)) and the definition of C_T defined in Eq. (7.2.1)) is

$$\chi = \frac{\frac{4L^2k_B\phi^2}{\pi^{5/2}}\Big[\sqrt{\frac{\alpha}{4\beta}}\big(e^{-\alpha\beta}-\sqrt{\pi\alpha\beta}\big)+\sqrt{\alpha\beta}\big(-\alpha e^{-\alpha\beta}-\sqrt{\frac{\pi\alpha}{4\beta}}\big)\Big]}{2\Big[L^2\phi^2\big(\frac{4}{3}-\phi^2\big)-\frac{4L^2\phi^2\sqrt{\alpha\beta}}{\pi^{5/2}}\big(e^{-\alpha\beta}-\sqrt{\pi\alpha\beta}\big)\Big]^{\frac{1}{2}}}.$$
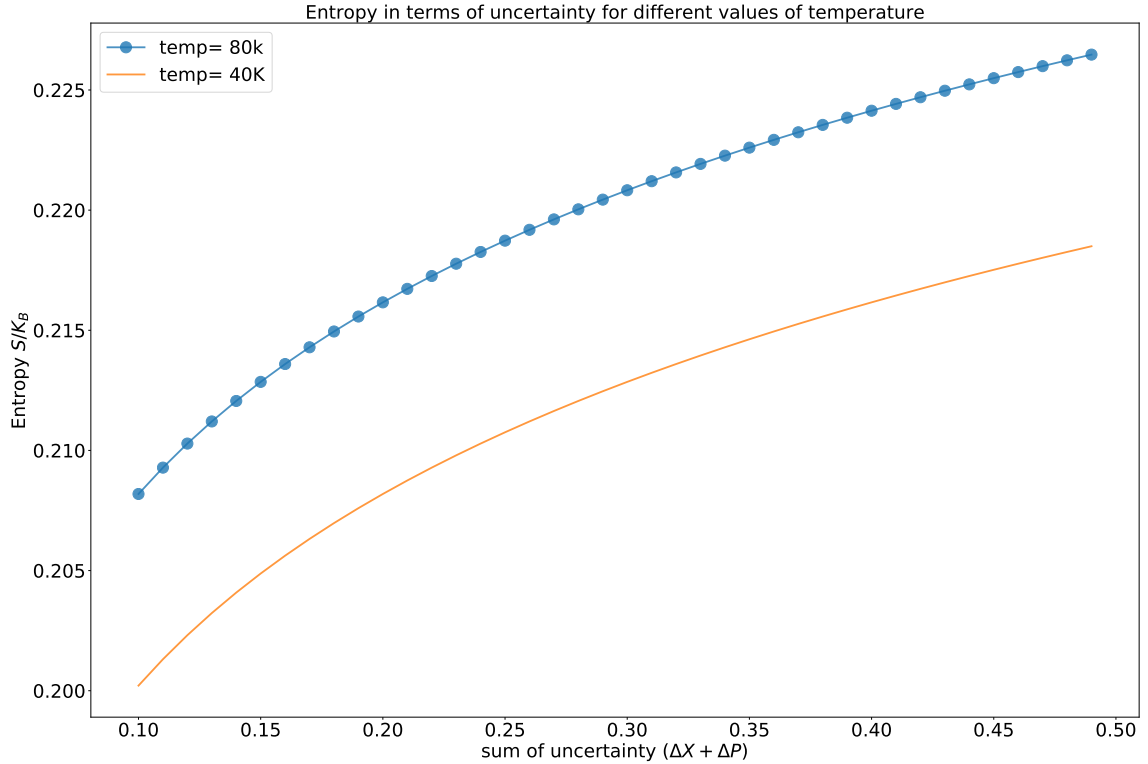
Figure 7.3. The variation of entropy from Eq. (7.2.2) for different temperature is shown. The scattered plot is for higher temperature and the solid line is for lower temperature.

From Fig. 7.3, we can infer that the entropy of the system increases along with the increase of the uncertainty of the observables. This is true when the system is kept at a different temperature. The entropy of the system are obtained by optimizing the UR over the compete set of bases of the considered system in Python with a complexity linear with the number of bases.

Till now entropy is the best-known measuring tool for entanglement. There is so far no standard method for the measure of entanglement for mixed states. If we can bridge a connection between these two quantities then it raises a question whether this can be a standard method for the entanglement measure.

For a given thermodynamic system, the knowledge of the Helmholtz free energy F is enough for determining all other thermodynamic variables for the given system. Here we

have developed the correlation of Helmholtz free energy with the uncertainty relation of the position and the momentum operator of the relativistic particle. This helps us to overcome the explicit requirement of internal energy of the system for the analysis of quantum thermodynamic system from uncertainty viewpoint. We can also explore and develop a theory which can explain the phase transition for relativistic particles in terms of their uncertainty relation. This is an open area to explore in the near future.

7.3   Bound on sum uncertainty for relativistic model of one dimensional potential well

The thorough analysis of the product uncertainty which produce better lower and upper bound using the method proposed in previous works [429, 448] results to zero. So, the product of variances of the specified observables is unable to capture the uncertainty for two incompatible observables. The reason behind this result is that the state of the system is an eigenstate of one of the observables. This causes the product of the uncertainties to vanish. We can overcome this issue if we invoke the sum of variances to capture the uncertainty of two incompatible observables. For the relativistic 1-D potential well, the sum of variance of two incompatible observable which results to the lower bound is defined as

$$\Delta A^2 + \Delta B^2 \geq \frac{1}{2} \sum_n \left(\left| \langle \psi_n | \bar{A} | \psi \rangle \right| + \left| \langle \psi_n | \bar{B} | \psi \rangle \right| \right)^2. \tag{7.3.1}$$

Here we replace A by X and B by P, according to the system we have considered for our analysis. This results to the upper bound of the relation for position and momentum. It is expressed as

$$\Delta X^2 + \Delta P^2 \geq \frac{1}{2} \sum_n \left(\left| \langle \psi_n | \bar{X} | \psi \rangle \right| + \left| \langle \psi_n | \bar{P} | \psi \rangle \right| \right)^2. \tag{7.3.2}$$

We can develop the upper bound of uncertainty relation for two incompatible observables when we compute the reverse uncertainty relation. We utilize the Dunkl-Williams inequality [461] to evolve the reverse relation. The mathematical form of the inequality is

$$\Delta A + \Delta B \leq \frac{\sqrt{2}\Delta(A-B)}{\sqrt{1 - \frac{Cov(A,B)}{\Delta A.\Delta B}}}. \tag{7.3.3}$$

Squaring both sides of the Eq. (7.3.3) we get

$$\Delta A^2 + \Delta B^2 \le \frac{2\Delta(A - B)^2}{1 - \frac{Cov(A,B)}{\Delta A \Delta B}} - 2\Delta A \Delta B, \tag{7.3.4}$$

where $Cov(A, B)$ is defined as $Cov(A, B) \equiv \frac{1}{2}\langle\{A, B\}\rangle - \langle A\rangle\langle B\rangle$, and $\Delta(A - B)^2 \equiv \langle(A - B)^2\rangle - \langle(A - B)\rangle^2$.

Now, for the system which we have considered as our working substance, we calculate the reverse relation for the position and the momentum operator. So, we substitute A by X and B by P in Eq. (7.3.4) which stands as

$$\begin{aligned}\Delta X^2 + \Delta P^2 &\le \frac{2\Delta(X - P)^2}{1 - \frac{Cov(X,P)}{\Delta X \Delta P}} - 2\Delta X \Delta P \\ &\le 4L^2\phi^{+2}(p)\left(\frac{1}{3} - \frac{1}{2(n\pi)^2}\right) + \frac{\pi^2\hbar^2 n^2}{4L^2} + 2m^2c^2.\end{aligned} \tag{7.3.5}$$

In Eq. (7.3.5), we have illustrated the reverse relation of the sum uncertainty relation without taking the thermal state under consideration. Now, we evaluate the reverse sum uncertainty relation from the correlation of the thermal variables. The mathematical form for the relation stands as

$$\begin{aligned}\Delta X_T^2 + \Delta P_T^2 &\le -\frac{8L^2\sqrt{\alpha\beta}}{\pi^{5/2}}\phi^{+2}(p)(e^{-\alpha\beta} - \sqrt{\pi\alpha\beta}) + \frac{8L^2}{3}\phi^{+2}(p) - 2L^2\phi^{+4}(p) \\ &\quad + \frac{\hbar^2\bar{n}^2\pi^3}{4L^2} + 4mc^2.\end{aligned} \tag{7.3.6}$$

The Eq. (7.3.6) express the upper bound of the sum uncertainty relation for our potential well model from the thermodynamic standpoint. The lower and upper bound of the system are obtained by optimizing the UR over the compete set of bases of the considered system. To do so, we have simulated Eq. (7.3.2) and Eq. (7.3.6) in Python with the linear complexity.

7.4 Relativistic Stirling cycle and bound on it's efficiency

Here we consider the Stirling cycle for a relativistic particle. The generic description of the process is discussed in section 2.8. We are going to evaluate the work and efficiency of the engine for both scenarios.

In the work [472], they have analyzed work done and efficiency for the heat engine in the non-relativistic limit. Here we have first developed heat engine in the relativistic limit where

the working substance is the one dimensional potential well. Following the similar method-
ology, we have analyzed the work done and the efficiency for the heat engine for a relativistic
particle. Along with that, we develop the work done by the engine and its efficiency from
the uncertainty relation viewpoint. We have considered a one dimensional potential well of
length $2L$ with a relativistic particle of mass m at temperature T_1 as the working substance
for our analysis. The energy for the system is equivalent to Eq. (2.6.11). The partition
function of our system is $Z_A = \sum_{n=1}^{\infty} e^{-\beta E_n} \approx \left(\frac{1}{2} \sqrt{\frac{\pi}{\beta \alpha}} e^{-\beta mc^2} \right)$. Now, when we insert a wall
isothermally it converts the one-dimensional infinite potential well into an infinite double
well potential. In this situation, the energy level for even values of n remain unchanged but
we see a shift for the odd ones. It overlaps with their nearest neighbor energy level. The
energy of the one-dimensional potential box that are created due to the partition is

$$E_{2n} = \frac{(2n)^2 \pi^2 \hbar^2}{2m(2L)^2} + mc^2, \tag{7.4.1}$$

which is evaluated by replacing n by $2n$ in Eq. (2.6.11). The partition function for the newly
formed partitioned potential well equivalent to Eq. (7.1.1) is

$$Z_B = \sum_n 2e^{-\beta_1 E_{2n}}.$$

The internal energy U_A and U_B is defined as $U_i \equiv -\partial lnZ_i/\partial \beta_1$, where $i = A, B$ and $\beta_1 = \frac{1}{k_B T_1}$. So, the internal energy are

$$U_A = U_B = \frac{1}{2\beta_1} + mc^2. \tag{7.4.2}$$

During the isothermal process, the heat exchange is expressed as

$$Q_{AB} \equiv U_B - U_A + k_B T_1 lnZ_B - k_B T_1 lnZ_A. \tag{7.4.3}$$

After the isothermal process, the system is connected to a heat bath at temperature T_2. The
partition function for this stage of the cycle is

$$Z_C = \sum_n 2e^{-\beta_2 E_{2n}}.$$

In the second stage of the cycle, the heat exchanged is given by the difference of the average

energies of the initial and the final states (similar to Eq. (7.4.2)). It is expressed as

$$Q_{CB} = U_C - U_B. \tag{7.4.4}$$

Here $U_C = -\partial ln Z_C / \partial \beta_2$ and $\beta_2 = \frac{1}{k_B T_2}$. In the next stage of the cycle, the system remains in the bath at temperature T_2 and we remove the wall isothermally. The energy for this stage of the cycle is same as given in Eq. (2.6.11). The partition function for the third stage of the cycle is

$$Z_D = \sum_n e^{-\beta_2 E_n},$$

where U_D can be similarly calculated as U_C. The heat exchanged for the third stage of the cycle (similar to Eq. (7.4.3)) stands as

$$Q_{CD} \equiv U_D - U_C + k_B T_2 ln Z_D - k_B T_2 ln Z_C. \tag{7.4.5}$$

Now, in the final stage of the cycle, the system reverts back to the first stage of the cycle, i.e., the system is now connected to the heat bath at temperature T_1. The energy exchange for the system when it reverts back to its initial stage is expressed as

$$Q_{DA} = U_A - U_D. \tag{7.4.6}$$

We calculate the total work done for this cycle in terms of the uncertainty relation of the position and the momentum operator. It is evaluated using Eq. (7.4.3), (7.4.4), (7.4.5) and (7.4.6) as

$$
\begin{aligned}
W &\equiv Q_{AB} + Q_{BC} + Q_{CD} + Q_{DA} \\
&= \frac{8L^2\alpha}{\hbar^2\pi^2}\left[f\, ln\Big(\frac{Z_B}{Z_A}\Big) + g\, ln\Big(\frac{Z_D}{Z_C}\Big) \right],
\end{aligned} \tag{7.4.7}
$$

where $f = \left[\frac{16c\sqrt{2mc}}{\pi^3\hbar^2}(\Delta X_{T_1} + \Delta P_{T_1} + C_{T_1}) \right]$ and $g = \left[\frac{16c\sqrt{2mc}}{\pi^3\hbar^2}(\Delta X_{T_2} + \Delta P_{T_2} + C_{T_2}) \right]$. The efficiency of this engine from thermal uncertainty relation standpoint using Eq. (7.4.3), (7.4.4), (7.4.5) and (7.4.6) is

$$
\begin{aligned}
\eta &\equiv 1 + \frac{Q_{BC} + Q_{CD}}{Q_{DA} + Q_{AB}} \\
&= \frac{\left(\bar{n}_{T_2}^2 \, ln\Big(\frac{Z_D}{Z_C}\Big) + \bar{n}_{T_1}^2 \, ln\Big(\frac{Z_B}{Z_A}\Big) \right)}{\left(-\bar{n}_{T_2}^2/2 + \bar{n}_{T_1}^2 \Big(ln\Big(\frac{Z_B}{Z_A}\Big) + 1/2 \Big) \right)}
\end{aligned}
$$
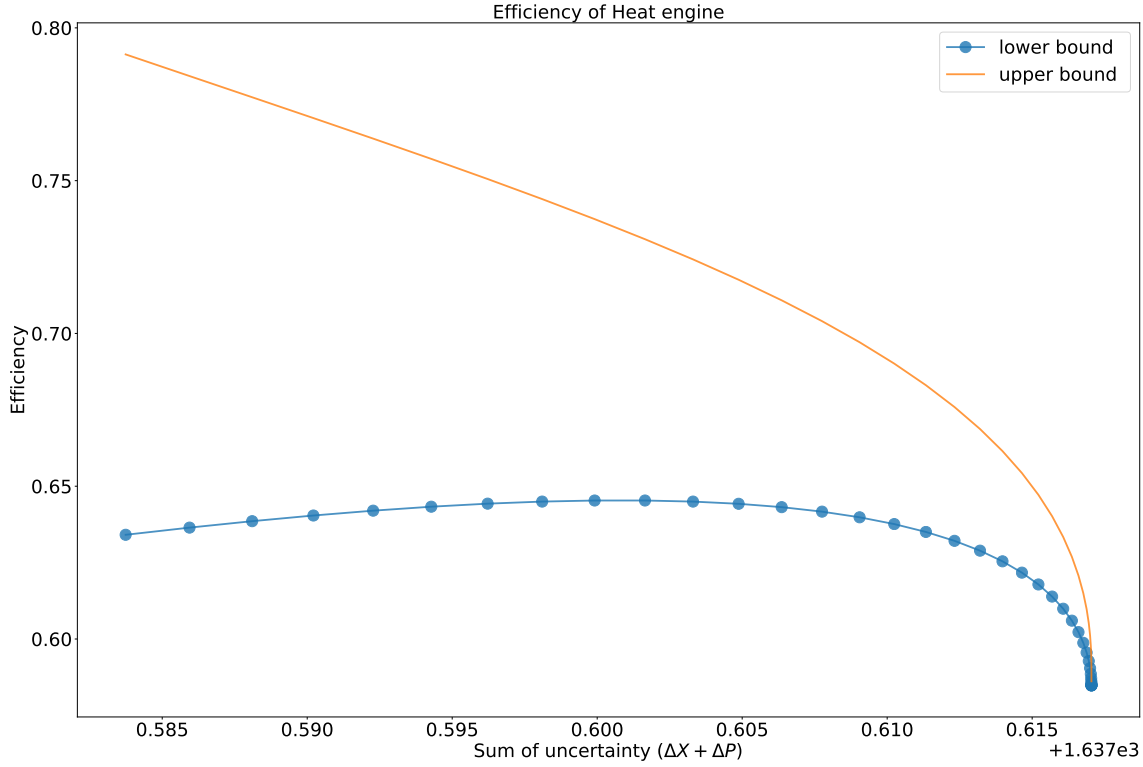
Figure 7.4. The efficiency bound for a relativistic model of heat engine.

$$
= \quad \frac{\left[g\, ln\!\left(\frac{Z_D}{Z_C}\right) + f\, ln\!\left(\frac{Z_B}{Z_A}\right) \right]}{\left[-g/2 + f\!\left(ln\!\left(\frac{Z_B}{Z_A}\right) + 1/2\right) \right]} . \tag{7.4.8}
$$

In Eq. (7.4.8), we have evaluated the upper and the lower bound of the efficiency with respect to the bound that we have analyzed for the thermal uncertainty relation of the position and the momentum operator. Here, f and g provides the required uncertainty relation for the explanation of the bound of the efficiency. We can evaluate the lower bound of f and g in the Eq. (7.4.8) from Eq. (7.3.1) and its upper bound from Eq. (7.3.4).

Here, we have evaluated the relation between the efficiency of a heat engine for a relativistic particle with the variance of position and momentum operator. The upper bound of the efficiency of the heat engine is monotonously decreasing function with the increase in temperature. From Fig. 7.4, we can infer that the variation of the lower bound with uncertainty is less for lower values of uncertainty, but there is a sudden dip when there is an increase in the uncertainty measure. The upper and lower bound of the efficiency of the heat engine predicts the same rate of accuracy when the uncertainty takes higher value. The lower and upper bound of the efficiency as described in Fig. 7.4 are obtained by optimizing the UR over the compete set of bases of the considered system in Python with linear complexity.

With the increase in the uncertainty, the conversion ratio of the heat engine decreases as

the thermal energy of the system is directly proportional to the uncertainty of the system. In the case of the upper bound of the efficiency which is depicted in terms of the uncertainty relation defined in Eq. (7.3.6), the decrease in the efficiency is more prominent due to the presence of the exponential component which causes exponential growth in the thermal energy of the engine and the dissipated heat over the work output. Whereas in the case of the lower bound we encounter a small variation of the efficiency for the lower value of the uncertainty. This can be easily analyzed from Eq. (7.3.2) where we encounter no exponential component which can depict a dominant effect on the thermal energy of the engine. If we equate the lower bound of the efficiency with the upper bound of the efficiency we encounter that it converges at high uncertainty. This show that for higher values of uncertainty the conversion ratio of the thermal energy to work reduces rapidly due to the steep growth in the thermal energy with higher uncertainty.

7.5 Chapter Summary

Heat engine plays a key role for a better comprehension of quantum thermodynamics. In this work, we have considered a potential well model with a relativistic particle confined in it, which acts as the working substance for the heat engine. Whether this can be globally extended to all the models that are considered for the analysis of heat engines and refrigerators is an open area to explore.

We have given the analytic formulation of the work and efficiency of the engine in terms of the thermal uncertainty relation. Based on our formulation, the physical properties of the heat engine and the thermodynamic variables are as follows.

(a) The total work and the efficiency of the heat engine for the relativistic particle depends on the position and momentum of the particle. The variation in the uncertainty relation of the position and the momentum of the particle has a direct impact on the efficiency rate and the work of the engine. The upper bound of the efficiency of the engine drops gradually when the uncertainty of the observable increases, whereas the lower bound of the efficiency decreases when the variation in the uncertainty relation is high.

(b) Our formulation develops a direct connection of every quantum thermodynamic variable with the uncertainty relation. Helmholtz free energy for this relativistic system conveys the dependence of the internal energy of the system with the thermal uncertainty relation. The entropy which can be evaluated from Helmholtz free energy thus has a dependency on the uncertainty relation. The entropy of the system increases when the uncertainty of the

incompatible observables increases for a definite temperature.

(c) The uncertainty relation is the cornerstone of quantum mechanics. Hereby applying this fundamental principle of quantum mechanics, we are able to predict the efficiency and the total work of the engine without performing any measurement. So, the measurement cost for the system gets reduced when we replace the classical model by a suitable quantum model, as has been done in this work.

All the well-known methods for the measurement of entanglement converges to the analysis of entropy [478]. Now, if the system that is being analyzed can be modeled with a quantum model, we can study the entanglement property from the uncertainty relation viewpoint for the system. If this method can explain the relativistic entanglement property, then this can act as a standard measure of entanglement. This might be a solution to the open problem of entanglement measure. A parallel analysis of our defined model for the non relativistic regime is shown in our work [36].

8 Quantum Thermal Engines and Refrigerators in Non-relativistic Non-Commutative Space

Contents

The contents in this chapter are based on the article in Ref. [40].

The modern-day challenge is to develop a more efficient heat engine to convert thermal energy to mechanical work with the different working mediums. Theoretical studies suggest that the limit to the efficiency of the engine, i.e., the Carnot limit, can be surpassed by exploiting the non-equilibrium reservoirs. Now the question is, can any working model in quantum regime exceed the Carnot efficiency, and can it boost the Coefficient of performance (COP) of the refrigerator?

In this chapter, we have proposed an approach to reach the threshold efficiency i.e., the Carnot efficiency of the thermal machine based on the non-commutative space structure. Progress in this direction but with different approaches is shown in the works [41, 480–482]. For our analysis, we utilize the latter version of non-commutative space-time where $\theta^{\mu\nu}$ is considered to be a function of the coordinates and momenta. Our prime motivation is to develop an engine and refrigerator in a non-commutative space where the working substance

will be the perturbed harmonic oscillator in this space. We employ this harmonic oscillator in the Stirling and Otto cycle which is the working principle for different engines and refrigerators. We analyze all the stages of the cycle to compute the efficiency of this model. The outcomes are astonishing when compared with the results of the usual spaces. We always observe higher efficiency in non-commutative space than the usual spaces. Along with that, the most interesting observation is that the efficiency is more for this space structure than the commutative phase space when we switch on the non-commutative parameter but it decreases with the increase in the parameter. Whereas, with the increase in the non-commutative parameter, the COP rises correspondingly. This guides us to the possibility of using non-commutative systems for the exploration of quantum information processing to obtain better results. One immediate question that arises is whether the defined non-commutative system is accessible physically. The obvious answer is yes and it is shown in previous works [462, 483]. The schematic analysis of the experimental model to access non-commutative space using optics is analyzed [462]. Using the same methodology, one can think of modeling the heat engine of non-commutative space.

The canonical partition function for the defined Hamiltonian (4.3.1) (as described in section 4.3) can be evaluated with the help of its corresponding eigenvalue to

$$
\begin{aligned}
Z &= \sum_n e^{-\beta E_n} \\
&= \frac{e^{\frac{\beta(2+\mu)^2\omega}{8\mu}} \sqrt{\frac{\pi}{2}} Erfc\left[\frac{\beta(2+\mu)\omega}{2\sqrt{2\beta\mu\omega}}\right]}{\sqrt{\beta\mu\omega}},
\end{aligned}
\tag{8.0.1}
$$

subjected to the condition that $Re[\beta\omega\mu] > 0$. We are neglecting the higher order terms because they tend to zero for the higher order. Erfc is the complementary error function, it is defined as $erfc(x) = \frac{\Gamma(1/2, x^2)}{\sqrt{\pi}}$, where $\Gamma(n, x)$ is the incomplete gamma function. It is expressed as $\Gamma(n, x) = (n-1)! e^x \sum_{k=0}^{n-1} \frac{x^k}{k!}$. We will now be able to evaluate all the thermodynamic variables in terms of the established partition function of the considered system for the analysis of the engine model.

8.1   Stirling heat cycle

The generic description of the quantum Stirling cycle with harmonic oscillator as the working medium is described in section 2.8.2. We will analyze the well-known *Stirling cycle* with non-commutating harmonic oscillator as the working substance. The four stages of the

Stirling cycle [36, 43, 146, 147, 472] (Fig. (2.4)) (as described in section 2.2) is as follows:

(i) The first step of the cycle is the *isothermal (A→B)* process. In this process, the working substance will be kept in contact with a heat bath of temperature T_h. The system stays in thermal equilibrium with the heat bath throughout every instant of time. The energy spectrum E_n and the internal energy U are changed as a result of the slow change in the working substance, i.e., the changes that take place in Hamiltonian (as described in section 4.3) during the execution of this phase. The Hamiltonian of the system changes from $H^{(1)}$ to $H^{(2)}$, where the change is depicted by the change of the parameter ω. So, heat is absorbed from the bath in this phase. The heat exchange during this phase of the cycle is:

$$Q_{AB} = U_B - U_A + k_B T_h ln Z_B - k_B T_h ln Z_A, \qquad (8.1.1)$$

where k_B is the Boltzmann constant. Here U_B and U_A describes the internal energy of the system at the end of this phase and the initial stage of the process. Similarly, Z_A describes the partition function for the initial stage of the process and Z_B describes the final stage of this phase.

(ii) The second phase of the cycle is the *isochoric (B→C)* process. During this process, the system undergoes an isochoric heat exchange. The system is connected to a bath with a lower temperature T_c, so heat is released. The heat exchange for this process is expressed as:

$$Q_{BC} = U_C - U_B. \qquad (8.1.2)$$

(iii) The third phase is an *isothermal (C→D)* process. During this phase of the cycle, the working substance is kept in contact with a bath of lower temperature T_c. Similar to phase one, the system is in thermal equilibrium with the bath. In this process, the Hamiltonian is reverted back to its initial stage (from $H^{(2)}$ to $H^{(1)}$). The heat exchange during this stage of the cycle is:

$$Q_{CD} = U_D - U_C + k_B T_c ln Z_D - k_B T_c ln Z_C. \qquad (8.1.3)$$

(iv) The last stage of the cycle is the *isochoric (D→A)* process. The system is connected back to the bath with a higher temperature T_h. The heat exchange for the last stage of the

cycle is expressed as:

$$Q_{DA} = U_A - U_D. \tag{8.1.4}$$

For all the phases, the internal energy of the system can be evaluated using the partition function as $U = -\frac{\partial lnZ}{\partial \beta}$. The different form of the partition function (Z_A, Z_B, Z_C, Z_D) arises due to the changes that occur in the Hamiltonian of the system during the different phases of the cycle. The total work done is $W_{tot} = Q_{AB} + Q_{BC} + Q_{CD} + Q_{DA}$. The efficiency of the Stirling heat cycle is expressed as:

$$\eta_{Stir} = 1 + \frac{Q_{BC} + Q_{CD}}{Q_{DA} + Q_{AB}}. \tag{8.1.5}$$
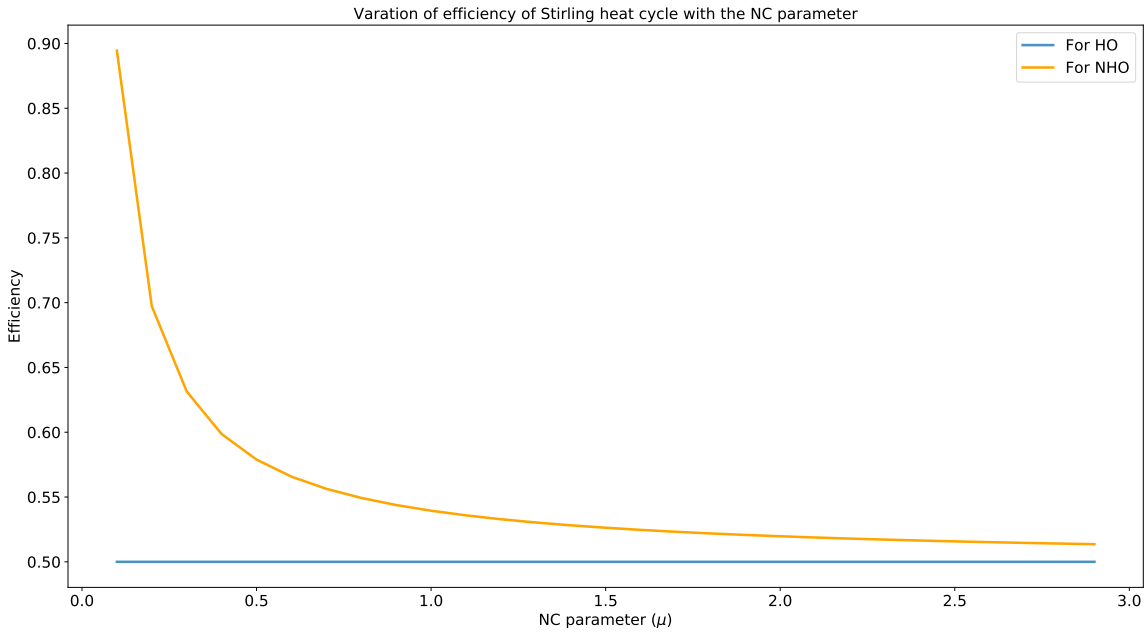
Figure 8.1. (Color Online) The variation of the efficiency of the Stirling cycle for the HO and NHO. The temperature of the hot bath and the cold bath is $T_h = 20K$ and $T_c = 10K$ respectively. The yellow and the blue solid line is the variation of the efficiency of NHO and HO with NC parameter, respectively.

8.2   Stirling refrigerator cycle

If we reverse the cycle, we will have a Stirling refrigerator [123]. Following the same methodology, as done above, we can analyze all four stages of the cycle.

(i) The first phase is the *isothermal* process. In this process, the system is paired to a

cold bath at temperature T_c. This is just the reverse of the first phase of the heat cycle. In this phase of the cycle, there is a quasi-static change of the Hamiltonian (as described in section 4.3) of the system which is described as in section 2.2. The entropy of the system changes during this process. The heat absorbed is:

$$Q_{AB} = T_c \Delta S. \tag{8.2.1}$$

(ii) The second stage is the *isochoric* process. During this stage of the cycle, the temperature of the system increases when connected to T_h from T_c. The mean internal energy of the system changes during this phase of the working cycle. The heat gain for this phase is:

$$Q_{BC} = U_C - U_B. \tag{8.2.2}$$

(iii) This phase is an *isothermal* process. During this stage of the cycle, the system is bridged with the hot reservoir with a temperature T_h. Heat is rejected from the system and is described as:

$$Q_{CD} = T_h \Delta S. \tag{8.2.3}$$

(iv) The last stage is an *isochoric* process. The system is reverted to the cold reservoir T_c from the hot reservoir T_h, which leads to a decrease in the internal energy of the system. The amount of heat released is:

$$Q_{DA} = U_A - U_D. \tag{8.2.4}$$

The entropy of the system can be evaluated from the partition function of the system as $S = \ln Z + \beta U$. The internal energy can be evaluated as shown while we have analyzed the heat cycle. The COP of the Stirling refrigerator cycle is expressed as:

$$COP_{Stir} = \frac{Q_{AB} + Q_{BC}}{W_T}, \tag{8.2.5}$$

where $W_T = Q_{AB} + Q_{BC} + Q_{CD} + Q_{DA}$ is the total work done on the system.

We can visualize the growth in the COP for the Stirling cycle for NHO due to the non-commutating parameter. Whereas for the case of HO the COP remains constant as it is independent of this parameter. For $\omega > \omega'$ and $\beta_h < \beta_c$ we encounter a steep rise in the COP with respect to the NC parameter as shown in Fig. (8.2). In Fig. (8.1), the efficiency of the engine decreases with the increase in the NC parameter. So the non-commutative is less
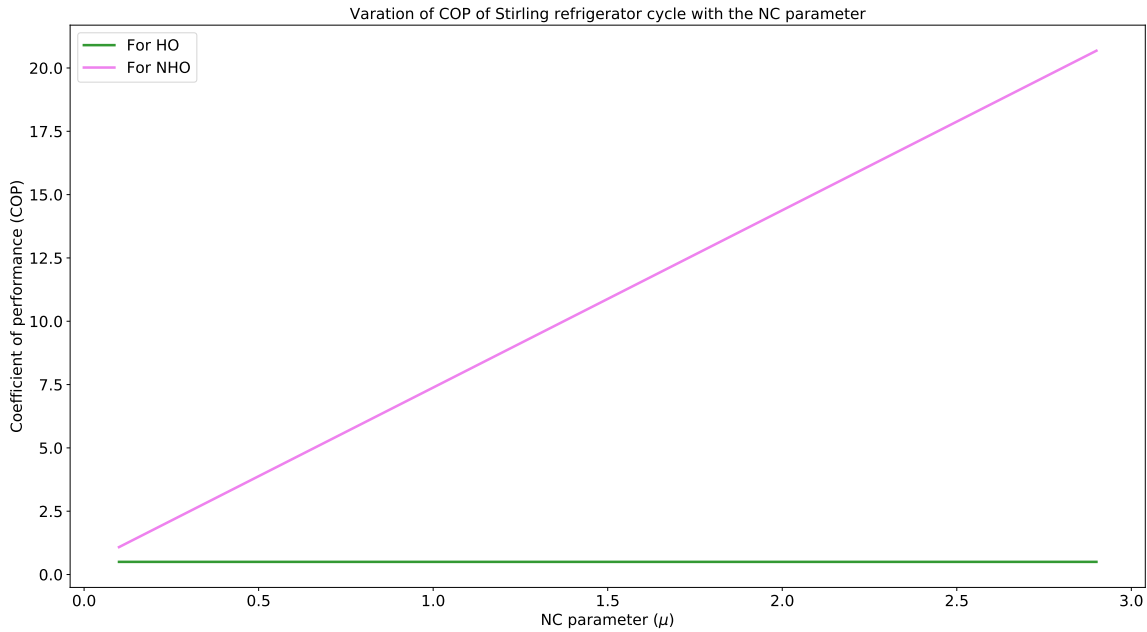
Figure 8.2. (Color Online) The variation of the COP of the Stirling refrigerator cycle for the Harmonic Oscillator (HO) and NHO. The temperature of the hot bath and the cold bath is $T_h = 20K$ and $T_c = 10K$ respectively. The violet and the green solid line is the variation of the COP of NHO and HO with NC parameter, respectively.

effective when the NC parameter is high for the engine model that we have considered for our analysis. For the generic statement of the less effectiveness of NC parameter on the engine model, we have to explore other cycles which is an open area for exploration.

The maximum attainable efficiency of the heat engine by the standard harmonic oscillator has been plotted as a reference point for the analysis of the advantage due to the NC space. Now, due to the change in the space structure, the standard Hamiltonian changes to the non-commutative harmonic oscillator by applying the transformation from the commutative space to the non-commutative space. So, to compare the advantage of the change introduced by the non-commutative space, we have considered the standard harmonic oscillator as a reference point. For the Stirling cycle, we can visualize the advantage in Fig. (8.1) and Fig. (8.2).

For the evaluation of the efficiency and the COP of the Stirling cycle as described in the Fig. 8.1 and Fig. 8.2 respectively, we have performed numerical simulation in Python with a complexity of $\mathcal{O}(n)$, where n describes the number of iteration of process for the variation of the non-commutative parameter.

8.3   Otto refrigerator cycle

The generic description of the quantum Otto cycle with harmonic oscillator as the working medium is described in section 2.8.1. Now, we will study the quantum *Otto refrigerator cycle* [110, 125, 484] with non-commutative space harmonic oscillator as the working substance. The four phases of the Otto refrigerator for our analysis are described as follows:

(i) The first phase of the cycle is an *isochoric (A→B)* process. During this process, the system is coupled to a cold reservoir at a temperature T_C while the Hamiltonian remains constant. The heat absorbed from the reservoir during this process is:

$$Q_{cold} = \sum_n E_n^{cold}(P_n^{hot} - P_n^{cold}), \tag{8.3.1}$$

where $P_n^{cold} = \frac{\exp(-\beta E_n)}{Z}|_{\beta=\beta_{cold},\omega=\omega'}$ and
$P_n^{hot} = \frac{\exp(-\beta E_n)}{Z}|_{\beta=\beta_{hot},\omega=\omega}$ represents the occupation probabilities of the system in the nth eigenstate and $E_n^{cold} = E_n$ for $\omega = \omega'$.

(ii) The second stage of the cycle is an *adiabatic (B→C)* process. During this phase of the cycle, the entropy of the system is conserved. Throughout the evolution of the system in this phase, the occupation distribution remains invariant.

(iii) The third stage of the cycle is an *isochoric (C→D)* heating process. In this process, the system is connected to a hot reservoir at temperature T_H. The heat rejected to the hot reservoir in this phase is:

$$Q_{hot} = \sum_n E_n^{hot}(P_n^{cold} - P_n^{hot}), \tag{8.3.2}$$

where $E_n^{hot} = E_n$ for $\omega = \omega$.

(iv) The last stage of the cycle is an *adiabatic (D→A)* process. In this process, the system changes quasi-statically while the entropy of the system remains constant during the execution of this phase. The total work done on the cycle can be evaluated as, $W_{total} = Q_{hot} + Q_{cold}$. The COP for the Otto refrigerator is defined as the ratio of the amount of heat removed from the cold reservoir to the net amount of work done on the system under analysis. It is represented as:

$$\Xi_{Otto} = \frac{Q_{cold}}{|W_{total}|}. \tag{8.3.3}$$

In the case of the Otto refrigerator, we have encountered a similar effect as in the case of the Stirling cycle. We have detected the growth in the COP for the Otto cycle for NHO due to the non-commuting parameter shown in Fig. (8.4). But in the case of HO, the COP
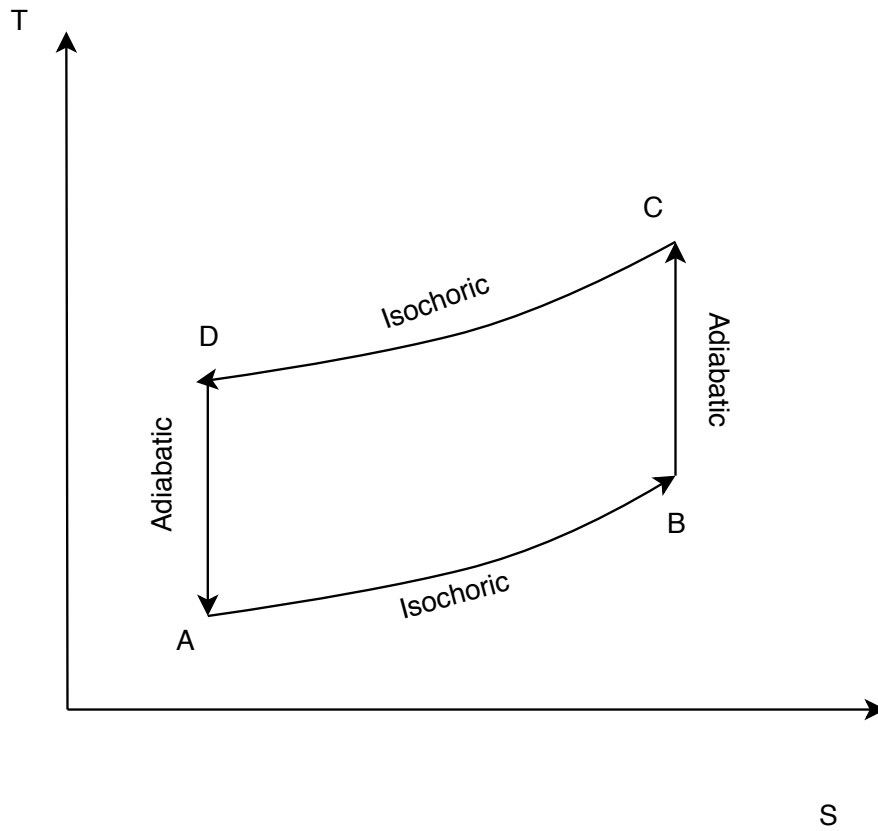
Figure 8.3. Schematic diagram for the four stages of the Otto cycle.
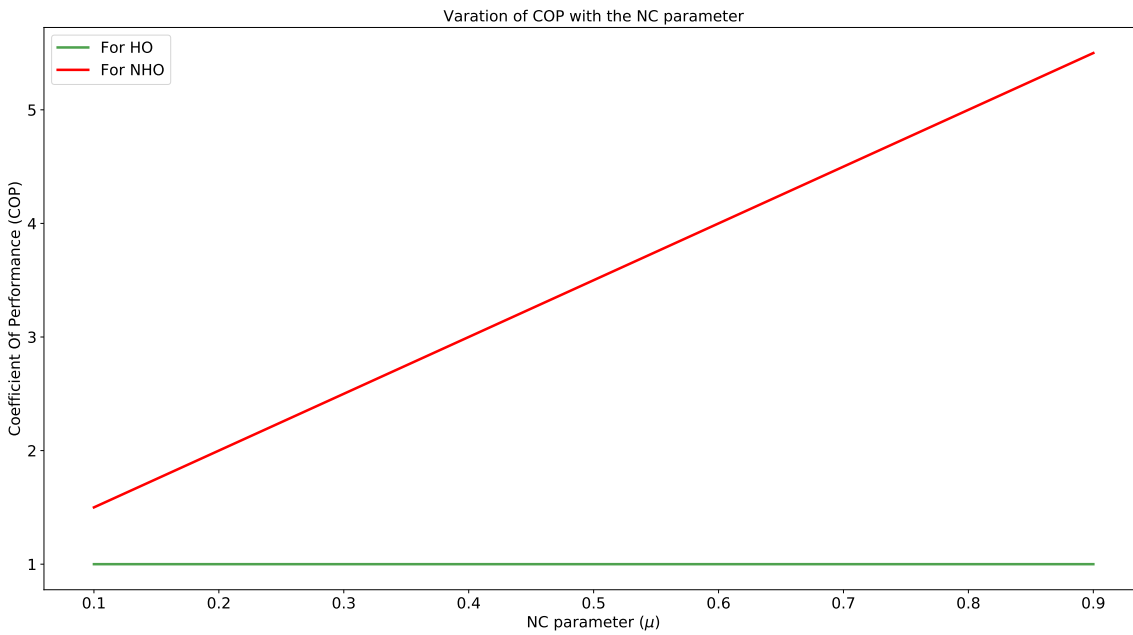
Figure 8.4. (Color Online) The plot depicts the evaluation of the COP of the Otto refrigerator for the HO and NHO. The temperature of the hot and the cold bath is $T_h = 20K$ and $T_c = 10K$ respectively. The red and the green solid line is the variation of the COP of NHO and HO with NC parameter, respectively.

remains constant. A steep rise in the coefficient of the NC parameter occurs for $\omega > \omega'$ and $\beta_h < \beta_c$, and this gives rise to this phenomenon. Following a similar pattern, as done during the analysis of the Stirling cycle, we have considered the maximum attainable efficiency of the heat engine by the standard harmonic oscillator has been plotted as a reference point for the analysis of the advantage due to the NC space. For the Otto cycle, we can visualize the advantage in Fig. (8.4). For the evaluation of the COP of the Otto refrigerator as described in the Fig. (8.4), we have numerically simulated the COP of the refrigerator. The simulation is carried out in Python with a complexity of $\mathcal{O}(n)$, where n describes the number of iteration of process for the variation of the non-commutative parameter.

The immediate question that pokes our intuition is whether it is feasible with the quantum technology we have? The answer to this is yes. One can analyze the non-commutative space effect using optical setup and measure the effectiveness of the non-commutative parameter as shown in [462]. They have provided a schematic representation of the experimental setup for the following analysis. Following the same methodology, we can develop the setup for the analysis of different thermodynamic cycles. For the experimental realization of the cycle in non-commutative space, one should keep in mind the basic ingredients that are required for the analysis. One of which is the availability of thermal heat baths for the different processes. The second one is about the measurement of the work performed during the different phases of the cycle, as in the case of the Otto cycle, the phases are two adiabatic processes. One of which expands the working medium and the other compresses the working medium. The third one is maintaining the thermal equilibrium during the thermalization processes. The experimental analysis of the engines and refrigerators of NC space is an open area to explore.

8.4   Chapter Summary

The non-commutative harmonic oscillator outperforms the harmonic oscillator in terms of the COP for the Stirling cycle and the Otto refrigerator. The contribution for this is provided by the non-commutative space parameter. So, we can infer that non-commutative is a boon for the refrigerators if considered for the growth of the COP. Whereas the NC parameter is less effective for a boost in the efficiency of the heat cycle for the considered model.

For the appropriate implementation of the Otto refrigerator, it requires a slow implementation of the adiabatic processes so that we can maintain no further coherence generation on the eigenstates of the non-commutative space Hamiltonian. If there is any change, then the mean population will also change. To achieve thermal equilibrium with the reservoir, the

system must spend a long time during the thermalization processes. The non-linearity that is generated in the Hamiltonian appears due to the non-commutative parameter, which requires some energy cost for the implementation of the cycle.

This model can result in a better resource in the applicable areas [485] of quantum theory which needs further analysis. This model can be used for the analysis of the coupled working medium as shown in previous works [136, 486, 487]. It can also be utilized for exploring the non-Markovian reservoirs in NC space. We have analyzed two thermodynamic cycles. One can analyze the different existing reversible cycles and irreversible cycles. It will be interesting to explore the effect of NC parameters in the irreversible cycles and on the quantum phase transition.

For the analysis of our work, we have used one of the existing models of the non-commutative space. To make the generic statement of the gain in COP for different cycles, one has to explore all the existing models in the non-commutative space. This is an open area to explore. One can also analyze the effect of the NC parameter on the different thermodynamic variables. We can analyze this model from an uncertainty viewpoint [36, 43, 429] to reduce the cost for the analysis of the cycles. Along with that, it will be interesting to explore the experimental realization of these cycles in NC space.

9

Quantum Thermal Engines with Coupled Harmonic Oscillator in Non-relativistic Non-Commutative Space

Contents

The contents in this chapter are based on the article in Ref. [41].

The thermodynamic machine has practical importance in the field of quantum computation and refrigeration in micro regimes [72]. Coupled quantum systems, as the working medium for heat engines, have been studied widely in previous works [136, 202]. It is shown in the work [136, 202] that with appropriate coupling the efficiency of the system can be increased compared with the uncoupled one. Experimental realization of the Otto cycle [488]

has also been analyzed.

In this chapter, we will describe our work, where we have considered a coupled harmonic oscillator as the working substance for the analysis of quantum cycles in commutative space and non-commutative spacetime. We have considered two non-commutative phase space structures for our analysis. Our ultimate goal is to inspect different quantum engine cycles with coupled harmonic oscillators as the working substance for considered non-commutative phase-space structures and also for the commutative space structure. Different heat cycles in the quantum realm have a harmonic oscillator as their working principle. We have considered two reversible cycles, i.e., the Stirling cycle and the Otto cycle for analysis. The efficiency of the cycle is evaluated for each engine cycle for commutative, and NC phase space structure after the working substance evolves through every stage of their individual cycles. The effects are astonishing when the cycles are in NC phase space.

In the case of the Otto cycle, the coupling strength of the coupled oscillator produce a constant efficiency in commutative phase space, but it gets a catalytic effect when the engine is in NC phase space. Similarly, when the Stirling cycle is analyzed with the coupled harmonic oscillator as the working medium the coupling strength results in higher efficiency than the decoupled oscillator. But in NC phase space the efficiency gets a boost and picks up the efficiency near to the ideal models of the engine cycles. The working medium is much more effective for the Stirling cycle than the Otto cycle in all forms of space structure that is analyzed in this work. Works with space structure with different approach is shown in [40, 480–482].

Though it seems to be mathematically feasible, one immediate question that comes to one's mind is regarding the physical accessibility of the NC phase space with the so-far existing modern quantum technology. Recent works for the physical accessibility of the NC phase space using quantum optics [462, 463] and Opto-mechanical [489] setup has been developed. So, the possibility of experimental verification and analysis of NC phase space will provide a boost for the exploration of quantum information theory in NC space structure.

The prime focus of this chapter is to analyze how the change in the space structure can affect the efficiency of the different quantum thermal engine models. For that, we have considered the traditional formalism of thermodynamics. The considered system is analyzed when the system reaches its equilibrium state. The non-equilibrium thermodynamics of the engines, which is referred to as finite-time thermodynamics has not been explored here. Non-equilibrium thermodynamics in NC space has been explored in some previous works [490, 491] that are mainly focused on the analysis of the Brownian motion in NC space structure.

They have shown that the master equation for the NC space boils down to the master equation of the ordinary space (commutative space) when the non-commutative parameter is equated to zero. Due to the non-commutative parameter, we encounter some extra terms which affect the results that we get from the ordinary space. The non-equilibrium thermodynamics of the engine models in NC space is an open area for exploration.

9.1   Otto cycle with coupled harmonic oscillator

The four stages of a quantum Otto cycle with harmonic oscillator as the working medium is schematically described in Fig. (2.6) as described in section 2.8.1. For our analysis, the four stages of the quantum Otto cycle with the coupled harmonic oscillator can be described as follows:

(1) In the first stage of the cycle which is the isochoric process, the working medium is coupled with the bath at temperature T_h. In other words, the Hamiltonian $H^{(1)}$ is attached to the hot bath. The system is represented by the density matrix $\rho_c^{(2)}$. The Hamiltonian is fixed throughout this process. The system approaches equilibrium with the bath at the end of this process. So, the final state of the system after this stage is given as $\rho_h^{(1)} = \frac{exp(-\beta_h H)}{Tr[exp(-\beta_h H)]}$, where $\beta_h = 1/k_B T_h$, with k_B as the Boltzmann constant. The amount of heat absorbed from the bath at temperature T_h is $Q_{hot} = Tr[H(\rho_h^{(1)} - \rho_c^{(2)})]$.

(2) The second stage of the cycle is the adiabatic process. The working medium in this phase is thermally isolated so that the quantum adiabatic theorem is valid throughout the process. The Hamiltonian of the system changes from $H^{(1)}$ to $H^{(2)}$. During this process, we do not encounter any heat exchange between the system and the bath. So, the change in energy is equivalent to the work done. The work done is described as:

$$W_1 = Tr[(\rho_h^{(1)} H^{(1)} - \rho_h^{(2)} H^{(2)})],$$

where $\rho_h^{(2)} = U_1 \rho_h^{(1)} U_1^\dagger$, with U_1 as the unitary operator which is associated with the adiabatic process. It is defined as:

$$U_1 = \mathscr{T} e^{[-(\frac{i}{\hbar}) \int_0^{\mathscr{T}} H(t)dt]},$$

where $\mathscr{T}$ represents the total time of evolution for the quasi-static process. Here $H(0) = H^{(1)}$ and $H(\mathscr{T}) = H^{(2)}$.

(3) The third stage is represented by the isochoric process. At this phase of the cycle the system is coupled with a cold bath at a temperature T_c. Similar to the stage one, the system

attains equilibrium with the cold bath at the end of this stage. The state of the system at this phase is described as $\rho_c^{(1)} = \frac{e^{(-\beta_c H^{(2)})}}{Tr[e^{(-\beta_c H^{(2)})}]}$. So, heat is rejected to the bath and is evaluated as $Q_{cold} = Tr[H^{(2)}(\rho_c^{(1)} - \rho_h^{(2)})]$.

(4) The last stage of the cycle is the adiabatic process. In this last phase of the cycle, the working substance is thermally isolated from the reservoir and at the end of this process, the system gets coupled with the hot bath. During this process, the Hamiltonian changes from $H^{(2)}$ to $H^{(1)}$. So, the work done in this process is:

$$W_2 = Tr[\rho_c^{(1)} H^{(2)} - \rho_c^{(2)} H^{(1)}],$$

which is equivalent to variation in the mean energy. Here $\rho_c^{(2)}$ is the density state of the system at the end of this process. It is defined as $\rho_c^{(2)} = U_2 \rho_c^{(1)} U_2^\dagger$, where U_2 is evaluated as:

$$U_2 = \mathscr{T} e^{[-(\frac{i}{\hbar}) \int_0^{\mathscr{T}} H(t)dt]}.$$

Here $H(0) = H^{(2)}$ and $H(\mathscr{T}) = H^{(1)}$.

During the execution of the process of the Otto cycle, the Hamiltonian of the system evolves from $H(0) = H^{(1)}$ to $H(\mathscr{T}) = H^{(2)}$. One can visualize that the NC space follows the standard master equation for the analysis of the evolution of the system as suggested by the previous analysis [491, 492].

9.1.1 In commutative phase space

Here, we will consider two coupled oscillators as our working substance. The Hamiltonian for this coupled system in commutative phase space is described in Eq. (4.4.12). Now we will consider the Otto cycle described above with the coupled system as the working medium.

During the first adiabatic process, the Hamiltonian of the working substance of the Otto cycle changes its initial value from $H^{(1)}$ to $H^{(2)}$ (which is described in section 4.4). The change in the Hamiltonian is due to the change in the eigenfrequency of the oscillators from ω_1 to ω_2. It reverts to its respective initial values after the execution of the second adiabatic process of the cycle. The total work done by the system is the sum of the contribution of the two oscillators. So, the work done is a function of the frequency of the oscillators and the coupling strength of the two oscillators. The frequency of the two oscillators is considered to be the same for our analysis. During the execution of the adiabatic process, it is assumed that there is no cross-over of the energy level of the Hamiltonian of the coupled oscillator. It is

also taken care of that the system abides by the quantum adiabatic theorem. So, the process occurs slowly enough such that the population of the eigenstate of the Hamiltonian remains constant throughout the process. The total amount of heat absorbed by the working medium from the hot bath is given by:

$$
\begin{aligned}
Q &= Tr[H(\rho_h^{(1)} - \rho_c^{(2)})] \\
&= \frac{\hbar \omega_1 e^{\zeta}}{2}\left(\coth\left[\frac{\beta_h \hbar \omega_1 e^{\zeta}}{2}\right] - \coth\left[\frac{\beta_c \hbar \omega_2 e^{\zeta}}{2}\right]\right) \\
&+ \frac{\hbar \omega_1 e^{-\zeta}}{2}\left(\coth\left[\frac{\beta_h \hbar \omega_1 e^{-\zeta}}{2}\right] - \coth\left[\frac{\beta_c \hbar \omega_2 e^{-\zeta}}{2}\right]\right).
\end{aligned}
\tag{9.1.1}
$$

The total work done of the Otto cycle is define $W = W_1 + W_2$. So, the work done for the Otto cycle with coupled HO as the working medium is expressed as:

$$
\begin{aligned}
W &= \frac{\hbar(\omega_1 - \omega_2)e^{\zeta}}{2}\left(\coth\left[\frac{\beta_h \hbar \omega_1 e^{\zeta}}{2}\right] - \coth\left[\frac{\beta_c \hbar \omega_2 e^{\zeta}}{2}\right]\right) \\
&+ \frac{\hbar(\omega_1 - \omega_2)e^{-\zeta}}{2}\left(\coth\left[\frac{\beta_h \hbar \omega_1 e^{-\zeta}}{2}\right] - \coth\left[\frac{\beta_c \hbar \omega_2 e^{-\zeta}}{2}\right]\right).
\end{aligned}
\tag{9.1.2}
$$

The efficiency of the coupled system which is considered as the working medium is defined as the ratio of total work over the total heat absorbed by this system during the execution of the process. It is given as:

$$
\eta_{otto_C} = \frac{W}{Q} = f(\zeta).
$$

Figure 9.1. (Color online) Efficiency of the Otto cycle as a function of the coupling parameter in commutative space with coupled HO as the working substance.

We have considered the hot reservoir temperature $T_h = 4K$ and that of the cold reservoir temperature $T_c = 1K$. The frequency for the coupled oscillator is considered as $\omega_1 = 4$ and $\omega_2 = 3$ for the evaluation of the efficiency of the Otto cycle with respect to the variation of the coupling strength. For the analysis of the efficiency of the engine, we have numerically simulated the efficiency factor with respect to the coupling parameter. The efficiency of the Otto cycle with coupled harmonic oscillator as the working substance remains constant with the change in the coupling parameter as shown in Fig. (9.1). The efficiency for the engine model with the coupled harmonic oscillator considered in our analysis produces an equivalent result to the previously studied models [202]. One can infer from all these different analyses that the coupling of harmonic oscillators does not provide any good advantage to the efficiency of this specific engine model. So, we can conclude that the coupling strength of the coupled oscillators results in a constant efficiency even for the two different approaches.

9.1.2   In non-commutative phase space

In the case of commutative space, the coupled oscillators as the working substances result in a constant efficiency with respect to the coupling strength of the system. Now here, we will analyze how the change in the phase space affects the thermodynamic process. The Hamiltonian of the two harmonic oscillators coupled with each other in the NC phase space is described in Eq. (4.4.12). Following the same methodology as used in the case of commutative space we will analyze the quantum Otto cycle in the NC phase space. We have considered even in NC space that the working medium will evolve to a Gibbs state when coupled to a heat bath similar to the previous analysis in this direction [490]. We have followed this throughout our analysis.

Similar to the case in commutative space, the Hamiltonian changes its initial value from $H^{(1)}$ to $H^{(2)}$ (which is described in section 4.4.1) during the first adiabatic process. The change in the Hamiltonian is due to the change in the eigenfrequency of the oscillators from ω_1 to ω_2. It goes back to its respective initial values after the second adiabatic process of the cycle. So, the work done is a function of the frequency of the oscillators, the coupling strength of the two oscillators, and the NC parameter of the phase space. For our analysis, the frequency of the two oscillators is considered to be the same throughout. We take care of the fact that there is no cross-over of the energy levels of the Hamiltonian which ultimately satisfies the quantum adiabatic theorem in the NC phase space. The net amount of heat absorbed is given as:

$$
\begin{aligned}
Q &= Tr[H(\rho_h^{(1)} - \rho_c^{(2)})] \\
&= \frac{\hbar\left(\omega_1 + \frac{K\theta}{2\hbar}\right)}{2}\left(\coth\left(\frac{\beta_h\hbar\left(\omega_1 + \frac{K\theta}{2\hbar}\right)}{2}\right) - \coth\left(\frac{\beta_c\hbar\left(\omega_2 + \frac{K\theta}{2\hbar}\right)}{2}\right)\right) \\
&+ \frac{\hbar\left(\omega_1 - \frac{K\theta}{2\hbar}\right)}{2}\left(\coth\left(\frac{\beta_h\hbar\left(\omega_1 - \frac{K\theta}{2\hbar}\right)}{2}\right) - \coth\left(\frac{\beta_c\hbar\left(\omega_2 - \frac{K\theta}{2\hbar}\right)}{2}\right)\right).
\end{aligned}
\tag{9.1.3}
$$

The total work done of the Otto cycle is defined as $W = W_1 + W_2$. So, the work done for the Otto cycle with coupled HO as the working medium in NC space is expressed as:

$$
\begin{aligned}
W &= \frac{\hbar\left(\omega_1 - \omega_2\right)}{2}\left(\coth\left(\frac{\beta_h\hbar\left(\omega_1 + \frac{K\theta}{2\hbar}\right)}{2}\right) - \coth\left(\frac{\beta_c\hbar\left(\omega_2 + \frac{K\theta}{2\hbar}\right)}{2}\right)\right) \\
&+ \frac{\hbar\left(\omega_1 - \omega_2\right)}{2}\left(\coth\left(\frac{\beta_h\hbar\left(\omega_1 - \frac{K\theta}{2\hbar}\right)}{2}\right) - \coth\left(\frac{\beta_c\hbar\left(\omega_2 - \frac{K\theta}{2\hbar}\right)}{2}\right)\right).
\end{aligned}
\tag{9.1.4}
$$

The efficiency of the coupled system is defined as the ratio of total work over the total heat absorbed by this system during the execution of the process. It is described as:

$$
\eta_{otto_{NC}} = \frac{W}{Q} = f(\theta).
$$

Similar to the case of commutative space, we have considered the hot reservoir temperature $T_h = 4K$ and that of the cold reservoir temperature $T_c = 1K$. The frequency for the coupled oscillator is considered as $\omega_1 = 4$ and $\omega_2 = 3$ for the evaluation of the efficiency of the Otto cycle with respect to the variation of the NC space parameter. For our analysis, we have fixed the coupling strength $\zeta = 2$ and the constant $K = 0.25$. Here we have numerically simulated the efficiency of the engine model in NC space structure with respect to the NC parameter. We can observe that the efficiency of the engine model (as shown in Fig. (9.2)) boils down to the efficiency of the commutative space when the NC parameter θ is close to zero. This satisfies the condition that the results produced by the system reduce to the commutative space when $\theta \to 0$. With the variation of the NC parameter, we observe that the efficiency increases monotonously for a certain range of the NC parameter. Then at a certain stage, the efficiency of the engine gets saturated with the variation of the NC parameter. So, we can infer that NC space provides a boost to the efficiency of the engine over the efficiency of the commutative space.

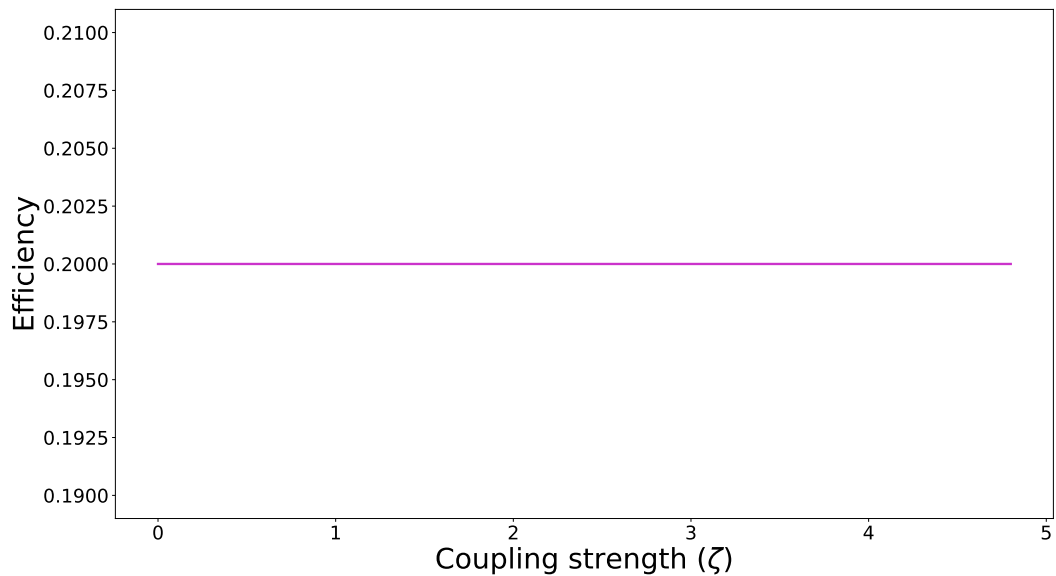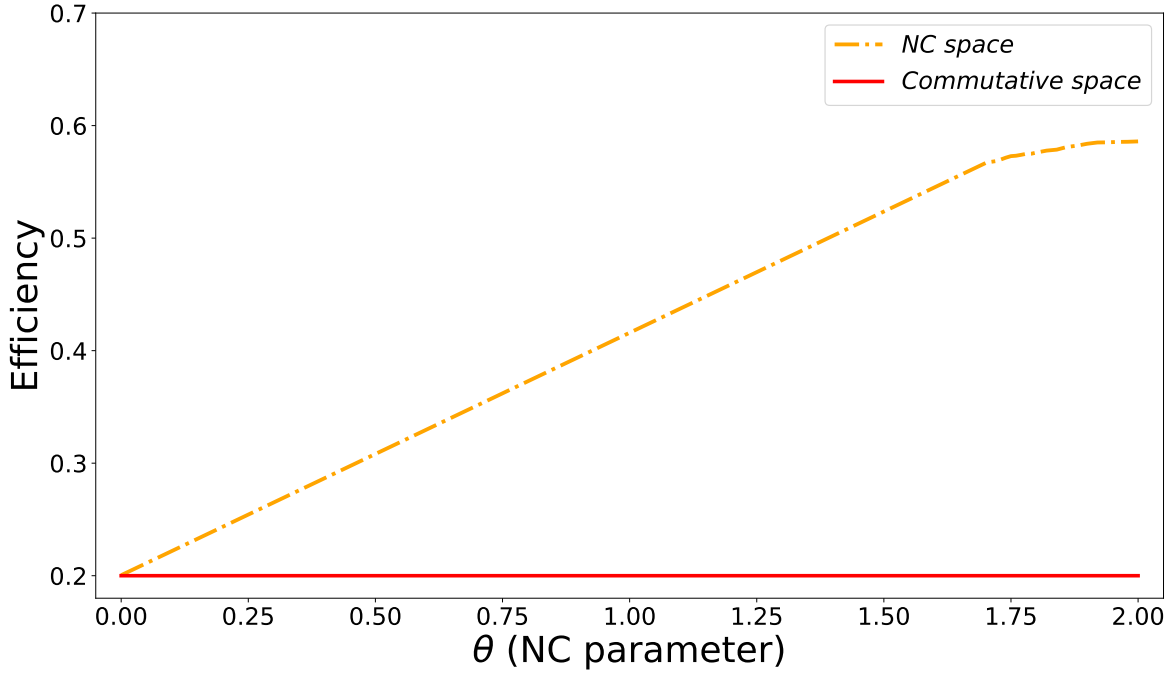**Figure 9.2.** (Color online) Efficiency of the Otto cycle as a function of the NC parameter with coupled HO as the working substance is shown. The orange dash dotted curve depicts the variation of the efficiency with respect to the NC parameter with a constant coupling factor. The red solid line depicts the efficiency of the commutative space with coupled HO as the working substance where the coupling constant $\zeta = 2$.

9.1.3 In generalized non-commutative phase space

In the case of non-commutative phase space, the coupled oscillators as the working substances result in a catalytic effect to the efficiency with respect to the NC space parameter of the system. The efficiency is high for the lower values of the NC parameter. Now, we will analyze how the generalized NC phase space affects the thermodynamic process. The Hamiltonian of the two coupled harmonic oscillators in the NC phase space is described in Eq. (4.4.14). Following the same methodology, as used in the case of non-commutative space we will analyze the quantum Otto cycle in the NC phase space.

In the case of generalized NC phase space, the Hamiltonian is separated into two parts as shown in Eq. (4.4.14). During the adiabatic process, the individual Hamiltonian changes from the initial values from $H^{(1)}$ to $H^{(2)}$ (which is described in section 4.4.2). The total Hamiltonian is the sum of the effect of these two Hamiltonians. The changes in the Hamiltonian is due to the change in the eigenfrequency of the oscillators, where the eigenfrequency for the first oscillator changes from ω_1 to ω_1' and for the second oscillator the frequency changes from ω_2 to ω_2'. After the second adiabatic process, the eigenfrequencies return to the respective initial stage. So, we can consider that the working substance is composed of two independent oscillators. The total work done is a result of the contribution of the two

oscillators. Therefore, the work done is a function of the frequency of the system and the NC phase space parameters. Similar to the previous cases, we have to take care of the fact that there is no cross-over of the energy levels of the total Hamiltonian during the execution of the adiabatic process. The total amount of heat absorbed by the system is described as:

$$
\begin{aligned}
Q &= Tr[H(\rho_h^{(1)} - \rho_c^{(2)})] \\
&= \frac{\omega_1}{2}\left(\coth\left[\frac{\beta_h\omega_1}{2}\right] - \coth\left[\frac{\beta_c\omega_1'}{2}\right]\right) + \frac{\omega_2}{2}\left(\coth\left[\frac{\beta_h\omega_2}{2}\right] - \coth\left[\frac{\beta_c\omega_2'}{2}\right]\right).
\end{aligned}
\tag{9.1.5}
$$

The total work done by the system is equivalent to the sum of the work done by the individual systems. So, the total work done for the system can be expressed as:

$$
\begin{aligned}
W &= \frac{(\omega_1 - \omega_1')}{2}\left(\coth\left[\frac{\beta_h\omega_1}{2}\right] - \coth\left[\beta_c\omega_1'\right]\right) \\
&+ \frac{(\omega_2 - \omega_2')}{2}\left(\coth\left[\frac{\beta_h\omega_2}{2}\right] - \coth\left[\beta_c\omega_2'\right]\right).
\end{aligned}
\tag{9.1.6}
$$

where the frequencies of the system is defined equivalent to the Eq. (4.4.16).

The efficiency of the coupled harmonic oscillator system for the generalized NC phase space is defined as the ratio of total work over the total heat absorbed by this system. It is described as:

$$
\eta_{otto_{GNC}} = \frac{W}{Q} = f(\gamma, \xi).
\tag{9.1.7}
$$
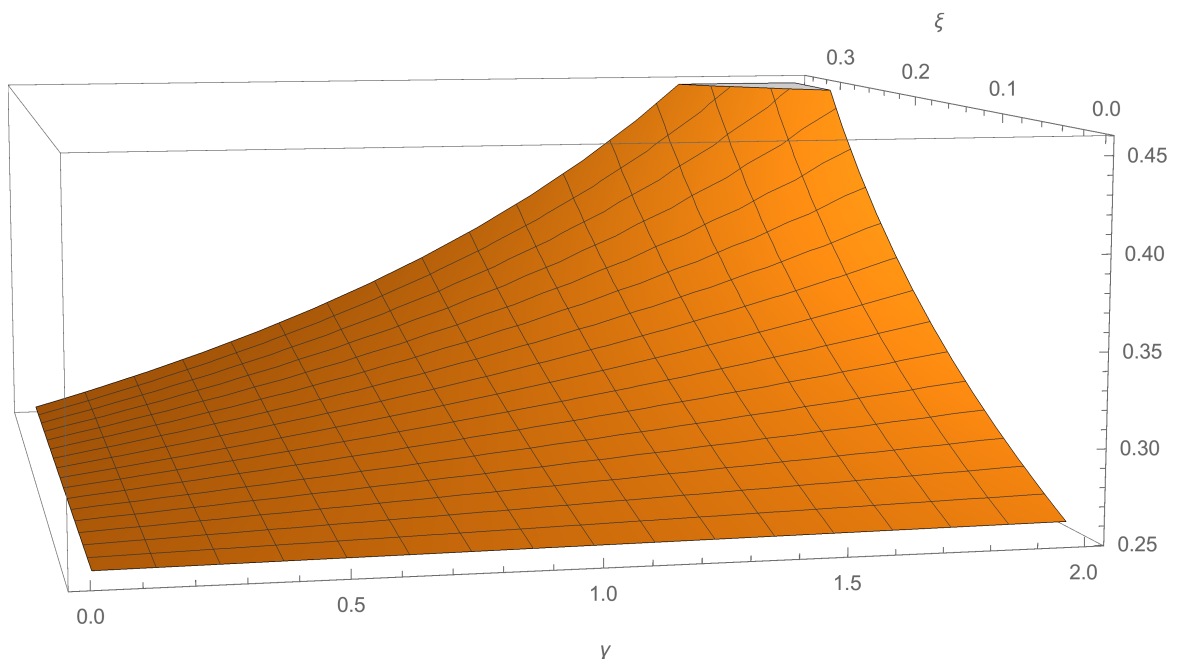
Figure 9.3. (Color online) Efficiency of the Otto cycle as a function of the NC parameters in generalized NC phase space parameters with coupled HO as the working substance.

Similar to the case of non-commutative space, we have considered the hot reservoir temperature $T_h = 4K$ and that of the cold reservoir temperature $T_c = 1K$ for the analysis of the Otto cycle in generalized NC phase space. Though we define this as generalized NC space, actually we incorporate the deformation in momentum space as well as the coordinate space. So, in this space structure, the NC effect increases than the above one. The frequency for the coupled oscillator is taken as $\omega_1 = 4$ and $\omega_2 = 3$ for the evaluation of the efficiency of the Otto cycle with respect to the variation of the generalized NC space parameters. The coupling strength is taken as $\zeta = 2$ and the constant $K = 0.25$ throughout the process. The three-dimensional plot (in Fig. (9.3)) shows the variation of the efficiency of the Otto cycle with coupled harmonic oscillator as the working substance in the generalized NC phase space. The variation of the NC parameter of the coordinate and the momentum space, i.e., ξ and γ in the graph shows that it has a direct impact on the efficiency of the engine. So, the so-called generalized NC space results in better efficiency of the engine compared to the NC space considered above for the analysis.

For the evaluation of the efficiency of the Otto cycle in commutative as well as non-commutative space we have performed numerically simulation. We have used Mathematica for deriving the solution of the equations and Python for data generation and ploting of the efficiency of the engine model.

9.2 Stirling cycle with coupled harmonic oscillator

The generic representation of the quantum Stirling cycle with the harmonic oscillator is described in section 2.8.2. Here in this work, we will consider coupled harmonic oscillator as our working medium for the analysis of the quantum Stirling cycle is commutative as well as non-commutative space structure. The four phases of the cycle for the considered working medium is described as follows:

(i)First stage of the Stirling cycle: the *isothermal process* $(A \rightarrow B)$. The working substance in this stage is coupled with the heat bath at temperature T_h. All the way round during the execution of this process, the system remains in thermal equilibrium with the hot reservoir. Due to the quasi-static changes in the Hamiltonian from $H^{(1)}$ to $H^{(2)}$ (where the Hamiltonian for the process is described in section 4.4) of the working medium, we encounter changes in the energy spectrum and the internal energy of the system. During this process, heat is extracted from the bath isothermally.

(ii) Second phase: the *isochoric process* $(B \rightarrow C)$. The system undergoes an isochoric

heat exchange while it goes through this phase of the cycle. The system is now decoupled from the hot reservoir and coupled with the cold reservoir at temperature T_c. So, heat gets released during this process of the cycle.

(iii) Third phase: the *isothermal process* $(C \rightarrow D)$. The system remains connected to the cold reservoir at temperature T_c throughout this process. This phase follows the same condition that is being followed during the execution of the first isothermal process. The system remains at thermal equilibrium with the reservoir. So, heat is rejected to the reservoir in this stage of the cycle where the Hamiltonian is reverted back to its initial state.

(iv) Fourth stage: the *isochoric process* $(D \rightarrow A)$. The system is decoupled from the cold reservoir and reverted to the hot reservoir at temperature T_h. So, heat is extracted from the bath in this process of the cycle.

The efficiency of the Stirling Cycle is defined as the ratio of work output to heat input. For our analysis, the efficiency with being a function of the coupling strength and the NC parameters in NC phase space.

9.2.1 Commutative phase space

Now, for our analysis, we will consider a coupled HO in commutative phase space as the working substance of the Stirling cycle. The Hamiltonian of the system is described in Eq. (4.4.6) of the section 4.4. The energy eigenvalues for this Hamiltonian are evaluated as conveyed in Eq. (4.4.7). The partition function for the considered system is described as:

$$Z = \sum_n e^{-\beta E_n}, = \frac{e^{-\beta\omega\cosh(\zeta)}}{\beta^2\omega^2}, \qquad (9.2.1)$$

where the system has to satisfy the condition $Re\left[e^{\zeta}\beta\omega\right] > 0$.

The heat exchange that takes place during the first stage (i.e, the isothermal process) of the Stirling cycle is:

$$Q_{AB} = U_A - U_B + \frac{1}{\beta_h}ln\Big(\frac{Z_{\omega_1,\beta_h}}{Z_{\omega_2,\beta_h}}\Big), \qquad (9.2.2)$$

One can evaluate the partition function Z_A, Z_B of the system using Eq. (9.2.1). The internal energy U_A, U_B is evaluated using the definition $U_i = -\partial lnZ_i/\partial\beta_h$, where $i = A, B$. The internal energy is described as:

$$U = -\frac{2}{\beta} - \omega\cosh(\zeta).$$

In the second phase of the cycle heat is released from the system. The heat exchange

throughout this process can be expressed as:

$$Q_{BC} = U_C - U_B. \tag{9.2.3}$$

The third phase is again a isothermal process. Heat gets rejected from the system in this stage. The heat exchange is represented as:

$$Q_{DC} = U_D - U_C + \frac{1}{\beta_c} ln\left(\frac{Z_{\omega_1,\beta_c}}{Z_{\omega_2,\beta_c}}\right), \tag{9.2.4}$$

where $U_i = -\partial ln Z_i / \partial \beta_h$ with $i = C, D$.

And in the final stage of the cycle the system undergoes an isochoric heat addition process. So, the heat addition to the system can be expressed as:

$$Q_{DA} = U_A - U_D. \tag{9.2.5}$$

The net work done for the cycle is $W_{tot_C} = Q_{AB} + Q_{BC} + Q_{CD} + Q_{DA}$. The efficiency of the Stirling heat cycle from Eq. (9.2.2), (9.2.3), (9.2.4) and (9.2.5) is defined as:

$$\eta_{Stir_C} = 1 + \frac{Q_{BC} + Q_{CD}}{Q_{DA} + Q_{AB}}.$$
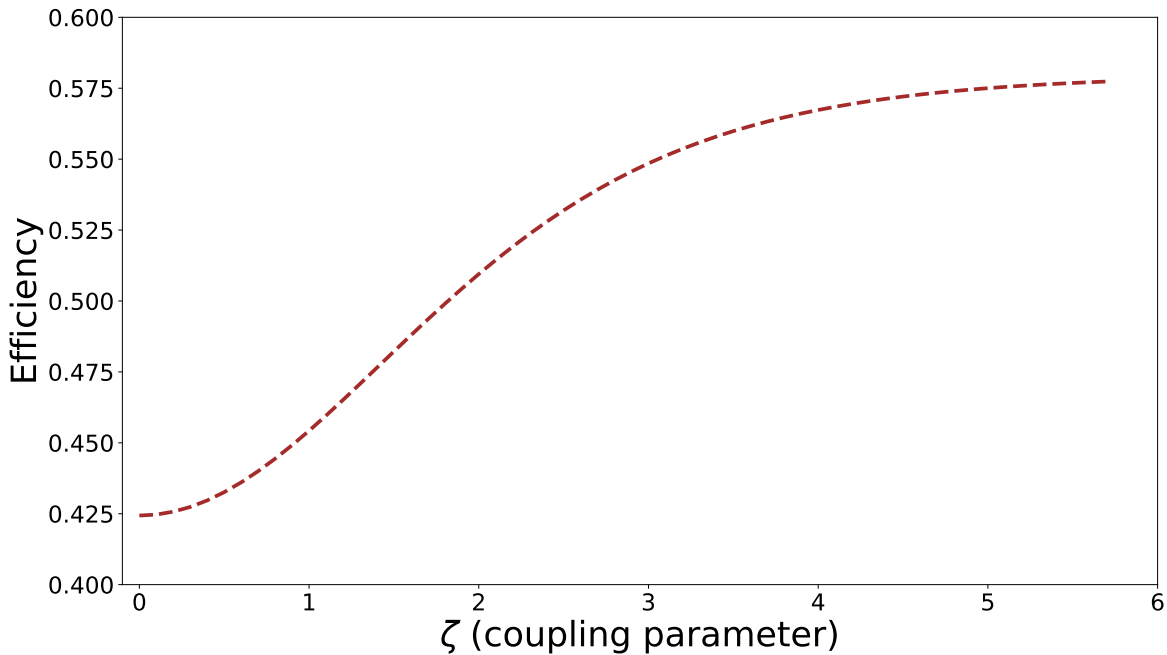
Figure 9.4. (Color online) Efficiency of the Stirling cycle with coupled HO as the working substance in commutative phase space.

The hot reservoir temperature is considered as $T_h = 4K$, and that of the cold reservoir

temperature $T_c = 1K$. For the analysis of the efficiency of the Stirling cycle with respect to the variation of the coupling strength, the frequency for the coupled oscillator is considered as $\omega_1 = 4$ and $\omega_2 = 2$. For our analysis, we have numerically simulated the efficiency of the Stirling cycle with respect to the coupling constant similar to the Otto cycle studied in the above section. The variation of the efficiency of the engine with respect to the coupling parameter is shown in Fig. (9.4). The efficiency shows very minute variation when the coupling constant is near zero. The efficiency monotonically increases for a certain range of the coupling constant. Then it gets saturated at a certain value of the coupling strength, and thereafter it remains constant with respect to the parameter. We encounter a high efficiency of the Stirling engine when compared with the Otto cycle with the coupled HO as the working medium.

9.2.2   Non-commutative phase space

In the case of commutative space, the coupled oscillators as the working substances result in a catalytic effect to the efficiency with respect to the coupling strength of the system. Now, we want to analyze how the change in the phase space affects the thermodynamic process. The Hamiltonian of the two harmonic oscillators coupled with each other in the NC phase space is described in Eq. (4.4.12). The energy eigenvalue of the Hamiltonian is expressed in the form shown in Eq. (4.4.13) of the section 4.4.1. Following the same methodology, as used in the case of commutative space, we will analyze the quantum Stirling cycle in the NC phase space.

The partition function for the system is evaluated and it takes the form:

$$Z \;=\; \sum_n e^{-\beta E_n} = \frac{-4}{\beta^2 \theta^2 (K - 4\omega^2)}, \tag{9.2.6}$$

subjected to the condition $Re\left[\frac{K\beta\theta}{2} + \beta \sqrt{K\theta^2\omega^2}\right] > 0$.

The heat exchange that occurs when the system undergoes the first stage of the Stirling cycle is:

$$Q_{AB} = U_A - U_B + \frac{1}{\beta_h} ln\left(\frac{Z_{\omega_1,\beta_h,\theta}}{Z_{\omega_2,\beta_h,\theta}}\right), \tag{9.2.7}$$

The partition function Z_A, Z_B of the system can be derived using Eq. (9.2.1). The internal energy U_A, U_B is evaluated using the definition $U_i = -\partial ln Z_i / \partial \beta_h$, where $i = A, B$.

In the second phase of the cycle heat is unleashed from the system. So, the heat exchange

throughout this process can be expressed as:

$$Q_{BC} = U_C - U_B. \tag{9.2.8}$$

The third phase is a isothermal process where heat gets rejected from the system. So, the heat exchange is represented as:

$$Q_{DC} = U_D - U_C + \frac{1}{\beta_c} ln\left(\frac{Z_{\omega_1, \beta_c, \theta}}{Z_{\omega_2, \beta_c, \theta}}\right), \tag{9.2.9}$$

where $U_i = -\partial ln Z_i / \partial \beta_h$ with $i = C, D$.

And in the last stage of the cycle the system undergoes an isochoric heat addition process. So, the heat addition to the system can be expressed as:

$$Q_{DA} = U_A - U_D. \tag{9.2.10}$$

The work done for the cycle is described as $W_{tot_{NC}} = Q_{AB} + Q_{BC} + Q_{CD} + Q_{DA}$. The efficiency of the Stirling heat cycle for the coupled harmonic oscillator as the working substance in NC phase space can be derived from Eq. (9.2.7), (9.2.8), (9.2.9) and (9.2.10). It is expressed as:

$$\eta_{Stir_{NC}} = 1 + \frac{Q_{BC} + Q_{CD}}{Q_{DA} + Q_{AB}}.$$

Similar to the commutative space model the hot reservoir temperature is $T_h = 4K$ and that of the cold reservoir temperature $T_c = 1K$. We take the frequency for the coupled oscillator as $\omega_1 = 4$ and $\omega_2 = 2$ for the evaluation of the efficiency of the Stirling cycle with respect to the variation of the NC space parameter. For our analysis we fix the coupling strength to $\zeta = 2$ and the constant at $K = 0.25$. The efficiency of the Stirling cycle (as shown in Fig. (9.5) in the NC phase space with coupled HO as the working medium increases with the increase of the NC parameter and attains a steady state after a certain value of the NC parameter. The efficiency of the engine is near to the efficiency of the ideal engine cycle. So, we can infer that the NC phase space provides a catalytic effect on the efficiency of the engine. In Fig. 9.5 we have shown the efficiency of the Stirling cycle in the commutative space (depicted by the solid line in the graph) for the coupling strength $\zeta = 2$. The variation of the efficiency with the NC parameter for the same coupling parameter is depicted by the dash-dot curve in the graph. The efficiency of the engine boils down to the efficiency of the commutative
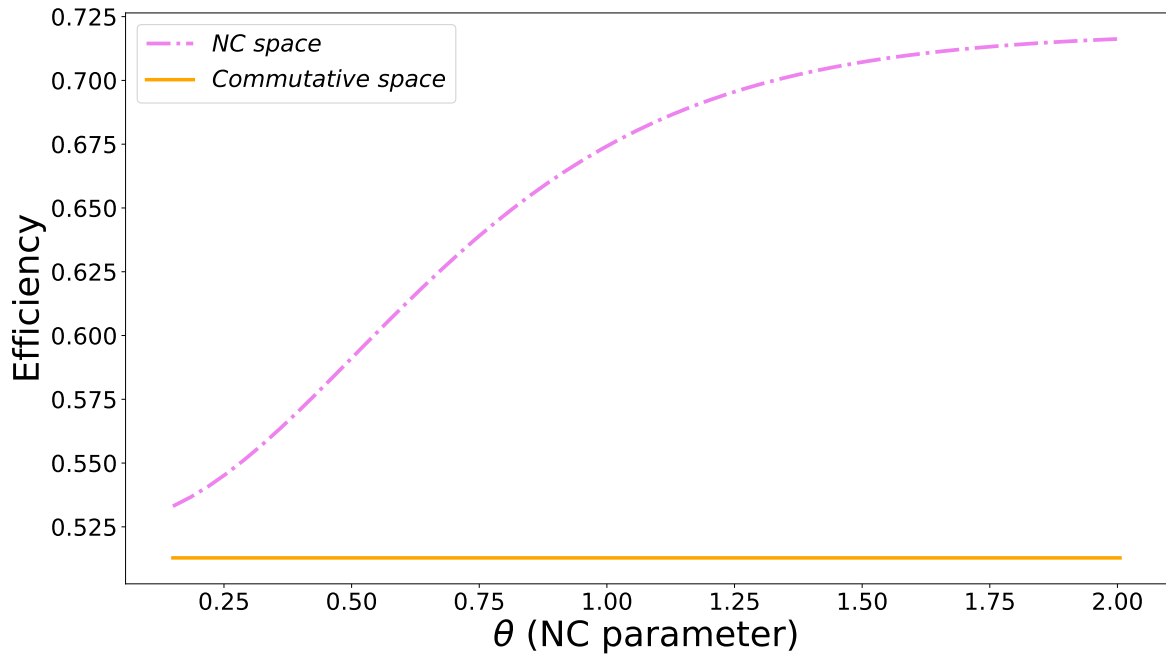
Figure 9.5. (Color online) Efficiency of the Stirling cycle with coupled HO as the working substance For a constant coupling factor is shown. The violet dash-dot curve depicts the change of the efficiency of the engine with respect to the NC parameter for a constant coupling factor $\zeta = 2$. The orange solid line describes the efficiency of the commutative space with the constant coupling constant $\zeta = 2$.

space when the NC parameter $\theta \rightarrow 0$. So, this satisfies the condition that the results of the system in NC space should reduce to the commutative space when the NC parameter is close to zero. We can infer from the graph that the engine in the NC space gets a boost for the NC parameter. Even the comparison of the efficiency of the Otto cycle with that of the Stirling cycle conveys that the working model provides a more catalytic effect on the efficiency of the Stirling cycle than that of the Otto cycle.

9.2.3   Generalized non-commutative phase space

In the case of non-commutative phase space, the coupled oscillators as the working substances give a boost to the efficiency with respect to the NC space parameter of the system. The efficiency increases with the increase of the NC parameter and shows a steady efficiency for the higher values. Now, we will study how the generalized NC phase space affects the thermodynamic process. The Hamiltonian of the two coupled harmonic oscillators in the NC phase space is described in Eq. (4.4.14), of the section 4.4.2. The energy eigenvalues are described in Eq. (4.4.15). Following the same methodology, as used in the case of non-commutative space, we will analyze the quantum Stirling cycle in the NC phase space.

In generalized NC phase space, the Hamiltonian is separated into two parts as shown in

Eq. (4.4.14). During the first stage of the cycle, i.e, the isothermal process, the individual Hamiltonian changes from the initial values from $H^{(1)}$ to $H^{(2)}$ to keep the system in thermal equilibrium with the hot reservoir. The total Hamiltonian of the system is the sum of the effect of these two Hamiltonian. The partition function for this system when evaluated results to:

$$Z = -\frac{2e^{\zeta - \frac{1}{2}\beta\omega}\cosh(\zeta)[4 + 2K(-K\gamma + \xi)^2 sech(\zeta)]^{1/2}}{\omega^2\beta^2[-2e^\zeta + 2e^{2\zeta}K^2\gamma\xi - K(K^2\gamma^2 + \xi^2)]}, \tag{9.2.11}$$

subjected to the condition $Re\left[e^\zeta\beta\omega\left(\sqrt{1 + \frac{e^\zeta K(-K\gamma+\xi)^2}{1+e^{2\zeta}}} + e^{2\zeta}\sqrt{1 + \frac{e^\zeta K(-K\gamma+\xi)^2}{1+e^{2\zeta}}} - \sqrt{1 + \frac{e^\zeta K(-K\gamma+\xi)^2}{-1+e^{2\zeta}}} + e^{2\zeta}\sqrt{1 + \frac{e^\zeta K(-K\gamma+\xi)^2}{-1+e^{2\zeta}}}\right) > 0\right]$

The heat exchange that takes place when the system undergoes the first stage of the Stirling cycle is:

$$Q_{AB} = U_A - U_B + \frac{1}{\beta_h}ln\left(\frac{Z_{\omega_1,\beta_h,\gamma,\xi}}{Z_{\omega_2,\beta_h,\gamma,\xi}}\right), \tag{9.2.12}$$

The partition function Z_A, Z_B of the system can be assessed using Eq. (9.2.1). The internal energy U_A, U_B is developed using the definition $U_i = -\partial lnZ_i/\partial\beta_h$, where $i = A, B$.

The Hamiltonian remains at $H^{(2)}$ while the temperature of the system decreases from T_h to T_c during the second phase of the cycle. As a result, heat is removed by the system to the reservoir and it can be mathematically defined as:

$$Q_{BC} = U_C - U_B. \tag{9.2.13}$$

In the third stage, the system remains coupled to the hot reservoir at temperature T_c, and the quasi-static changes in the Hamiltonian are depicted by the change of the Hamiltonian from $H^{(2)}$ to $H^{(1)}$. Heat exchange for this phase of the cycle is given as:

$$Q_{DC} = U_D - U_C + \frac{1}{\beta_c}ln\left(\frac{Z_{\omega_1,\beta_c,\gamma,\xi}}{Z_{\omega_2,\beta_c,\gamma,\xi}}\right), \tag{9.2.14}$$

where $U_i = -\partial lnZ_i/\partial\beta_h$ with $i = C, D$.

During the fourth stage of the cycle in generalized NC space, the system Hamiltonian stays as it is in $H^{(1)}$ while the temperature changes from T_c to T_h as the system is reverted back to the initial stage of the cycle. The heat exchange throughout this stage of this cycle is described as:

$$Q_{DA} = U_A - U_D. \tag{9.2.15}$$

The grand total work done for the cycle is $W_{tot_{GNC}} = Q_{AB} + Q_{BC} + Q_{CD} + Q_{DA}$. The efficiency of the Stirling heat cycle for the coupled harmonic oscillator as the working sub-
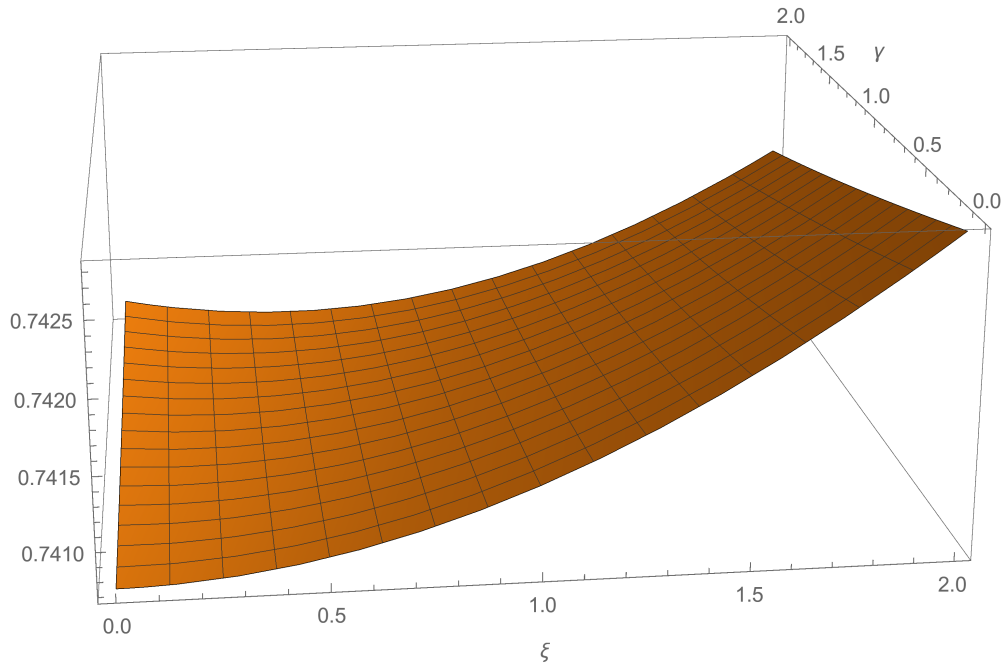
Figure 9.6. (Color online) Efficiency of the Stirling cycle with coupled HO as the working substance for generalized non-commutative phase space.

stance in generalized NC phase space can be derived from Eq. (9.2.12), (9.2.13), (9.2.14) and (9.2.15). It is expressed as:

$$\eta_{Stir_{GNC}} = 1 + \frac{Q_{BC} + Q_{CD}}{Q_{DA} + Q_{AB}}.$$

Following the same values of the parameters as done in the case of non-commutative space, we considered the hot reservoir temperature $T_h = 4K$ and that of the cold reservoir temperature $T_c = 1K$ for the analysis of the Stirling cycle in generalized NC phase space. The frequency for the coupled oscillator is taken as $\omega_1 = 4$ and $\omega_2 = 2$ for the evaluation of the efficiency of the Stirling cycle with respect to the variation of the generalized NC space parameters. Throughout the process the coupling strength is $\zeta = 2$ and the constant is $K = 0.25$. The three-dimensional plot (in Fig. (9.6)) shows the variation of the efficiency of the Stirling cycle with the coupled harmonic oscillator as the working substance in the generalized NC phase space. The variation in the parameter ξ and γ in the graph shows a prominent effect on the efficiency of the engine in this space structure model. The efficiency of the Stirling cycle for $\zeta = 2$ in commutative space is about 0.63. With the same value of the coupling constant, we can see that the efficiency of the engine is high in the generalized NC space model. This indicates that the deformation of the space, which is depicted by the non-commutative parameter of both the coordinate and the momentum space influences the efficiency. If we compare the efficiency of the Stirling cycle with that of the Otto cycle we

visualize that the maximum attainable efficiency for both the cycle is near about the same but slightly higher for the Stirling cycle.

For the evaluation of the efficiency of the Stirling cycle in commutative as well as non-commutative space we have performed numerically simulation. We have used Mathematica for deriving the solution of the equations and Python for data generation and ploting of the efficiency of the engine model.

9.3   Chapter Summary

To summarize, we analyzed quantum heat engines with coupled harmonic oscillators as the working medium for the commutative and the non-commutative space. The coupled harmonic oscillator in non-commutative phase space out-performs the oscillator in the commutative space in terms of the efficiency of both the quantum cycles that are being analyzed. In the case of the Otto cycle, the efficiency is high for the lower values of the NC parameter. Even if it shows a monotonous decrease in the efficiency of the Otto cycle, it remains higher than the expected efficiency in the commutative space. Whereas in the case of the Stirling cycle we encounter a steep boost with the increase of the NC parameter. It tends to reach the efficiency of the ideal cycle. So, we can infer that the working medium considered for our analysis is an effectual working substance for the Stirling cycle than that of the quantum Otto cycle. Even in the case of generalized NC phase space, the efficiency gets a catalytic effect for the NC parameter over the commutative phase space. The non-linearity that we encounter in the Hamiltonian is the consequence of the NC parameter of the non-commutative phase space.

Some of the previous works [40, 480] have explored the influence of NC space in thermodynamic cycles. They have shown that the NC space provides a catalytic effect to the efficiency of the engine as well as the refrigerator models. Most of the analyses have claimed that the system is model-dependent. So to provide a generic statement that the high engine efficiency in NC space is universal, further analysis in this direction is required.

For the analysis and implementation of the quantum Otto cycle, one has to maintain a quasi-static adiabatic process to prevent coherence generation in the Hamiltonian of the considered system. This should be kept in mind while the execution of the adiabatic process so that one can prevent the mean population change. During the thermalization process of the cycle, to achieve the thermal equilibrium state where the system is coupled with the reservoirs, the system must stay coupled with the bath for a longer period of time. It will

be interesting to analyze various thermodynamic processes by using the general form of coupling of the harmonic oscillator as the working substance.

10 Quantum Thermal Engines in Relativistic Non-Commutative Space

Contents

The contents in this chapter are based on the review article in Ref. [42].

In this chapter, we have considered non-commutative spacetime with relativistic and GUP correction for our analysis. Our prime motivation is to inspect the quantum engine cycles for different working mediums in relativistic non-commutative spacetime with GUP correction. Here, the working medium, that we have considered for the analysis is one-dimensional potential well and the harmonic oscillator. We make use of this working medium for the analysis of the Stirling cycle, which depicts the working principle for different quantum heat engines and refrigerators. We evaluate the efficiency of the cycle after the working mediums evolve through every phase of the cycle. The outcomes are surprising in the case of relativistic NC spacetime. We visualize that when the working medium is the one-dimensional potential well, we get a constant efficiency of the engine, whereas, during the case of the harmonic oscillator as the working substance, the efficiency increases rapidly with the variation of the NC parameter of the spacetime. The NC parameter gives a catalytic effect to the efficiency with the harmonic oscillator as the working medium. This leads us to the possibility of analyzing and exploring quantum information theory from the NC spacetime perspective. One inevitable question that pokes our mind is regarding the physical

accessibility of the non-commutative spacetime with the existing quantum technology. In the context of experimental verification and analysis of the signatures of the NC spacetime effect, we encounter recent development in this direction using quantum optics [463] and Opto-mechanical [489] setups.

10.1　Quantum heat cycles in NC with GUP corrections

Quantum heat engines and refrigerators are analyzed for different systems as the working substance. We will consider the 1-D potential well with relativistic and GUP correction as the working substance for the engine model. We will also take into account the harmonic oscillator (HO) with relativistic and GUP correction as the working substance for the engine model. Our purpose is to analyze the better working medium for the heat engine cycles in non-commutative space in the relativistic realm. For our analysis, we will study the Stirling engine cycle for both cases. In the non-commutative phase space, the working medium that we will consider for the analysis of the Stirling cycle will evolve to a Gibbs state which we will consider for our analysis following the same analogy as shown in previous works [490].

Stirling cycle, a reversible thermodynamic cycle, is a four-stroke engine that comprises two isothermal processes and two isochoric processes. The pressure-volume (P-V) diagram of the Stirling cycle in the classical regime is depicted in Fig. (2.4) of the section 2.2.

10.1.1　Stirling cycle with 1-D well as working substance in the NC space

Here, we analyze the Stirling cycle with 1-D potential well as the working substance. A Stirling cycle [123, 146, 147, 200] consists of four stages, two of which are isothermal processes, and the remaining two processes are isochoric in nature. The detailed description of the generic process of the analysis of the quantum Stirling cycle with infinite potential well as the working medium is described in section 2.8. The process will be analyzed for infinite potential well as the working substance in the relativistic non-commutative space in this section.

In previous works [43, 472, 493, 494], they have studied the work done and the efficiency for the heat engine in the non-relativistic and relativistic regime in commutative space. In this work, we first develop the heat engine in the NC spacetime with relativistic and GUP correction with one-dimensional potential well as the working medium. Following the same

analogy in the previous works, we analyze the work done and the efficiency of the heat engine for NC spacetime.

Some previous works [491, 492] have explored the non-equilibrium thermodynamics in non-commutative space structure. They have shown that the master equation for the non-commutative space narrows down to the usual master equation when one equates the non-commutative parameter to zero. The presence of the non-commutative parameter enhances the results that are generally encountered in the ordinary space without violating the usual master equation. We have considered that our system follows the same usual master equation in the non-commutative space as suggested in the works [491, 492]. In our analysis, we have considered that only the system will encounter the effect of the non-commutative space.

Now, we will take a 1-D potential well having a length $2L$ in NC spacetime with a particle inside the system having mass m at temperature T_1 as the working medium for our analysis. The physical energy for this system is identical to Eq. (4.4.15).

The partition function [476] of our system is:

$$
\begin{aligned}
Z_A &= \sum_n e^{-\beta_1 E_n} \\
&= \frac{1}{\sqrt{\pi} \sqrt{\frac{\beta_1 \hbar^2 (2 + 3\alpha \zeta^2 m^2 c^2)}{L^2 m}}},
\end{aligned}
\tag{10.1.1}
$$

where $\beta_1 = \frac{1}{k_B T_1}$ and k_B is the Boltzmann constant.

Now, in the first stage of the cycle, we divide the 1-D well into a double potential well by inserting a partition isothermally. During this process, even energy levels remain therein, but we observe a shift in the odd levels. The odd ones merge with the nearest neighbor, i.e., the even energy level. So, the energy after the insertion takes the form:

$$
E_{2n} = -\frac{(2n)^2 \hbar^2 \pi^2}{8mL^2} \left[1 + \frac{3}{2} \alpha \zeta^2 m^2 c^2\right] - \frac{\hbar^4}{8m^2 c^2} \left[\frac{(2n)\pi}{2L}\right]^4,
\tag{10.1.2}
$$

which evolves by substituting n by $2n$ in Eq. (4.6.9). The partition function after the insertion of the well is defined equivalent to Eq. (10.1.1) as:

$$
Z_B = \sum_n 2 e^{-\beta_1 E_{2n}}.
$$

In the isothermal process, the heat exchange takes the form:s

$$
Q_{AB} = U_B - U_A + k_B T_1 ln Z_B - k_B T_1 ln Z_A.
\tag{10.1.3}
$$

The internal energy U_A and U_B is described as $U_i = -\partial ln Z_i / \partial \beta_1$, where $i = A, B$.

During the second stage of the cycle, the system is connected to the cold bath at a temperature T_2. The partition function takes the form:

$$Z_C = \sum_n 2e^{-\beta_2 E_{2n}}.$$

The heat exchanged during this stage of this cycle is interpreted by the difference of the average energies for the initial and final states. It takes the form:

$$Q_{CB} = U_C - U_B, \tag{10.1.4}$$

where $U_C = -\partial ln Z_C / \partial \beta_2$ and $\beta_2 = \frac{1}{k_B T_2}$. In the third phase of the cycle, we remove the wall isothermally. The energy during this stage of the cycle reverts back and is the same as given in Eq. (4.6.9). The partition function becomes:

$$Z_D = \sum_n e^{-\beta_2 E_n},$$

where U_D can be evaluated similarly as U_C. The heat exchanged (similar to Eq. (10.1.3)) becomes:

$$Q_{CD} = U_D - U_C + k_B T_2 ln Z_D - k_B T_2 ln Z_C. \tag{10.1.5}$$

In the fourth stage of the cycle, the system falls back into the first phase of the cycle, i.e., the system is bridged back to the heat reservoir at temperature T_1. The heat exchange for the system is expressed as:

$$Q_{DA} = U_A - U_D. \tag{10.1.6}$$

The total work done for this cycle is evaluated using Eq. (10.1.3), (10.1.4), (10.1.5) and (10.1.6) as:

$$W \;\; = \;\; Q_{AB} + Q_{BC} + Q_{CD} + Q_{DA}.$$

The efficiency of this engine is defined using Eq. (10.1.3), (10.1.4), (10.1.5) and (10.1.6) as:

$$\eta_{Stir} \;\; = \;\; 1 + \frac{Q_{BC} + Q_{CD}}{Q_{DA} + Q_{AB}}.$$
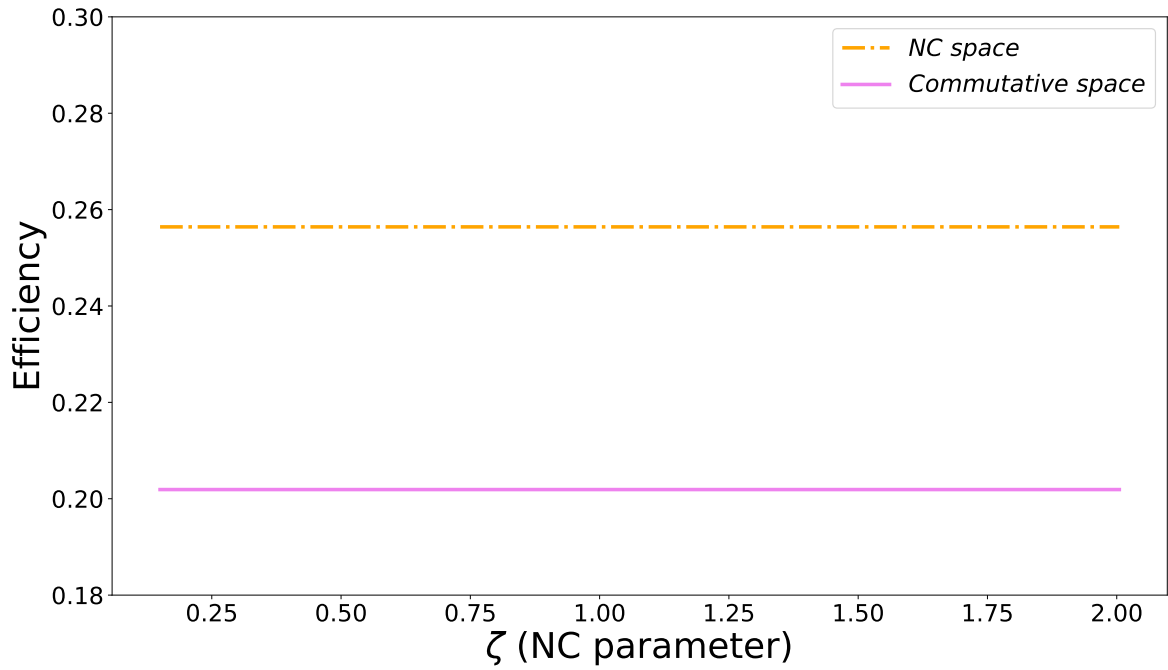
Figure 10.1. (Color online) Variation of the efficiency of Stirling cycle with the NC parameter of the system with 1-D potential as the working substance. The violet solid line depicts the efficiency of the cycle in commutative phase space and the orange dashed-dot curve represents the efficiency in non-commutative phase space.

We have considered $T_1 = 2K$ and $T_2 = 1K$ for the evaluation the efficiency of the Stirling engine (shown in Fig. (10.1)) with the variation of the NC parameter. The efficiency of the engine has been numerically analyzed with the results of the partition function and the internal energy of the system. We have considered the length of the potential well as $5\,nm$. The efficiency of the engine is constant with the variation of the parameter. So, for this working medium, we do not encounter any boost in the efficiency of the cycle. If we analyze the engine cycle with this working medium in commutative space, the efficiency results in a constant value which is near about (0.2) for a fixed length of the potential well. Along with that, we encounter that the efficiency of the engine is not up to the mark with the relativistic and GUP correction working medium. We can infer from the plot shown in Fig. (10.1) that the non-commutative parameter has lost its impact when we have considered this model as the working medium. The gain in the efficiency of the engine is provided by the relativistic correction. This is quite surprising as we have encountered gain due to the non-commutative parameters as shown in previous works [40, 41, 480, 481]. This feature of suppressing the non-commutative effect with relativistic correction needs further investigation.

10.1.2   Stirling cycle with harmonic oscillator in NC space

Now, we analyze the Stirling cycle having a harmonic oscillator with relativistic and GUP
correction as the working substance. A Stirling cycle [123, 146, 147, 200], consists of four
stages, two isothermal processes, and the remaining two processes are isochoric. The schematic
representation of the Stirling engine cycle with HO as a working substance is shown in
Fig. 2.7 of the section 2.8.2.

The physical energy of the system is equivalent to Eq. (4.6.10). Now, the partition function [476] for the system is defined as:

$$
\begin{aligned}
Z &= \sum_n e^{-\beta E_n} \\
&= \frac{2(\frac{2\pi}{5})^{\frac{1}{2}} e^\kappa \chi}{\Theta},
\end{aligned}
\tag{10.1.7}
$$

where $\kappa = \frac{\beta \Xi}{640 c^2 m \left(-1 + 4 c^2 m^2 \alpha \zeta^2\right)}$, $\Xi = \left(-1024 c^6 m^4 \alpha \zeta^2 + 256 m^6 \alpha^2 \zeta^4 - 35 \hbar^2 \omega^2 + 280 c^2 \hbar^2 m^2 \alpha \zeta^2 \omega^2 - 16 c^4 m^2 \left(-64 + 35 \hbar^2 m^2 \alpha^2 \zeta^4 \omega^2\right)\right)$, $\Theta = \sqrt{\beta \omega^2 (4 \alpha \zeta^2 - 1)}$ and
$\chi = 1 + erf\left[\frac{\hbar \beta \omega \left(16 c^4 m^3 \alpha \zeta^2 + 5 \hbar \omega - 4 c^2 m \left(8 + 5 \hbar m \alpha \zeta^2 \omega\right)\right)}{\Theta}\right]$. Here erf is the error function [479] which
is defined as $erf(x) = \pi^{-\frac{1}{2}} \Gamma(\frac{1}{2}, x^2)$, where $\Gamma(\alpha, x)$ is known as incomplete gamma function [495].

(i) The first stage: *isothermal (A→B) process.* During this phase, the working medium
is attached with a heat reservoir of temperature T_h. Throughout this process, the system will
be in thermal equilibrium with the heat bath. The changes in the energy spectrum and the
internal energy of the system take place as a result of quasistatic changes that occurs to the
working medium. These changes are due to the changes that occur in the Hamiltonian of the
system when the system evolves during this process. The heat exchange that occurs during
the first stage of the Stirling cycle is:

$$
Q_{AB} = U_B - U_A + k_B T_h ln Z_B - k_B T_h ln Z_A,
\tag{10.1.8}
$$

where k_B is the Boltzmann constant. The partition function Z_A, Z_B for the phases can be cal-
culated using Eq. (10.1.7). The internal energy U_A and U_B is described as $U_i \equiv -\partial ln Z_i / \partial \beta_h$,
where $i = A, B$.

(ii) The second phase: *isochoric (B→C) process.* During this phase, the system evolves
under an isochoric heat exchange. The system is coupled with a bath at a temperature T_c, so

heat will be released in this process. So, the heat exchange is expressed as:

$$Q_{BC} = U_C - U_B. \tag{10.1.9}$$

(iii) Third phase: *isothermal (C→D)* process. In this process, the working substance remains coupled with the bath at temperature T_c. Similar to the first isothermal process, the system during this process is at thermal equilibrium with the bath. Heat gets released in this phase. The heat exchange takes the form:

$$Q_{CD} = U_D - U_C + k_B T_c ln Z_D - k_B T_c ln Z_C. \tag{10.1.10}$$

where $U_C = -\partial ln Z_C / \partial \beta_c$ and $\beta_c = \frac{1}{k_B T_c}$.

(iv) The fourth phase: *isochoric (D→A)* process. The system falls back into the bath with temperature T_h. The heat exchange for this stage is expressed as:

$$Q_{DA} = U_A - U_D. \tag{10.1.11}$$

The total work done for this process is $W_{tot} = Q_{AB} + Q_{BC} + Q_{CD} + Q_{DA}$. The efficiency of the Stirling heat cycle from Eq. (10.1.8), (10.1.9), (10.1.10) and (10.1.11) is expressed as:

$$\eta_{Stir} = 1 + \frac{Q_{BC} + Q_{CD}}{Q_{DA} + Q_{AB}}.$$

We have considered $T_1 = 2K$, $T_2 = 1K$, $\omega = 4$ and $\omega' = 3$ for the evaluation the efficiency of the Stirling engine (shown in Fig. (10.2)) with the variation of the NC parameter. We numerically analyze the efficiency of the engine. There is a steep increase in the efficiency of the Stirling cycle with the variation of the NC parameter. So, for this working medium with relativistic and GUP correction, we encounter a catalytic effect in the efficiency of the cycle with the increase of the NC parameter. The range of the NC parameter is considered in such a way that it does not exceed the extreme quantum gravity limit [496]. Though it seems like that the efficiency of the engine is monotonously increasing with the NC parameter, there is a bound on it due to the accessible range of the NC parameter. Following the methodology proposed in [463, 489], one can have the experimental realization of the engine models in
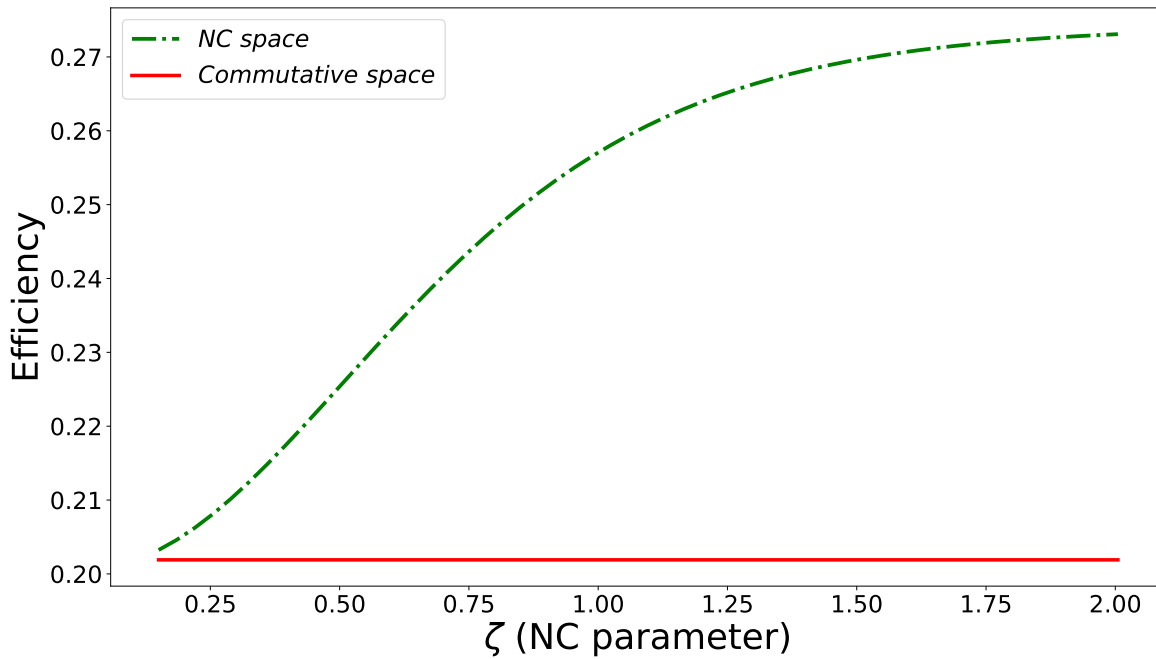
Figure 10.2. (Color online) The green dash-dot curve shows the variation of the efficiency of the engine cycle with the NC parameter of the system with non-commutative HO with relativistic and GUP effect as the working substance. The red solid line is the efficiency of the harmonic oscillator.

NC spacetime with a harmonic oscillator as the working medium. We can infer from the plot shown in Fig. (10.2) that the non-commutative parameter along with the relativistic correction has an impact on the efficiency of the engine. It is a surprising fact that this model when considered as the working medium for the same engine we can visualize the effect of both the relativistic as well as the non-commutative parameter. The model dependency of the non-commutative parameter is confirmed from this analysis.

For the evaluation of the efficiency of the Stirling cycle for the two different working mediums in the relativistic non-commutative space, we have numerically simulated the efficiency of the engine. We have used Mathematica for deriving the solution of the equations and Python for data generation and ploting of the efficiency of the engine model.

10.2   Chapter Summary

The non-commutative harmonic oscillator with relativistic and GUP correction as a working medium for the Stirling cycle, out-performs the harmonic oscillator as a working medium in terms of the efficiency of the cycle. With the increase in the NC parameter, the efficiency of the engine gets a boost. We have considered the range of the NC parameter in such a way that it is bounded by the extreme quantum gravity limit. We encounter a catalytic effect

in the efficiency of the cycle with the harmonic oscillator as the working substance. But we get a constant efficiency with 1-D infinite potential well as the working medium for the same cycle. So, we can infer that the harmonic oscillator model is an effectual working substance relativistic NC spacetime over the 1-D infinite potential well model. The effect of non-linearity that we encounter in the Hamiltonian appears due to the NC parameter along with the GUP correction. This requires energy for the implementation in the thermodynamic cycles.

For the analysis and implementation of the quantum Otto cycle in the relativistic NC spacetime, one has to maintain a quasi-static adiabatic process to prevent coherence generation in the Hamiltonian of the considered system. This should be kept in mind while the execution of the adiabatic process so that one can prevent the mean population change. During the thermalization process of the cycle, to achieve the thermal equilibrium state where the system is coupled with the reservoirs, the system must stay coupled with the bath for a longer period of time. It will be interesting to analyze various thermodynamic processes by using the general form of coupling of the harmonic oscillator as the working substance.

In different application areas of the quantum theory [485], the relativistic NC spacetime can be a better resource. This is an open area for exploration. In previous works [136, 486, 487], coupled working medium has been analyzed. One can utilize the NC spacetime for the analysis of coupled working medium, and it can be further extended for the exploration of non-Markovian reservoirs in relativistic NC spacetime. Here, in our work, we have analyzed the heat cycle. For the generic statement about the boost on efficiency for the engine cycle in NC spacetime, further investigation of the existing heat cycles is required. Even one can study the nature of the coefficient of performance for the refrigerator cycles using the different spacetime models. It will be fascinating to study the effect of the NC spacetime even in the irreversible cycles [497, 498] and how they affect the quantum phase transition.

11 Thermodynamics, Quantum Computer and Information Paradox

Contents

11.1   Quantum Thermal Process in Quantum Computer

We know that the standard second law of thermodynamics proposed by Clausius set up constraints on the thermodynamics processes like the efficiency of the engine. Similarly, we encounter that each thermodynamic formulation provides constraints to the evolution of the physical process that it can undergo. The constraints that are imposed on the system, can be determined by the dynamics that characterize the respective framework. For example, in the case of fluctuation relation [499,500] and thermodynamic uncertainty relation [210,501,502] we can derive the constraints by applying external driving, but it is forbidden in the case of resource theoretic approach [83,503]. In the work [504], they use the principle "information from violation" for the evaluation of the devices, which demands an adequate amount of isolation from the external environment for the correct execution of the operation. Quantum computers, as well as quantum simulators which are the emerging quantum technology, fall

into this category. The experimental analysis of the violation of the thermodynamic constraints, which results in the identification of the non-unitary evolution of the system in the quantum computer was first proposed in the work [504]. Simulating of open quantum systems has been explored in the work [505], where the evolution of the system is supervised by the time-independent master equation and the parameters are considered to be fixed.

A universal system will be offered by the quantum computing system for the experimental demonstration of the essential thermodynamic phenomena in the quantum realm. But it remains a challenging problem to simulate open quantum systems as we are unable to tune physically the control parameters of the systems and also we encounter difficulties to measure the work extraction. This is due to the that for the analysis of the work extraction we need to physically tune the control parameter. In the case of quantum computers, there is a constraint that no one is allowed to tune the parameters. The tuning of the parameter is forbidden as they are optimized in the system to reduce the noise in the system. In a recent work [506], they have proposed a way to overcome this tuning difficultly for the simulation of the finite-time isothermal process, which is one of the fundamental thermodynamic processes for the analysis of thermal machines. So, for the analysis, we need to know how to simulate all the four quantum thermodynamic processes, i.e., isothermal, adiabatic, isochoric, and isobaric processes. In their work, they have introduced a virtual way by which one can tune the control parameter. So, the dynamics of the system can be analyzed with the help of quantum gates which will encode the parameter changes. The isothermal process is complicated for the simulation as in this process we encounter Hamiltonian change, as well as the interaction with the thermal bath. So, for the implementation, a discrete step method was considered for the analysis of the thermal process, where the discrete steps consist of series of rudimentary processes. Each step of the process either consists of an adiabatic process or an isochoric process. In the case of the adiabatic process, the physically tuning of the parameter is replaced by the unitary evolution with the help of quantum gates, and in the case of the isochoric process, the dissipative evolution of the system is taken care of by the quantum channel simulation [507–509]. The quantum channel simulation acts as a substitute for the environment [504, 510, 511]. Having this preliminary finding and along with that, if we are able to simulate the required thermodynamics process, then we will be able to analyze different quantum thermal engines like the Stirling cycle, and Otto cycles in the universal quantum computer with different quantum systems as their working medium.

11.2   Quantum Information Paradox in Quantum Computer

The contents in this section are based on the article in Ref. [512].

In a very recent work as stated in section 4.7, they have proposed a method to tackle the black hole information loss paradox. In this chapter, we will present a work, based on similar principles, where we will apply this formalism in a binary black hole system and show it can be successfully analyzed with a three-qubit system for binary black hole system and measurements of this generates pseudo-random state operators which are in excellent agreement with the theoretical values. We present an experimental setup for our model and perform quantum optical simulation via the quantum state tomographic process[1] [513]. So far we have been considering the situation where there is no correlation between the two qubits of the binary black hole system. Now, we have considered a situation that there exists a correlation between the qubits of the binary black-hole. This can be described by using the pseudo-density operator formalism by considering the interaction between the qubits of the binary black hole with the particle above the event horizon. Interestingly the results show an excellent agreement with our proposed theoretical proposal.

11.2.1   Mathematical Modeling of the Black Hole with Pseudo Density Operator

It is a known fact that the Schwarzschild metric describes the space-time continuum in the presence of the black hole. A particle crossing the horizon is equivalent to swapping of the signature of the metric, i.e., the spatial and the temporal components [399]. Now in the quantum realm, if one considers a quantum phase factor, then the change in the spatial and the temporal is simply conveyed by the conjugate of the defined phase factor. So, the transpose operation of the density matrix can describe the effect of the in-falling quantum system. The transpose operation so defined is a positive operation but defies to represent a completely positive operation, which indicates that if one performs a transpose operation on

---

[1]It is not possible to estimate a quantum state from a single experimental run, due to no-clone theorem. As a result, it is necessary to reconstruct the state multiple times and do the measurements number of times on a different basis. Basic state tomography involves the estimation of the expectation values of all the operators (we parameterize any given quantum states of a system with respect to a set of operators), and if one can reconstruct all the operators then the experiment is said to be tomographically complete.
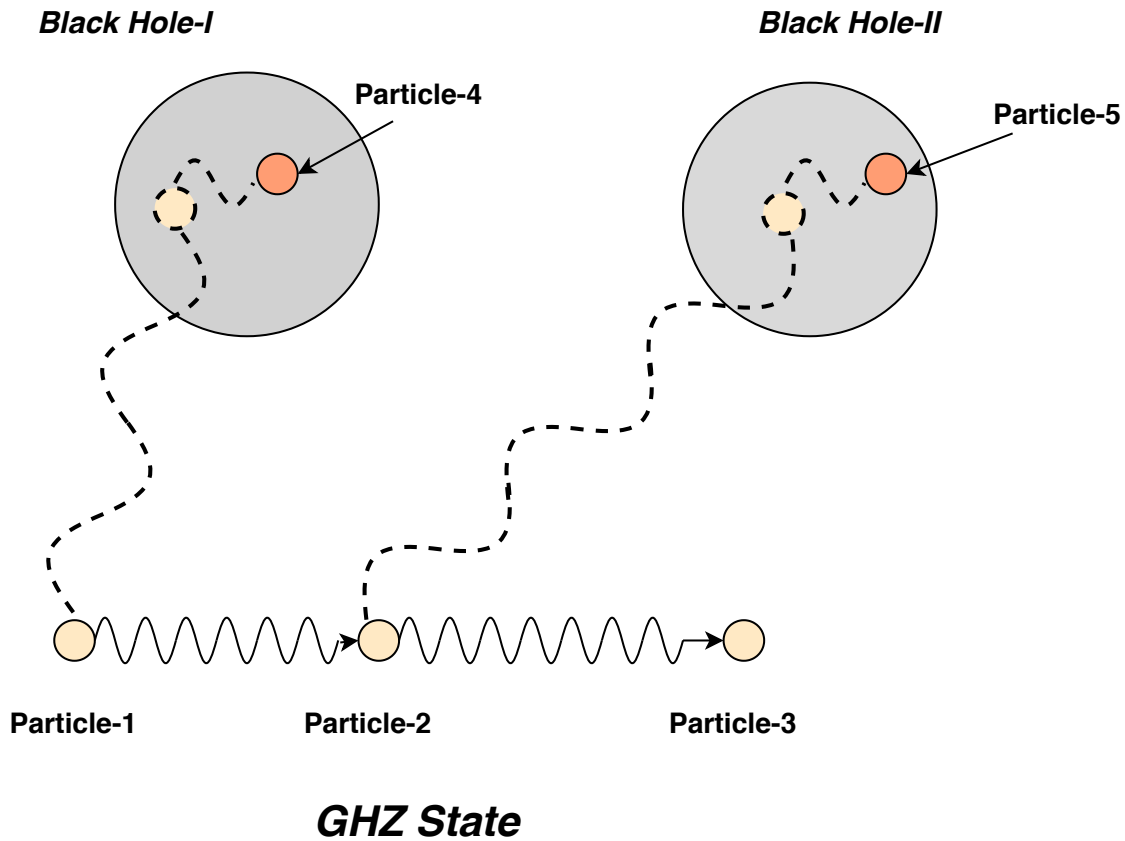
Figure 11.1. This is the schematic representation of the process of the black hole evaporation for a binary system from a pseudo-density operator framework.

one of the three-party entanglement system, the state of the system may not turn out being a valid density matrix. For this, pseudo density operator (PDO) are used to explain this phenomenon [514], which can accommodate non-positive operations like Hermitian transformations as well. We are going to exploit this fact to neutralize the violation of the monogamy principle of the entanglement theory during the evaporation of the black hole.

Here, we consider a maximally entangled Greenberger–Horne–Zeilinger (GHZ) state (three-qubit system) and a binary black hole system with pure states. We name the three particles maximally entangled as particle 1 and so on. We consider that two particles from this system fall in the binary black hole system, as shown in Fig. (11.1). Particle 1 falls in black hole 1 and particle 2 in black hole 2. Once inside, the particles will entangle with particles from inside the black hole environment, we name them particle 4 and 5 in the two black holes successively. We implement this setup as per the optical setup shown in Fig. (11.2) and then, we do the tomographic reconstruction of the state to analyze the black hole evaporation from an information theory standpoint. The simulation returns a pseudo-density matrix which can then be compared to our true value pseudo-density operator (ρ_{true}, which depicts the theoretical expectation of the state) via a distance measure between the
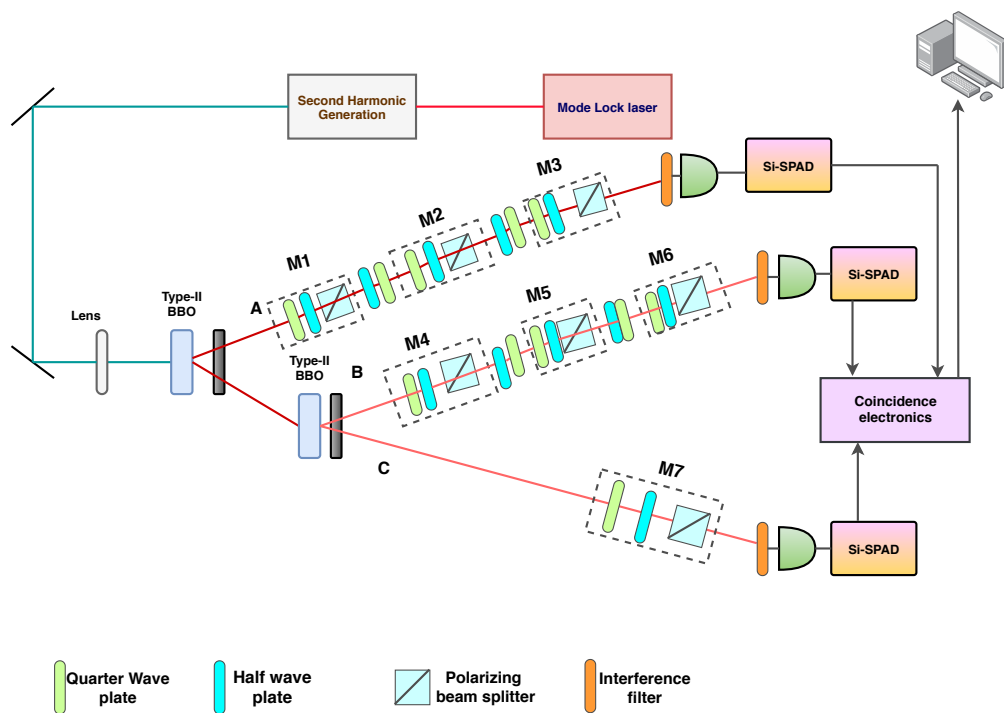
Figure 11.2. Experimental setup of the process. Here a GHZ state is generated by using two sets of β−barium borate (BBO) type-II crystal. Three sets of measurements are considered on photon A, B, where the measurements are considered for three different times (t_1, t_2 and t_3 respectively) and a single measurement for the photon C.

two and give a figure of merit on the comparison of measurement values between the particle entangled inside the black hole and that outside. We present this comparison in terms of a fidelity score. We show that the fidelity score is sensitive to the method of estimation that are used in our analysis. We have used three different methods: maximum likelihood, and two variants of linear inversion techniques to do the state tomography, yet our overall fidelity score is excellent, inferring that it is possible to do the measurement of the particle that is inside the black hole via the measurement of the particle that is outside.

A density matrix bestows the probability distribution of the pure states, i.e., $\rho = \sum_j a_j |\phi_j\rangle\langle\phi_j|$, where a_j describes the probability of the pure state $|\phi_j\rangle$. The expectation value of a Pauli matrix is defined as $\langle a \rangle = tr(a\rho)$. So, we can describe an alternative approach to formulate the density matrix in terms of the Pauli operator. So, for an n-qubit system, the general density operator in terms of the Pauli operators is defined as

$$\rho_n = \frac{1}{2^n} \sum_{\alpha_1=0}^{3} \cdots \sum_{\alpha_n=0}^{3} \langle \bigotimes_{\beta=1}^{n} \sigma_{\alpha_\beta} \rangle \bigotimes_{\beta=1}^{n} \sigma_{\alpha_\beta}, \tag{11.2.1}$$

where $\sigma_0 = \mathbb{I}$, $\sigma_1 = X$, $\sigma_2 = Y$, $\sigma_3 = Z$. Whereas the PDOs generalises these operators and contains the statistics of the time domain. A general form of the PDO for a n-qubit is described as:

$$P_n = \frac{1}{2^n} \sum_{\alpha_1=0}^{3} \cdots \sum_{\alpha_n=0}^{3} \langle \{\sigma_{\alpha_\beta}\}_{\beta=1}^{n} \rangle \bigotimes_{\beta=1}^{n} \sigma_{\alpha_\beta}. \tag{11.2.2}$$

If one consider a set of event $\{E_1, E_2, \cdots, E_m\}$, for each event E_β we can have a single qubit Pauli measurement operator $\sigma_{\alpha_\beta} \in \{\sigma_0, \cdots, \sigma_3\}$. Now for any specific choice of Pauli measurement operator $\{\sigma_{\alpha_\beta}\}_{j=1}^{n}$, we consider $\langle \{\sigma_{\alpha_\beta}\}_{\beta=1}^{n} \rangle$ as the expectation value product of the result of these measurements. This can be in space or in time. The PDOs shares many properties in common with the density matrix. All PDOs are necessarily Hermitian in nature, trace one. The main difference of the PDOs with the density matrix is that they are not necessarily positive operators, i.e., they can possess negative eigenvalues.

We will now try to comprehend the working principle of PDOs relevant to the problem under study. Let us consider a maximally mixed state for a three-qubit system. Now, we will describe a physical process where a system of qubits is measured at two different times. The measurements are performed in the complimentary Pauli bases X, Y, and Z. The outcome of the measurement statistics can be expressed by an operator, the quantum density operator. This quantum density operator is the pseudo-density operator [514] which is described as
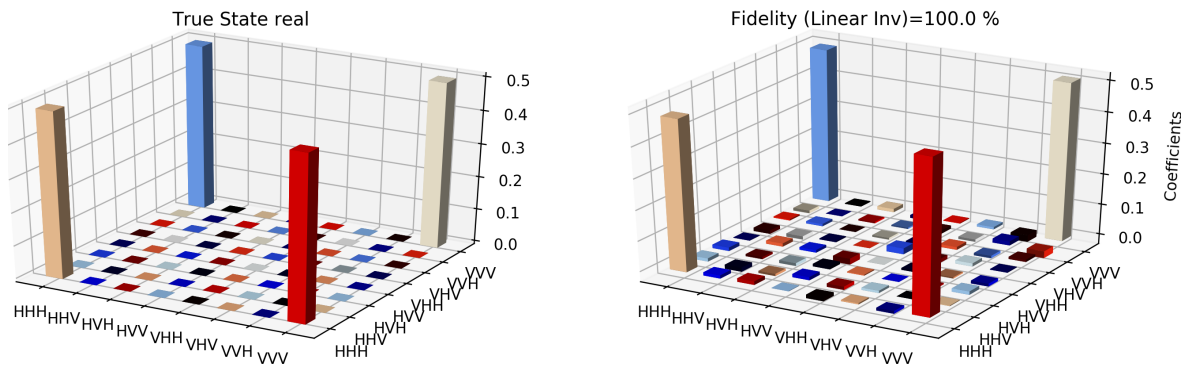
Figure 11.3. Tomographic reconstruction of the reduced pseudo-density operator P_{143} using the linear inversion method. The real part of the theoretical expectation (depicted by the true state in the plot) and the real part of the reduced pseudo-density operator is compared here.

$$P_{123} = \frac{1}{8}[I + X_1X_2X_3 + Y_1Y_2Y_3 + Z_1Z_2Z_3], \qquad (11.2.3)$$

where the subscripts indicate the index of qubits. One can obtain the reduced state of the subsystem by tracing out the subsystem whose information is not of concern. Surprisingly, one can represent the pseudo-density operators by executing a partial transpose operation over the maximally entangled basis of the respective dimension. We use this model to understand what happened to the three-particle entangled qubits when two of the qubits are falling into the binary black hole system. We use P_{123} to describe the state of the system where it is considered that two of the qubits is falling into the binary black hole. This is schematically explained in Fig. (11.1).

Based on this reasoning, we will propose a PDO to model the problem under execution. Here, a three-qubit entangled state is considered, out of them, two of the particles gets further entangled with two other particles in the binary black hole system. We would explain that the black hole information problem and binary black hole system can be explained by contemplating the PDO model, which is represented by Eq. (11.2.3). This PDO represents a three-qubit entangled system, out of which two of the entangled particles cross the event horizon and fall into the black hole and there the particles get entangled with a qubit. This proposed method describing the correlations associated with the black-hole evaporation is in agreement with that proposed by [428], and the explanation of the black hole ringdown stage boils down to the equivalent two-qubit system from the three-qubit system.
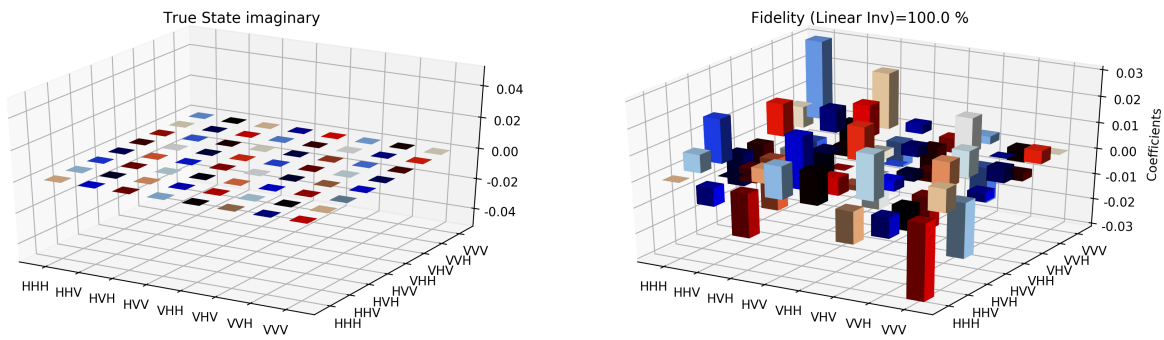
Figure 11.4. Tomographic reconstruction of the reduced pseudo-density operator P_{143} using the linear inversion method. The imaginary part of the theoretical expectation (depicted by the true state in the plot) and the imaginary part of the reduced pseudo-density operator is compared here.
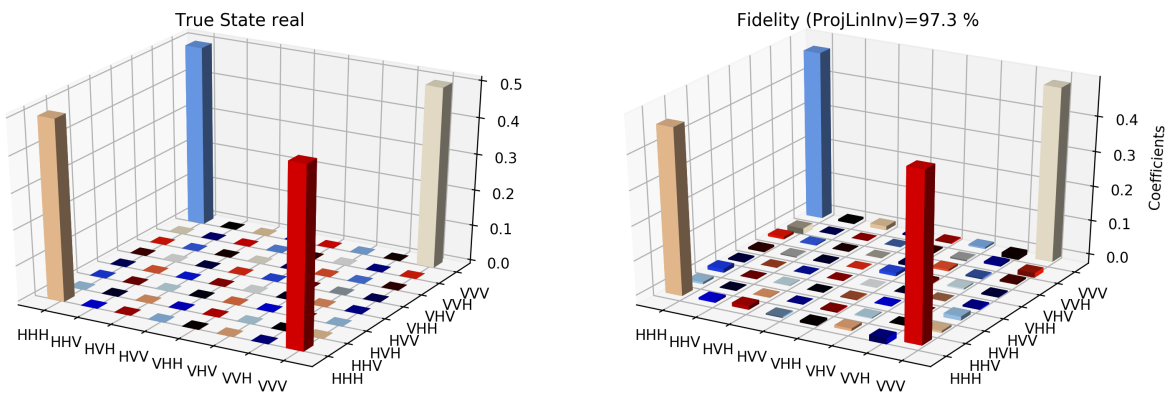
Figure 11.5. Similar to Fig.11.3, state tomography reconstruction of the reduced pseudo-density operator P_{143} is conducted using the projected linear inversion method. The real part of the theoretical expectation (depicted by the true state in the plot) and the reduced pseudo-density operator is compared.
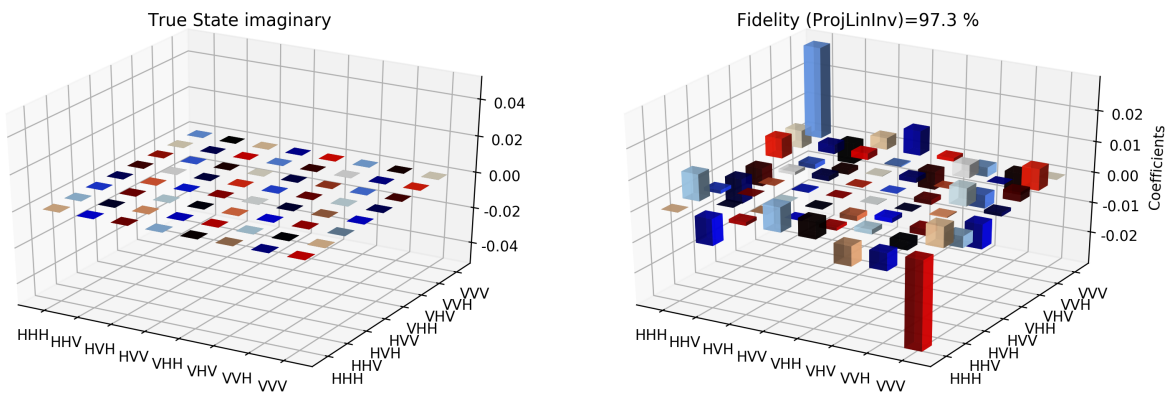
Figure 11.6. Similar to Fig.11.4, state tomography reconstruction of the reduced pseudo-density operator P_{143} is conducted using the projected linear inversion method. The imaginary part of the theoretical expectation (depicted by the true state in the plot) and the reduced pseudo-density operator is compared.
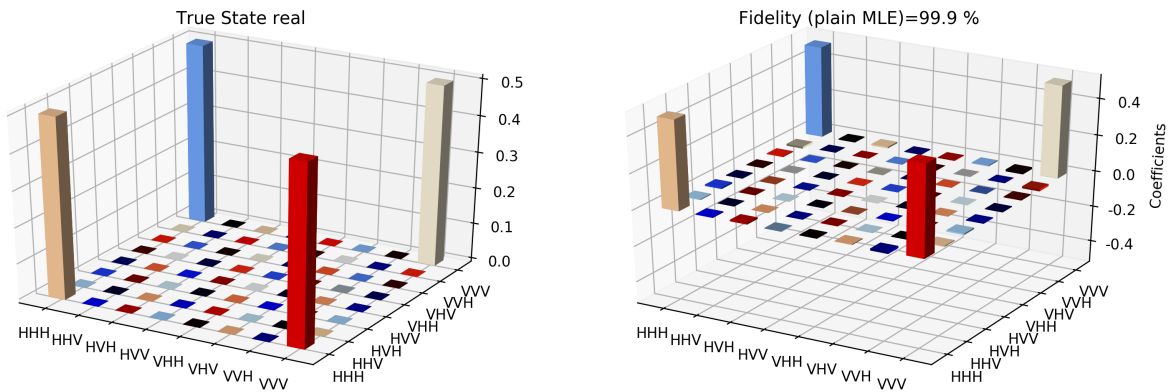
Figure 11.7. State tomography reconstruction of the reduced pseudo-density operator P_{143} is conducted using the maximum likelihood estimation method. The real part of the theoretical expectation (depicted by the true state in the plot) and the reduced pseudo-density operator is compared.
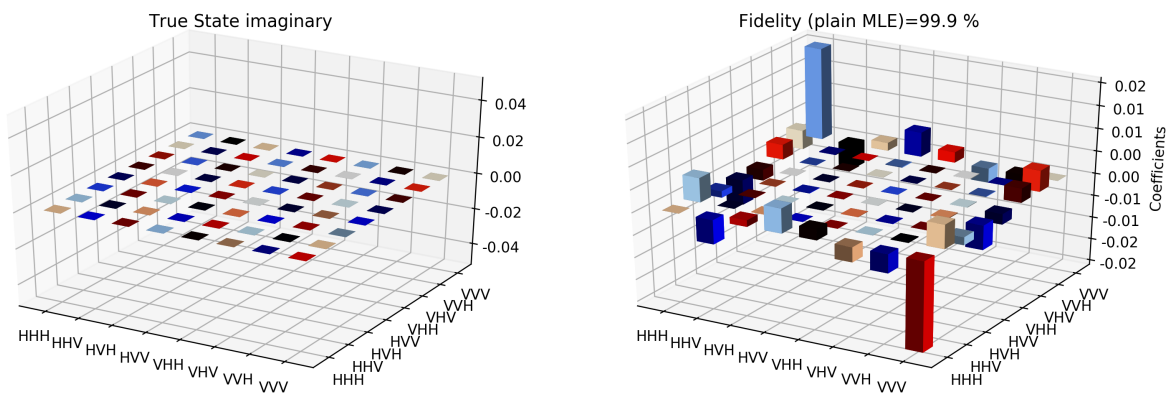
Figure 11.8. State tomography reconstruction of the reduced pseudo-density operator P_{143} is conducted using the maximum likelihood estimation method. The imaginary part of the theoretical expectation (depicted by the true state in the plot) and the reduced pseudo-density operator is compared.
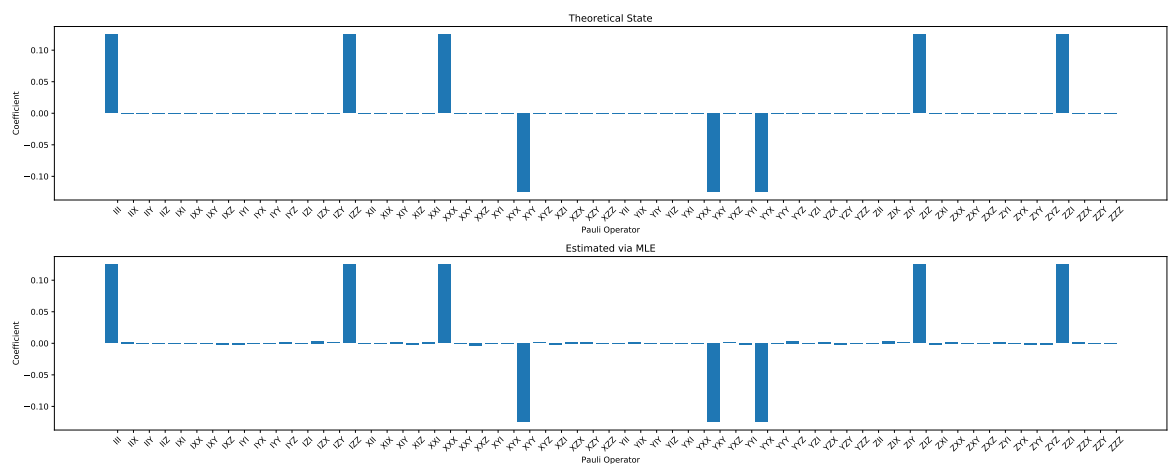
Figure 11.9. The comparison of state tomographic reconstruction of the pseudo-density operator P_{143} and the theoretical state (depicted by the true state in the plot) after the execution of the measurement.
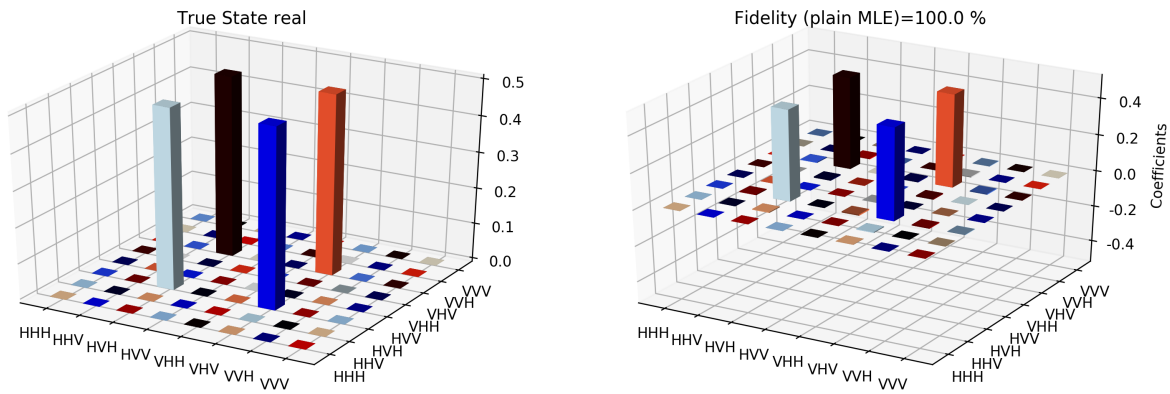
Figure 11.10. State tomography reconstruction of the reduced pseudo-density operator P_{453} is conducted using the maximum likelihood estimation method. The imaginary part of the theoretical expectation (depicted by the true state in the plot) and the reduced pseudo-density operator is compared.
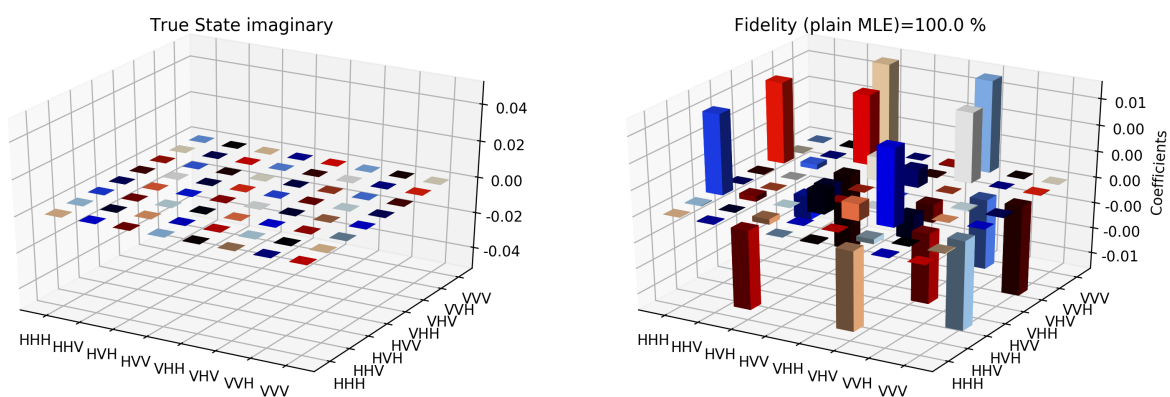
Figure 11.11. State tomography reconstruction of the reduced pseudo-density operator P_{453} is conducted using the maximum likelihood estimation method. The imaginary part of the theoretical expectation (depicted by the true state in the plot) and the reduced pseudo-density operator is compared.

11.2.2 Analysis Using Rigetti Quantum Computer

We are going to explain the binary black hole evaporation theory with the help of the PDO model. We will take into account that a three-qubit entangled state is created above the event horizon. Now one of the particles of the GHZ state that is created due to the process of Hawking radiation falls into one of the black holes of the binary black hole system, and the second particle falls in the second black hole. Time like correlation is developed between them. Now when the two particles that have fallen in the black hole get entangled respectively with a qubit in the black hole, the system can be represented by a five-qubit entangled pseudo-state. The total pseudo-density operator for the system can be described as

$$P_{12345} = \frac{1}{2^5}\Big[I + \Sigma_{123} - \Sigma_{143} - \Sigma_{413} - \Sigma_{253} - \Sigma_{523}\Big], \qquad (11.2.4)$$

where $\Sigma_{ijk} = X_i X_j X_k + Y_i Y_j Y_k + Z_i Z_j Z_k$. The Eq. (11.2.4) is based on the framework outlined in [428]. According to the conjecture proposed in the work [428], they have considered that the time-like correlation is positive, and whereas the spatial correlation component is negative. This is based on the metric signature convention in general relativity, which typically follows the $[+,-,-,-]$ (or $[-,+,+,+]$) convention where the positive sign is for the temporal component and the remaining three negative signs are for the spatial component. Following the same convention, we have defined the pseudo density operator for our system in Eq. (11.2.4). The correlation described by the pseudo density for this system does not obey the monogamy principle of entanglement theory. We will now use this PDO to explain the binary black hole system and discuss how the merger of the black hole boils down equivalent to the two-qubit system.

So far in the analysis of the binary black hole system, the correlation between the qubits of the two black hole was not taken under consideration. Here we will consider the case, where the correlation between the two qubits (interaction term) in the binary black hole systems are taken into account. The pseudo-density operator with this correlation is expressed as

$$P_{12345} = \frac{1}{2^5}\Big[I + \Sigma_{123} - \Sigma_{143} - \Sigma_{413} - \Sigma_{253} - \Sigma_{523} - \Sigma_{453}\Big], \qquad (11.2.5)$$

where the term Σ_{453} represents the correlation of the qubits of the two black hole systems. Similar to the process conducted above for the analysis of P_{123}, we execute the state tomographic reconstruction of the state P_{453}, which can be obtained from Eq. (11.2.5) by tracing out the information of the particle one and two (which can be depicted as $P_{453} = \frac{1}{8}(\mathbb{I} - \Sigma_{453})$).

If two-qubits systems (like A and B) are maximally correlated they cannot be correlated with a third qubit C. For this convention, there exists a trade-off between the amount of entanglement between the qubits A and B, and the same between the qubits A and C. One can express this mathematically using the Coffman-Kundu-Wootters (CKW) monogamy inequality [515, 516] as

$$C_{AB}^2 + C_{AC}^2 \leq C_{A(BC)}^2, \tag{11.2.6}$$

where C_{AB}, C_{AC} represents the concurrences between A and B, and between A and C respectively, while $C_{A(BC)}$ is the concurrence between subsystems A and BC. C_{AB} is defined as $C_{AB} = max\{0, \lambda_1 - \lambda_2 - \lambda_3 - \lambda_4\}$. Here the (λ_i) represents the square root of the eigenvalues of the matrix $\rho_{ij}(\sigma_y \otimes \sigma_y)\rho_{ij}^\star(\sigma_y \otimes \sigma_y)$, where $\rho_{ij}^\star$ depicts the complex conjugate of the density matrix and σ_y the Pauli matrix. The monogamy inequality can also be expressed in terms of entanglement measures as

$$E(A|B) + E(A|C) \leq E(A|BC). \tag{11.2.7}$$

For N qubit [517] the definition can be extended as

$$E(A|B_1) + E(A|B_2) + \cdots + E(A|B_{N-1}) \leq E(A|B_1 B_2 \dots B_{N-1}). \tag{11.2.8}$$

Using the equation (11.2.8), we can analyze the monogamy inequality for our system. This is violated by our pseudo operator P_{12345}.

The above proposed PDO describes the binary black hole evaporation which incorporates the monogamy violation principle. This is possible because PDOs can be used to describe the maximally temporal correlation as well as maximally spatial correlation.

To describe this process, we execute a quantum optical simulation of this framework. Here, we are not going to describe any experimental test results, but we will illustrate our theoretical model via qubit simulation using quantum virtual machines (we have considered rigetti quantum computer for the simulation). Through our experiment, we first generate a three-particle entangled pair of photons (A, B, C). Now, after the two-particle falls into the black hole the correlation between the individual particles that have fallen and the particle that is above the event horizon is in the same maximally entangled state, which is observed by measuring the photon A and B in three different times (t_1, t_2 and t_3). Whereas, the correlation between the particles that have fallen inside the black hole, and has developed a spatial entanglement there, which can be comprehended by measuring the photons A, B,

C at the same time t_1. So, we reconstruct the relevant statistics of the PDO P_{12345}. This is established by constructing the different ensemble of the particles under study.

In the optical schematic, we have generated a GHZ state using a type-II β-Barium Borate (BBO) crystal [518]. A mode lock laser has been considered for the generation of a laser beam of 808 nm wavelength. This beam is then passed through a second harmonic generator after which it gets injected into a 0.5 nm thick BBO crystal of type-II to generate a parametric down-conversion (PDC) [518, 519]. After the generation of the two-photon beam, the second photon beam is again injected into a BBO crystal to produce two further beams. These generate a three-photon entangled state. The maximally entangled state is $|GHZ\rangle = \frac{1}{\sqrt{2}}\big(|HHH\rangle + |VVV\rangle\big)$, where H and V represents the horizontal and the vertical polarisation components respectively. These are generated from the interaction of the PDC cone [520].

In two of the photon paths (A, B), two sets of measurements is conducted here in cascades $(M_1, M_2, M_3$ for photon path A and M_4, M_5, M_6 for the photon path B). Each of these measurement systems when unfolded, consists of a quarter-wave plate (QWP), then a half-wave plate (HWP), and a polarizing beam splitter (PBS). We have inserted a set of HWP and QWP between two measurements so that, one can compensate for the polarisation that occurred due to the previous measurement. After the measurement, the photon A, B, and C are passed through the band-pass interference filter, which filters the photon beam. After the filtration process, it passed through the multi-mode optical fibers connected to silicon single-photon avalanche diodes (Si-SPADs). The output is then sent to the coincidence electronics for the analysis.

We will perform a quantum state tomography reconstruction [521, 522] on branch A. In this case, we are able to extract the temporal correlation for the system which can be described as $P_{123} = \frac{1}{8}(I + \Sigma_{123})$ and to understand the spatial correlation we have conducted a tomographical reconstruction of the reduced pseudo density state P_{143} of the system. Similarly, one can develop the other reduced pseudo-density state by a similar chronology.

The state tomographic reconstruction of the state P_{123} is shown in Figs. (11.3-11.8). For the analysis, we have considered three different methods to estimate and reconstruction of the state. The results so generated using these methods are in excellent agreement with the theoretical expectations as stated by the fidelity (F), which is the measure that evaluates the closeness of the state expressed by the density matrix to that of the original pure state $|\psi\rangle$, F can have a value between $[0, 1]$. For maximum likelihood estimation (MLE), linear inversion and projected linear inversion the fidelity is $F = 99.9\%$, 100% and 97.3% respectively (shown

Method	Fidelity Score
Linear Inversion	1.0
Projected Linear Inversion	0.973
MLE	0.999

Table 11.1. Table showing the fidelity score F obtained from the three different methods used in the tomography used. Since F can't exceed values of 0.5 in the classical limit, it shows that there is true entanglement beyond the classical limit. Also, the deviation in the models shows that better entanglement distillation could resolve this difference in values.

in table (11.1)). The state tomographic reconstruction of the state P_{143} results similar to P_{123}. The simulation of the monogamy inequality of the considered pseudo-density matrix shows that it violates the monogamy principal. The detailed plots of the analysis of P_{143} are not shown as they are similar in nature.

It is however interesting to note the fluctuations in the imaginary part of each of the plots. Although the absence of any fluctuations in the real axis compels us to believe that it is simply not background noise, originating from measurement error. If we compare our imaginary plot results to that of the [428] plots, we see clearly there are much more fluctuations in our binary black hole system set up. It is not clear to us at the moment what are the origins of these fluctuations, but definitely, it points to some perturbations on the quantum state measurements of the pseudo-random operators originating specifically from our system's set up (hence essentially a quantum phenomenon). We speculate this could be any deviations around the horizon of the black hole. In the future, we plan to verify this analysis with an optomechanical setup [462, 523] and further explore in the Planck regime for any possible deviation in the horizon of the black hole. We look forward to studying the cause of such anomaly in the imaginary axis values and exploring it further in future works along with a similar framework as presented by [524].

For the analysis of the interaction between the two qubits of the two black hole systems, we have considered a different basis of the GHZ state [525], from which we can return to the usual form by some local operation. One can obtain the maximally entangled state by adopting the selected photons spatially which belongs to the intersection of two parametric down-conversion cones. The process properly compensates for the temporal and the phase effect [520]. To measure the spatial correlation (like $P_{453} = \frac{1}{8}(\mathbb{I} - \Sigma_{453})$) we measure the correlation between M_4, M_5 and M_7, provided that M_6 performs the same polarization projection as that of M_4 and M_5. By this process, we reconstruct the reduced pseudo-density operator tomographically which actually corresponds to the spatial entangled state that is
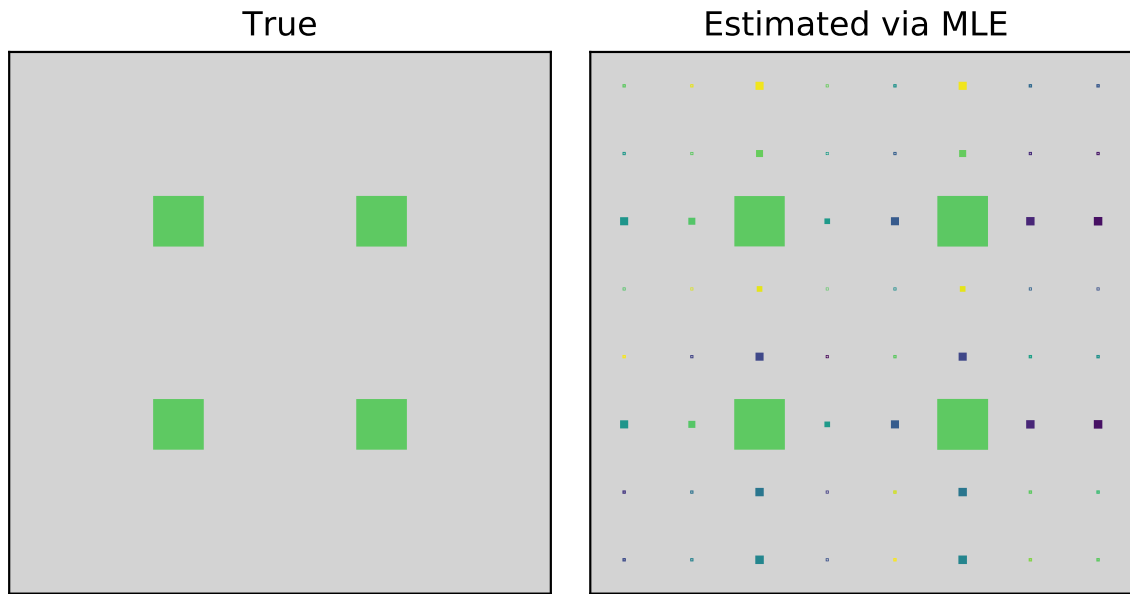
Figure 11.12. Comparison of the two dimensional projection plot between the estimated state P_{453} and the true state.

formed between the particles 4, 5, and 3 within the black hole. The state tomographic reconstruction of the system shows a complete agreement with the proposed theoretical model for the analysis as shown in Fig. (11.10). Similar to the state tomographic analysis of P_{123}, we also encounter fluctuations in the imaginary part of the plot which we can speculate as to the effect due to the interaction of the two qubits in the binary black hole system.

11.2.3 Gravitational Waves as a context

So far, we have described an alternative method to explain the entanglement paradox in the binary black hole system. We have incorporated the pseudo-density matrix formalism to explain this phenomenon. We have considered that Hawking radiation, which is the cause for the phenomenology of the black hole evaporation, can be well established from the pseudo-density formalism point of view in such a binary system, in agreement with the conjecture presented by [428]. For the analysis, we have considered PDO in terms of the Pauli operators for the three-qubit system, where two of them fall into the binary black hole system and get entangled there. We have used a quantum optical set up to demonstrate these phenomena by simulations using a quantum virtual machine. The state tomographic reconstruction shows that the pseudo-density operator can appropriately describe the correlation that violates monogamy.

The first detection of gravitational waves in 2015 [526, 527] has opened many new possibilities for us in understanding many fundamentals of physics and the Universe. Recent

works [528, 529], have shown signs that there is a scope for using the gravitational waves as an effective tool for understanding the Hawking radiation and probe into the black hole physics. Lately, works also show [530–535] that it is very much possible to extend the standard framework of Hawking radiation in a single black hole to that of a binary black hole system (both non-spinning and spinning). In this context, upcoming gravitational waves detection programs like laser interferometer space antenna (LISA) [536] are well designed. They will target objects like binary black hole systems typically a supermassive galactic black hole orbited by a stellar black hole [536]. For such large mass ratio systems, [529] has shown how there will be Hawking radiation exchange between the two merging black holes and also that this exchange will not be attenuated by other physical parameters like the tidal force, relative motion, etc. In addition, they proposed that such exchanged Hawking radiation will lead to the production of gravitational waveforms different than those predicted by the classical theory of gravity and in future tests of gravitational waves, it is highly likely that such precision measurement can be recorded.

Also in their work, [528] has shown how binary gravitational systems can be expected to produce entangled signal emissions and how laser interferometer gravitational-wave observatory (LIGO)-like detectors can be used to detect them. In what follows, we put forward a thought experiment, trying to bridge this gap and make more use between the theoretical conjectures and the observational artefacts available from gravitational waves. We also explore it's verification possibilities.

In the work [529], the authors stated that owing to the effects of Hawking radiation from the binary black hole systems, the emitted gravitational waves will have a deviation in their characteristics from that predicted by the semi-classical theories of gravity. However, we suggest that the exchanged Hawking radiation between the two black holes will not hinder the normal entanglement process to propagate, exactly as outlined in our current work. We make an assumption that in an unlikely situation if simultaneously Hawking radiation and gravitational waves were both emitted from the outside neighborhood of the horizon of a binary black hole system, the entanglement information that would be imprinted in both these carriers would be the same, essentially describing the previous quantum state's information within the common envelope of the binary black hole's horizon [2]. A verification of this thought experiment is proposed with our optomechanical setup. If future observations of the gravitational waves are available with better precision, then we can replace the laser beam

---

[2]Although realistically that will never be possible to observe them simultaneously, as measurable Hawking radiation will be produced at a much much later stage in the lifetime of a black hole.

source in our optical setup with the characteristics waves of the gravitational waves (treating both as standard electromagnetic waves) and perform the optical simulations with the real data. In spite of the fact, that the gravitational waves detected are not the Hawking radiation waves from the black hole, but in the situation described above, they should carry the same entanglement imprint to that of Hawking radiation if they were simultaneous at the time of emission. If this is experimentally verified as we suggest with our optical setup, then we can do away with the requirement of detecting Hawking radiation separately for retrieval of quantum state information from inside the black hole. If the results provide satisfactory verification of the conjecture we proposed with good agreement between the theoretical and the experimental values, in our optical setup using the gravitational waves, then we will verify our above assumption.

This could potentially open new possibilities with the use of the gravitational waves as a tool for understanding the black hole paradox and information retrieval. We can explore the possibility of understanding the quantum states of the particles inside the black hole which would be in spatial entanglement with the particles from outside (which in our case is particles 1, 3 and 4) or in other words we can have the possibility to access the information of the inside of a black hole. The other possibility being, the gravitational waves detected being originated from the binary black hole system as explained before, if, via reverse engineering, the entanglement information which these waves will carry can be successfully segregated [537, 538], we can also do a verification of our proposed conjecture and try to explore the same set of questions with a stronger benchmark.

11.3 Chapter Summary

To summarize, in the first phase of this chapter, we have discussed how one can simulate a thermodynamic system using quantum gates in a quantum computer, and propose that if we can simulate the thermodynamic processes like adiabatic, isothermal, isochoric, and isobaric processes, then we can have an experimental validation of thermal machines with different working medium using a quantum computer. And in the second phase of the chapter, we have verified the conjecture presented by [428] with a different system than theirs. We also tried to explore the possibilities of how their novel work could be brought to more practical setups, from where we can try to exploit our current available black hole observational information in the form of the gravitational waves and make use of our conjecture for its experimental verification as well as explore the idea of real black hole entanglement related observational

experiments in near future. We would also like to mention, that we have analyzed the post-merger equilibrium state (ring down) of a reduced binary black hole system. We have seen that our setup can reproduce the results presented in [428] of a single black hole system under such conditions. Additionally, we have encountered some interesting results from our analysis like the fluctuations in the imaginary plots (see section 11.2.2). As discussed already, the origin of these fluctuations is expected to be not just due to noise but due to some effect of the system. We plan to continue the investigation on the origins of these fluctuations and it's consequences.

Recent new developments in open quantum systems have drawn our attention to the possibility to extend the current project from this perspective. The dynamics of a system interacting with an environment can be analyzed in the framework of open quantum systems. One can express the thermalization phenomena of the Hawking radiation from a Schwarzschild or a de Sitter spacetime from an open quantum system framework [539–541]. Our model conjectured here can be suited to explore with open quantum systems.

12 Conclusion

Thermodynamics is always motivated by experimental analysis. One of the primary purposes of the field is to develop principles that convey to us what are the type of machine we can develop and the limit in the performance of these machines. For the quest of quantum thermodynamics, the important point is to identify the quantum effects that disregard classical elucidation. A recent study to explore thermodynamics from quantum information and computation point of view got the limelight due to the fact that their effects provide an advantage over the classical realization of the process. This framework is utilized to investigate the void between classical and quantum computation. So, there happens to be an intimate relation between quantum information and quantum thermodynamics dated back to Maxwell, Landauer, Szilard, and Bennett. The analysis of the computation process from the thermodynamic viewpoint has been one of the central points of attraction for the researchers of physics as well as computer science. It got initiated from the physical Church-Turing thesis, where they conveyed that every computational process is physical. Various approaches have been considered for the analysis of the different computational processes. With the advent of the modern statistical theory, the research in this area got boosted. Not only in the field of computer science, we also encounter its application in different fields from chemical networks, molecular biology, and even in neurology. In this thesis, I discussed the basic problem of relating thermodynamics and quantum mechanics from a variety of angles mainly focusing on the analysis of thermal machines.

Hereafter, I will discuss the main results of the thesis along with its possible future directions inspired by the analysis of the work that is carried out in this thesis. First and foremost, we did a survey where we have presented an overview of the impact of thermodynamics in the field of computation, mainly the artificial process (computer science theory) and the information theory. For the information theory, we will consider only the error-correcting codes. We have considered some specific computational models and then explored their processing from a thermodynamic viewpoint. Error correction is an important part of any

computational process. The analysis of these protocols from a thermodynamic viewpoint is at their baby stage. Error correction codes in terms of the thermodynamic process are also explored in this thesis. Further investigation in this direction is required to get a better understanding of the bond between thermodynamics and the computational process. For example, in the case of finite automata, one can investigate the maximum thermodynamic cost that is required to accept a language for automata. Also one can calculate the minimal cost for any deterministic automata. One can also work on developing a theory to analyze the non-deterministic finite-state automata in terms of thermodynamics. Models to describe the complex Turing machine, and also network theory from the thermodynamic viewpoint is an open area of research. Along with that from an information perspective modeling of the error correction models by the physical system to explain it thermodynamically needs further investigation. In recent work, the authors have shown that there a similarity between the quantum heat engine and quantum error correction codes. They have strengthened their intuition by making a complete analysis of the thermodynamic properties of the quantum engine-based error correction codes. So the thermodynamic approach to explaining the error correction is an open book to read.

In the next phase of the thesis, we have explored thermal machines with different quantum mechanical effects. In this phase of the thesis, our primary motivation is to find alternative approaches to enhance the efficiency and the coefficient of performance (COP) of the thermal machine and also reduce the cost of measurement. For this purpose, we have considered various working models with quantum signatures for the exploration of quantum thermal machines. In one approach, we have considered potential well as the working medium for the analysis of thermal machines like Stirling engine in both non-relativistic as well as the relativistic regime. In this work, we have bridged a connection between the thermodynamic variables and the uncertainty relation of the incompatible observables for the quantum mechanical system that is being considered for the analysis. We encountered that there is a direct connection between the thermodynamic variables and the canonical formalism of the uncertainty relation. We have developed the thermal uncertainty relation where we have applied the bounds of the canonical uncertainty relation to study the behavior of the efficiency in terms of the uncertainty relation. We visualized that the efficiency of the quantum thermal machines that can be predicted with the knowledge of uncertainty relation without performing any projective measurement on the system. The effect of the uncertainty relation is prevalent for both regimes.

Now, being fascinated by the question of whether the change in the space structure pro-

vides a boost in the performance of the thermal engine, we considered different deformed space structures in the literature to explore quantum thermal machines. We considered a simple harmonic oscillator thermal machine in NC space, and then the performance of the thermal machine was compared with ordinary space thermal machines. We encounter that the space structure provides a boost to the performance of the engine. To explore further deep into this problem we considered coupled harmonic oscillator for the analysis of thermal machines. In this work, we have considered generalized deformed space structure for the analysis. We visualized a boost in the efficiency of the heat engines for these models. This work was further extended in the relativistic limit to explore whether it holds in this regime or not. We find the same outcome in this regime. Along with that, we have proposed a way to analyze the information loss paradox with the help PDO model by simulating the system in Righetti quantum computer. Along with that, we have also proposed a Gedanken experiment for the gravitational wave using the quantum optical approach, which can be implemented for a better understanding of the working principle behind these gravitational waves. The basis of this project was to visualize the power of the quantum computation tool to explain different physical phenomena of the universe.

Though the primary perspective of the thesis was to analyze the different processes to enhance the efficiency of the thermal machine, we provide some approaches through which we can have the experimental analysis of relativistic thermal machines. The bound to the efficiency that is provided by the uncertainty relation also sustain in case of the experimental realization as it depends on the working medium (i.e. potential well, harmonic oscillator, and so on). But it is independent of the process through which it is experimentally verified.

In recent times, the trapped ion is one of the profound quantum technology which plays a vital role in the experimental validation of various aspects of quantum information. It also plays an important role in the field of quantum thermodynamics for the implementation of harmonic thermal machines [467,488,542–544]. One looks into logical trapped-ion technology first when one envisions the experimental implementation of an oscillator-based thermal machine. So we can expect that our model can be experimentally implemented by trapped ion technology. Recent development has shown that one can implement relativistic Brownian motion with 2D materials like graphene chips [545]. Following the same methodology, one can design a relativistic harmonic thermal machine with 2D materials.

Now, we would try to explore the future prospect of the works of this thesis. The work which explores the connection between the uncertainty relation with the thermodynamic variables can be a backbone to develop a bridge of connection between the relativistic heat

engines with the relativistic condensed matter physics. Several approaches to design materials for non-relativistic engines and refrigerators are explored. Thus, it may also be possible to design materials for the analysis of the relativistic engines using the relativistic density functional theory. Cycles, when accompanied by the quantum phase transition, have a direct impact on thermodynamic performance. So, one possible application of our work could be to develop a connection between the uncertainty relations associated with the thermodynamics cycles with the quantum phase transition. Along with that, one can even explore the holographic interpretation of entanglement entropy of anti-de Sitter (ADS)/conformal field theory (CFT) from an uncertainty viewpoint. We visualized that NC space has an impact on the performance of the thermal machine. So we can expect that the NC phase space can be an effectual resource for different application areas of the quantum theory, which needs further exploration.

Various other coupled working medium is used for the analysis of quantum cycles. One can make use of the NC phase space structure to analyze these models for the cycles, and even can extend it for exploring non-Markovian reservoirs. For our analysis, we have focused on quantum heat cycles. One can study the effect of the non-commutative phase space on the coefficient of performance of the quantum refrigerator cycles for coupled oscillators and even for other working substances. The analysis of the existing thermodynamic cycles in NC phase space is required to provide the generic statement about the catalytic effect it yields to the efficiency of the cycles. The analysis of the irreversible and continuous cycles, and quantum phase transition in NC phase space needs exploration to visualize the effect of the NC parameter in different thermodynamic processes. The challenging task in the NC space is to analyze the NC spacetime in the relativistic regime. Recent work has analyzed the different potential problems in the NC spacetime with relativistic correction. This gives us the insight to analyze the thermodynamic process in the relativistic realm of NC phase space which needs exploration. One can utilize the generalized uncertainty principle to instigate a bound not only in the efficiency of the different cycles but even to the various thermodynamic process by getting motivated from previous works.

The experimental realization of the NC phase space with our existing technology will provide a boost for the analysis of thermodynamic processes and quantum information theory in NC spacetime. Dey and Hussin in their work have shown that non-commutative systems result in more entanglement than the usual quantum systems. The experimental validation of this will provide a boost in the study of entanglement theory and its application to the different areas of quantum information theory.

It is a well-known fact that different systems have different heat signatures. One can utilize this property of the system for various purposes such as for security in cryptographic protocols. So one can explore the communications protocols, crypto-systems from a thermodynamic viewpoint. Algorithms in the form of a search algorithm from a thermodynamic viewpoint have already been analyzed. Further exploration in this direction is an open area of research. Thermodynamic analysis of quantum computations needs a rigorous investigation for a better understanding of quantum computers and to develop hardware with lower cost functions.

Simulation of thermodynamic system in quantum computer is a challenging work as quantum computer constraints the tuning of the control parameter. These are forbidden as they are optimized to reduce the noise. We can design a simulation of thermodynamic cycle in quantum computer provided that we can simulate the thermodynamics processes. This will help us to experimentally analyze different thermodynamic cycles as well as different thermodynamic frameworks.

Bibliography

[1] B. Woodcroft *et al.*, *The Pneumatics of Hero of Alexandria: From the Original Greek*. Charles Whittingham, 1851.

[2] R. Clausius, *On the motive power of heat and the laws which can be deduced therefrom regarding the theory of heat*, *Annalen der Physik* **155** no. 4, (1850) 500–524.

[3] J. D. Bekenstein, *Black holes and entropy*, *Physical Review D* **7** no. 8, (1973) 2333.

[4] J. M. Bardeen, B. Carter, and S. W. Hawking, *The four laws of black hole mechanics*, *Communications in mathematical physics* **31** no. 2, (1973) 161–170.

[5] S. W. Hawking, *Particle creation by black holes*, *Communications in mathematical physics* **43** no. 3, (1975) 199–220.

[6] E. Schrödinger, *Die gegenwärtige situation in der quantenmechanik*, *Naturwissenschaften* **23** no. 49, (1935) 823–828.

[7] E. Schrödinger, *Mathematical proceedings of the cambridge philosophical society*, in *Mathematical Proceedings of the Cambridge Philosophical Society*, vol. 31, pp. 555–563. 1935.

[8] C. Carathéodory, *Untersuchungen über die grundlagen der thermodynamik*, *Mathematische Annalen* **67** no. 3, (1909) 355–386.

[9] H. Callen, *Thermodynamics and an introduction to thermostatistics. john wiley & sons*, *New York* (1985) .

[10] E. H. Lieb and J. Yngvason, *The physics and mathematics of the second law of thermodynamics*, *Physics Reports* **310** no. 1, (1999) 1–96.

[11] E. H. Lieb and J. Yngvason, *A fresh look at entropy and the second law of thermodynamics*, *Statistical Mechanics* (2000) 365–370.

[12] H. E. Scovil and E. O. Schulz-DuBois, *Three-level masers as heat engines*, *Physical Review Letters* **2** no. 6, (1959) 262.

[13] J. Geusic, E. S.-D. Bois, R. De Grasse, and H. Scovil, *Three level spin refrigeration and maser action at 1500 mc/sec*, *Journal of Applied Physics* **30** no. 7, (1959) 1113–1114.

[14] R. Alicki, *The quantum open system as a model of the heat engine*, *Journal of Physics A: Mathematical and General* **12** no. 5, (1979) L103.

[15] R. Kosloff, *A quantum mechanical open system as a model of a heat engine*, *The Journal of chemical physics* **80** no. 4, (1984) 1625–1631.

[16] S. Lloyd and L. Viola, *Engineering quantum dynamics*, *Physical Review A* **65** no. 1, (2001) 010101.

[17] F. Binder, L. A. Correa, C. Gogolin, J. Anders, and G. Adesso, *Thermodynamics in the quantum regime*, *Fundamental Theories of Physics* **195** (2018) .

[18] S. Deffner and S. Campbell, *Quantum Thermodynamics: An introduction to the thermodynamics of quantum information*. Morgan & Claypool Publishers, 2019.

[19] K. Maruyama, F. Nori, and V. Vedral, *Colloquium: The physics of maxwell's demon and information*, *Reviews of Modern Physics* **81** no. 1, (2009) 1.

[20] C. H. Bennett, *Notes on landauer's principle, reversible computation, and maxwell's demon*, *Studies In History and Philosophy of Science Part B: Studies In History and Philosophy of Modern Physics* **34** no. 3, (2003) 501–510.

[21] L. Szilard, *Über die entropieverminderung in einem thermodynamischen system bei eingriffen intelligenter wesen*, *Zeitschrift für Physik* **53** no. 11-12, (1929) 840–856.

[22] R. Landauer, *Irreversibility and heat generation in the computing process*, *IBM journal of research and development* **5** no. 3, (1961) 183–191.

[23] R. Landauer *et al.*, *Information is physical*, *Physics Today* **44** no. 5, (1991) 23–29.

[24] C. H. Bennett, *The thermodynamics of computation—a review*, *International Journal of Theoretical Physics* **21** no. 12, (1982) 905–940.

[25] E. T. Jaynes, *Information theory and statistical mechanics*, *Physical review* **106** no. 4, (1957) 620.

[26] E. T. Jaynes, *Information theory and statistical mechanics. ii*, *Physical review* **108** no. 2, (1957) 171.

[27] J. Goold, M. Huber, A. Riera, L. Del Rio, and P. Skrzypczyk, *The role of quantum information in thermodynamics—a topical review*, *Journal of Physics A: Mathematical and Theoretical* **49** no. 14, (2016) 143001.

[28] S. Vinjanampathy and J. Anders, *Quantum thermodynamics*, *Contemporary Physics* **57** no. 4, (2016) 545–579.

[29] C. P. Kempes, D. Wolpert, Z. Cohen, and J. Pérez-Mercader, *The thermodynamic efficiency of computations made in cells across the range of life*, *Philosophical Transactions of the Royal Society A: Mathematical, Physical and Engineering Sciences* **375** no. 2109, (2017) 20160343.

[30] A. W. Burks, *Von neumann's self-reproducing automata*, tech. rep., MICHIGAN UNIV ANN ARBOR LOGIC OF COMPUTERS GROUP, 1969.

[31] L. Brillouin, *Science and information theory*. Courier Corporation, 2013.

[32] E. Fredkin and T. Toffoli, *Conservative logic*, *International Journal of theoretical physics* **21** no. 3-4, (1982) 219–253.

[33] C. H. Bennett, *Logical reversibility of computation*, *IBM journal of Research and Development* **17** no. 6, (1973) 525–532.

[34] R. W. Keyes and R. Landauer, *Minimal energy dissipation in logic*, *IBM Journal of Research and Development* **14** no. 2, (1970) 152–157.

[35] K. K. Likharev, *Classical and quantum limitations on energy consumption in computation*, *International Journal of Theoretical Physics* **21** no. 3-4, (1982) 311–326.

[36] P. Chattopadhyay, A. Mitra, G. Paul, and V. Zarikas, *Bound on efficiency of heat engine from uncertainty relation viewpoint*, *Entropy* **23** no. 4, (2021) 439.

[37] F. Wu, Z. Yang, L. Chen, X. Liu, and S. Wu, *Work output and efficiency of a reversible quantum otto cycle*, *Thermal science* **14** no. 4, (2010) 879–886.

[38] L. Chen, X. Liu, Y. Ge, F. Wu, and F. Sun, *Ecological optimisation of irreversible harmonic oscillator carnot refrigerator*, *Journal of the Energy Institute* **86** no. 2, (2013) 85–96.

[39] F. Wu, L. Chen, F. Sun, C. Wu, and Q. Li, *Generalized model and optimum performance of an irreversible quantum brayton engine with spin systems*, *Physical Review E* **73** no. 1, (2006) 016103.

[40] P. Chattopadhyay, *Non-commutative space: boon or bane for quantum engines and refrigerators*, *The European Physical Journal Plus* **135** no. 3, (2020) 1–11.

[41] T. Pandit, P. Chattopadhyay, and G. Paul, *Non-commutative space engine: a boost to thermodynamic processes*, *arXiv preprint arXiv:1911.13105* (2019) .

[42] P. Chattopadhyay, T. Pandit, A. Mitra, and G. Paul, *Quantum cycle in relativistic non-commutative space with generalized uncertainty principle correction*, *arXiv preprint arXiv:2010.06672* (2020) .

[43] P. Chattopadhyay and G. Paul, *Relativistic quantum heat engine from uncertainty relation standpoint*, *Scientific reports* **9** no. 1, (2019) 1–12.

[44] E. Munoz and F. J. Pena, *Quantum heat engine in the relativistic limit: The case of a dirac particle*, *Physical Review E* **86** no. 6, (2012) 061108.

[45] Y. Yin, L. Chen, and F. Wu, *Performance of quantum stirling heat engine with numerous copies of extreme relativistic particles confined in 1d potential well*, *Physica A: Statistical Mechanics and its Applications* **503** (2018) 58–70.

[46] A. Purwanto, H. Sukamto, B. A. Subagyo, M. Taufiqi, *et al.*, *Two scenarios on the relativistic quantum heat engine*, *Journal of Applied Mathematics and Physics* **4** no. 07, (2016) 1344.

[47] S. W. Hawking, *Black holes and thermodynamics*, *Physical Review D* **13** no. 2, (1976) 191.

[48] T. Padmanabhan, *Gravity and the thermodynamics of horizons*, *Physics Reports* **406** no. 2, (2005) 49–125.

[49] U. Gürsoy, E. Kiritsis, L. Mazzanti, and F. Nitti, *Holography and thermodynamics of 5d dilaton-gravity*, *Journal of High Energy Physics* **2009** no. 05, (2009) 033.

[50] K. Huang, *Introduction to statistical physics*. CRC press, 2009.

[51] E. P. Gyftopoulos and G. P. Beretta, *Thermodynamics: foundations and applications*. Courier Corporation, 2005.

[52] M. W. Zemansky, *Heat and thermodynamics: an intermediate textbook*, .

[53] S. J. Farlow, *Partial differential equations for scientists and engineers*. Courier Corporation, 1993.

[54] P. C. Cross and H. C. Eckstrom, *The third law of classical thermodynamics*, *The Journal of Chemical Physics* **10** no. 5, (1942) 287–291.

[55] W. Nernst, *The New Heat Theorem: Its foundations in theory and experiment*. Taylor & Francis, 1969.

[56] L. Bryant, *The silent otto*, *Technology and Culture* **7** no. 2, (1966) 184–200.

[57] L. Boltzmann, *On certain questions of the theory of gases*, *Nature* **51** no. 1322, (1895) 413–415.

[58] J. W. Gibbs, *On the equilibrium of heterogeneous substances*, .

[59] K. Sharp and F. Matschinsky, *Translation of ludwig boltzmann's paper "on the relationship between the second fundamental theorem of the mechanical theory of heat and probability calculations regarding the conditions for thermal equilibrium" sitzungberichte der kaiserlichen akademie der wissenschaften. mathematisch-naturwissen classe. abt. ii, lxxvi 1877, pp 373-435 (wien. ber. 1877, 76: 373-435). reprinted in wiss. abhandlungen, vol. ii, reprint 42, p. 164-223, barth, leipzig, 1909*, *Entropy* **17** no. 4, (2015) 1971–2009.

[60] H. Spohn, *Entropy production for quantum dynamical semigroups*, *Journal of Mathematical Physics* **19** no. 5, (1978) 1227–1230.

[61] E. Muñoz, F. J. Peña, and A. González, *Magnetically-driven quantum heat engines: The quasi-static limit of their efficiency*, *Entropy* **18** no. 5, (2016) 173.

[62] M. Campisi, P. Talkner, and P. Hänggi, *Fluctuation theorem for arbitrary open quantum systems*, *Physical review letters* **102** no. 21, (2009) 210401.

[63] M. Campisi, P. Hänggi, and P. Talkner, *Colloquium: Quantum fluctuation relations: Foundations and applications*, *Reviews of Modern Physics* **83** no. 3, (2011) 771.

[64] H. Quan and H. Dong, *Quantum crooks fluctuation theorem and quantum jarzynski equality in the presence of a reservoir*, *arXiv preprint arXiv:0812.4955* (2008) .

[65] A. Del Campo, J. Goold, and M. Paternostro, *More bang for your buck: Super-adiabatic quantum engines*, *Scientific reports* **4** no. 1, (2014) 1–5.

[66] E. Geva and R. Kosloff, *A quantum-mechanical heat engine operating in finite time. a model consisting of spin-1/2 systems as the working fluid*, *The Journal of chemical physics* **96** no. 4, (1992) 3054–3067.

[67] T. Feldmann and R. Kosloff, *Performance of discrete heat engines and heat pumps in finite time*, *Physical Review E* **61** no. 5, (2000) 4774.

[68] Y. Rezek and R. Kosloff, *Irreversible performance of a quantum harmonic heat engine*, *New Journal of Physics* **8** no. 5, (2006) 83.

[69] R. Kosloff and A. Levy, *Quantum heat engines and refrigerators: Continuous devices*, *Annual Review of Physical Chemistry* **65** (2014) 365–393.

[70] U. Harbola, S. Rahav, and S. Mukamel, *Quantum heat engines: A thermodynamic analysis of power and efficiency*, *EPL (Europhysics Letters)* **99** no. 5, (2012) 50005.

[71] A. E. Allahverdyan, K. Hovhannisyan, and G. Mahler, *Optimal refrigerator*, *Physical Review E* **81** no. 5, (2010) 051129.

[72] N. Linden, S. Popescu, and P. Skrzypczyk, *How small can thermal machines be? the smallest possible refrigerator*, *Physical review letters* **105** no. 13, (2010) 130401.

[73] M. J. Henrich, F. Rempp, and G. Mahler, *Quantum thermodynamic otto machines: A spin-system approach*, *The European Physical Journal Special Topics* **151** no. 1, (2007) 157–165.

[74] P. Skrzypczyk, A. J. Short, and S. Popescu, *Work extraction and thermodynamics for individual quantum systems*, *Nature communications* **5** no. 1, (2014) 1–8.

[75] J. Gemmer, M. Michel, and G. Mahler, *Quantum thermodynamics: Emergence of thermodynamic behavior within composite quantum systems*, vol. 784. Springer, 2009.

[76] A. Riera, C. Gogolin, and J. Eisert, *Thermalization in nature and on a quantum computer*, *Physical Review Letters* **108** no. 8, (2012) 080402.

[77] S. Trotzky, Y.-A. Chen, A. Flesch, I. P. McCulloch, U. Schollwöck, J. Eisert, and I. Bloch, *Probing the relaxation towards equilibrium in an isolated strongly correlated one-dimensional bose gas*, *Nature physics* **8** no. 4, (2012) 325–330.

[78] P. O. Boykin, T. Mor, V. Roychowdhury, F. Vatan, and R. Vrijen, *Algorithmic cooling and scalable nmr quantum computers*, *Proceedings of the National Academy of Sciences* **99** no. 6, (2002) 3388–3393.

[79] W. S. Bakr, P. M. Preiss, M. E. Tai, R. Ma, J. Simon, and M. Greiner, *Orbital excitation blockade and algorithmic cooling in quantum gases*, *Nature* **480** no. 7378, (2011) 500–503.

[80] J. Baugh, O. Moussa, C. A. Ryan, A. Nayak, and R. Laflamme, *Experimental implementation of heat-bath algorithmic cooling using solid-state nuclear magnetic resonance*, *Nature* **438** no. 7067, (2005) 470–473.

[81] L. J. Schulman, T. Mor, and Y. Weinstein, *Physical limits of heat-bath algorithmic cooling*, *Physical review letters* **94** no. 12, (2005) 120501.

[82] F. Rempp, M. Michel, and G. Mahler, *Cyclic cooling algorithm*, *Physical Review A* **76** no. 3, (2007) 032325.

[83] M. Horodecki and J. Oppenheim, *Fundamental limitations for quantum and nanoscale thermodynamics*, *Nature communications* **4** no. 1, (2013) 1–6.

[84] L. Del Rio, J. Åberg, R. Renner, O. Dahlsten, and V. Vedral, *The thermodynamic meaning of negative entropy*, *Nature* **474** no. 7349, (2011) 61–63.

[85] D. Mandal and C. Jarzynski, *Work and information processing in a solvable model of maxwell's demon*, *Proceedings of the National Academy of Sciences* **109** no. 29, (2012) 11641–11645.

[86] A. Ferraro, A. García-Saez, and A. Acín, *Intensive temperature and quantum correlations for refined quantum measurements*, *EPL (Europhysics Letters)* **98** no. 1, (2012) 10009.

[87] M. Kliesch, C. Gogolin, M. Kastoryano, A. Riera, and J. Eisert, *Locality of temperature*, *Physical review x* **4** no. 3, (2014) 031019.

[88] S. Hernández-Santana, A. Riera, K. V. Hovhannisyan, M. Perarnau-Llobet, L. Tagliacozzo, and A. Acín, *Locality of temperature in spin chains*, *New Journal of Physics* **17** no. 8, (2015) 085007.

[89] L. Masanes and J. Oppenheim, *A derivation (and quantification) of the third law of thermodynamics*, *arXiv preprint arXiv:1412.3828* (2014) .

[90] F. Brandao, M. Horodecki, N. Ng, J. Oppenheim, and S. Wehner, *The second laws of quantum thermodynamics*, *Proceedings of the National Academy of Sciences* **112** no. 11, (2015) 3275–3279.

[91] M. Lostaglio, *The resource theory of quantum thermodynamics*. PhD thesis, Imperial College London, 2016.

[92] N. H. Y. Ng and M. P. Woods, *Resource theory of quantum thermodynamics: Thermal operations and second laws*, in *Thermodynamics in the Quantum Regime*, pp. 625–650. Springer, 2018.

[93] C. Jarzynski, *Nonequilibrium equality for free energy differences*, *Physical Review Letters* **78** no. 14, (1997) 2690.

[94] C. Jarzynski, *Equilibrium free-energy differences from nonequilibrium measurements: A master-equation approach*, *Physical Review E* **56** no. 5, (1997) 5018.

[95] G. E. Crooks, *Entropy production fluctuation theorem and the nonequilibrium work relation for free energy differences*, *Physical Review E* **60** no. 3, (1999) 2721.

[96] G. E. Crooks, *Path-ensemble averages in systems driven far from equilibrium*, *Physical review E* **61** no. 3, (2000) 2361.

[97] S. Mukamel, *Quantum extension of the jarzynski relation: Analogy with stochastic dephasing*, *Physical review letters* **90** no. 17, (2003) 170604.

[98] P. Talkner, E. Lutz, and P. Hänggi, *Fluctuation theorems: Work is not an observable*, *Physical Review E* **75** no. 5, (2007) 050102.

[99] G. E. Crooks, *On the jarzynski relation for dissipative quantum dynamics*, *Journal of Statistical Mechanics: Theory and Experiment* **2008** no. 10, (2008) P10023.

[100] P. Talkner, M. Campisi, and P. Hänggi, *Fluctuation theorems in driven open quantum systems*, *Journal of Statistical Mechanics: Theory and Experiment* **2009** no. 02, (2009) P02025.

[101] G. Huber, F. Schmidt-Kaler, S. Deffner, and E. Lutz, *Employing trapped cold ions to verify the quantum jarzynski equality*, *Physical review letters* **101** no. 7, (2008) 070403.

[102] S. An, J.-N. Zhang, M. Um, D. Lv, Y. Lu, J. Zhang, Z.-Q. Yin, H. Quan, and K. Kim, *Experimental test of the quantum jarzynski equality with a trapped-ion system*, *Nature Physics* **11** no. 2, (2015) 193–199.

[103] T. Xiong, L. Yan, F. Zhou, K. Rehan, D. Liang, L. Chen, W. Yang, Z. Ma, M. Feng, and V. Vedral, *Experimental verification of a jarzynski-related information-theoretic equality by a single trapped ion*, *Physical review letters* **120** no. 1, (2018) 010601.

[104] L. Mazzola, G. De Chiara, and M. Paternostro, *Measuring the characteristic function of the work distribution*, *Physical review letters* **110** no. 23, (2013) 230602.

[105] T. B. Batalhão, A. M. Souza, L. Mazzola, R. Auccaise, R. S. Sarthour, I. S. Oliveira, J. Goold, G. De Chiara, M. Paternostro, and R. M. Serra, *Experimental reconstruction of work distribution and study of fluctuation relations in a closed quantum system*, *Physical review letters* **113** no. 14, (2014) 140601.

[106] G. De Chiara, A. J. Roncaglia, and J. P. Paz, *Measuring work and heat in ultracold quantum gases*, *New Journal of Physics* **17** no. 3, (2015) 035004.

[107] J. Gemmer and J. Anders, *From single-shot towards general work extraction in a quantum thermodynamic framework*, *New Journal of Physics* **17** no. 8, (2015) 085006.

[108] S.-Y. Wang, *Single-shot work extraction in quantum thermodynamics revisited*, *Journal of Physics A: Mathematical and Theoretical* **51** no. 3, (2017) 035305.

[109] M. N. Bera, A. Riera, M. Lewenstein, and A. Winter, *Generalized laws of thermodynamics in the presence of correlations*, *Nature communications* **8** no. 1, (2017) 1–6.

[110] H.-T. Quan, Y.-x. Liu, C.-P. Sun, and F. Nori, *Quantum thermodynamic cycles and quantum heat engines*, *Physical Review E* **76** no. 3, (2007) 031105.

[111] M. A. Nielsen and I. Chuang, *Quantum computation and quantum information*, 2002.

[112] A. Peres, *Quantum theory: concepts and methods*, vol. 57. Springer Science & Business Media, 2006.

[113] E. Bento, G. Viswanathan, M. da Luz, and R. Silva, *Third law of thermodynamics as a key test of generalized entropies*, *Physical Review E* **91** no. 2, (2015) 022105.

[114] L. Pauling and E. Eastman, *Quantum mechanics and the third law of thermodynamics*, *The Journal of Chemical Physics* **4** no. 6, (1936) 393–394.

[115] M. G. Raizen, *Demons entropy and the quest for absolute zero*, *Scientific American* **304** no. 3, (2011) 54–59.

[116] M. Kolář, D. Gelbwaser-Klimovsky, R. Alicki, and G. Kurizki, *Quantum bath refrigeration towards absolute zero: Challenging the unattainability principle*, *Physical review letters* **109** no. 9, (2012) 090601.

[117] E. Torrontegui and R. Kosloff, *Quest for absolute zero in the presence of external noise*, *Physical Review E* **88** no. 3, (2013) 032103.

[118] A. Levy, R. Alicki, and R. Kosloff, *Quantum refrigerators and the third law of thermodynamics*, *Physical Review E* **85** no. 6, (2012) 061126.

[119] M. Born and V. Fock, *Beweis des adiabatensatzes*, *Zeitschrift für Physik* **51** no. 3-4, (1928) 165–180.

[120] J. E. Avron and A. Elgart, *Adiabatic theorem without a gap condition*, *Communications in mathematical physics* **203** no. 2, (1999) 445–463.

[121] H. T. Quan, *Quantum thermodynamic cycles and quantum heat engines. ii.*, *Physical Review E* **79** no. 4, (2009) 041129.

[122] H. Wang, *Quantum-mechanical brayton engine working with a particle in a one-dimensional harmonic trap*, *Physica Scripta* **87** no. 5, (2013) 055009.

[123] X.-L. Huang, X.-Y. Niu, X.-M. Xiu, and X.-X. Yi, *Quantum stirling heat engine and refrigerator with single and coupled spin systems*, *The European Physical Journal D* **68** no. 2, (2014) 1–8.

[124] R. Uzdin and R. Kosloff, *The multilevel four-stroke swap engine and its environment*, *New Journal of Physics* **16** no. 9, (2014) 095003.

[125] R. Kosloff and Y. Rezek, *The quantum harmonic otto cycle*, *Entropy* **19** no. 4, (2017) 136.

[126] C. M. Bender, D. C. Brody, and B. K. Meister, *Quantum mechanical carnot engine*, *Journal of Physics A: Mathematical and General* **33** no. 24, (2000) 4427.

[127] J. Arnaud, L. Chusseau, and F. Philippe, *Carnot cycle for an oscillator*, *European journal of physics* **23** no. 5, (2002) 489.

[128] R. Dillenschneider and E. Lutz, *Energetics of quantum correlations*, *EPL (Europhysics Letters)* **88** no. 5, (2009) 50003.

[129] N. Brunner, M. Huber, N. Linden, S. Popescu, R. Silva, and P. Skrzypczyk, *Entanglement enhances cooling in microscopic quantum refrigerators*, *Physical Review E* **89** no. 3, (2014) 032115.

[130] G. Xiao and J. Gong, *Construction and optimization of a quantum analog of the carnot cycle*, *Physical Review E* **92** no. 1, (2015) 012118.

[131] B. Gardas and S. Deffner, *Thermodynamic universality of quantum carnot engines*, *Physical Review E* **92** no. 4, (2015) 042126.

[132] I. A. Martínez, É. Roldán, L. Dinis, D. Petrov, J. M. Parrondo, and R. A. Rica, *Brownian carnot engine*, *Nature physics* **12** no. 1, (2016) 67–70.

[133] D. Türkpençe, F. Altintas, M. Paternostro, and Ö. E. Müstecaplioğlu, *A photonic carnot engine powered by a spin-star network*, *EPL (Europhysics Letters)* **117** no. 5, (2017) 50002.

[134] J. Roßnagel, O. Abah, F. Schmidt-Kaler, K. Singer, and E. Lutz, *Nanoscale heat engine beyond the carnot limit*, *Physical review letters* **112** no. 3, (2014) 030602.

[135] H. Wang, S. Liu, and J. He, *Thermal entanglement in two-atom cavity qed and the entangled quantum otto engine*, *Physical Review E* **79** no. 4, (2009) 041113.

[136] G. Thomas and R. S. Johal, *Coupled quantum otto cycle*, *Physical Review E* **83** no. 3, (2011) 031135.

[137] X. Huang, T. Wang, X. Yi, *et al.*, *Effects of reservoir squeezing on quantum systems and work extraction*, *Physical Review E* **86** no. 5, (2012) 051105.

[138] X. Huang, H. Xu, X. Niu, and Y. Fu, *A special entangled quantum heat engine based on the two-qubit heisenberg xx model*, *Physica Scripta* **88** no. 6, (2013) 065008.

[139] F. Altintas, A. Ü. Hardal, and Ö. E. Müstecaplıoglu, *Quantum correlated heat engine with spin squeezing*, *Physical Review E* **90** no. 3, (2014) 032102.

[140] F. Altintas and Ö. E. Müstecaplıoğlu, *General formalism of local thermodynamics with an example: Quantum otto engine with a spin-1/2 coupled to an arbitrary spin*, *Physical Review E* **92** no. 2, (2015) 022142.

[141] B. Karimi and J. Pekola, *Otto refrigerator based on a superconducting qubit: Classical and quantum performance*, *Physical Review B* **94** no. 18, (2016) 184503.

[142] G. A. Barrios, F. Albarrán-Arriagada, F. Cárdenas-López, G. Romero, and J. Retamal, *Role of quantum correlations in light-matter quantum heat engines*, *Physical Review A* **96** no. 5, (2017) 052119.

[143] B. Reid, S. Pigeon, M. Antezza, and G. De Chiara, *A self-contained quantum harmonic engine*, *EPL (Europhysics Letters)* **120** no. 6, (2018) 60006.

[144] E. Munoz and F. J. Pena, *Magnetically driven quantum heat engine*, *Physical Review E* **89** no. 5, (2014) 052107.

[145] F. J. Pena and E. Munoz, *Magnetostrain-driven quantum engine on a graphene flake*, *Physical Review E* **91** no. 5, (2015) 052152.

[146] G. Agarwal and S. Chaturvedi, *Quantum dynamical framework for brownian heat engines*, *Physical Review E* **88** no. 1, (2013) 012130.

[147] V. Blickle and C. Bechinger, *Realization of a micrometre-sized stochastic heat engine*, *Nature Physics* **8** no. 2, (2012) 143–146.

[148] R. Kosloff, *Quantum thermodynamics: A dynamical viewpoint*, *Entropy* **15** no. 6, (2013) 2100–2128.

[149] D. J. Griffiths and D. F. Schroeter, *Introduction to quantum mechanics*. Cambridge University Press, 2018.

[150] *über den anschaulichen inhalt der quantentheoretischen kinematik und mechanik*, .

[151] E. H. Kennard, *Zur quantenmechanik einfacher bewegungstypen*, *Zeitschrift für Physik* **44** no. 4, (1927) 326–352.

[152] H. Weyl, *Group theory and quantum mechanics*, 1931.

[153] E. Schr ö things, *"U about force-free movement in relativistic quantum mechanics*. Academy of Sciences in commission at W. de Gruyter and Company, 1930.

[154] H. P. Robertson, *The uncertainty principle*, *Physical Review* **34** no. 1, (1929) 163.

[155] H. Robertson, *An indeterminacy relation for several observables and its classical interpretation*, *Physical Review* **46** no. 9, (1934) 794.

[156] J. Hilgevoord, *The uncertainty principle for energy and time*, *American Journal of Physics* **64** no. 12, (1996) 1451–1456.

[157] L. Rosenfeld, *in Ergodic Theories*. P. Caldirola, ed. (Academic Press, New York), 1961.

[158] A. Einstein, B. Podolsky, and N. Rosen, *Can quantum-mechanical description of physical reality be considered complete?*, *Phys. Rev.* **47** (May, 1935) 777–780.

[159] M. Reid, P. Drummond, W. Bowen, E. G. Cavalcanti, P. K. Lam, H. Bachor, U. L. Andersen, and G. Leuchs, *Colloquium: the einstein-podolsky-rosen paradox: from concepts to applications*, *Reviews of Modern Physics* **81** no. 4, (2009) 1727.

[160] H. M. Wiseman, S. J. Jones, and A. C. Doherty, *Steering, entanglement, nonlocality, and the einstein-podolsky-rosen paradox*, *Physical review letters* **98** no. 14, (2007) 140402.

[161] J. S. Bell, *On the einstein podolsky rosen paradox*, *Physics Physique Fizika* **1** no. 3, (1964) 195.

[162] J. F. Clauser, M. A. Horne, A. Shimony, and R. A. Holt, *Proposed experiment to test local hidden-variable theories*, *Phys. Rev. Lett.* **23** (Oct, 1969) 880–884.

[163] R. Simon, *Peres-horodecki separability criterion for continuous variable systems*, *Physical Review Letters* **84** no. 12, (2000) 2726.

[164] J. S. Ivan, S. Chaturvedi, E. Ercolessi, G. Marmo, G. Morandi, N. Mukunda, and R. Simon, *Entanglement and nonclassicality for multimode radiation-field states*, *Physical Review A* **83** no. 3, (2011) 032118.

[165] H. Nha, *Entanglement condition via su (2) and su (1, 1) algebra using schrödinger-robertson uncertainty relation*, *Physical Review A* **76** no. 1, (2007) 014305.

[166] J. Gillet, T. Bastin, and G. Agarwal, *Multipartite entanglement criterion from uncertainty relations*, *Physical Review A* **78** no. 5, (2008) 052317.

[167] L. Song, X. Wang, D. Yan, and Z.-S. Pu, *Entanglement conditions for tripartite systems via indeterminacy relations*, *Journal of Physics B: Atomic, Molecular and Optical Physics* **41** no. 1, (2007) 015505.

[168] J. S. Ivan, K. K. Sabapathy, N. Mukunda, and R. Simon, *Invariant theoretic approach to uncertainty relations for quantum systems*, *arXiv preprint arXiv:1205.5132* (2012) .

[169] S. Mal, T. Pramanik, and A. Majumdar, *Detecting mixedness of qutrit systems using the uncertainty relation*, *Physical Review A* **87** no. 1, (2013) 012105.

[170] J. Oppenheim and S. Wehner, *The uncertainty principle determines the nonlocality of quantum mechanics*, *Science* **330** no. 6007, (2010) 1072–1074.

[171] T. Pramanik and A. S. Majumdar, *Fine-grained uncertainty relation and nonlocality of tripartite systems*, *Physical Review A* **85** no. 2, (2012) 024103.

[172] A. Dey, T. Pramanik, and A. Majumdar, *Fine-grained uncertainty relation and biased nonlocal games in bipartite and tripartite systems*, *Physical Review A* **87** no. 1, (2013) 012120.

[173] I. Devetak and A. Winter, *Distillation of secret key and entanglement from quantum states*, *Proceedings of the Royal Society A: Mathematical, Physical and engineering sciences* **461** no. 2053, (2005) 207–235.

[174] J. M. Renes and J.-C. Boileau, *Conjectured strong complementary information tradeoff*, *Physical review letters* **103** no. 2, (2009) 020402.

[175] M. Berta, M. Christandl, R. Colbeck, J. M. Renes, and R. Renner, *The uncertainty principle in the presence of quantum memory*, *Nature Physics* **6** no. 9, (2010) 659–662.

[176] W. Heisenberg, *Über den anschaulichen inhalt der quantentheoretischen kinematik und mechanik*, in *Original Scientific Papers Wissenschaftliche Originalarbeiten*, pp. 478–504. Springer, 1985.

[177] H. Weyl, *The theory of groups and quantum mechanics*. Courier Corporation, 1950.

[178] E. Schrödinger, *Discussion of probability relations between separated systems*, in *Mathematical Proceedings of the Cambridge Philosophical Society*, vol. 31, pp. 555–563, Cambridge University Press. 1935.

[179] E. Schrödinger, *Discussion of probability relations between separated systems*, in *Mathematical Proceedings of the Cambridge Philosophical Society*, vol. 32, pp. 446–450, Cambridge University Press. 1936.

[180] L. Maccone and A. K. Pati, *Stronger uncertainty relations for all incompatible observables*, *Physical review letters* **113** no. 26, (2014) 260401.

[181] M. Koashi, *Unconditional security of quantum key distribution and the uncertainty principle*, in *Journal of Physics: Conference Series*, vol. 36, pp. 98–102. 2006.

[182] M. Koashi, *Simple security proof of quantum key distribution via uncertainty principle*, *arXiv preprint quant-ph/0505108* (2005) .

[183] C. A. Fuchs and A. Peres, *Quantum-state disturbance versus information gain: Uncertainty relations for quantum information*, *Physical Review A* **53** no. 4, (1996) 2038.

[184] H. F. Hofmann and S. Takeuchi, *Violation of local uncertainty relations as a signature of entanglement*, *Physical Review A* **68** no. 3, (2003) 032103.

[185] A. Osterloh, *Entanglement and its facets in condensed matter systems*, *arXiv preprint arXiv:0810.1240* (2008) .

[186] O. Marty, M. Epping, H. Kampermann, D. Bruß, M. B. Plenio, and M. Cramer, *Quantifying entanglement with scattering experiments*, *Physical Review B* **89** no. 12, (2014) 125117.

[187] O. Gühne, *Characterizing entanglement via uncertainty relations*, *Physical review letters* **92** no. 11, (2004) 117903.

[188] V. Giovannetti, S. Lloyd, and L. Maccone, *Advances in quantum metrology*, *Nature photonics* **5** no. 4, (2011) 222.

[189] D. Mondal, C. Datta, and S. Sazim, *Quantum coherence sets the quantum speed limit for mixed states*, *Physics Letters A* **380** no. 5-6, (2016) 689–695.

[190] I. Marvian, R. W. Spekkens, and P. Zanardi, *Quantum speed limits, coherence, and asymmetry*, *Physical Review A* **93** no. 5, (2016) 052331.

[191] S. Deffner and S. Campbell, *Quantum speed limits: from heisenberg's uncertainty principle to optimal quantum control*, *Journal of Physics A: Mathematical and Theoretical* **50** no. 45, (2017) 453001.

[192] D. P. Pires, M. Cianciaruso, L. C. Céleri, G. Adesso, and D. O. Soares-Pinto, *Generalized geometric quantum speed limits*, *Physical Review X* **6** no. 2, (2016) 021031.

[193] L. Xiao, K. Wang, X. Zhan, Z. Bian, J. Li, Y. Zhang, P. Xue, and A. K. Pati, *Experimental test of uncertainty relations for general unitary operators*, *Optics Express* **25** no. 15, (2017) 17904–17910.

[194] W. Ma, Z. Ma, H. Wang, Z. Chen, Y. Liu, F. Kong, Z. Li, X. Peng, M. Shi, F. Shi, *et al.*, *Experimental test of heisenberg's measurement uncertainty relation based on statistical distances*, *Physical review letters* **116** no. 16, (2016) 160405.

[195] S.-Y. Baek, F. Kaneda, M. Ozawa, and K. Edamatsu, *Experimental violation and reformulation of the heisenberg's error-disturbance uncertainty relation*, *Scientific reports* **3** (2013) 2221.

[196] L. Schiff, *Quantum mechanics mcgraw-hill*, *New York* **19752** (1955) 267–280.

[197] D. J. Griffiths, *Introduction to quantum mechanics, 2nd, Pearson, Chapter2. The time-independent schrodinger equation* (2005) 90–91.

[198] M. Peskin, *An introduction to quantum field theory*. CRC press, 2018.

[199] P. Alberto, S. Das, and E. C. Vagenas, *Relativistic particle in a box: Klein–gordon versus dirac equations*, European Journal of Physics **39** no. 2, (2018) 025401.

[200] H. Saygin and A. Şişman, *Quantum degeneracy effect on the work output from a stirling cycle*, Journal of Applied Physics **90** no. 6, (2001) 3086–3089.

[201] T. D. Kieu, *The second law, maxwell's demon, and work derivable from quantum heat engines*, Physical review letters **93** no. 14, (2004) 140403.

[202] G. Thomas, M. Banik, and S. Ghosh, *Implications of coupling in quantum thermodynamic machines*, Entropy **19** no. 9, (2017) 442.

[203] P. Chattopadhyay and G. Paul, *Revisiting thermodynamics in computation and information theory*, arXiv preprint arXiv:2102.09981 (2021) .

[204] C. H. Bennett, *Time/space trade-offs for reversible computation*, SIAM Journal on Computing **18** no. 4, (1989) 766–776.

[205] U. Seifert, *Stochastic thermodynamics, fluctuation theorems and molecular machines*, Reports on progress in physics **75** no. 12, (2012) 126001.

[206] J. M. Parrondo, J. M. Horowitz, and T. Sagawa, *Thermodynamics of information*, Nature physics **11** no. 2, (2015) 131–139.

[207] G. Diana, G. B. Bagci, and M. Esposito, *Finite-time erasing of information stored in fermionic bits*, Physical Review E **87** no. 1, (2013) 012111.

[208] G. Lan, P. Sartori, S. Neumann, V. Sourjik, and Y. Tu, *The energy–speed–accuracy trade-off in sensory adaptation*, Nature physics **8** no. 5, (2012) 422–428.

[209] T. E. Ouldridge, C. C. Govern, and P. R. ten Wolde, *Thermodynamics of computational copying in biochemical systems*, Physical Review X **7** no. 2, (2017) 021004.

[210] A. C. Barato and U. Seifert, *Thermodynamic uncertainty relation for biomolecular processes*, Physical review letters **114** no. 15, (2015) 158101.

[211] D. H. Wolpert, *Extending landauer's bound from bit erasure to arbitrary computation*, arXiv preprint arXiv:1508.05319 (2015) .

[212] P. Strasberg, J. Cerrillo, G. Schaller, and T. Brandes, *Thermodynamics of stochastic turing machines*, *Physical Review E* **92** no. 4, (2015) 042104.

[213] O. J. Maroney, *Does a computer have an arrow of time?*, *Foundations of Physics* **40** no. 2, (2010) 205–238.

[214] M. Li and P. M. Vitányi, *Mathematical theory of thermodynamics of computation*. Citeseer, 1992.

[215] J. E. Hopcroft and R. Motwani, *Rotwani, and jd ullman. introduction to automata theory, languages and computability*, 2000.

[216] A. Church, *Am turing. on computable numbers, with an application to the entscheidungs problcm. proceedings of the london mathematical society, 2 s. vol. 42 (1936–1937), pp. 230–265.*, *The Journal of Symbolic Logic* **2** no. 1, (1937) 42–43.

[217] J. E. Savage, *Models of computation. vol. 136*, 1998.

[218] S. Arora and B. Barak, *Computational complexity: a modern approach*. Cambridge University Press, 2009.

[219] B. J. Copeland, *The church-turing thesis*, .

[220] M. B. Pour-El and I. Richards, *Noncomputability in models of physical phenomena*, *International Journal of Theoretical Physics* **21** no. 6-7, (1982) 553–555.

[221] C. Moore, *Unpredictability and undecidability in dynamical systems*, *Physical Review Letters* **64** no. 20, (1990) 2354.

[222] D. H. Wolpert, *The stochastic thermodynamics of computation*, *Journal of Physics A: Mathematical and Theoretical* **52** no. 19, (2019) 193001.

[223] P. Arrighi, *An overview of quantum cellular automata*, *Natural Computing* **18** no. 4, (2019) 885–899.

[224] C. Wüthrich, *A quantum-information-theoretic complement to a general-relativistic implementation of a beyond-turing computer*, *Synthese* **192** no. 7, (2015) 1989–2008.

[225] C. Moore and S. Mertens, *The nature of computation*. OUP Oxford, 2011.

[226] O. Goldreich, *P, NP, and NP-Completeness: The basics of computational complexity*. Cambridge University Press, 2010.

[227] K. Gödel, *On formally undecidable propositions of Principia Mathematica and related systems*. Courier Corporation, 1992.

[228] B. J. Copeland, C. J. Posy, and O. Shagrir, *Computability: Turing, gödel, church, and beyond*. MIT Press, 2013.

[229] M. Baaz, C. H. Papadimitriou, H. W. Putnam, D. S. Scott, and C. L. Harper Jr, *Kurt Gödel and the foundations of mathematics: Horizons of truth*. Cambridge University Press, 2011.

[230] S. Aaronson, *Guest column: Np-complete problems and physical reality*, *ACM Sigact News* **36** no. 1, (2005) 30–52.

[231] M. Sipser, *Introduction to the theory of computation*, *ACM Sigact News* **27** no. 1, (1996) 27–29.

[232] M. Li, P. Vitányi, *et al.*, *An introduction to Kolmogorov complexity and its applications*, vol. 3. Springer, 2008.

[233] T. M. Cover and J. A. Thomas, *Elements of information theory*, 2012.

[234] R. M. Gray, *Entropy and information theory*. Springer Science & Business Media, 2011.

[235] D. J. MacKay and D. J. Mac Kay, *Information theory, inference and learning algorithms*. Cambridge university press, 2003.

[236] M. M. Wilde, *Quantum information theory*. Cambridge University Press, 2013.

[237] M. Hayashi, *Quantum information theory*, *Graduate Texts in Physics, Springer* (2017) .

[238] C. E. Shannon, *A mathematical theory of communication*, *The Bell system technical journal* **27** no. 3, (1948) 379–423.

[239] R. W. Hamming, *Error detecting and error correcting codes*, *The Bell system technical journal* **29** no. 2, (1950) 147–160.

[240] M. WILLIAMS and S. FJ, *Nja the theory of error correcting codes*, 1978.

[241] D. R. Hankerson, D. Hoffman, D. Leonard, C. Lindner, K. Phelps, C. Rodger, and J. Wall, *Coding theory and cryptography: The essentials. new york: M*, 2000.

[242] V. Pless, *Introduction to the theory of error-correcting codes*, vol. 48. John Wiley & Sons, 1998.

[243] P. W. Shor, *Scheme for reducing decoherence in quantum computer memory*, *Physical review A* **52** no. 4, (1995) R2493.

[244] J. Preskill, *Reliable quantum computers*, *Proceedings of the Royal Society of London. Series A: Mathematical, Physical and Engineering Sciences* **454** no. 1969, (1998) 385–410.

[245] A. Y. Kitaev, *Quantum computations: algorithms and error correction*, *Russian Mathematical Surveys* **52** no. 6, (1997) 1191.

[246] E. Knill, R. Laflamme, and W. H. Zurek, *Resilient quantum computation*, *Science* **279** no. 5349, (1998) 342–345.

[247] D. Gottesman, *Theory of fault-tolerant quantum computation*, *Physical Review A* **57** no. 1, (1998) 127.

[248] D. Gottesman, *An introduction to quantum error correction and fault-tolerant quantum computation*, in *Quantum information science and its contributions to mathematics, Proceedings of Symposia in Applied Mathematics*, vol. 68, pp. 13–58. 2010.

[249] S. J. Devitt, W. J. Munro, and K. Nemoto, *Quantum error correction for beginners*, *Reports on Progress in Physics* **76** no. 7, (2013) 076001.

[250] D. A. Lidar and T. A. Brun, *Quantum error correction*. Cambridge university press, 2013.

[251] B. M. Terhal, *Quantum error correction for quantum memories*, *Reviews of Modern Physics* **87** no. 2, (2015) 307.

[252] P. Benioff, *Quantum mechanical hamiltonian models of turing machines*, *Journal of Statistical Physics* **29** no. 3, (1982) 515–546.

[253] J. H. Reif, *Complexity of the mover's problem and generalizations*, in *20th Annual Symposium on Foundations of Computer Science (sfcs 1979)*, pp. 421–427, IEEE. 1979.

[254] J. D. Norton, *Brownian computation is thermodynamically irreversible*, *Foundations of Physics* **43** no. 11, (2013) 1384–1410.

[255] D. Chu and R. E. Spinney, *A thermodynamically consistent model of finite-state machines*, *Interface focus* **8** no. 6, (2018) 20180037.

[256] G. E. Crooks, *Nonequilibrium measurements of free energy differences for microscopically reversible markovian systems*, *Journal of Statistical Physics* **90** no. 5-6, (1998) 1481–1487.

[257] D. H. Wolpert, A. Kolchinsky, and J. A. Owen, *A space–time tradeoff for implementing a function with master equation dynamics*, *Nature communications* **10** no. 1, (2019) 1–9.

[258] C. H. Bennett and R. Landauer, *The fundamental physical limits of computation*, *Scientific American* **253** no. 1, (1985) 48–57.

[259] A. de Castro, *One-way-ness in the input-saving (turing) machine*, *Physica A: Statistical Mechanics and its Applications* **415** (2014) 473–478.

[260] A. C. Barato and U. Seifert, *An autonomous and reversible maxwell's demon*, *EPL (Europhysics Letters)* **101** no. 6, (2013) 60001.

[261] D. Mandal, H. Quan, and C. Jarzynski, *Maxwell's refrigerator: an exactly solvable model*, *Physical review letters* **111** no. 3, (2013) 030602.

[262] S. Deffner and C. Jarzynski, *Information processing and the second law of thermodynamics: An inclusive, hamiltonian approach*, *Physical Review X* **3** no. 4, (2013) 041003.

[263] A. C. Barato and U. Seifert, *Stochastic thermodynamics with information reservoirs*, *Physical Review E* **90** no. 4, (2014) 042150.

[264] P. Strasberg, G. Schaller, T. Brandes, and C. Jarzynski, *Second laws for an information driven current through a spin valve*, *Physical Review E* **90** no. 6, (2014) 062107.

[265] E. B. Davies, *Markovian master equations*, *Communications in mathematical Physics* **39** no. 2, (1974) 91–110.

[266] J. D. Norton, *On brownian computation*, in *International Journal of Modern Physics: Conference Series*, vol. 33, p. 1460366, World Scientific. 2014.

[267] A. Kolchinsky and D. H. Wolpert, *Thermodynamic costs of turing machines*, *Physical Review Research* **2** no. 3, (2020) 033312.

[268] C. Van den Broeck *et al.*, *Stochastic thermodynamics: A brief introduction*, *Physics of Complex Colloids* **184** (2013) 155–193.

[269] M. Esposito and C. Van den Broeck, *Three faces of the second law. i. master equation formulation*, *Physical Review E* **82** no. 1, (2010) 011143.

[270] P. Cotogno, *Hypercomputation and the physical church-turing thesis.*, *British Journal for the Philosophy of Science* **54** no. 2, (2003) .

[271] A. R. Calderbank and P. W. Shor, *Good quantum error-correcting codes exist*, *Physical Review A* **54** no. 2, (1996) 1098.

[272] A. M. Steane, *Error correcting codes in quantum theory*, *Physical Review Letters* **77** no. 5, (1996) 793.

[273] A. R. Calderbank, E. M. Rains, P. W. Shor, and N. J. Sloane, *Quantum error correction and orthogonal geometry*, *Physical Review Letters* **78** no. 3, (1997) 405.

[274] A. R. Calderbank, E. M. Rains, P. Shor, and N. J. Sloane, *Quantum error correction via codes over gf (4)*, *IEEE Transactions on Information Theory* **44** no. 4, (1998) 1369–1387.

[275] D. Gottesman, *Class of quantum error-correcting codes saturating the quantum hamming bound*, *Physical Review A* **54** no. 3, (1996) 1862.

[276] D. Gottesman, *Stabilizer codes and quantum error correction*, *arXiv preprint quant-ph / 9705052* (1997) .

[277] V. Vedral, *Landauer's erasure, error correction and entanglement*, *Proceedings of the Royal Society of London. Series A: Mathematical, Physical and Engineering Sciences* **456** no. 1996, (2000) 969–984.

[278] C. Cafaro and P. van Loock, *An entropic analysis of approximate quantum error correction*, *Physica A: Statistical Mechanics and its Applications* **404** (2014) 34–46.

[279] V. Korepin and J. Terilla, *Thermodynamic interpretation of the quantum error correcting criterion*, *Quantum Information Processing* **1** no. 4, (2002) 225–242.

[280] J. Kempe, D. Bacon, D. A. Lidar, and K. B. Whaley, *Theory of decoherence-free fault-tolerant universal quantum computation*, *Physical Review A* **63** no. 4, (2001) 042307.

[281] A. Osterloh, L. Amico, G. Falci, and R. Fazio, *Scaling of entanglement close to a quantum phase transition*, *Nature* **416** no. 6881, (2002) 608–610.

[282] D. P. DiVincenzo, D. Bacon, J. Kempe, G. Burkard, and K. B. Whaley, *Universal quantum computation with the exchange interaction*, *nature* **408** no. 6810, (2000) 339–342.

[283] A. Y. Kitaev, *Fault-tolerant quantum computation by anyons*, *Annals of Physics* **303** no. 1, (2003) 2–30.

[284] M. Freedman, A. Kitaev, M. Larsen, and Z. Wang, *Topological quantum computation*, *Bulletin of the American Mathematical Society* **40** no. 1, (2003) 31–38.

[285] C. H. Bennett, D. P. DiVincenzo, J. A. Smolin, and W. K. Wootters, *Mixed-state entanglement and quantum error correction*, *Physical Review A* **54** no. 5, (1996) 3824.

[286] E. Knill and R. Laflamme, *Theory of quantum error-correcting codes*, *Physical Review A* **55** no. 2, (1997) 900.

[287] E. Lieb, T. Schultz, and D. Mattis, *Two soluble models of an antiferromagnetic chain*, *Annals of Physics* **16** no. 3, (1961) 407–466.

[288] O. C. de Beauregard, *The computer and the heat engine*, *Foundations of physics* **19** no. 6, (1989) 725–727.

[289] I. Prigogine and G. Nicolis, *Self-organisation in nonequilibrium systems: towards a dynamics of complexity*, in *Bifurcation analysis*, pp. 3–12. Springer, 1985.

[290] S. Ishioka and N. Fuchikami, *Thermodynamics of computing: Entropy of nonergodic systems*, *Chaos: An Interdisciplinary Journal of Nonlinear Science* **11** no. 3, (2001) 734–746.

[291] N. Shimizu, Y. Harada, N. Miyamoto, and E. Goto, *A new a/d converter with quantum flux parametron*, *IEEE Transactions on Magnetics* **25** no. 2, (1989) 865–868.

[292] E. GOTO, N. Yoshida, K. Loe, and W. Hioe, *A study on irreversible loss of information without heat generation*, in *Foundations Of Quantum Mechanics In The Light Of New Technology: Selected Papers from the Proceedings of the First through Fourth International Symposia on Foundations of Quantum Mechanics*, pp. 389–395, World Scientific. 1996.

[293] G. Banegas and D. J. Bernstein, *Low-communication parallel quantum multi-target preimage search*, in *International Conference on Selected Areas in Cryptography*, pp. 325–335, Springer. 2017.

[294] R. Beals, S. Brierley, O. Gray, A. W. Harrow, S. Kutin, N. Linden, D. Shepherd, and M. Stather, *Efficient distributed quantum computing*, *Proceedings of the Royal Society A: Mathematical, Physical and Engineering Sciences* **469** no. 2153, (2013) 20120686.

[295] D. J. Bernstein, *Cost analysis of hash collisions: Will quantum computers make sharcs obsolete*, *SHARCS* **9** (2009) 105.

[296] S. R. Fluhrer, *Reassessing grover's algorithm.*, *IACR Cryptol. ePrint Arch.* **2017** (2017) 811.

[297] R. Perlner and Y.-K. Liu, *Thermodynamic analysis of classical and quantum search algorithms*, *arXiv preprint arXiv:1709.10510* (2017) .

[298] P. C. Van Oorschot and M. J. Wiener, *Parallel collision search with cryptanalytic applications*, *Journal of cryptology* **12** no. 1, (1999) 1–28.

[299] G. Brassard, P. Høyer, and A. Tapp, *Quantum cryptanalysis of hash and claw-free functions*, in *Latin American Symposium on Theoretical Informatics*, pp. 163–169, Springer. 1998.

[300] V. Giovannetti, S. Lloyd, and L. Maccone, *Quantum random access memory*, *Physical review letters* **100** no. 16, (2008) 160501.

[301] S. Tani, *An improved claw finding algorithm using quantum walk*, in *International Symposium on Mathematical Foundations of Computer Science*, pp. 536–547, Springer. 2007.

[302] C. Zalka, *Grover's quantum searching algorithm is optimal*, *Physical Review A* **60** no. 4, (1999) 2746.

[303] W. Pauli, C. P. Enz, and K. von Meyenn, *Writings on physics and philosophy*. Springer, 1994.

[304] W. Pauli, *Letter to rj oppenheimer (1946), in 'wolfgang pauli, scientific correspondence', vol. iii, p. 380, ed. k. von meyenn*, 1993.

[305] H. S. Snyder, *Quantized space-time*, *Physical Review* **71** no. 1, (1947) 38.

[306] A. Connes, *Introduction to noncommutative differential geometry*, *Lectures Notes in Physics; Springer: Berlin/Heidelberg, Germany* **1111** (1984) 3–16.

[307] A. Connes, J. Cuntz, M. A. Rieffel, and G. Yu, *Noncommutative geometry*, *Oberwolfach Reports* **10** no. 3, (2014) 2553–2629.

[308] E. Witten, *Non-commutative geometry and string field theory*, *Nuclear Physics B* **268** no. 2, (1986) 253–294.

[309] S. Doplicher, K. Fredenhagen, and J. E. Roberts, *The quantum structure of spacetime at the planck scale and quantum fields*, *Communications in Mathematical Physics* **172** no. 1, (1995) 187–220.

[310] A. Connes, M. R. Douglas, and A. Schwarz, *Noncommutative geometry and matrix theory*, *Journal of High Energy Physics* **1998** no. 02, (1998) 003.

[311] M. Sheikh-Jabbari, *More on mixed boundary conditions and d-branes bound states*, *Physics Letters B* **425** no. 1-2, (1998) 48–54.

[312] N. Seiberg and E. Witten, *String theory and noncommutative geometry*, *Journal of High Energy Physics* **1999** no. 09, (1999) 032.

[313] F. Ardalan, H. Arfaei, and M. M. Sheikh-Jabbari, *Noncommutative geometry from strings and branes*, *Journal of High Energy Physics* **1999** no. 02, (1999) 016.

[314] M. R. Douglas and N. A. Nekrasov, *Noncommutative field theory*, *Reviews of Modern Physics* **73** no. 4, (2001) 977.

[315] A. A. Bichl, J. M. Grimstrup, L. Popp, M. Schweda, and R. Wulkenhaar, *Perturbative analysis of the seiberg–witten map*, *International Journal of Modern Physics A* **17** no. 16, (2002) 2219–2231.

[316] R. J. Szabo, *Quantum field theory on noncommutative spaces*, *Physics Reports* **378** no. 4, (2003) 207–299.

[317] E. Akofor, A. Balachandran, and A. Joseph, *Quantum fields on the groenewold–moyal plane*, *International Journal of Modern Physics A* **23** no. 11, (2008) 1637–1677.

[318] R.-G. Cai and N. Ohta, *Lorentz transformation and light-like noncommutative sym*, *Journal of High Energy Physics* **2000** no. 10, (2000) 036.

[319] T. Filk, *Divergencies in a field theory on quantum space*, *Physics Letters B* **376** no. 1-3, (1996) 53–58.

[320] N. Seiberg, L. Susskind, and N. Toumbas, *Space/time non-commutativity and causality*, *Journal of High Energy Physics* **2000** no. 06, (2000) 044.

[321] L. Susskind, *The quantum hall fluid and non-commutative chern simons theory*, *arXiv preprint hep-th/0101029* (2001) .

[322] R. Jackiw, *Physical instances of noncommuting coordinates*, in *Proceedings of the Second Meeting on CPT and Lorentz Symmetry, Bloomington, USA, 15-18 August, 2001*, p. 142, World Scientific. 2002.

[323] V. V. Dvoeglazov, *A note on noncommutativity*, *Physics Essays* **31** no. 3, (2018) 340–341.

[324] G. Magro, *Noncommuting coordinates in the landau problem*, *arXiv preprint quant-ph/0302001* (2003) .

[325] C. Duval and P. Horvathy, *The exotic galilei group and the "peierls substitution"*, *Physics Letters B* **479** no. 1-3, (2000) 284–290.

[326] C. Duval and P. Horvathy, *Exotic galilean symmetry in the non-commutative plane and the hall effect*, *Journal of Physics A: Mathematical and General* **34** no. 47, (2001) 10097.

[327] P. Horváthy, *The non-commutative landau problem*, *Annals of Physics* **299** no. 1, (2002) 128–140.

[328] P. Horváthy, *Anomalous hall effect in noncommutative mechanics*, *Physics Letters A* **359** no. 6, (2006) 705–706.

[329] J. Gamboa, M. Loewe, and J. Rojas, *Noncommutative quantum mechanics*, *Physical Review D* **64** no. 6, (2001) 067901.

[330] J. Gamboa, F. Mendez, M. Loewe, and J. Rojas, *The landau problem and noncommutative quantum mechanics*, *Modern Physics Letters A* **16** no. 32, (2001) 2075–2078.

[331] J. Gamboa, F. Mendez, M. Loewe, and J. Rojas, *Noncommutative quantum mechanics: The two-dimensional central field*, *International Journal of Modern Physics A* **17** no. 19, (2002) 2555–2565.

[332] H. Falomir, J. Gamboa, J. Lopez-Sarrion, F. Mendez, and P. Pisani, *Magnetic-dipole spin effects in noncommutative quantum mechanics*, *Physics Letters B* **680** no. 4, (2009) 384–386.

[333] V. Nair and A. Polychronakos, *Quantum mechanics on the noncommutative plane and sphere*, *Physics Letters B* **505** no. 1-4, (2001) 267–274.

[334] B. Morariu and A. P. Polychronakos, *Quantum mechanics on the noncommutative torus*, *Nuclear Physics B* **610** no. 3, (2001) 531–544.

[335] S. Bellucci, A. Nersessian, and C. Sochichiu, *Two phases of the noncommutative quantum mechanics*, *Physics Letters B* **522** no. 3-4, (2001) 345–349.

[336] S. Bellucci and A. Nersessian, *Phases in noncommutative quantum mechanics on (pseudo) sphere*, *Physics Letters B* **542** no. 3-4, (2002) 295–300.

[337] S. Bellucci and A. Yeranyan, *Noncommutative quantum scattering in a central field*, *Physics Letters B* **609** no. 3-4, (2005) 418–423.

[338] A. Smailagic and E. Spallucci, *Isotropic representation of the noncommutative 2d harmonic oscillator*, *Physical Review D* **65** no. 10, (2002) 107701.

[339] A. Smailagic and E. Spallucci, *Noncommutative 3d harmonic oscillator*, *Journal of Physics A: Mathematical and General* **35** no. 26, (2002) L363.

[340] A. Smailagic and E. Spallucci, *Feynman path integral on the non-commutative plane*, *Journal of Physics A: Mathematical and General* **36** no. 33, (2003) L467.

[341] M. Chaichian, P. Prešnajder, M. Sheikh-Jabbari, and A. Tureanu, *Aharonov–bohm effect in noncommutative spaces*, *Physics Letters B* **527** no. 1-2, (2002) 149–154.

[342] M. Chaichian, M. Långvik, S. Sasaki, and A. Tureanu, *Gauge covariance of the aharonov–bohm phase in noncommutative quantum mechanics*, *Physics Letters B* **666** no. 2, (2008) 199–204.

[343] A. A. Deriglazov, *Quantum mechanics on noncommutative plane and sphere from constrained systems*, *Physics Letters B* **530** no. 1-4, (2002) 235–243.

[344] L. Jonke and S. Meljanac, *Representations of non-commutative quantum mechanics and symmetries*, *The European Physical Journal C-Particles and Fields* **29** no. 3, (2003) 433–439.

[345] I. Dadic, L. Jonke, and S. Meljanac, *Harmonic oscillator on noncommutative spaces*, *arXiv preprint hep-th/0301066* (2003) .

[346] F. G. Scholtz, B. Chakraborty, S. Gangopadhyay, and A. G. Hazra, *Dual families of noncommutative quantum systems*, *Physical Review D* **71** no. 8, (2005) 085005.

[347] F. G. Scholtz, B. Chakraborty, S. Gangopadhyay, and J. Govaerts, *Interactions and non-commutativity in quantum hall systems*, *Journal of Physics A: Mathematical and General* **38** no. 45, (2005) 9849.

[348] F. Scholtz, B. Chakraborty, J. Govaerts, and S. Vaidya, *Spectrum of the non-commutative spherical well*, *Journal of Physics A: Mathematical and Theoretical* **40** no. 48, (2007) 14581.

[349] S. Gangopadhyay and F. G. Scholtz, *Path-integral action of a particle in the noncommutative plane*, *Physical review letters* **102** no. 24, (2009) 241602.

[350] S. Alavi and S. Abbaspour, *Dynamical noncommutative quantum mechanics*, *Journal of Physics A: Mathematical and Theoretical* **47** no. 4, (2014) 045303.

[351] C. Bastos, O. Bertolami, N. C. Dias, and J. N. Prata, *Violation of the robertson-schrödinger uncertainty principle and noncommutative quantum mechanics*, *Physical Review D* **86** no. 10, (2012) 105030.

[352] S. Dulat and K. Li, *Quantum hall effect in noncommutative quantum mechanics*, *The European Physical Journal C* **60** no. 1, (2009) 163–168.

[353] F. S. Bemfica and H. O. Girotti, *Born series and unitarity in noncommutative quantum mechanics*, *Physical Review D* **77** no. 2, (2008) 027704.

[354] F. S. Bemfica and H. O. Girotti, *Noncommutative quantum mechanics: Uniqueness of the functional description*, *Physical Review D* **78** no. 12, (2008) 125009.

[355] F. S. Bemfica and H. O. Girotti, *Noncommutative quantum mechanics as a gauge theory*, *Physical Review D* **79** no. 12, (2009) 125024.

[356] S. Dey and A. Fring, *Noncommutative quantum mechanics in a time-dependent background*, *Physical Review D* **90** no. 8, (2014) 084005.

[357] M. Hounkonnou, J. Allognon, E. Baloïtcha, J. Bukweli-Kyemba, and H. Mweene, *Quantum mechanics of a two-dimensional anharmonic oscillator in a non-commutative phase space*, *Physica Scripta* **90** no. 1, (2014) 015207.

[358] L. Gouba, *A comparative review of four formulations of noncommutative quantum mechanics*, *International Journal of Modern Physics A* **31** no. 19, (2016) 1630025.

[359] M. Chaichian, M. Sheikh-Jabbari, and A. Tureanu, *Hydrogen atom spectrum and the lamb shift in noncommutative qed*, *Physical Review Letters* **86** no. 13, (2001) 2716.

[360] M. Demetrian and D. Kochan, *Quantum mechanics on non-commutative plane*, *arXiv preprint hep-th/0102050* (2001) .

[361] F. Bopp, *Is quantum mechanics a particular classical statistical mechanics?*, in *Annals of the Henri Poincar Institute 'e*, vol. 15, pp. 81–112. 1956.

[362] H. J. Groenewold, *On the principles of elementary quantum mechanics*, in *On the Principles of Elementary Quantum Mechanics*, pp. 1–56. Springer, 1946.

[363] T. Curtright, D. Fairlie, and C. Zachos, *Features of time-independent wigner functions*, *Physical Review D* **58** no. 2, (1998) 025002.

[364] J. E. Moyal, *Quantum mechanics as a statistical theory*, in *Mathematical Proceedings of the Cambridge Philosophical Society*, vol. 45, pp. 99–124, Cambridge University Press. 1949.

[365] B. Hiley, *A note on the role of idempotents in the extended heisenberg algebra*, in *Proc. of the Int. Meeting of ANPA*, vol. 22, pp. 107–121. 2001.

[366] C. Bastos and O. Bertolami, *Berry phase in the gravitational quantum well and the seiberg–witten map*, *Physics Letters A* **372** no. 34, (2008) 5556–5559.

[367] C. Bastos, O. Bertolami, N. C. Dias, and J. N. Prata, *Noncommutative quantum mechanics and quantum cosmology*, *International Journal of Modern Physics A* **24** no. 15, (2009) 2741–2752.

[368] A. Kokado, T. Okamura, and T. Saito, *Noncommutative quantum mechanics and the seiberg-witten map*, *Physical Review D* **69** no. 12, (2004) 125007.

[369] O. Bertolami and P. Leal, *Aspects of phase-space noncommutative quantum mechanics*, *Physics Letters B* **750** (2015) 6–11.

[370] C. Acatrinei, *Path integral formulation of noncommutative quantum mechanics*, *Journal of High Energy Physics* **2001** no. 09, (2001) 007.

[371] G. Mangano, *Path integral approach to noncommutative space–times*, *Journal of Mathematical Physics* **39** no. 5, (1998) 2584–2591.

[372] H. Christiansen and F. Schaposnik, *Noncommutative quantum mechanics and rotating frames*, *Physical Review D* **65** no. 8, (2002) 086005.

[373] H. Tan, *A coherent-state-based path integral for quantum mechanics on the moyal plane*, *Journal of Physics A: Mathematical and General* **39** no. 49, (2006) 15299.

[374] D. M. Gitman and V. Kupriyanov, *Path integral representations in noncommutative quantum mechanics and noncommutative version of berezin–marinov action*, *The European Physical Journal C* **54** no. 2, (2008) 325–332.

[375] C. Acatrinei, *Lagrangian versus quantization*, *arXiv preprint hep-th/0212321* (2002) .

[376] H. Weyl, *quantum mechanics and group theory*, *magazine for "u r physics* **46** no. 1-2, (1927) 1–46.

[377] E. P. Wigner, *On the quantum correction for thermodynamic equilibrium*, in *Part I: Physical Chemistry. Part II: Solid State Physics*, pp. 110–120. Springer, 1997.

[378] N. C. Dias and J. N. Prata, *Generalized weyl–wigner map and vey quantum mechanics*, *Journal of Mathematical Physics* **42** no. 12, (2001) 5565–5579.

[379] C. Bastos, O. Bertolami, N. C. Dias, and J. N. Prata, *Weyl–wigner formulation of noncommutative quantum mechanics*, *Journal of mathematical physics* **49** no. 7, (2008) 072101.

[380] C. Bastos, N. Dias, and J. Prata, *Wigner measures in noncommutative quantum mechanics*, *Communications in Mathematical Physics* **299** no. 3, (2010) 709–740.

[381] M. Wakimoto, *Fock representations of the affine lie algebra a 1 (1)*, *Communications in mathematical physics* **104** no. 4, (1986) 605–609.

[382] R. V. Mendes, *Quantum mechanics and non-commutative space-time*, *Physics Letters A* **210** no. 4-5, (1996) 232–240.

[383] C. Rohwer, K. Zloshchastiev, L. Gouba, and F. Scholtz, *Noncommutative quantum mechanics—a perspective on structure and spatial extent*, *Journal of Physics A: Mathematical and Theoretical* **43** no. 34, (2010) 345302.

[384] J. Ben Geloun and F. Scholtz, *Coherent states in noncommutative quantum mechanics*, *Journal of mathematical physics* **50** no. 4, (2009) 043505.

[385] M. M. Nieto and D. R. Truax, *Squeezed states for general systems*, *Physical review letters* **71** no. 18, (1993) 2843.

[386] B. Bagchi and A. Fring, *Minimal length in quantum mechanics and non-hermitian hamiltonian systems*, *Physics Letters A* **373** no. 47, (2009) 4307–4310.

[387] S. Dey and A. Fring, *Squeezed coherent states for noncommutative spaces with minimal length uncertainty relations*, *Physical Review D* **86** no. 6, (2012) 064038.

[388] S. Ghosh and P. Roy, *"stringy" coherent states inspired by generalized uncertainty principle*, *Physics Letters B* **711** no. 5, (2012) 423–427.

[389] S. Dey, A. Fring, and T. Mathanaranjan, *Non-hermitian systems of euclidean lie algebraic type with real energy spectra*, *Annals of Physics* **346** (2014) 28–41.

[390] J. dos Santos, F. S. Luiz, O. S. Duarte, and M. H. Moussa, *Non-hermitian noncommutative quantum mechanics*, *The European Physical Journal Plus* **134** no. 7, (2019) 332.

[391] A. Jellal, M. Schreiber, and E. H. El Kinani, *Two coupled harmonic oscillators on noncommutative plane*, *International Journal of Modern Physics A* **20** no. 07, (2005) 1515–1529.

[392] B. Lin, S. Jing, and T. Heng, *Deformation quantization for coupled harmonic oscillators on a general noncommutative space*, *Modern Physics Letters A* **23** no. 06, (2008) 445–456.

[393] P. Feinsilver, *Discrete analogues of the heisenberg-weyl algebra*, *Monatshefte für Mathematik* **104** no. 2, (1987) 89–108.

[394] V. Todorinov, P. Bosso, and S. Das, *Relativistic generalized uncertainty principle*, *Annals of Physics* **405** (2019) 92–100.

[395] A. Kempf, G. Mangano, and R. B. Mann, *Hilbert space representation of the minimal length uncertainty relation*, *Physical Review D* **52** no. 2, (1995) 1108.

[396] S. Das and E. C. Vagenas, *Universality of quantum gravity corrections*, *Physical review letters* **101** no. 22, (2008) 221301.

[397] A. Einstein, *Relativity: The Special and the General Theory-100th Anniversary Edition*. Princeton University Press, 2019.

[398] S. M. Carroll, *Lecture notes on general relativity*, *arXiv preprint gr-qc/9712019* (1997) .

[399] K. S. Thorne, C. W. Misner, and J. A. Wheeler, *Gravitation*. Freeman, 2000.

[400] K. Schwarzschild, *Sitzungsberichte deut. acad. wiss. berlin, kl. math*, *Phys. Tech* (1916) 189–196.

[401] R. P. Kerr, *Gravitational field of a spinning mass as an example of algebraically special metrics*, *Physical review letters* **11** no. 5, (1963) 237.

[402] H. Reissner, *"U about the self-gravity of the electric field according to einstein's theory, annals of physics* **355** no. 9, (1916) 106–120.

[403] G. Nordstrom, *On the energy of the gravitational field in einstein's theory ii verhandl, Koninkl. Ned. Akad. Wetenschap., Afdel. Natuurk., Amsterdam* **26** (1918) 1201–1208.

[404] I. Novikov and V. Frolov, *Physics of black holes*, vol. 27. Springer Science & Business Media, 2013.

[405] E. Poisson, *A relativist's toolkit: the mathematics of black-hole mechanics*. Cambridge university press, 2004.

[406] C. DeWitt-Morette, *Gravitational radiation and gravitational collapse*, vol. 64. Springer Science & Business Media, 1974.

[407] L. Susskind and J. Lindesay, *Introduction To Black Holes, Information And The String Theory Revolution, An: The Holographic Universe*. World Scientific, 2004.

[408] A. K. Pati and S. L. Braunstein, *Impossibility of deleting an unknown quantum state*, *Nature* **404** no. 6774, (2000) 164–165.

[409] W. K. Wootters and W. H. Zurek, *A single quantum cannot be cloned*, *Nature* **299** no. 5886, (1982) 802–803.

[410] G. Chiribella and C. M. Scandolo, *Conservation of information and the foundations of quantum mechanics*, in *EPJ Web of Conferences*, vol. 95, p. 03003, EDP Sciences. 2015.

[411] S. Luo, *Information conservation and entropy change in quantum measurements*, *Physical Review A* **82** no. 5, (2010) 052103.

[412] M. Horodecki and R. Horodecki, *Are there basic laws of quantum information processing?*, *Physics Letters A* **244** no. 6, (1998) 473–481.

[413] L. Susskind, *String theory and the principle of black hole complementarity*, *Physical Review Letters* **71** no. 15, (1993) 2367.

[414] O. C. Stoica, *Revisiting the black hole entropy and the information paradox*, *Advances in High Energy Physics* **2018** (2018) .

[415] E. C. Vagenas, A. F. Ali, and H. Alshal, *Gup and the no-cloning theorem*, *The European Physical Journal C* **79** no. 3, (2019) 1–5.

[416] R. Geroch, *Energy extraction*, *Annals of the New York Academy of Sciences* **224** no. 1, (1973) 108–117.

[417] M. Takahashi, S. Nitta, Y. Tatematsu, and A. Tomimatsu, *Magnetohydrodynamic flows in kerr geometry-energy extraction from black holes*, *The Astrophysical Journal* **363** (1990) 206–217.

[418] J. D. Bekenstein, *Black holes and entropy*, in *JACOB BEKENSTEIN: The Conservative Revolutionary*, pp. 307–320. World Scientific, 2020.

[419] G. W. Gibbons and S. W. Hawking, *Euclidean quantum gravity*. World Scientific, 1993.

[420] R. Penrose and R. Floyd, *Extraction of rotational energy from a black hole*, *Nature Physical Science* **229** no. 6, (1971) 177–179.

[421] B. Carter, *Axisymmetric black hole has only two degrees of freedom*, *Physical Review Letters* **26** no. 6, (1971) 331.

[422] I. Semiz, *Dyon black holes do not violate cosmic censorship*, *Classical and Quantum Gravity* **7** no. 3, (1990) 353.

[423] J. D. Bekenstein, *Generalized second law of thermodynamics in black-hole physics*, *Phys. Rev. D* **9** (Jun, 1974) 3292–3300.

[424] W. Israel, *Third law of black-hole dynamics: a formulation and proof*, *Physical review letters* **57** no. 4, (1986) 397.

[425] D. Sciama, *Black holes and their thermodynamics*, *Vistas in Astronomy* **19** (1976) 385–401.

[426] D. Bigatti and L. Susskind, *Tasi lectures on the holographic principle*, in *Strings, branes and gravity*, pp. 883–933. World Scientific, 2001.

[427] L. Susskind, *The world as a hologram*, *Journal of Mathematical Physics* **36** no. 11, (1995) 6377–6396.

[428] C. Marletto, V. Vedral, S. Virzì, E. Rebufello, A. Avella, F. Piacentini, M. Gramegna, I. P. Degiovanni, and M. Genovese, *Non-monogamy of spatio-temporal correlations and the black hole information loss paradox*, Entropy **22** no. 2, (2020) 228.

[429] P. Chattopadhyay, A. Mitra, and G. Paul, *Probing uncertainty relations in non-commutative space*, International Journal of Theoretical Physics **58** no. 8, (2019) 2619–2631.

[430] J. Zhang, Y. Zhang, and C.-s. Yu, *Rényi entropy uncertainty relation for successive projective measurements*, Quantum Information Processing **14** no. 6, (2015) 2239–2253.

[431] C. Hyeon and W. Hwang, *Physical insight into the thermodynamic uncertainty relation using brownian motion in tilted periodic potentials*, Physical Review E **96** no. 1, (2017) 012156.

[432] L. Jia, Z. Tian, and J. Jing, *Entropic uncertainty relation in de sitter space*, Annals of Physics **353** (2015) 37–47.

[433] J. Feng, Y.-Z. Zhang, M. D. Gould, and H. Fan, *Uncertainty relation in schwarzschild spacetime*, Physics Letters B **743** (2015) 198–204.

[434] F. Scardigli and R. Casadio, *Gravitational tests of the generalized uncertainty principle*, The European Physical Journal C **75** no. 9, (2015) 425.

[435] M. Bojowald, S. Brahma, U. Büyükçam, and T. Strobl, *States in non-associative quantum mechanics: uncertainty relations and semiclassical evolution*, Journal of High Energy Physics **2015** no. 3, (2015) 93.

[436] U. Singh, A. K. Pati, and M. N. Bera, *Uncertainty relations for quantum coherence*, Mathematics **4** no. 3, (2016) 47.

[437] X. Guo, P. Wang, and H. Yang, *The classical limit of minimal length uncertainty relation: revisit with the hamilton-jacobi method*, Journal of Cosmology and Astroparticle Physics **2016** no. 05, (2016) 062.

[438] R. Schwonnek, L. Dammeier, and R. F. Werner, *State-independent uncertainty relations and entanglement detection in noisy systems*, Physical review letters **119** no. 17, (2017) 170404.

[439] S. Bagchi and A. K. Pati, *Uncertainty relations for general unitary operators*, *Physical Review A* **94** no. 4, (2016) 042104.

[440] P. Busch, T. Heinonen, and P. Lahti, *Heisenberg's uncertainty principle*, *Physics Reports* **452** no. 6, (2007) 155–176.

[441] M. J. Hall, *Exact uncertainty approach in quantum mechanics and quantum gravity*, *General Relativity and Gravitation* **37** no. 9, (2005) 1505–1515.

[442] L. Mandelstam and I. Tamm, *The uncertainty relation between energy and time in non-relativistic quantum mechanics*, in *Selected Papers*, pp. 115–123. Springer, 1991.

[443] B.-Q. Wang, C.-Y. Long, Z.-W. Long, and T. Xu, *Solutions of the schrödinger equation under topological defects space-times and generalized uncertainty principle*, *The European Physical Journal Plus* **131** no. 10, (2016) 378.

[444] A. Plato, C. Hughes, and M. Kim, *Gravitational effects in quantum mechanics*, *Contemporary Physics* **57** no. 4, (2016) 477–495.

[445] A. Kempf, G. Mangano, and R. B. Mann, *Hilbert space representation of the minimal length uncertainty relation*, *Phys. Rev. D* **52** (Jul, 1995) 1108–1118. https://link.aps.org/doi/10.1103/PhysRevD.52.1108.

[446] J. Maziero, *The maccone-pati uncertainty relation*, *Revista Brasileira de Ensino de Física* **39** no. 4, (2017) .

[447] K. Wang, X. Zhan, Z. Bian, J. Li, Y. Zhang, and P. Xue, *Experimental investigation of the stronger uncertainty relations for all incompatible observables*, *Physical Review A* **93** no. 5, (2016) 052108.

[448] D. Mondal, S. Bagchi, and A. K. Pati, *Tighter uncertainty and reverse uncertainty relations*, *Physical Review A* **95** no. 5, (2017) 052117.

[449] D. V. Anosov and A. A. Bolibruch, *The Riemann-Hilbert Problem: A Publication from the Steklov Institute of Mathematics Adviser: Armen Sergeev*, vol. 22. Springer Science & Business Media, 2013.

[450] G. F. B. Riemann, *On the hypotheses which lie at the bases of geometry*, *J. Tokyo Math. Soc.* **7** (1895) 65–78.

[451] B. Riemann, *Mathematical werke*, 1953.

[452] D. Deutsch, *Uncertainty in quantum measurements*, *Physical Review Letters* **50** no. 9, (1983) 631.

[453] Y. Huang, *Variance-based uncertainty relations*, *Physical review a* **86** no. 2, (2012) 024101.

[454] J. Sánchez, *Entropic uncertainty and certainty relations for complementary observables*, *Physics Letters A* **173** no. 3, (1993) 233–239.

[455] J. Sánchez-Ruiz, *Improved bounds in the entropic uncertainty and certainty relations for complementary observables*, *Physics Letters A* **201** no. 2-3, (1995) 125–131.

[456] Z. Puchała, Ł. Rudnicki, K. Chabuda, M. Paraniak, and K. Życzkowski, *Certainty relations, mutual entanglement, and nondisplaceable manifolds*, *Physical Review A* **92** no. 3, (2015) 032109.

[457] V. Balasubramanian, S. Das, and E. C. Vagenas, *Generalized uncertainty principle and self-adjoint operators*, *Annals of Physics* **360** (2015) 1–18.

[458] M. S. Moslehian and L.-E. Persson, *Reverse cauchy–schwarz inequalities for positive c*-valued sesquilinear forms*, *arXiv preprint arXiv:0905.4065* (2009) .

[459] D. Ilisevic, S. Varosanec, *et al.*, *On the cauchy-schwarz inequality and its reverse in semi-inner product c*-modules*, *Banach Journal of Mathematical Analysis* **1** no. 1, (2007) 78–84.

[460] E.-Y. Lee, *A matrix reverse cauchy–schwarz inequality*, *Linear algebra and its applications* **430** no. 2-3, (2009) 805–810.

[461] P. Cerone and S. S. Dragomir, *Mathematical inequalities: a perspective*. CRC Press, 2010.

[462] I. Pikovski, M. R. Vanner, M. Aspelmeyer, M. Kim, and Č. Brukner, *Probing planck-scale physics with quantum optics*, *Nature Physics* **8** no. 5, (2012) 393–397.

[463] S. Dey, A. Bhat, D. Momeni, M. Faizal, A. F. Ali, T. K. Dey, and A. Rehman, *Probing noncommutative theories with quantum optical experiments*, *Nuclear Physics B* **924** (2017) 578–587.

[464] L. A. Correa, J. P. Palao, D. Alonso, and G. Adesso, *Quantum-enhanced absorption refrigerators*, *Scientific reports* **4** (2014) 3949.

[465] R. Dorner, S. R. Clark, L. Heaney, R. Fazio, J. Goold, and V. Vedral, *Extracting quantum work statistics and fluctuation theorems by single-qubit interferometry*, *Physical review letters* **110** no. 23, (2013) 230601.

[466] A. Dechant, N. Kiesel, and E. Lutz, *All-optical nanomechanical heat engine*, *Physical review letters* **114** no. 18, (2015) 183602.

[467] O. Abah, J. Rossnagel, G. Jacob, S. Deffner, F. Schmidt-Kaler, K. Singer, and E. Lutz, *Single-ion heat engine at maximum power*, *Physical review letters* **109** no. 20, (2012) 203006.

[468] K. Zhang, F. Bariani, and P. Meystre, *Quantum optomechanical heat engine*, *Physical review letters* **112** no. 15, (2014) 150602.

[469] A. Mari and J. Eisert, *Cooling by heating: Very hot thermal light can significantly cool quantum systems*, *Physical review letters* **108** no. 12, (2012) 120602.

[470] W. H. Zurek, *Maxwell's demon, szilard's engine and quantum measurements*, in *Frontiers of nonequilibrium statistical physics*, pp. 151–161. Springer, 1986.

[471] C. Ou and S. Abe, *Exotic properties and optimal control of quantum heat engine*, *EPL (Europhysics Letters)* **113** no. 4, (2016) 40009.

[472] G. Thomas, D. Das, and S. Ghosh, *Quantum heat engine based on level degeneracy*, *Physical Review E* **100** no. 1, (2019) 012123.

[473] P. Alberto, C. Fiolhais, and V. Gil, *Relativistic particle in a box*, *European Journal of Physics* **17** no. 1, (1996) 19.

[474] V. Alonso, S. De Vincenzo, and L. Mondino, *On the boundary conditions for the dirac equation*, *European Journal of Physics* **18** no. 5, (1997) 315.

[475] G. Menon and S. Belyi, *Dirac particle in a box, and relativistic quantum zeno dynamics*, *Physics Letters A* **330** no. 1-2, (2004) 33–40.

[476] F. Reif, *Fundamentals of statistical and thermal physics*. Waveland Press, 2009.

[477] W. Niedenzu, V. Mukherjee, A. Ghosh, A. G. Kofman, and G. Kurizki, *Quantum engine efficiency bound beyond the second law of thermodynamics*, *Nature communications* **9** no. 1, (2018) 1–13.

[478] M. B. Plenio and S. S. Virmani, *An introduction to entanglement theory*, in *Quantum Information and Coherence*, pp. 173–209. Springer, 2014.

[479] L. C. Andrews, *Special functions of mathematics for engineers*, vol. 49. Spie Press, 1998.

[480] J. F. Santos and A. E. Bernardini, *Quantum engines and the range of the second law of thermodynamics in the noncommutative phase-space*, *The European Physical Journal Plus* **132** no. 6, (2017) 1–11.

[481] J. F. Santos, *Noncommutative phase-space effects in thermal diffusion of gaussian states*, *Journal of Physics A: Mathematical and Theoretical* **52** no. 40, (2019) 405306.

[482] J. F. Santos, *Heat flow and noncommutative quantum mechanics in phase-space*, *Journal of Mathematical Physics* **61** no. 12, (2020) 122101.

[483] A. Fring, L. Gouba, and F. G. Scholtz, *Strings from position-dependent noncommutativity*, *Journal of Physics A: Mathematical and Theoretical* **43** no. 34, (2010) 345401.

[484] R. Long and W. Liu, *Performance of quantum otto refrigerators with squeezing*, *Physical Review E* **91** no. 6, (2015) 062137.

[485] M. Huber, M. Perarnau-Llobet, K. V. Hovhannisyan, P. Skrzypczyk, C. Klöckl, N. Brunner, and A. Acín, *Thermodynamic cost of creating correlations*, *New Journal of Physics* **17** no. 6, (2015) 065008.

[486] T. Zhang, W.-T. Liu, P.-X. Chen, and C.-Z. Li, *Four-level entangled quantum heat engines*, *Physical Review A* **75** no. 6, (2007) 062102.

[487] J. Wang, Z. Ye, Y. Lai, W. Li, and J. He, *Efficiency at maximum power of a quantum heat engine based on two coupled oscillators*, *Physical Review E* **91** no. 6, (2015) 062134.

[488] J. Roßnagel, S. T. Dawkins, K. N. Tolazzi, O. Abah, E. Lutz, F. Schmidt-Kaler, and K. Singer, *A single-atom heat engine*, Science **352** no. 6283, (2016) 325–329.

[489] M. Khodadi, K. Nozari, S. Dey, A. Bhat, and M. Faizal, *A new bound on polymer quantization via an opto-mechanical setup*, Scientific reports **8** no. 1, (2018) 1–6.

[490] H. Girotti, *Noncommutative quantum field theories*, arXiv preprint hep-th/0301237 (2003) .

[491] N. C. Dias and J. N. Prata, *Exact master equation for a noncommutative brownian particle*, Annals of Physics **324** no. 1, (2009) 73–96.

[492] S. Ghorashi and M. B. Harouni, *Decoherence of quantum brownian motion in noncommutative space*, Physics Letters A **377** no. 13, (2013) 952–956.

[493] P. Chattopadhyay, A. Mitra, G. Paul, and V. Zarikas, *Bound on efficiency of heat engine from uncertainty relation viewpoint*, Entropy **23** no. 4, (2021) 439.

[494] S. Singh, *Quantum brayton engine of non-interacting fermions in a one dimensional box*, International Journal of Theoretical Physics **59** no. 9, (2020) 2889–2900.

[495] P. Amore, *Asymptotic and exact series representations for the incomplete gamma function*, EPL (Europhysics Letters) **71** no. 1, (2005) 1.

[496] L. B. Castro and A. E. Obispo, *Generalized relativistic harmonic oscillator in minimal length quantum mechanics*, Journal of Physics A: Mathematical and Theoretical **50** no. 28, (2017) 285202.

[497] X. Liu, L. Chen, F. Wu, and F. Sun, *Fundamental optimal relation of an irreversible quantum carnot heat pump with spin-1/2 systems*, Mathematical and computer modelling **54** no. 1-2, (2011) 190–202.

[498] A. Dalkıran, E. Açıkkalp, and N. Caner, *Analysis of a quantum irreversible otto cycle with exergetic sustainable index*, Physica A: Statistical Mechanics and its Applications **453** (2016) 316–326.

[499] M. Esposito, U. Harbola, and S. Mukamel, *Nonequilibrium fluctuations, fluctuation theorems, and counting statistics in quantum systems*, Reviews of modern physics **81** no. 4, (2009) 1665.

[500] M. Campisi, P. Hänggi, and P. Talkner, *Erratum: Colloquium: Quantum fluctuation relations: Foundations and applications [rev. mod. phys. 83, 771 (2011)]*, *Reviews of Modern Physics* **83** no. 4, (2011) 1653.

[501] K. Macieszczak, K. Brandner, and J. P. Garrahan, *Unified thermodynamic uncertainty relations in linear response*, *Physical review letters* **121** no. 13, (2018) 130601.

[502] A. M. Timpanaro, G. Guarnieri, J. Goold, and G. T. Landi, *Thermodynamic uncertainty relations from exchange fluctuation theorems*, *Physical review letters* **123** no. 9, (2019) 090604.

[503] M. Lostaglio, *An introductory review of the resource theory approach to thermodynamics*, *Reports on Progress in Physics* **82** no. 11, (2019) 114001.

[504] I. Henao, R. Uzdin, and N. Katz, *Experimental detection of microscopic environments using thermodynamic observables*, *arXiv preprint arXiv:1908.08968* (2019) .

[505] G. García-Pérez, M. A. Rossi, and S. Maniscalco, *Ibm q experience as a versatile experimental testbed for simulating open quantum systems*, *npj Quantum Information* **6** no. 1, (2020) 1–10.

[506] J.-F. Chen, Y. Li, and H. Dong, *Simulating finite-time isothermal processes with superconducting quantum circuits*, *Entropy* **23** no. 3, (2021) 353.

[507] H. Lu, C. Liu, D.-S. Wang, L.-K. Chen, Z.-D. Li, X.-C. Yao, L. Li, N.-L. Liu, C.-Z. Peng, B. C. Sanders, *et al.*, *Experimental quantum channel simulation*, *Physical Review A* **95** no. 4, (2017) 042310.

[508] K. A. Fisher, R. Prevedel, R. Kaltenbaek, and K. J. Resch, *Optimal linear optical implementation of a single-qubit damping channel*, *New Journal of Physics* **14** no. 3, (2012) 033016.

[509] D.-S. Wang, D. W. Berry, M. C. De Oliveira, and B. C. Sanders, *Solovay-kitaev decomposition strategy for single-qubit channels*, *Physical review letters* **111** no. 13, (2013) 130504.

[510] H. Wang, S. Ashhab, and F. Nori, *Quantum algorithm for simulating the dynamics of an open quantum system*, *Physical Review A* **83** no. 6, (2011) 062317.

[511] H.-Y. Su and Y. Li, *Quantum algorithm for the simulation of open-system dynamics and thermalization*, *Physical Review A* **101** no. 1, (2020) 012328.

[512] A. Mitra, P. Chattopadhyay, G. Paul, and V. Zarikas, *Binary black hole information loss paradox and future prospects*, *Entropy* **22** no. 12, (2020) 1387.

[513] D. Greenbaum, *Introduction to quantum gate set tomography*, *arXiv preprint arXiv:1509.02921* (2015) .

[514] J. F. Fitzsimons, J. A. Jones, and V. Vedral, *Quantum correlations which imply causation*, *Scientific reports* **5** no. 1, (2015) 1–7.

[515] V. Coffman, J. Kundu, and W. K. Wootters, *Distributed entanglement*, *Physical Review A* **61** no. 5, (2000) 052306.

[516] T. J. Osborne and F. Verstraete, *General monogamy inequality for bipartite qubit entanglement*, *Physical review letters* **96** no. 22, (2006) 220503.

[517] X.-N. Zhu and S.-M. Fei, *Entanglement monogamy relations of qubit systems*, *Physical Review A* **90** no. 2, (2014) 024304.

[518] D. R. Hamel, L. K. Shalm, H. Hübel, A. J. Miller, F. Marsili, V. B. Verma, R. P. Mirin, S. W. Nam, K. J. Resch, and T. Jennewein, *Direct generation of three-photon polarization entanglement*, *Nature Photonics* **8** no. 10, (2014) 801–807.

[519] M. H. Rubin, D. N. Klyshko, Y. Shih, and A. Sergienko, *Theory of two-photon entanglement in type-ii optical parametric down-conversion*, *Physical Review A* **50** no. 6, (1994) 5122.

[520] M. Genovese, *Research on hidden variable theories: A review of recent progresses*, *Physics Reports* **413** no. 6, (2005) 319–396.

[521] Y. I. Bogdanov, G. Brida, M. Genovese, S. Kulik, E. Moreva, and A. Shurupov, *Statistical estimation of the efficiency of quantum state tomography protocols*, *Physical review letters* **105** no. 1, (2010) 010404.

[522] D. F. V. James, P. G. Kwiat, W. J. Munro, and A. G. White, *Measurement of qubits*, *Phys. Rev. A* **64** (Oct, 2001) 052312.

[523] P. Bosso, S. Das, I. Pikovski, and M. R. Vanner, *Amplified transduction of planck-scale effects using quantum optics*, *Physical Review A* **96** no. 2, (2017) 023849.

[524] J. Abedi and N. Afshordi, *Echoes from the abyss: A highly spinning black hole remnant for the binary neutron star merger gw170817*, *Journal of Cosmology and Astroparticle Physics* **2019** no. 11, (2019) 010.

[525] M. M Cunha, A. Fonseca, and E. O Silva, *Tripartite entanglement: Foundations and applications*, *Universe* **5** no. 10, (2019) 209.

[526] J. Aasi, B. Abbott, R. Abbott, T. Abbott, M. Abernathy, K. Ackley, C. Adams, T. Adams, P. Addesso, R. Adhikari, *et al.*, *Advanced ligo*, *Classical and quantum gravity* **32** no. 7, (2015) 074001.

[527] **LIGO Scientific Collaboration and Virgo Collaboration** Collaboration, B. P. e. a. Abbott, *Observation of gravitational waves from a binary black hole merger*, *Phys. Rev. Lett.* **116** (Feb, 2016) 061102.

[528] T. Krisnanda, G. Y. Tham, M. Paternostro, and T. Paterek, *Observable quantum entanglement due to gravity*, *npj Quantum Information* **6** no. 1, (2020) 1–6.

[529] H. Li and J. Wang, *Towards the merger of hawking radiating black holes*, *arXiv preprint arXiv:2002.08048* (2020) .

[530] J. L. Friedman, K. Uryū, and M. Shibata, *Thermodynamics of binary black holes and neutron stars*, *Physical Review D* **65** no. 6, (2002) 064035.

[531] K. Uryū, E. Gourgoulhon, and C. Markakis, *Thermodynamics of magnetized binary compact objects*, *Physical Review D* **82** no. 10, (2010) 104054.

[532] A. Le Tiec, L. Blanchet, and B. F. Whiting, *First law of binary black hole mechanics in general relativity and post-newtonian theory*, *Physical Review D* **85** no. 6, (2012) 064039.

[533] A. Zimmerman, A. G. Lewis, and H. P. Pfeiffer, *Redshift factor and the first law of binary black hole mechanics in numerical simulations*, *Physical review letters* **117** no. 19, (2016) 191101.

[534] A. Le Tiec and P. Grandclément, *Horizon surface gravity in corotating black hole binaries*, *Classical and Quantum Gravity* **35** no. 14, (2018) 144002.

[535] S. B. Giddings, *Observational strong gravity and quantum black hole structure*, *International Journal of Modern Physics D* **25** no. 12, (2016) 1644014.

[536] P. Amaro-Seoane, H. Audley, S. Babak, J. Baker, E. Barausse, P. Bender, E. Berti, P. Binetruy, M. Born, D. Bortoluzzi, *et al.*, *Laser interferometer space antenna*, *arXiv preprint arXiv:1702.00786* (2017) .

[537] Z. Zhao, Y.-A. Chen, A.-N. Zhang, T. Yang, H. J. Briegel, and J.-W. Pan, *Experimental demonstration of five-photon entanglement and open-destination teleportation*, *Nature* **430** no. 6995, (2004) 54–58.

[538] K. Edamatsu, *Entangled photons: generation, observation, and characterization*, *Japanese Journal of Applied Physics* **46** no. 11R, (2007) 7175.

[539] X.-M. Liu and W.-B. Liu, *Researching on hawking effect in a kerr space time via open quantum system approach*, *Advances in High Energy Physics* **2014** (2014) .

[540] J. Hu, W. Zhou, and H. Yu, *Dynamics of an elementary quantum system outside a radiating schwarzschild black hole*, *Physical Review D* **88** no. 8, (2013) 085035.

[541] F. C. Lombardo and G. J. Turiaci, *Dynamics of an acoustic black hole as an open quantum system*, *Physical Review D* **87** no. 8, (2013) 084028.

[542] S. T. Dawkins, O. Abah, K. Singer, and S. Deffner, *Single atom heat engine in a tapered ion trap*, in *Thermodynamics in the Quantum Regime*, pp. 887–896. Springer, 2018.

[543] L. Lamata, J. León, T. Schätz, and E. Solano, *Dirac equation and quantum relativistic effects in a single trapped ion*, *Physical review letters* **98** no. 25, (2007) 253005.

[544] R. Gerritsma, G. Kirchmair, F. Zähringer, E. Solano, R. Blatt, and C. Roos, *Quantum simulation of the dirac equation*, *Nature* **463** no. 7277, (2010) 68–71.

[545] A. Pototsky, F. Marchesoni, F. V. Kusmartsev, P. Hänggi, and S. E. Savel'ev, *Relativistic brownian motion on a graphene chip*, *The European Physical Journal B* **85** no. 10, (2012) 1–8.